

# **DUAL FRAME SYSTEMS OF BUCKLING RESTRAINED BRACES**

Teză destinată obținerii  
titlului științific de doctor inginer  
la  
Universitatea "Politehnica" din Timișoara  
în domeniul INGINERIE CIVILĂ  
de către

**Ing. Sorin BORDEA**

Președinte:

Prof.Dr.Ing. Gheorghe LUCACI, Decan Facultatea de Construcții,  
Universitatea "Politehnica" din  
Timișoara

Conducător științific:

Prof.Dr.Ing.Dr.H.C. Dan DUBINA,                      Universitatea "Politehnica"  
Timișoara

Referenți științifici:

Prof.Dr.Ing. Andre PLUMIER,                      Universitatea Tehnică din Liege,  
Belgia

Prof.Dr.Ing. Dan LUNGU,                      Universitatea Tehnică de  
Construcții București

Prof.Dr.Ing. Daniel GRECEA,                      Universitatea "Politehnica" din  
Timișoara

Ziua susținerii tezei: 19. februarie 2010

Seriile Teze de doctorat ale UPT sunt:

- |                        |   |
|------------------------|---|
| 1. Automatică          | 7. Inginerie Electronică și Telecomunicații |
| 2. Chimie              | 8. Inginerie Industrială                    |
| 3. Energetică          | 9. Inginerie Mecanică                       |
| 4. Ingineria Chimică   | 10. Știința Calculatoarelor                 |
| 5. Inginerie Civilă    | 11. Știința și Ingineria Materialelor       |
| 6. Inginerie Electrică |   |

Universitatea „Politehnica” din Timișoara a inițiat seriile de mai sus în scopul diseminării expertizei, cunoștințelor și rezultatelor cercetărilor întreprinse în cadrul școlii doctorale a universității. Seriile conțin, potrivit H.B.Ex.S Nr. 14 / 14.07.2006, tezele de doctorat susținute în universitate începând cu 1 octombrie 2006.

Copyright © Editura Politehnica – Timișoara, 2006

Această publicație este supusă prevederilor legii dreptului de autor. Multiplicarea acestei publicații, în mod integral sau în parte, traducerea, tipărirea, reutilizarea ilustrațiilor, expunerea, radiodifuzarea, reproducerea pe microfilme sau în orice altă formă este permisă numai cu respectarea prevederilor Legii române a dreptului de autor în vigoare și permisiunea pentru utilizare obținută în scris din partea Universității „Politehnica” din Timișoara. Toate încălcările acestor drepturi vor fi penalizate potrivit Legii române a drepturilor de autor.

România, 300159 Timișoara, Bd. Republicii 9,  
tel. 0256 403823, fax. 0256 403221  
e-mail: editura@edipol.upt.ro

## Acknowledgements

The thesis was developed during my activity (2005 – 2010) within the Department of Steel Structures and Structural Mechanics CMMC, the Center of Excellence in the Mechanics of Materials and Safety of Structures CEMSIG, from the “Politehnica” University of Timișoara.

I would like to express my gratitude to my advisor, Prof. Dr. Ing. Dr. h.c. Dan Dubină, for all his support and guidance throughout my research activity. His advices and comments along these years made it possible for me to conclude my work.

My special thanks to Assoc. Prof. Dr. Ing. Aurel Stratan, for his support and assistance, for his valuable advices that helped me to develop the experimental program. During these 5 years of research activity, his patience and attitude encouraged me to finalize the thesis.

I would like also to thank Assoc. Prof. Dr. Ing. Florea Dinu for his assistance in numerical modeling and also for helping me finalize the proofread the thesis.

My thanks also go my colleagues, PhD Student Filip Vacarescu Norin, PhD Student Gelu Danku and PhD Student Calin Neagu, for their assistance in the laboratory work.

Many thanks to Assoc. Prof. Dr. Ing. Tamas Nagy, for his advices and assistance in the field of RC building frames and FRP retrofitting techniques.

Thanks to Dr. Ing. Nicu Munteanu, for helping me to pursue the experimental work. Thanks also to Ing. Popa Viorel, for helping me in the management of the research contracts.

Thanks to Dan Scarlat, whose professional experience and involvement helped me in the laboratory work.

My thanks to Prof. Dr. Ing. Daniel Grecea, Assoc. Prof. Dr. Ing. Raul Zaharia, Assoc. Prof. Dr. Ing. Viorel Ungureanu, Assoc. Prof. Dr. Ing. Adrian Ciutina, Senior Lecturer Dr. Ing. Adrian Dogariu, Dr. Ing. Ramona Gabor, PhD Student Andrei Crisan for their assistance and suggestions.

I am grateful to my parents and sister, for teaching me the most beautiful things of my life, for all the unconditional support. I hope I have made them proud.

Bordea, Sorin

**Title of the thesis:** Dual Frame Systems with Buckling Restrained Braces

Teze de doctorat ale UPT, Seria 5, Nr. 53, Editura Politehnica, 2010, 244 pagini, 199 figuri, 36 tabele.

ISSN:1842-581X

ISBN: 978-606-554-059-0

Keywords:

Buckling Restrained Brace, reinforced concrete frame structure, gravity load design, local retrofitting, global retrofitting, modeling parameters for Buckling Restrained Braces, acceptance criteria for Buckling Restrained Braces, seismic reduction factor  $q$ , nonlinear static analysis (pushover), nonlinear dynamic analysis (timehistory), nonlinear incremental dynamic analysis, experimental tests, unbounded materials, performance based seismic evaluation/design.

Abstract:

The thesis aims at investigating the behavior of reinforced concrete frame structures retrofitted with dissipative buckling restrained brace systems.

On this purpose, numerical investigations and experimental tests were conducted, in order to evaluate the effectiveness and the functionality of a buckling restrained brace system and its influence on a reinforced concrete portal frame. Modeling parameters for buckling restrained braces were determined. Acceptance criteria were proposed for this particular case, then a performance based seismic evaluation and design was applied on the case study. Finally, the seismic reduction factor ( $q$ ) was evaluated by means of nonlinear analysis and compared to the experimental values. A methodology for the performance based evaluation and design was proposed.

Numerical analysis performed on the retrofitted reinforced concrete frame has shown an improvement of the seismic performance. The final experimental results confirmed and validated the buckling restrained system functionality both at local level (BRB element and its connections with reinforced concrete elements) and at global level (RC frame behavior).



## TABLE OF CONTENTS

Table of contents .....	5
Notations, abbreviations, acronyms .....	8
List of tables.....	14
List of figures .....	15
Rezumat .....	21
Summary .....	24
<b>1. INTRODUCTION</b>	
1.1 Subject of the thesis (motivation) .....	27
1.2 Objectives and goals .....	28
1.3 Research framework.....	28
<b>1. BUCKLING RESTRAINED BRACING SYSTEMS FOR NEW AND EXISTING BUILDING STRUCTURES</b>	
2.1 Hystory and concept of the dissipative systems .....	29
2.2 Buckling restrained braces: principle, model and advantages .....	29
2.3 Comparison with other removable passive hysteretic devices installed within the framed structure .....	42
2.3.1. INERD devices.....	42
2.3.2. EBF with removable link .....	43
2.3.3. Hysteretic dampers (CV+Hysteretic dampers) .....	45
2.3.4. Shear walls of low yield steel (AISC2005) .....	46
2.3.5. Self-centering devices .....	48
2.3.6. Shape Memory Alloy Systems.....	50
2.4 The advantages of using buckling restrained braces.....	51
2.5 Research development regarding buckling restrained bracesystems and their use in seismic resistant building frames.....	52
2.6 Specific provisions in design codes .....	65
2.7 Research objectives of the thesis .....	73
<b>3. MODELS AND METHODS FOR PERFORMANCE BASED ANALYSIS AND DESIGN</b>	
3.1 General concept of performance based seismic approach.....	77
3.2 Performance based evaluation of existing buildings before and after retrofiting: methodologies and general criteria.....	80
3.3 Models and performance criteria for materials .....	81
3.4 Models and performance criteria for elements.....	87
3.4.1. Type of models.....	87
3.4.2. Performance criteria for elements .....	90
3.5 Global analysis: principles and methods.....	96
3.5.1. Nonlinear static procedure .....	96
3.5.2. Summary of the N2 method .....	98
3.5.3. Nonlinear dynamic procedure (NDP).....	99
3.6 Case study: application of BRB to an existing RC building .....	101
3.6.1. Frame design and strengthening solution.....	102
3.6.2. Strengthening solution .....	103
3.7 Analysis procedure .....	103
3.8 Modeling for pushover analysis .....	104
3.9 Performance assessment .....	107
3.9.1. Initial RC frame (MRF).....	107
3.9.2. Strengthening with buckling restrained braces.....	108
3.9.3. Strengthening by fiber reinforced polymers.....	108
3.9.4. Strengtening by BRB and FRP.....	108

6 Table of contents

---

3.10	Conclusions .....	110
4.	CHARACTERISATION AND EVALUATION OF BUCKLING RESTRAINED BRACES: EXPERIMENTAL PROGRAM	
4.1	Test arrangements .....	111
4.1.1.	Introduction .....	111
4.1.2.	Test arrangements.....	111
4.2	Experimental setup, proposed BRB system and loading protocol .....	114
4.2.1.	BRB specimens.....	114
4.2.2.	Test setup .....	115
4.2.3.	Test results .....	117
4.3	Conclusions .....	121
5.	PERFORMANCE BASED EVALUATION AND RETROFIT OF REINFORCED CONCRETE BUILDING FRAMES: CASE STUDY	
5.1	Building description .....	123
5.1.1.	Geometry .....	123
5.1.2.	Loads .....	125
5.1.3.	Materials .....	126
5.1.4.	Members .....	126
5.1.5.	BRB seismic upgrade of RC frames.....	128
5.2	Performace based seismic evaluation of initial and retrofitted reinforced concrete frame .....	132
5.2.1.	Preliminary considerations .....	132
5.2.1.1.	Elements controlled by flexure .....	132
5.2.1.2.	Elements controlled by shear .....	134
5.2.1.3.	Rebars overlapping along the elements.....	135
5.2.1.4.	Beams controlled by inadequate anchorage of reinforcement into beam-column joint .....	135
5.2.1.5.	Columns with axial loads exceeding $0.7P_0$ .....	136
5.2.1.6.	Earthquake hazard level EHL - conversion coefficients of PGA for different EHL (according to national standard).....	136
5.2.1.7.	Evaluation of performance with nonlinear pushover analysis (N2 method) .....	137
5.2.1.8.	Time History analysis.....	137
5.2.2.	Pushover analysis .....	138
5.2.3.	Nonlinear dybnameic analysis .....	143
5.2.4.	Incremental dynamic analysis (IDA).....	148
5.3	Conclusions .....	151
6.	EXPERIMENTAL QUALIFICATION OF BRB SYSTEMS FOR SEISMIC RETROFIT OF REINFORCED CONCRETE FRAMED STRUCTURES	
6.1	Introduction .....	152
6.2	Frame model .....	152
6.2.1.	RC frame .....	152
6.2.2.	Details of the concrete frame .....	153
6.2.3.	Characteristics of BRB system .....	154
6.3	Testing setup.....	157
6.3.1.	Testing rig and connection between BRB and RC frame .....	157
6.3.2.	Monitoring device and measurements.....	161
6.4	Loading protocol .....	165
6.4.1.	Monotonic tests .....	165
6.4.2.	Cyclic tests .....	167
6.5	Experimental results.....	167

6.5.1. Observations and direct measurements .....	167
6.5.2. Evaluation of results.....	177
6.6 Conclusions .....	183
7. PROPOSAL DESIGN METHOD FOR THE RETROFITTING OF REINFORCED CONCRETE BUILDING FRAMES WITH BUCKLING RESTRAINED BRACE SYSTEM	184
8. CONCLUSIONS AND PERSONAL CONTRIBUTIONS.....	187
Bibliography .....	192
Annexes I .....	198
Annexes II.....	243

## NOTATIONS, ABBREVIATIONS, ACRONYMS

### Notations

#### Chapter 1

$q$  Seismic reduction factor

#### Chapter 2

$Y(x)$  Transverse deflection

$q(x)$  Transverse distributed load

$A$  area where the brace is in either tension or compression

$A_o$  original area

$A_c$  Area of the inner core

$A_j$  Area of the end core

$A_t$  Area of the transition core

$E_i$  Young's modulus of inner core

$E_o I_o$  Flexural rigidity of the outer tube

$E I_{trans}$  Flexural stiffness of the core member at a section near the end of the steel tube

$C_{max}$  Maximum compressive brace strengths at a given axial deformation level

$I_i$  Moment of inertia of the inner steel core

$L$  length where the brace is in either tension or compression

$L_o$  original length

$L_b$  Length of the core at a section near the end of the steel tube

$L_c$  Length of the core segment

$L_f$  Effective length of the core

$L_{fb}$  Effective length of the core at a section near the end of the steel tube

$L_j$  End core length

$L_j$  Length of the end joint regions

$L_t$  Transition zone length

$L_{wp}$  Work point to work point length

$P$  Axial load

$P_e$  Euler buckling load

$P_{cr}$  Critical load

$P_{e\_trans}$  Euler buckling load at a section near the end of the steel tube

$P_{max}$  Maximum compressive strength

$P_y$  Axial yield load

$P_{yc}$  Nominal yield strength of the core section

$T_{max}$  Maximum tensile brace strengths at a given axial deformation level

$\beta$  Imperfect unbonding

$\varepsilon$  axial strain

$\varepsilon_{wp}$  Brace overall strain

$\varepsilon_c$  BRB core inelastic upper bound strain

$\Phi$  Angle between the brace and the horizontal beam

$\theta$  Inter-story drift

$\Delta_t$	is the axial deformation at expected tensile yielding load
$\sigma_y$	Yield stress
$\Omega$	Material over-strength of the core steel
$\Omega_h$	Strain hardening factors of the core steel
<b>Chapter 3</b>	
$b''$	Width of confined core measured outside of the hoops
$f_c'$	Confined concrete is the cylinder strength
$f_{cm}$	Mean value of concrete cylinder compressive strength core measured to outside the hoops
$f_{ctd}$	Design tensile strength
$f_t$	Tensile strength
$f_{yk}$ or $f_{0.2k}$	Yield strength
$f_{y,max}$	Maximum actual yield strength
$s_h$	Spacing of hoops
$\epsilon_{c1}$	Strain at peak stress
$ \epsilon_{cu1} $	Nominal ultimate strain
$\rho_s$	Ratio of volume of transversal reinforcement to volume of concrete
$\alpha_{cc}$	Coefficient taking into account of long term effects on the compressive strength and unfavorable effects resulting from the way the load is applied.
$\alpha_{ct}$	Coefficient taking into account of long term effects on the tensile strength and unfavorable effects resulting from the way the load is applied.
$\epsilon_{uk}$ and $f_t/f_{yk}$	Ductility
$\gamma_c$	Partial safety factor for concrete;
<b>Chapter 4</b>	
$f_y$	Characteristic yield strength of BRB steel plate
$f_u$	Ultimate limit strength of steel of BRB steel plate
A%	Elongation
$D_y$	Yielding displacement of the BRB element
$E_{pl}$	Energy corresponding to the attainment of ultimate plastic displacement
$E_y$	Energy corresponding to the attainment of displacement $D_y$
$F_y$	Yielding force
$\beta$	Compression-strength adjustment factor
$\omega$	Tension strength adjustment factor
$\mu\%$	Energy based ductility index
$\Delta_b$	Brace deformation
$\Delta_{by}$	Brace yield deformation
$\Delta_{bm}$	Design story drift
<b>Chapter 5</b>	
a	Minimum concrete cover depth (2.5 cm)

## 10 Notations, abbreviations, acronyms

---

$b$	Cross section width
$b_w$	Beams width
CS	Cross section
$d$	Distance from the extreme compression fiber to the center of tension reinforcement
$f_c'$	Characteristic concrete strength
$f_{ck}$	Characteristic compressive strength of concrete
$f_{sk}$	Characteristic yield strength of rebars
$f_y$	Characteristic strength of reinforcement
$f_{ySC}$	Measured yield strength of the steel core
$h$	Cross section height
$h_0$	Distance from compressed fiber of cross section to middle of tensed rebar ( $d$ )
$h_i$	Height of level $i$ relative to the base of the frame
$l_{bmin}$	minimum anchorage/overlapping length ( $l_{b,av}$ )
$l_{b,reqd}$	basic required anchorage length ( $l_{b,req}$ )
$m_i$	Mass at level $i$
Ag	Gross cross section area
C	Conforming concrete (confined concrete)
$E_s$	Reinforcement young modulus
$K_e$	Effective stiffness of the BRB element
NC	Nonconforming concrete (unconfined concrete)
P	Axial force
$P_o$	nominal axial load strength at zero eccentricity
$P_{max}$	Maximum axial force in each different cross section extracted from preliminary nonlinear pushover analysis
$Q_b$	shear strength of concrete
$Q_{cap}$	shear strength
$Q_e$	shear strength of stirrups
$Q_i$	shear strength of inclined rebars
R	partial behavior factor which characterize strictly the behavior of the structure
$R_R$	contribution of structural redundancy
$R_y$	Ratio of the expected yield stress to the specified minimum yield stress
$R_\mu$	seismical reduction factor due to the ductility of the structure
$T_c$	corner period at the upper limit of the constant acceleration region of the elastic spectrum corner period
$V_{max}$	maximum shear force in each different cross section extracted from preliminary nonlinear pushover analysis
$V_s$	strength provided by the hoops
$\beta_1$	Coefficient of depth from the compressed edge - according to Park and Paulay $\beta_1=0.85$ if $f_c' < 27.6$ [N/mm <sup>2</sup> ] and is reduced continuously at a rate of 0.05 for each 6.89 N/mm <sup>2</sup> of strength in excess of 27.6 N/mm <sup>2</sup> (acc to Park and Paulay) - Reinforced Concrete Structures (1975) - p58/59 and fig. 4.1.
$\lambda_1$	the acceleration multiplier for first yielding
$\lambda_u$	acceleration multiplier for the ultimate limit state
$\mu$	displacement ductility factor

$\rho$	Tensed reinforcement
$\rho'$	Compressed reinforcement
$\rho_{bal}$	Reinforcement ratio producing balanced strain conditions according to Park and Paulay - Reinforced Concrete Structures (1975)
$\Delta_t$	Axial deformation at expected tensile yielding load
$\Delta_u$	Ultimate displacement of the BRB element
$\Delta_y$	Yield displacement of the BRB element
$\Phi$	Rebar diameter
$\Omega$	Multiplicative factor of axial force
$\Omega_i$	Maximum overstrength
Chapter 6	
$n_{bolts}$	number of the bolts
$D_y$	Yielding displacement of the RC frame
$F_f$	friction force
$F_t$	maximum force applied to all bolts
$M_s$	torque moment of a pretensed bolt
$\sigma_{pl}$	plate pressure
Abbreviations	
BPL	Building Performance Levels
BRB	Buckling restrained bracing
BRBF	Buckling restrained braced frame
BRB-C-L	left BRB element cyclically loaded
BRB-C-R	right BRB element cyclically loaded
BRBS	Buckling restrained bracing system
CBF	Centrally braced frame
CP	Collapse prevention
DBDM	Displacement Based Design Method
DL	dead load
EBF	Eccentrically braced frames
EHL	Earthquake hazard level
EQ	seismic load
FBDM	Force Based Design Method
FEM	Finite element method
GLD	Gravity load designed
IO	Immediate occupancy
LS	Life safety
LL	live load
MDOF	Multi Degree of Freedom
MRF	Moment resisting frame
MRF+BRB	Moment resisting frame global retrofitted by buckling restrained braces
MRF+FRP	Moment resisting frame local retrofitted by fiber reinforced polymers (carbon fiber)
MRF+FRP+BRB	Moment resisting frame local retrofitted by fiber reinforced polymers (carbon fiber) and global retrofitted by buckling restrained braces
MRI	Medium recurrence interval

## 12 Notations, abbreviations, acronyms

---

PBSA	Performance based seismic assessment
PBSD	Performance based seismic design
PBSE	Performance based seismic evaluation
PGA	Peak Ground Acceleration
PVC	Polyvinylchloride (polyethylene)
PE	Probability to exceed
RC	Reinforced concrete
SDOF	Single Degree of Freedom
SLS	Serviceability limit state
SMA	Shape memory alloy
SL	snow load
ULS	Ultimate limit state
WL	wind load
Acronyms	
AISC	American Institute of Steel Constructions ( <a href="http://www.aisc.org/">http://www.aisc.org/</a> )
ARUP	global firm of designers, engineers, planners and business consultants ( <a href="http://info.arup.com/">http://info.arup.com/</a> )
ASCE	American Society of Civil Engineers ( <a href="http://www.asce.org/">http://www.asce.org/</a> )
CEMSIG	Research Center for Mechanics of Materials and Structural Safety - CEMSIG is a RTD (Research and Technical Development) unit of the "Politehnica" University of Timisoara, at the Faculty of Civil Engineering, Department of Steel Structures and Structural Mechanics ( <a href="http://cemsig.ct.upt.ro/cemsig/index.php">http://cemsig.ct.upt.ro/cemsig/index.php</a> )
COST C26	<i>Urban Habitat Constructions under Catastrophic Events</i> ; an European Action in order to increase the knowledge of the behaviour of constructions in urban habitat under catastrophic events, when exposed to extreme events ( <a href="http://www.cost.esf.org/">http://www.cost.esf.org/</a> )
ECCS	European Convention for Constructional Steelwork ( <a href="http://www.steelconstruct.com/">http://www.steelconstruct.com/</a> )
EN10002-1	European standard specifies the method for tensile testing of metallic materials
EN10025:1993	European code regarding " <i>Hot rolled products of non-alloy structural steels. Technical delivery conditions</i> "
EN10051ClassA	European code regarding steel hot rolled products
EN 1998-1	European seismic standard for the <i>Design of structures for earthquake resistance</i>
FEMA	Federal Emergency Management Agency is an agency of the United States Department of Homeland Security ( <a href="http://www.fema.gov/">http://www.fema.gov/</a> )
NEHRP	National Earthquake Hazards Reduction Program ( <a href="http://www.nehrp.gov/">http://www.nehrp.gov/</a> )
NIPON STEEL	Japanese company, producer of steel and steel products ( <a href="http://www.nsc.co.jp/en/index.html">http://www.nsc.co.jp/en/index.html</a> )
NTC	Italian standard, " <i>Norme Tecniche per le Costruzioni</i> " ( <a href="http://esse1.mi.ingv.it/">http://esse1.mi.ingv.it/</a> )
PROHITECH	<i>Earthquake PROtection of HIstorical Buildings by Reversible Mixed TECHnologies</i> ; a European FP6 project whose main scope was the research project is to develop sustainable methodologies for the use of reversible mixed technologies in the seismic protection of existing



	constructions, with particular emphasis to historical and monumental buildings ( <a href="http://www.prohitech.com/">http://www.prohitech.com/</a> )
PN-II-RU-TD	Romanian <i>National Project for Young Researchers</i> financed by CNCISIS (National Council of Scientific Research from Higher Education) ( <a href="http://www.cncsis.ro/">http://www.cncsis.ro/</a> )
ST 009-2005	Romanian code regarding reinforcement material quality „ <i>Specificație tehnică privind produse din oțel utilizate ca armături: cerințe și criterii de performanță</i> ”
STAS 438/1-89	Romanian code regarding reinforcement material quality „ <i>Produse de oțel pentru armarea betonului. Oțel beton laminat la cald. Mărci și condiții tehnice de calitate</i> ”
STEELRETRO	<i>STEEL Solutions for Seismic RETROfit and Upgrade of Existing Constructions</i> ; a RFCS (Research Fund for Coal and Steel) European Project

## LIST OF TABLES

Table 2.1	Yield and maximum forces evaluated from nominal and measured characteristics
Table 2.1	Pe/Py Ratios (by Watanabe et al., 1988)
Table 2.2	Test Specimens
Table 2.3	Steel Braces in Tension Acceptance Criteria for Nonlinear Procedures—Structural Steel Components (FEMA356/ASCE41)
Table 2.4	Acceptance Criteria for BRBs
Table 3.1	Numerical Acceptance Criteria for Linear Procedures—Reinforced Concrete Infilled Frames
Table 3.2	FEMA 356 modeling parameters and numerical acceptance criteria for nonlinear procedures - RC beams
Table 3.3	FEMA 356 modeling parameters and numerical acceptance criteria for nonlinear procedures - RC columns
Table 3.4	FEMA 356 modeling parameters and numerical acceptance criteria for nonlinear procedures - RC beam-column joints
Table 3.5	FEMA 356 modeling parameters and numerical acceptance criteria for nonlinear procedures – member controlled by flexure
Table 3.6	FEMA 356 modeling parameters and numerical acceptance criteria for nonlinear procedures – member controlled by shear
Table 3.7	FEMA 356 modeling parameters and numerical acceptance criteria for nonlinear procedures – braces in tension
Table 3.8	Type of gravity loads
Table 3.9	Load combinations
Table 3.10	Verification of beams
Table 3.11	Verification of columns
Table 3.12	Equivalent yield strength of the reinforcements
Table 3.13	Column stiffness reduction according to FEMA356
Table 3.14	The fundamental period of vibration and the target displacements for the considered structure
Table 3.15	Displacement demand and acceptance criteria (FEMA), in mm
Table 4.1	Yielding displacements and yielding forces for BRB, for different unbonding materials
Table 4.2	Summary of cyclic tests
Table 4.3	Dissipative energy of the BRBs
Table 4.4	Ultimate displacement of BRB from cyclic test vs. acceptance criteria
Table 5.1	$\Omega$ values in case of constant BRB steel core plates for all levels
Table 5.2	$\Omega$ values in case of variable BRB steel core plates cross section
Table 5.3	modeled stiffness and real stiffness ratio
Table 5.4	BRB modeling parameters for the final benchmark analysis
Table 5.5	BRB modeling parameters for the final benchmark analysis
Table 5.6	Earthquake hazard levels
Table 5.7	Plastic rotations and deformations in elements for static and dynamic nonlinear analysis
Table 5.8	Values of partial behavior factor q
Table 6.1	Theoretical vs. quality certificate vs. experimental rebars samples material characteristics
Table 6.2	Theoretical vs. experimental BRB characteristics and parameters
Table 6.3	Material characteristics of the BRB steel core plates
Table 6.4	q factor values for RC frame structure, before and after retrofitting

## LIST OF FIGURES

- Figure 2.1 Buckling-restrained unbonded steel brace
- Figure 2.2 CBF vs. BRB
- Figure 2.3 Cross-sections of various buckling-restrained braces developed in Japan ..
- Figure 2.4 BRBS on Steel/RC MRF as a V and/or inverted V, or as diagonals
- Figure 2.5 Examples of BRB bracing configurations, (a) Diagonal bracing, (b) Chevron bracing, (c) V bracing, (d) X bracing
- Figure 2.6 BRBS - RC MRF connections: local connections and continuously connections
- Figure 2.7 Local connections: in-plane of RC frame (F.M. Mazzolani)
- Figure 2.8 "Continuously" connected to the RC frame (infilled steel braced frame connections) - in-plane of RC frame - the RC frame - drilled bolts / chemical anchors
- Figure 2.9 Concept of a type of buckling-restrained brace
- Figure 2.10 Components of buckling restrained brace
- Figure 2.11 Gap between mortar and restrained yielding element
- Figure 2.12: a) Unbonded brace under axial loading, b) distributed load along the inner core in the deformed configuration, c) distributed load along the encasing mortar/outer tube
- Figure 2.13 Modes of overall brace instability
- Figure 2.14 Dimensions of core length and work point to work point length
- Figure 2.15 Profile of steel core member in the double tube BRB
- Figure 2.16 Schematic of brace deformation versus inter-story drift angle relationship
- Figure 2.17 Brace strain to story drift ratio versus brace angle relationship
- Figure 2.18: a) Splice plate details for single - cored BRB end connections; b) Double tee to gusset connection detail for double cored BRB end join
- Figure 2.19 Diagram of brace force displacement
- Figure 2.20 INERD pin connection in test frame
- Figure 2.21 INERD U connection in test frame
- Figure 2.22 a) Pin device; b) U device
- Figure 2.23 Comparaisons U-device vs. Pin device
- Figure 2.24 Deformed pin connections after test
- Figure 2.25 Bolted link concepts
- Figure 2.26 a) Failure by connection degradation at the LH6-c2 specimen plastic; b) web buckling at the LL4-c1 specimen
- Figure 2.27 Force-total deformation relationships  $V-\gamma_T$  for specimens LL4-c1 and LH4-c1
- Figure 2.28 Test on full-scale frame with bolted links  
Single-story tested frame
- Figure 2.29 Comparison between numerical and experimental second floor hysteresis loops: (a) Second floor (test), (b) second floor (numerical)
- Figure 2.30 Typical photographs showing specimen at ultimate stage
- Figure 2.31 Hysteresis behavior of the specimens
- Figure 2.32 Global view of the structure retrofitted by means of: a) steel shear panels; b) aluminium shear panels
- Figure 2.33 Post-tensioned RCS frame
- Figure 2.34 Connection details
- Figure 2.35 Test set-up
- Figure 2.36 Beam moment versus drift relationship

- Figure 2.37 Specimen failure modes
- Figure 2.38 A large crack during a loading test. The crack closes after the loading test
- Figure 2.39 Buckling Restrained Braces sandwiched between precast concrete panels
- Figure 2.40 Sub-assembly test of BRB sandwiched between precast concrete panels a) Test setup; b) hysteretic behavior
- Figure 2.41 System test of BRB Subassemblies test of BRB sandwiched between precast concrete panels a) Test setup; b) hysteretic behavior
- Figure 2.42 BRB end details
- Figure 2.43 Section of four test specimens, a) Type 1; b) type 2; c) type 3; d) type 4
- Figure 2.44 Cyclic response of four test specimen a) Type 1; b) type 2; c) type 3; d) type 4
- Figure 2.45 Cyclic response of Unbonded Braces s) Specimen 2; b) specimen 3
- Figure 2.46 Composite confined hysteretic damper. a) Test specimen; b) steel core
- Figure 2.47 Hysteresis response of composite confined hysteretic damper
- Figure 2.48 Star Seismic buckling – restrained brace, a) Single tube configuration; b) multitube configuration
- Figure 2.49 End details and typical hysteresis response. a) End details; b) hysteresis response
- Figure 2.50 Details of buckling inhibiting brace a) Overall view; b) load carrying element; c) A-A section; d) B-B section from
- Figure 2.51 Typical response of buckling – inhibiting brace
- Figure 2.52 Steel – only buckling inhibiting brace: a) Components; b) load – carrying core steel; c) cross sections; d) hysteresis response
- Figure 2.53 Geometry of buckling – restrained brace test specimens
- Figure 2.54 Buckling restrained brace effect of unbonding materials on axial load difference
- Figure 2.55 Double tube buckling restrained brace
- Figure 2.56 Osaka International Convention Center (“damage tolerant” structural design, \$420 million project, completed in 1999, 721000 s.f., 13+2 stories, h=300 ft, 370 braces, largest 73 ft with  $P_y = 1200$  kips)
- Figure 2.57 Toyota stadium
- Figure 2.58 Nippon TV Headquarters, Tokyo (1.4 million s.f., 32+2 stories, h=630 ft, 68 braces, L=60 ft.,  $P_y = 2400$  kips)
- Figure 2.59 Hewlett Packard Co. – Building 5, Corvallis Campus
- Figure 2.60 Exterior exposition system, rectangular tube type: (upper left) SANKYO New Tokyo Headquarter Building (Tokyo, 1997); Nippon Television Tower (Tokyo, 2003) (lower left); Roppongi Hills (Tokyo, 2002); Seismic reinforcement of US Federal Government Building (Salt Lake, U.S., 2001)
- Figure 2.61 a) Osaka International Convention Centre, Japans b) UC Davis Plant & Enviromental Facility, California
- Figure 2.62 Kaiser Santa Clara under construction
- Figure 2.63 Braced Frame elevation at Grid Line C at Wallace F. Bennett Federal Building (N-S direction, E-end of building)
- Figure 2.64 Joint detail of the braced frame elevation at Grid Line C at Wallace F. Bennett Federal Building
- Figure 2.65 Joint detail of the braced frame elevation at Grid Line C at Wallace F. Bennett Federal Building
- Figure 2.66 Wallace F. Bennett Federal Building Before Retrofittting and After Retrofittting

- Figure 2.67 Application of BRB to Constructions of the Tzu-Chi Culture Building ( TV Station)
- Figure 2.68 Connection detail for application of BRB to Constructions of the Tzu-Chi Culture Building (TV Station)
- Figure 2.69 University of Marche (Italy)
- Figure 2.70 Generalized Force-Deformation Relation for Steel Elements or Components (FEMA356/ASCE41)
- Figure 3.1 Matrix of performance objectives for buildings, recommended in Vision 2000
- Figure 3.2 Normalized force versus deformation, FEMA 356
- Figure 3.3 Capacity spectrum method, ATC-40
- Figure 3.4 Relationship between seismic hazard intensity and structural performance
- Figure 3.5 Kent & Park unconfined concrete definition
- Figure 3.6 Stress-strain curve for concrete confined by rectangular hoops, Kent and Park
- Figure 3.7 Some proposed stress-strain curves for concrete confined by rectangular hoops. (a) Chan and Blume et al., (b) Baker, (c) Roy and Sozen, (d) Soliman and Yu, (e) Sargin et al.
- Figure 3.8 Stress-strain curve for nonlinear structural analysis, Eurocode 2
- Figure 3.9 Idealisation of the stress-strain curve for steel reinforcements: (a) elastic perfectly plastic curve; (b) trilinear curve; (c) complete curve
- Figure 3.10 Stress-strain diagrams of typical reinforcing steel (absolute values are shown for tensile stress and strain)
- Figure 3.11 Idealised and design stress-strain diagrams for reinforcing steel (for tension and compression)
- Figure 3.12 Structural element modeling (OpenSees)
- Figure 3.13 Fiber model for discretization of a composite section
- Figure 3.14 Elastic plastic hinge modeling
- Figure 3.15 Deformed frames for application of plastic zones and plastic hinges methods
- Figure 3.16 Generalized Component Force-Deformation relations for depicting modeling and acceptance criteria: a) deformation; b) deformation ratio; c) component or element deformation acceptance criteria
- Figure 3.17 Comparison between IDA curve and pushover static pushover curve
- Figure 3.18 Relative interstorey drift vs. seismic multiplication factor  $\lambda$  for several records
- Figure 3.19 Frame geometry and characteristic beam and column cross-sections
- Figure 3.20 Lateral load pattern
- Figure 3.21 Elastic response spectrum for construction site
- Figure 3.22 Kent & Park unconfined concrete definition
- Figure 3.23 M- $\Phi$  relationship
- Figure 3.24 BRB behavior model
- Figure 3.25 Effect of confinement by FRP on the moment-curvature relationship corresponding to an axial force of 389.6 KN from seismically combination of column section A.
- Figure 3.26 Plastic hinges with inelastic deformations larger than the ULS capacity at the target displacement
- Figure 3.27 Pushover curves of the analyzed frames
- Figure 3.28 Interstorey drift demands at the target displacement

- Figure 4.1 Geometry of the tested BRB element  
Figure 4.2 Subassembly BRB test, according to AISC 2005  
Figure 4.3 Type I subassembly  
Figure 4.4 Test setup for Type II subassembly  
Figure 4.5 Reinforced concrete frame considered in the experimental program  
Figure 4.6 Manufacturing of BRB elements: wrapped BRB elements; centering and fixing inside the tubes; pouring the concrete in vertical position  
Figure 4.7 Test setup  
Figure 4.8 The monotonic behavior of the BRB tests (compression vs. tension)  
Figure 4.9 The AISC and ECCS loading protocols for cyclic tests  
Figure 4.10 Hysteretic behavior of the BRB with PVC transparent film unbonding material, AISC and ECCS loading protocols  
Figure 4.11 Monotonic tests vs. the envelopes from AISC and ECCS loading protocols for PVC transparent film  
Figure 4.12 Steel core deformations (local buckling)  
Figure 4.13. The elongation of the steel core plate is visible using scale marks on the transversal stiffeners of the end connection segment
- Figure 5.1 STEELRETRO reference benchmark RC building model and BRB system distribution  
Figure 5.2 External frame in X direction and interior central frame in Y direction  
Figure 5.3 Plan view of the first and second floor and direction of ribs in the floor  
Figure 5.4 Floor structure  
Figure 5.5 Elastic and design response spectrum  
Figure 5.6 a) Reinforced concrete nonlinear model based on Kent and Park; b) modified Park nonlinear model for steel reinforcement  
Figure 5.7 Definition of reinforced concrete beam elements  
Figure 5.8 Splitting of elements on RC elements in X direction and Y directions (plastic hinges modeled at the end of each element)  
Figure 5.9 a) Moment – rotation relation based on FEMA procedure; b) P-M-M surface interaction  
Figure 5.10 BRB tri-linear model in X direction  
Figure 5.11 BRB trilinear model in Y direction  
Figure 5.12 Definition of reinforced concrete cross section  
Figure 5.13 Cracks distribution in a beam element with opening from lower/upper part of the element  
Figure 5.14 Steel-Retro Benchmark building – overlapping of longitudinal reinforcements  
Figure 5.15 Steel-Retro Benchmark building – Anchorage of the reinforcing bars in the exterior joint  
Figure 5.16 Selection of seismic hazard and performance levels for structural and nonstructural members.  
Figure 5.17 Pushover curves in X direction  
Figure 5.18 Pushover curves in Y direction  
Figure 5.19 Demand and capacity diagram of the equivalent SDOF system MRF - X direction  
Figure 5.20 Demand and capacity diagram of the equivalent SDOF system MRF+FRP - X direction  
Figure 5.21 Demand and capacity diagram of the equivalent SDOF system MRF+BRB - X direction

- Figure 5.22 Demand and capacity diagram of the equivalent SDOF system MRF+FRP+BRB - X direction
- Figure 5.23 Demand and capacity diagram of the equivalent SDOF system MRF - Y direction
- Figure 5.24 Demand and capacity diagram of the equivalent SDOF system MRF+FRP - Y direction
- Figure 5.25 Demand and capacity diagram of the equivalent SDOF system MRF+BRB - Y direction
- Figure 5.26 Demand and capacity diagram of the equivalent SDOF system MRF+FRP+BRB - Y direction
- Figure 5.27 Artificial elastic response spectra of the artificial accelerograms vs. elastic response spectra, 5% damping
- Figure 5.28 Example of an artificial accelerogram used in time history analysis
- Figure 5.29 position of reference point for top displacement
- Figure 5.30 History of top displacement on X direction for MRF, at IO, LS and CP, 2<sup>nd</sup> accelerogram
- Figure 5.31 History of top displacement on X direction for MRF+FRP, at IO, LS and CP, 2<sup>nd</sup> accelerogram
- Figure 5.32 Location of plastic hinges for LS, frame in X direction, MRF structure, 2<sup>nd</sup> accelerogram
- Figure 5.33 History of top displacement on X direction for MRF+BRB, at IO, LS and CP, 2<sup>nd</sup> accelerogram
- Figure 5.34 History of top displacement on X direction for MRF+BRB+FRP, at IO, LS and CP, 2<sup>nd</sup> accelerogram
- Figure 5.35 Location of plastic hinges for LS, frame in X direction, MRF+BRB+FRP structure, 2<sup>nd</sup> accelerogram
- Figure 5.36 Definition of behavior factor
- Figure 5.37 Nodes followed in IDA
- Figure 5.38 Relative interstory drift vs. seismic multiplication factor  $\lambda$  in X direction
- Figure 5.39 Relative interstory drift vs. seismic multiplication factor  $\lambda$  in Y direction
- Figure 6.1 RC frame location: a) 3D view; b) plan view of the third floor
- Figure 6.2 RC elements cross sections (columns and beam)
- Figure 6.3 RC frame and node details: a) rebars bent in the joints; b) formwork of the concrete frame
- Figure 6.4 Characteristics of concrete used for: a) RC frame; b) BRB infill material
- Figure 6.5 BRB composition and geometry (unbonding material – polyethylene foil, 1mm thick)
- Figure 6.6 Modeling parameters for BRB element (bilinear force-displacement relation)
- Figure 6.7 BRB steel plate specimens (5 for mechanical cut and 6 for flame cut)
- Figure 6.8 Stress-strain curves for BRB steel core material
- Figure 6.9 Testing rig and the loading system: a) scheme of the testing rig; b) RC portal frame (MRF); c) RC portal frame and BRB system (MRF+BRB)
- Figure 6.10 Column base connection
- Figure 6.11 Column base and BRB connections
- Figure 6.12 Column base and BRB to column connections: a) BRB and RC column; c) FEM modeling; d) detail of the BRB - RC connection
- Figure 6.13 Friction between BRB connection and the beam
- Figure 6.14 Numerical simulation: a) RC beam – BRB connection; b) RC beam – BRB connection: pressure under the steel plate due to bolts prestressing

- Figure 6.15 Measurement of the vertical displacement of the connection between BRB and column
- Figure 6.16 Measurement of the horizontal displacement of the connection between BRB and column
- Figure 6.17 Measurement devices distribution: Horizontal on RC beam
- Figure 6.18 Measurement devices distribution: on BRB elements
- Figure 6.19 Measurement devices distribution: on RC frame
- Figure 6.20 Experimental results of MRF vs. MRF+BRB: Monotonic Test
- Figure 6.21 Evaluation of  $D_y$  from MRF monotonic test - method 1
- Figure 6.22 Evaluation of  $D_y$  from MRF monotonic test - method 2
- Figure 6.23 ECCS loading history for cyclic test
- Figure 6.24 RC frame under cyclic load
- Figure 6.25 RC frame under cyclic load – development of bending cracks
- Figure 6.26 RC frame under cyclic load – development of shear cracks
- Figure 6.27 RC frame under cyclic load – failure of the node
- Figure 6.28 MRF + BRB under cyclic load
- Figure 6.29 MRF+BRB under cyclic load – bending moment cracks
- Figure 6.30 MRF+BRB under cyclic load – shear cracks at ultimate stage
- Figure 6.31 Initial RC frame vs. retrofitted frame
- Figure 6.32 Left BRB during cyclic test
- Figure 6.33 Right BRB during cyclic test
- Figure 6.34 BRB steel core plates during cyclic test
- Figure 6.35 BRB to column connection after cyclic test
- Figure 6.36 Connection between RC column and BRB - influence of horizontal displacement
- Figure 6.37 Connection between RC column and BRB – influence of vertical displacement
- Figure 6.38 Behavior of connection between BRB and left RC column during cyclic test
- Figure 6.39 Behavior of connection between BRB and right RC column during cyclic test
- Figure 6.40 Connection between BRB and beam during cyclic test – influence of horizontal action
- Figure 6.41 Connection between RB and beam during cyclic test – hysteretic curve
- Figure 6.42 a) Numerical vs. experimental Results (Pushover Analysis vs. Monotonic test)
- Figure 6.43 Analytical vs. Experimental Results (Pushover Analysis vs. Monotonic & Cyclic Test)
- Figure 6.44 a) Envelope of the MRF cyclic test; b) Envelope of the MRF+BRB cyclic test
- Figure 6.45 a) Preliminary value of the seismic reduction factor  $q$  based on envelopes of MRF and MRF+BRB hysteretic curves
- Figure 6.46 Evaluation of  $D_y$  from positive envelope of MRF cyclic test
- Figure 6.47 Evaluation of  $D_y$  from negative envelope of MRF cyclic test
- Figure 6.48 Evaluation of  $D_y$  from positive envelope of MRF+BRB cyclic test
- Figure 6.49 Evaluation of  $D_y$  from negative envelope of MRF+BRB cyclic test



## Rezumat

Teza de doctorat are ca subiect reabilitarea clădirilor în cadre din beton armat proiectate la încărcări gravitaționale cu ajutorul unor sisteme disipative din contravântuiri cu flambaj împiedicat BRB. Contravântuirea cu flambaj împiedicat are ca avantaj principal comportarea similară la întindere și la compresiune.

Obiectivul principal al acestui studiu îl reprezintă investigarea și validarea unui sistem disipativ de contravântuiri cu flambaj împiedicat, destinat reabilitării la nivel global a clădirilor existente. Scopul final este acela de a crea o metodologie de evaluare și proiectare bazată pe performanță PBSE/PBSD pentru reabilitarea cadrelor din beton armat cu ajutorul sistemului de contravântuiri cu flambaj împiedicat BRB. Acest lucru poate asigura protecția clădirilor la acțiuni seismice în conformitate cu cerințele normelor seismice moderne. În același timp, validarea acestei soluții face posibilă aplicarea sistemului BRB la clădiri noi cu structuri în cadre metalice sau din beton armat.

Teza este împărțită în 8 capitole și demonstrează eficacitatea sistemului BRB atât din punct de vedere numeric (analize structurale globale pe cadre) cât și din punct de vedere experimental (teste pe cadre cu un singur nivel).

### **Capitolul I: Introducere**

Se prezintă subiectul tezei (motivarea), obiectivele și scopurile, justificarea în contextul actual și cadrul tezei în contextul programelor de cercetare naționale și internaționale în care autorul tezei și centrul de cercetare CEMSIG este implicat.

### **Capitolul II: Sisteme de contravântuiri cu flambaj împiedicat pentru clădiri noi și existente.**

Al doilea capitol reprezintă o monografie referitoare la utilizarea sistemelor de contravântuiri cu flambaj împiedicat. Acest capitol scoate în evidență principiul de funcționare al unui element BRB, modelul de calcul și posibilele avantaje față de sistemele convenționale. Acestea sunt descrise în literatura de specialitate sau în recomandările unor norme internaționale, cum ar fi AISC2005. În același timp, se încearcă identificarea unor "noi ținte" de importanță majoră în ceea ce privește cercetarea sistemului BRB. Un astfel de exemplu îl constituie determinarea factorului de reducere seismică ( $q$ ) pentru cadre din beton armat reabilite cu sistemul BRB și obținerea unui criteriu de acceptare, particular, în conformitate cu FEMA356 (ASCE41), pentru elementele de tip BRB studiate.

### **Capitolul III: Modele și metode pentru analiza bazată pe performanță.**

În prima parte a capitolului, sunt prezentate principiile de modelare pentru metodele de analiză neliniară și criteriul de acceptare conform FEMA356 (ASCE41), împreună cu metodologia evaluării/proiectării bazate pe performanță (PBSE /PBSD). În cea de-a doua parte a capitolului, este prezentată analiza unui cadru plan dintr-o clădire în cadre din beton armat dimensionată doar la încărcări gravitaționale după normele românești din anii 1960. Analiza statică neliniară a fost aplicată pentru clădirea nereabilitată și reabilitată. Sistemul BRB a fost introdus ca un sistem în V inversat, articulat la capete, iar pentru modelarea lui s-au folosit, în primă fază, parametrii obținuți din analogia cu sistemele BRB similare din literatura de specialitate. Chiar dacă unele elemente ale cadrului au avut nevoie de întărire locală, rezultatele pot fi considerate încurajatoare datorită unei contribuții

semnificative a sistemului BRB. Această concluzie rezultă din analiza rezultatelor pentru trei parametri de bază: rezistență, rigiditate și capacitate de disipare.

Astfel, a apărut ideea continuării studiului numeric cu un studiu experimental pentru a determina cerințele unui element BRB în termeni de deplasare. Acest ultim pas al analizei a fost efectuat pentru a oferi datele de intrare pentru testele experimentale descrise în capitolul IV.

#### **Capitolul IV: Caracterizarea și evaluarea contravântuirilor cu flambaj împiedicat: program experimental.**

Programul experimental descris în acest capitol reprezintă un pionierat în cercetarea din România. Pe baza rezultatelor obținute în capitolul III, s-a proiectat o tipologie de elemente de tip BRB, care apoi au fost executate și testate experimental în laborator. Regimul de încărcare a fost de tip monoton și ciclic. Elementul BRB încercat experimental este alcătuit dintr-o platbandă de oțel introdusă într-un tub de oțel umplut apoi cu beton. Pentru prevenirea frecării dintre platbanda de oțel și beton, au fost folosite trei tipuri diferite de materiale de interfață și anume folie de polietilenă de 1 mm grosime, carton bituminat cu o grosime de 2 mm respectiv cauciuc cu o grosime de 3 mm. În acest fel, au rezultat 12 elemente BRB care au fost încercate în cadrul laboratorului CEMSIG. Rezultatele experimentale au arătat ca elementele BRB și-au dovedit funcționalitatea, îndeplinind cerințele de deformație obținute în analizele descrise în capitolul III. Dintre cele 3 materiale de interfață studiate, folia de polietilenă (PVC) a condus la rezultatele cele mai bune. În concluzie, rezultatele obținute experimental s-au dovedit încurajatoare pentru o cercetare mai complexă atât din punct de vedere numeric (capitolul V) cât și experimental (capitolul VI).

#### **Capitolul V: Evaluarea bazată pe performanță și reabilitarea unei clădiri în cadre din beton armat: studiu de caz.**

Scopul principal al capitolului l-a constituit investigarea unei clădiri în cadre din beton armat existente în vederea reabilitării seismice utilizând diferite sisteme metalice. Astfel, pe baza experienței acumulate în modelarea și analiza numerică a cadrelor din beton armat (parametrii de modelare obținuți pentru elementele BRB în capitolul IV și metodologia descrisă în capitolul III), s-a făcut o evaluare bazată pe performanța a clădirii și s-a decis reabilitarea clădirii. Clădirea de beton armat aleasă ca studiu de caz este o clădire istorică, construită în prima jumătate a secolului 20 în orașul Toscana din Italia. Trebuie precizat că această alegere este motivată de faptul că cercetarea s-a efectuat în cadrul proiectului Steel Retro (2007-2010) având ca parteneri 11 universități, institute de cercetare și companii de profil din 8 țări europene, printre care România și Italia.

Pentru dimensionarea sistemului BRB, s-a utilizat un factor de reducere seismică  $q=4$ . S-a utilizat același sistem BRB în V inversat articulată la capete descris în capitolul III. Rezultatele numerice au dovedit încă o dată posibilitatea îmbunătățirii performanțelor seismice ale unei clădiri în cadre din beton armat prin reabilitarea cu sistemul BRB, dar și faptul că acest lucru necesită și o întărire locală a elementelor din beton armat. Analizele neliniare statice și dinamice s-au aplicat utilizându-se modelul de spectru elastic din EC8, însă considerându-se caracteristicile terenului din locația clădirii. După reabilitare, în urma analizelor statice neliniare s-a observat o îmbunătățire considerabilă a comportamentului la nivel de rezistență și rigiditate, precum și o reducere a deplasării țintă. Pentru analiza dinamică, s-au folosit șapte accelerograme artificiale. S-a observat că în urma reabilitării cu sistemul BRB, performanța clădirii s-a îmbunătățit. Astfel, dacă

pentru structura inițială era îndeplinit doar obiectivul de performanță de Ocupare Imediată, structura reabilitată a îndeplinit inclusiv obiectivul de performanță de Evitare a Colapsului,

Pentru determinarea factorului de reducere  $q$  al clădirii reabilitate cu sistemul BRB (fără influența confinării), s-a efectuat o analiză incrementală dinamică aplicând cele 7 accelerograme pe două direcții ortogonale, scalate prin factori de scalare de la 0.1 până la 2.0. Rezultatele obținute au confirmat valoarea factorului  $q=4$  folosit în dimensionare.

#### **Capitolul VI: Validarea experimentală a unui sistem de contravântuiri cu flambaj împiedicat utilizat pentru reabilitarea structurilor în cadre din beton armat.**

[1] *În urma rezultatelor pozitive obținute prin analize statice și dinamice neliniare, a fost izolat un cadru portal de beton armat din clădirea analizată, în vederea realizării unor încercări experimentale. Obiectivul acestui capitol l-a reprezentat validarea experimentală a rezultatelor obținute pe clădirea reabilitată studiată în capitolul V. În acest scop, cadrul portal izolat a fost testat la scara 1:1 în laboratorul CEMSIG. Cadrul a fost testat la încărcări de tip monoton și ciclic, cu și fără*

PROHITECH WP6 (Leader Darko Beg) "SET-UP OF ADVANCED REVERSIBLE MIXED TECHNOLOGIES FOR SEISMIC PROTECTION BUCKLING RESTRAINED BRACES AS SOLUTION FOR SEISMIC UPGRADING OF EXISTING RC STRUCTURES" M. D'Aniello, G. Della Corte, F.M. Mazzolani University of Naples Federico II, Italy Datasheet n. 01.06.01.01abilitate cu sistemul BRB testate la încărcări monotone și ciclice). Aceste teste au avut ca scop și verificarea îmbinărilor dintre sistemul BRB și elementele de beton armat.

În urma acestor teste, atât elementele BRB cât și sistemul de prindere și-au demonstrat funcționalitatea. Valoarea factorului de reducere  $q$  determinată experimental a fost foarte apropiată de valoarea obținută în analizele neliniare din capitolul V.

#### **Capitolul VII: Metoda de dimensionare propusă pentru reabilitarea unui cadru de beton armat cu sistemul de contravântuiri cu flambaj împiedicat.**

Pe baza studiilor realizate în capitolele III – VI, s-a propus o metodologie coerentă care prezintă pașii de urmat pentru realizarea unei evaluări/proiectări bazate pe performanță a sistemului BRB în cazul reabilitării seismice a cadrelor din beton armat dimensionate la încărcări gravitaționale.

#### **Capitolul VIII: Concluzii și contribuții personale**

Capitolul sintetizează concluziile tezei și prezintă principalele contribuții ale tezei cu privire la tematica subiectului.

## Summary

The thesis investigates the retrofitting of reinforced concrete frame buildings designed for gravity loads only by means of steel dissipative devices based on Buckling Restrained Brace systems BRB. The main advantage of the BRB system is given by the similar behavior in tension and in compression.

The main objective of the study aims at investigating and validating a dissipative solution base on a BRB system, in order to retrofit the existing buildings. The scope is to define a performance based evaluation/design methodology (PBSE/PBSD) for the retrofit of RC frames by means of BRB system. This will result in an improvement of the seismic protection of existing buildings according to the requirements expressed in the new seismic codes. In the same time, the validation of this solution may give the possibility to apply this system for new steel and concrete frame buildings.

The thesis is divided in 8 chapters and demonstrates the efficiency of the BRB systems by means of numerical analysis (structural analysis on RC frames) and experimental investigations (experimental tests on single level RC Frames).

### **Chapter I: Introduction.**

It presents the subject of the thesis (motivation), the objectives and goals, their justifications in the present context, together with the framework of the thesis within the national/international projects in which the author of the thesis and the CEMSIG research center were involved.

### **Chapter II: Buckling Restrained Bracing Systems for New and Existing Building Structures.**

Second chapter presents a state of the art related to applications of BRB system. This chapter emphasis the background of the BRB element, its principle, the computation models and the possible advantages of such systems. Provisions from seismic codes are also referred (eg. AISC2005). In the same time, the thesis looks for "new targets" of major importance regarding the research of BRB elements (e.g. seismic reduction factor  $q$  for RC frames retrofitted with BRB systems, particular acceptance criteria for BRB elements, according to FEMA356 (ASCE41).

### **Chapter III: Models and Methods for Performance Based Analysis and Design.**

In the first part of chapter, the principles of modeling for nonlinear analysis methods and the acceptance criteria according to FEMA356 (ASCE41) together with its methodology regarding the performance based seismic evaluation/design (PBSE/PBSD) are presented. In the second part of the chapter is presented the nonlinear analysis of a RC frame building, designed for gravity loads (GLD), according to Romanian design codes from 1960s. Static nonlinear analysis was applied both for unretrofitted and retrofitted building. An inverted V BRB system pinned at both ends was used. For modeling, the parameters obtained by analogies with similar BRB systems from the literature were applied. Even some RC elements needed local strengthening, the results were considered positive due to a significant global contribution of the BRB system in terms of strength, stiffness and dissipation capacity.

Thus, emerged the idea of continuing the numerical study with an experimental program in order to evaluate the BRB displacement demands. This last

step of analysis was done in order to determine the input values for the experimental tests described in chapter IV.

#### **Chapter IV: Characterization and Evaluation of Buckling Restrained Braces: Experimental Program.**

The experimental program presented in this chapter represents a pioneering research in Romania. Based on the results obtained in chapter III, a typology of BRB element is designed and manufactured and then tested experimentally in the laboratory. The loading program comprised both monotonic and cyclic tests. The tested BRB consisted of a steel core inserted in a steel tube filled with concrete. Three different types of unbonded materials, in order to prevent the friction between steel core and infill concrete, were used (PVC transparent film of 1mm thick, asphaltic bitumen of 2 mm thick and rubber of 3 mm thick). In this way, 12 BRB elements were built and experimentally tested at CEMSIG laboratory. The experimental results proved that the BRB elements were properly designed and manufactured and in the same time proved their functionality by fulfilling the deformations demands obtained from the analysis performed in chapter III. Also, the polyethylene (PVC) proved to be the best unbonded material from the studied ones. As a consequence, the obtained results proved to be encouraging for a more complex research, developed both numerically (chapter V) and experimentally (chapter VI).

#### **Chapter V: Performance Based Evaluation and Retrofit of Reinforced Concrete Building Frames: Case Study.**

The research presented in this chapter was focused on the evaluation of an existing reinforced concrete building designed for gravity loads, retrofitted with different steel systems. Based on the numerical and experimental results obtained in previous chapters, a performance based evaluation of the RC frame building was applied before and after retrofitting. The building from the case study is a historical building built during the first half of 20 century, located in Toscana, Italy. The reason for this selection is that the research was done in the framework of STEELRETRO project. This project was developed in the period 2007-2010 and involved 11 partners from 8 European countries, including Romania and Italy.

A seismic reduction factor of  $q=4$  was used for the design of BRB system. The same inverted V BRB system with pinned connections at both ends as in chapter III was applied. The numerical results proved once again the possibility of seismic improvement of existing RC building frames designed for gravity load by retrofitting with BRB systems, but also the necessity of local retrofitting of RC elements. Nonlinear static and dynamic analyses were performed using EC8 elastic spectrum but adapted to the soil characteristics from the location of the building. Nonlinear static analysis of the retrofitted frame demonstrated an improved behaviour in terms of strength, stiffness and a reduction of the target displacement.

For dynamic analysis, seven artificial accelerograms were applied. Results have shown an improved performance of the frame. If initial RC frame fulfilled the IO objective level only, after retrofitting the structure fulfilled the LS and CP performance objectives.

In order to evaluate the seismic reduction factor  $q$  for retrofitted frame (without taking into account the effect of the confinement), an incremental dynamic analysis was performed by scaling the intensity with scaling factors up to 2.0. The results confirmed the value of seismic reduction factor  $q=4$  used in design.

**Chapter VI: Experimental Qualification of a BRB System for Seismic Retrofit of Reinforced Concrete Framed Structure.**

Following the positive results from the nonlinear static and dynamic analysis, a RC portal frame was isolated from the case study building, in order to develop an experimental program. The objective of this chapter is represented by the experimental validation of the retrofitting technique presented in chapter V. For this purpose, the portal frame isolated from the building was tested in CEMSIG laboratory at 1:1 scale. The portal frame was tested both monotonically and cyclically with/without BRB system. The connecting system between BRB elements and RC elements was detailed and designed.

The experimental program comprised 4 RC frames of 3.2m height and 4.5m span, 2 RC frames without any retrofitting and 2 retrofitted with BRB. They were tested under monotonic and cyclic loads. Following these tests, the BRB system and the connections proved their functionality. The  $q$  factor used in design was confirmed by the tests.

**Chapter VII: Proposal Design Method for the Retrofitting of Reinforced Concrete Building Frames with Buckling Restrained Brace System.**

Based on the studies presented in chapters III – VI, a coherent methodology was proposed in order to perform a PBSE/PBSD for seismic retrofitting of existing RC frames with BRB systems.

**Chapter VIII: Conclusions and Personal Contributions.**

This chapter synthesizes all conclusions of the thesis and main contributions regarding this subject.

# 1. INTRODUCTION

## 1.1 Subject of the thesis (motivation)

Romania is located in a zone of high seismic activity. Reinforced concrete structures built before the 1960's were designed so as to resist mainly gravity loads and wind. The main deficiencies of these reinforced concrete frames are related to the poor detailing and lack of capacity design, leading to reduced local and global ductility. Nowadays, when such types of structures are subjected to structural evaluation, according to the current seismic design provisions, one finds out that strengthening is needed in almost all cases. The main deficiencies of the structures are:

- poor anchorage length of bottom bars at the supports;
- inclined reinforcement used for shear force resistance;
- open stirrups, largely spaced (20 - 25 cm) in potential plastic zones;
- weak materials (concrete with a compressive strength between 12.5 - 20.5 N/mm<sup>2</sup>, and steel rebars (usually smooth rebars, not ribbed) with a yielding strength of 235 N/mm<sup>2</sup>;
- lack of or insufficient stirrups in the beam-column joints;
- weak columns resulting in floor collapse.

The seismicity of Romania is mainly due to the seismic activity within the Vrancea region. The Vrancea seismic region is an area of intermediate to deep seismicity (60 - 180 km). The first major earthquake was historically reported on August the 29<sup>th</sup> 1471 (probable magnitude between 6.9 and 7.1). Since 1471, three other major earthquakes have been historically reported (in 1738, 1802 and 1838), with magnitudes between 6.7 and 7.9. A devastating earthquake stroke Romania in 1940 (depth of 133 km, moment magnitude of 7.7). The most devastating earthquake was recorded on Mars the 4<sup>th</sup> 1977 (94 km depth and a moment magnitude of 7.5). More than 1570 casualties and 11300 injured people were recorded. Numerous buildings collapsed or were severely damaged. 32,900 apartments were destroyed or severely affected, and the overall seismic loss was estimated at more than 2 Billion US \$. Most of these buildings were reinforced concrete buildings with 2 to 16 storeys, with or without infill masonry walls.

The upgrading of the existing buildings is a difficult task, due to the costs implied and for technical reasons. Several strengthening methods were developed, aiming at improving the performances of the existing buildings in the case of seismic events, including base insulation systems, structural systems equipped with dampers and/or energy dissipative devices (passive or with active/semi-active controlled response).

Hysteretic systems with buckling restrained braces BRB have entered during the last decade in the engineering practice of the earthquake resistant structures. There are already numerous relevant applications in new buildings or in the case of existing RC frame buildings, most of them in Japan and USA. There are special provisions regarding the structural design of buildings fit-out with these types of devices in the recent editions of Japanese and American standards. Unfortunately, there are no provisions in the European standards.

The main advantage of the BRB system is based on good stiffness, especially in the case of V or inverted V systems and also very good ductility compared with the conventional centric braces. That is why the importance of BRB systems is increasing, especially for existent RC frame buildings with a small strength capacity to respond earthquake action. The adoption of BRB systems assures the fulfillment of strength, stiffness and ductility simultaneously.

The application of this system in the European context assumes the definition of the behavior factor  $q$ , of the overstrength requirements and ductility in order to establish acceptance criteria for the BRB elements. Furthermore, each different application needs a system calibration and the evaluation of the design and performance parameters. This represents the main purpose of the present thesis and its main objective.

## 1.2 Objectives and Goals

The main objective of the thesis is represented by the investigation and validation of a steel dissipative solution of a buckling restrained system (BRB) for the global retrofitting of existing RC frame buildings designed for gravity loads (GLD). The validation of this solution makes its application possible on new steel/concrete frame buildings.

The objectives of the thesis are:

- to operate a synthesis of the actual state of knowledge concerning the theoretical background, the design methodology and rules for the application of the BRB system to new buildings and to existing buildings, in order to enhance their seismic performance;
- to propose and qualify by testing a Buckling Restrained Brace technical solution;
- to apply and evaluate the performance of seismic BRB technology for the retrofitting of an existing RC frame building;
- to evaluate the behavior factor  $q$  and to propose a design method for the BRB seismic upgrading of RC building frames.

## 1.3 Research framework

The results of the studies, analyses and of the experimental part, represented a point of interest within the framework of two international projects: PROHITECH and STEEL RETRO. The involvement in these projects was performed through CEMSIG, from the CMMC department of the Civil Engineering Faculty of Timisoara. Also, all results were disseminated by the participation of the author at national/international conferences and meetings, and also the involvement of the author as director in a TD national project founded by CNCSIS. The results of the research presented in this thesis were also presented in two European research projects, one TD national project, and one COST/ESF action, as follows:

PN – II – RU – TD – 2008 – 3 „Proiecte de Cercetare pentru Tineri Doctoranzi ” TD 55/2008 “Studiul sistemelor cu cadre duale cu contravântuiri metalice comprimate cu flambaj împiedecat” – project manager (2008/2009)

UE/RFSR-CT-2007-00050 „Steel Solutions for Seismic Retrofit and Upgrade of Existing Constructions” STEEL RETRO – research assistant (2008 – present)

PROHITECH FP6 INCO-CT-2004-509119/2004 Earthquake Protection of Historical Buildings by Reversible Mixed Technologies – member in the research team

PROACTEX 31042/2007 „Sisteme structurale si solutii tehnologice inovative pentru protectia cladirilor la actiuni extreme in contextul cerintelor pentru dezvoltare durabila” - member in the research team

COST C26 – COST Action C26 – Urban Habitat Constructions under Catastrophic Events – program participant



## **2. BUCKLING RESTRAINED BRACING SYSTEMS FOR NEW AND EXISTING BUILDING STRUCTURES**

### **2.1. History and concept of dissipative systems**

The history of modern earthquake engineering is relatively new and started in the second decade of the last century, with the introduction of first seismic regulations in USA and Japan. Since then, seismic code provisions developed continuously, and special efforts have been made to coordinate these actions in order to reduce the losses. This was accompanied by important changes in the materials, fabrication, erection and quality assurance for constructions. These activities still continue on several directions, including the development of new structural systems (e.g. buckling restrained braces).

The kinetic energy introduced in the structure during an earthquake may be partially consumed, by transforming it into potential energy through plastic deformation. If the cumulated plastic deformation energy is larger than the assimilation capacity of the structure, the collapse of the structure takes place. In order to avoid this scenario, with regard to structures design for gravity load conditions, but also to new structures (steel, concrete), the introduction of dissipative elements may reduce the risk of failure.

### **2.2. Buckling Restrained Braces: Principle, Model and Advantages**

#### **History of the development**

The BRBs were introduced for the first time in Japan during the 1980's. Since then, many buildings have been equipped with 'unbonded' braces manufactured by Nippon Steel Corporation. After several tests carried out in 1999 at the University of Berkeley, California, the technology has also been implemented in the USA, by utilizing BRBs for the seismic retrofitting of the UC Davis Plant and Environmental Sciences. The use of BRB technology is increasingly introduced worldwide, with a growing number of buildings that use buckling-restrained braces as a primary lateral force-resisting system. This strong development is also certified by several research studies carried out during the last years in USA, Taiwan and Japan [1].

The application of BRBs in Europe started in Italy and followed the same development trend.

During a major earthquake, a large amount of kinetic energy is introduced into a structure. The manner in which this energy is dissipated determines the level of damage. All building codes recognize that it is not economically feasible to dissipate the seismic energy within the elastic capacity of the materials. The common strategy is therefore to accept that the structure may yield, but to ensure that it yields in a controlled location and a ductile manner. The underlying idea is that a successful ductile structure is one in which yielding occurs in designated elements or "structural fuses" limiting the building-up of forces in the structure. In traditional braced frames, braces are the structural fuses. They yield in compression and tension and absorb energy. However, buckling in compression leads to a sudden loss of stiffness and a progressively degrading behavior which limits the amount of energy dissipation [2].

Several attempts have been made in order to solve the buckling problem. However, these were unsuccessful until Wada, whose team developed the Unbonded

30 Buckling restrained bracing systems for new and existing building structures - 2

Brace™. The buckling of the central steel core is prevented by encasing it over its length in a steel tube filled with mortar, concrete or different aggregates. The term "Unbonded Brace™" derives from the need to provide a slip surface or unbonding layer between the steel core and the surrounding concrete, so that axial loads are taken only by the steel core. The materials and geometry in this slip layer have been carefully designed and constructed so as to allow relative movement between the steel element and the concrete. It simultaneously inhibits local buckling of the steel as it yields in compression. The concrete and steel tube encasement provides sufficient flexural strength and stiffness as to prevent global buckling of the brace, allowing the core to undergo fully-reversed axial yield cycles without loss of stiffness or strength. The concrete and steel tube also helps to resist local buckling [2].

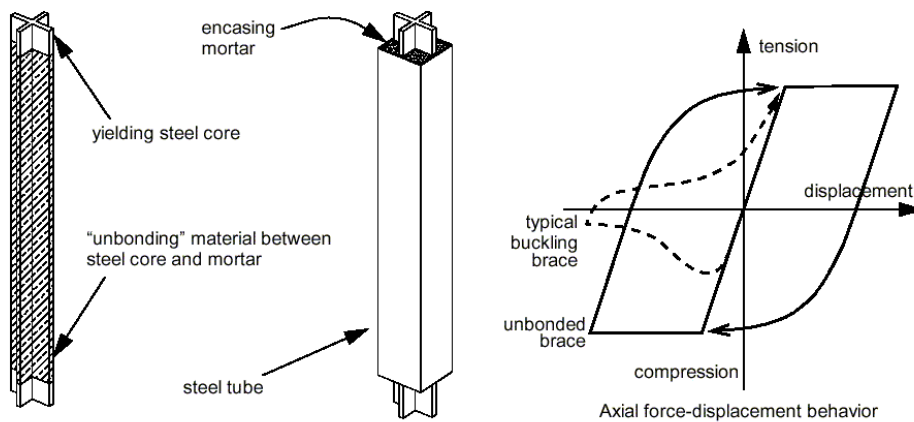


Figure 2.1 Buckling-restrained unbonded steel brace [3]

The following figure presents the difference between a conventional brace CBF and a BRB.

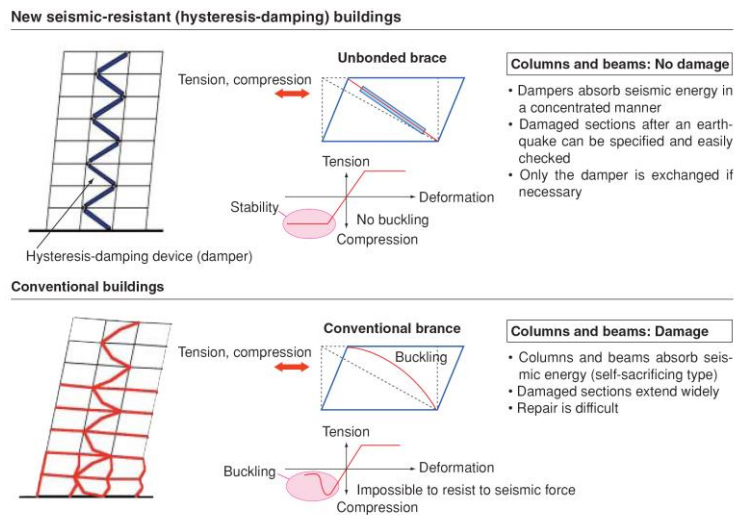


Figure 2.2 CBF vs. BRB [4]

In contrast with the behavior of a typical bracing element, a BRB results in stable hysteretic behavior and provides a more stable and effective seismic resisting element. The brace exhibits nearly identical properties in tension and compression and has the ability to undergo numerous cycles of inelastic deformations without degrading or fracturing. Since these braces do not need to be designed so as to resist buckling, the brace forces are generally lower. This results in lower forces in the superstructure and foundation [2].

A variety of "unbonded braces" having various materials and geometries have been proposed and studied extensively over the last 10-15 years [5]. A summary of the early development of unbonded braces which use a steel core inside a concrete-filled steel tube is provided in Watanabe et al., 1988. In fact, the concept of "damage tolerant structures" - in which the primary structural system is designed to remain elastic while all energy dissipation occurs in specially-detailed components of the lateral force-resisting system - is gaining broad acceptance in Japan [6].

### **BRBS definition and constructive systems**

#### **Types of cross sections**

Several types of BRB sections have been developed and currently used in engineering practice, such as a rectangular or cruciform section of the yielding steel core and a concrete filled tube section the restraining steel encasement, as shown in Figure 2.3a to Figure 2.3d. Figure 2.3e to Figure 2.3h show other BRB configurations in which no filling material is used, and hence no unbonding material has to be provided [7].

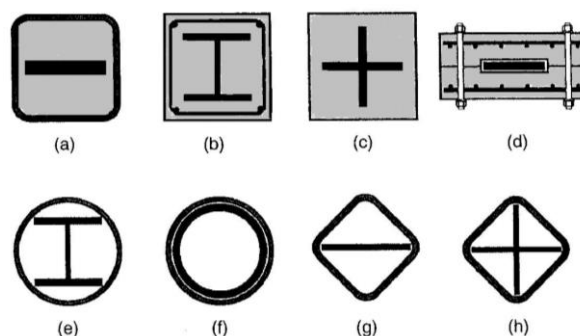


Figure 2.3 Cross-sections of various buckling-restrained braces developed in Japan [7]

#### **Methods of active core embedment**

The BRB elements may also be divided in function of the embedment of the steel (active) core:

- a steel tube filled with concrete/mortar/aggregates (Figure 2.3.a)
- cast in RC (Figure 2.3.b)
- cast- in plain concrete (Figure 2.3.c)
- active core embedded in a detachable RC tube (Figure 2.3.d)
- embedded in a steel tube, with no infill material (Figure 2.3.e, Figure 2.3.h)

- in a detachable steel tube

All these ways of embedment were applied with or without unbonded materials (rubber, polyethylene, resins).

According to Sabbeli [8], as there is no strength or stiffness degradation permitted in the braces, and because the tension and the compression strengths are

32 Buckling restrained bracing systems for new and existing building structures - 2

almost equal, the single diagonal configuration is allowed without any penalty. The single-diagonal configuration is also an effective way to take advantage of the high strengths possible for BRBs. K-bracing is not permitted.

The Chevron (V or inverted-V) configuration is also popular for BRBF, as it maintains some openness for the frame. Because of the balance between brace tension and compression strength, the beam is required to resist only modest loads; a deflection limit is also imposed so as to prevent excessive vertical beam displacement. BRB members can dissipate large amounts of the energy input by a strong earthquake through stable tension-compression yield cycles, thus minimizing damage in primary structural elements to a large extent. BRBs can be installed in the bracing system of the structure as diagonal members, chevron or V braces, or as X configuration bracing, as shown in Figure 2.4. As it may be seen, BRBs may be applied in existing RC MRF buildings with or without infilled masonry, as V or inverted V systems, in the middle span of the structure or as a diagonal inside the external spans [8].

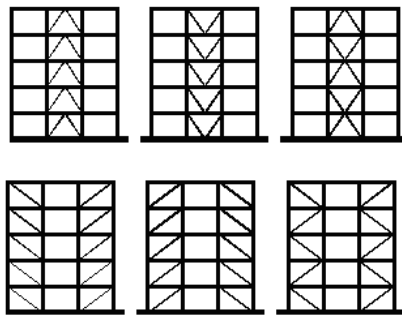


Figure 2.4 BRBS on Steel/RC MRF as a V and/or inverted V, or as diagonals

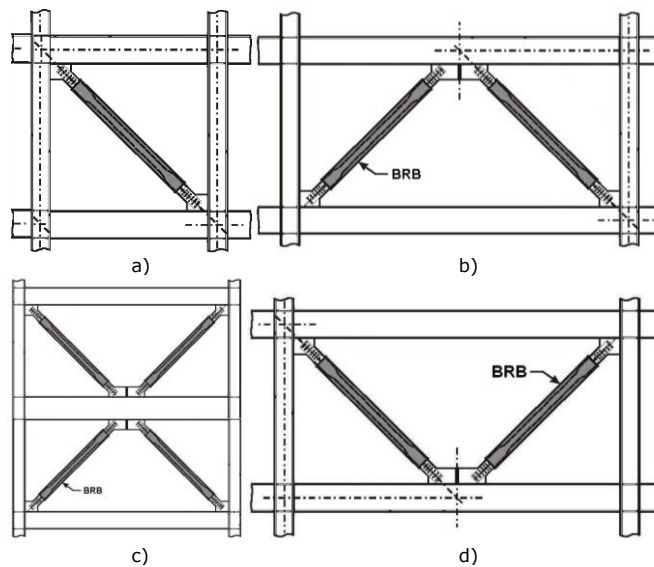


Figure 2.5 Examples of BRB bracing configurations, (a) Diagonal bracing, (b) Chevron bracing, (c) V bracing, (d) X bracing [9]

Figure 2.6 shows different types of connections between existing building and BRBs:

- local connections, may be applied to in-plane/out-of-plane of the RC MRF;
- continuous connections, as infilled steel braced frames with BRB braced frames (in-plane of the RC MRF) or as a steel braced frame system around the exterior of the building (out-of-plane of RC MRF).

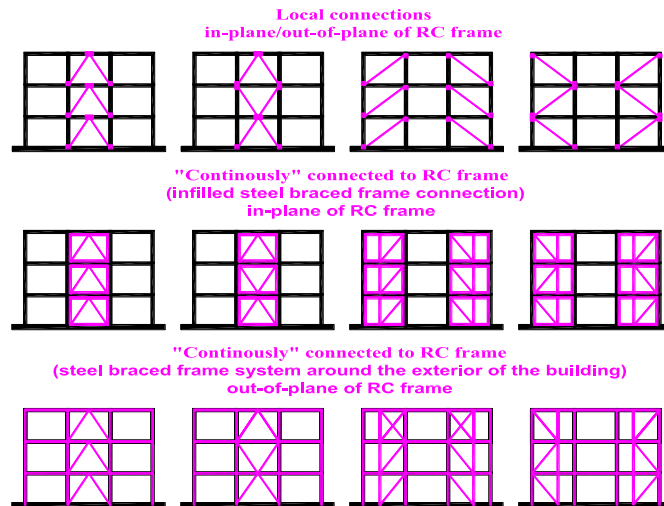


Figure 2.6 BRBS - RC MRF connections: local connections and continuous connections

Figure 2.7 presents a detail of a bolted connection; these bolts may be drilled bolts, chemical anchors, or preloaded bolts applied at the end of the RC cross section.

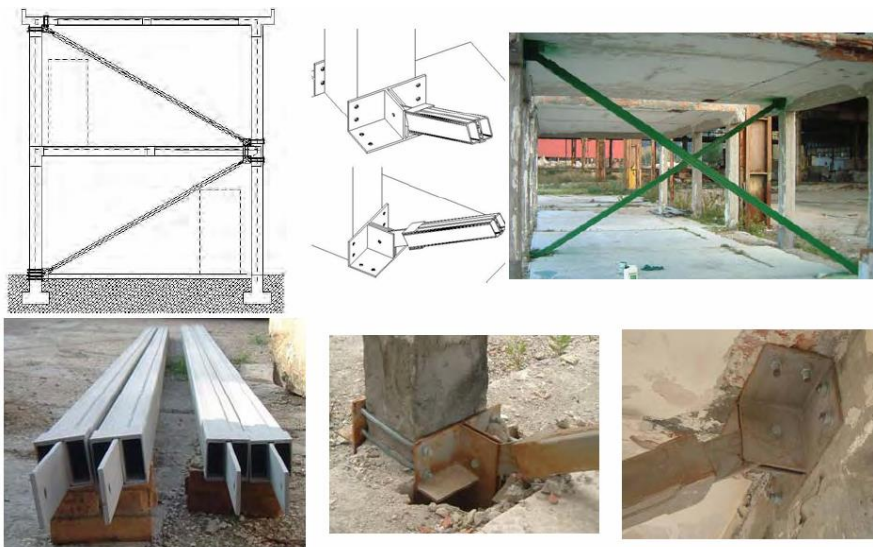


Figure 2.7 Local connections: in-plane of RC frame (F.M. Mazzolani) [10]

34 Buckling restrained bracing systems for new and existing building structures - 2

The same principle may be applied in the case of continuous connections with chemical anchors between the steel element and the RC element or with shear connectors and chemical anchors (Figure 2.8).

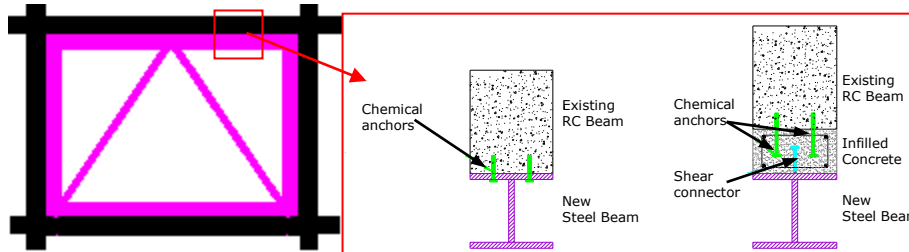


Figure 2.8 "Continuously" connected to the RC frame (infilled steel braced frame connections) - in-plane of RC frame - the RC frame - drilled bolts / chemical anchors

BRBs can be installed in new steel or reinforced concrete buildings or bridges, and can effectively be used in the seismic upgrading of existing structures.

**Design of BRB systems**  
**BRB Components**

Uang and Nakashima, [11] give details about BRB components (Figure 2.9 and Figure 2.10):

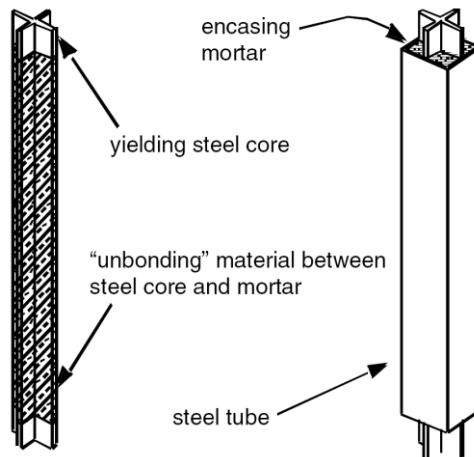


Figure 2.9 Concept of a type of buckling-restrained brace [12]

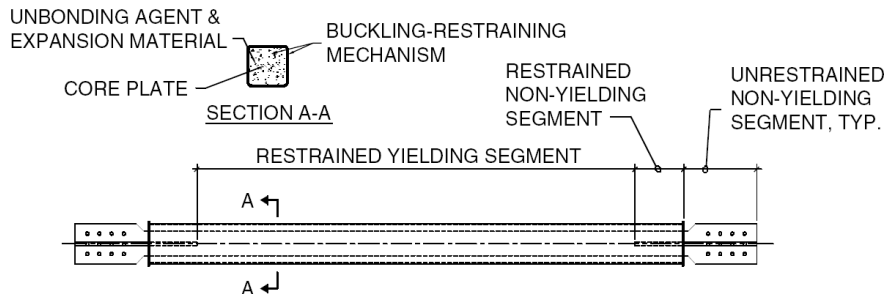


Figure 2.10 Components of a buckling restrained brace [13]

**The restrained yielding segment**

This steel segment has rectangular or cruciform cross sections. As this segment is designed to yield under cyclic loading, mild steel (or low-yield steel) is desirable. Alternatively, high-strength low-alloy steel (e.g. A572 Gr.50 steel) has also been used. Also desirable are steel materials with predictable yield strength with small variations. This property is essential for a reliable capacity design of BRBs.

**The restrained non-yielding segment**

This segment, which is surrounded by the casing and mortar, is usually an extension of the restrained yielding segment but with an enlarged area meant to ensure the elastic response. This can be achieved by widening the restrained yielding segment. It is also common that stiffeners be welded so as to increase the cross-sectional area in this region.

**The unrestrained non-yielding segment**

This segment is usually an extension of the restrained non-yielding segment. This segment is also called the steel core projection. It is common that this segment be designed as a bolted connection for site erection, but other connections such as pin connections or welded connections are also possible. The design considerations of this segment include (i) construction tolerance for the ease of site erection and to facilitate the removal and (ii) local buckling prevention.

**The unbonding agent and expansion material**

Inert material needs to be used that can effectively minimize or eliminate the transfer of shear force between the restrained steel segment and the mortar; materials like rubber, silicon grease or mastic tape have also been used. The restrained yielding segment is expected to experience small-amplitude buckling in higher modes due to the presence of the restraining mechanism. The gap needs to be sufficiently wide as to allow for the expansion of the yielding steel core in compression. Otherwise the friction that is created by the bearing action between the expanding yielding steel and mortar can force the buckling restraining mechanism to carry some axial load. On the other hand, if the gap is too wide, the buckling amplitude and the associated curvature of the buckled steel-yielding segment can be large, which would reduce the low-cycle fatigue resistance of the yielding segment. For the evaluation of the design gap, the Poisson ratio in the elastic (0.3) and yielding (0.5) range may be considered. The design gap is also a function of the maximum design strain. If a width transition between the restrained yielding and the non-yielding segments is used, a longitudinal gap ("interior reserve space" in Figure 2.11) in front of the widened non-yielding segment also needs to be provided so as to avoid direct bearing between the steel segment and the mortar. Such bearing action would unexpectedly increase the compressive capacity of the brace beyond the expected design strength, which is not desirable from the viewpoint of the capacity design and also increases the possibility of an unbalanced load if a chevron bracing configuration is used. Figure 2.11 also shows the exterior space that is needed so as to avoid the contact between the splice plates and the buckling-restraining mechanism.



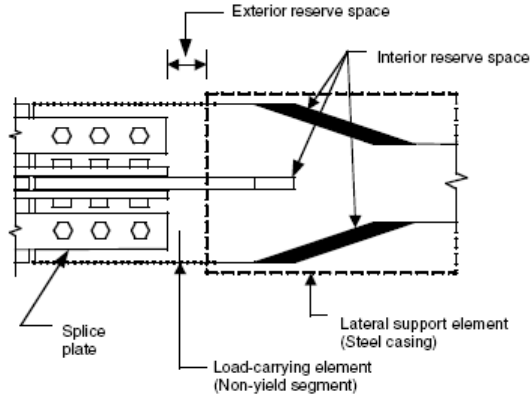


Figure 2.11 Gap between mortar and restrained yielding element

**The buckling-restraining mechanism**

This mechanism is typically composed of mortar and steel casing (e.g., hollow structural shape). But BRBs that do not use mortar have also been proposed. Proper mix design is needed in order to ensure a sufficient compressive strength for the mortar. Otherwise, the mortar cannot effectively restrain the buckling amplitude of the restrained yielding segment.

**Calculation Model**

The global stability of the unbonded brace can be estimated directly from the theory of buckling [14]. Figure 2.12: a shows the diagram of an unbonded brace in compression, while Figure 2.12: b and Figure 2.12: .c show the distributed forces on the steel core and the encasing mortar/outer tube in the deformed configuration. The unknown distributed load, shown in Figure 2.12: b is the transverse reaction of the outer tube/encasing mortar along the inner steel core. Using the system of axes shown in Figure 2.12: the equilibrium of the inner steel core in its deformed configuration is given by

$$E_i I_i \frac{d^4 y(x)}{dx^4} + P \frac{d^2 y(x)}{dx^2} = -q(x) \tag{2.1}$$

The minus sign on the right-hand side of Equation 2.1 results from the fact that  $q(x)$  acts on the direction opposite to the deflection  $y(x)$ . The equal and opposite distributed load  $q(x)$  is loading the encasing mortar/outer tube as shown in Figure 2.12: .b. The equilibrium of a segment of the beam gives:

$$E_o I_o \frac{d^4 y(x)}{dx^4} = q(x) \tag{2.2}$$

The elimination of the unknown distributed load,  $q(x)$ , in Equations 2.1 and 2.2 gives:

$$E_i I_i \frac{d^4 y(x)}{dx^4} + P \frac{d^2 y(x)}{dx^2} = -E_o I_o \frac{d^4 y(x)}{dx^4} \tag{2.3}$$

which, after rearranging terms, yields a homogeneous Euler equation

$$\frac{d^4 y(x)}{dx^4} + \frac{P}{E_i I_i + E_o I_o} \frac{d^2 y(x)}{dx^2} = 0 \tag{2.4}$$



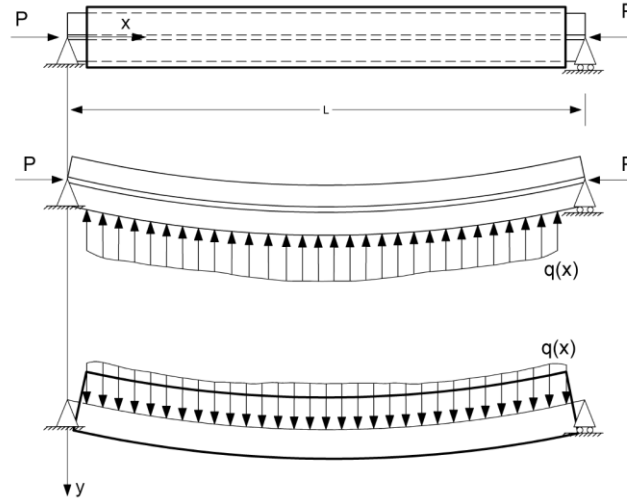


Figure 2.12: a) Unbonded brace under axial loading, b) distributed load along the inner core in the deformed configuration, c) distributed load along the encasing mortar/outer tube [14]

For a brace with buckling length  $L$ , Equation 2.4 yields the critical buckling load of the brace:

$$P_{cr} = P_e = \frac{\pi^2}{L_f^2} (E_i I_i + E_o I_o) \quad (2.5)$$

Neglecting the bending rigidity of the inner steel core  $E_i I_i$ , Equation 2.5 simplifies to:

$$P_{cr} = P_e \approx \frac{\pi^2 E_o I_o}{L_f^2} \quad (2.6)$$

Therefore,

$$\frac{P_e}{P_y} \leq 1.0 \quad \frac{P_e}{P_y} \leq 1.0 \quad (2.7)$$

Equation 2.6 indicates that the critical load of the unbonded brace is merely the Euler buckling load of the outer tube. Accordingly, the global stability of the brace is ensured when the Euler buckling load of the tube,  $P_{cr}$ , exceeds the yielding load of the core,

$$P_y = \sigma_y A_c \quad (2.8)$$

In order to accommodate the axial yielding of the steel core, and to prevent the instability of the sleeve, the detailing of BRB end connections must be able to transmit forces to the core without permitting significant stress to develop in the sleeve. The end connections must also be designed so as to preclude modes of overall brace instability (as shown in Figure 2.13); they are therefore designed as to have higher yield strength than the core within the sleeve so that yielding be confined to a limited length of the core.

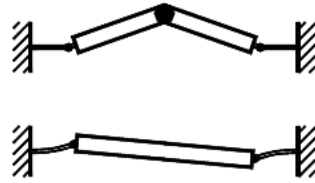


Figure 2.13 Modes of overall brace instability [8]

When properly designed and detailed, steel casing should not resist any significant axial load. To avoid the buckling of BRBs, Watanabe et al. (1988) suggested that the steel casing should be designed for a sufficient flexural stiffness such that

$$\frac{P_e}{P_y} \leq 1.0 \quad (2.9)$$

In order to confine the BRBs' inelastic deformations inside the restraining tube, the cross sectional area ( $A_c$ ) of the energy dissipation core segment ( $L_c$ ) needs to be smaller than that of the end joint regions ( $L_j$ ). The schematic configuration is illustrated in Figure 2.14, in which  $L_c$  and  $L_{wp}$  represent the core length and the work-point to work-point length, respectively.

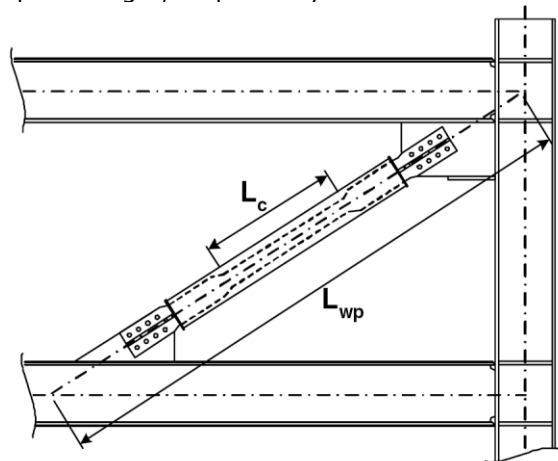


Figure 2.14 Dimensions of core length and work point to work point length [15]

It is confirmed by tests that the effective stiffness,  $K_e$  of the BRB considering the variation of cross sectional area along the length of the brace can be accurately predicted by:

$$K_e = \frac{EA_j A_c A_t}{A_j A_c L_c + 2A_c A_t L_j + 2A_c A_j L_t} \quad (2.10)$$

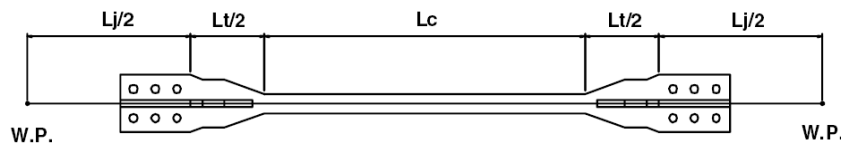


Figure 2.15 Profile of a steel core member in the double tube BRB [15]

The relationships between the brace overall strain ( $\epsilon_{wp}$ ) and the inter-storey drift  $\theta$  can be approximated as:

$$\epsilon_{wp} = \frac{\theta \sin 2\phi}{2} \tag{2.11}$$

The strain-to-drift ratio versus the beam angle  $\phi$  relationships given in Equation 2.11 are plotted in Figure 2.17.

where, the ratio of the core length and the work-point to work-point dimension is:

$$a = \frac{L_c}{L_{wp}} \tag{2.12}$$

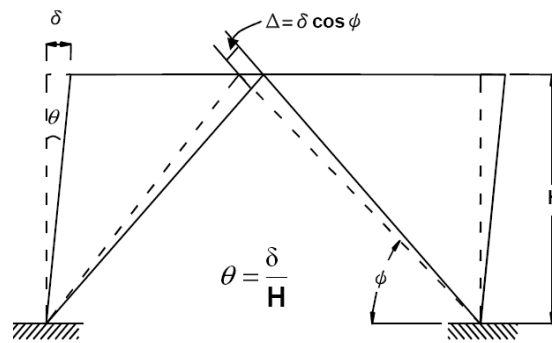


Figure 2.16 Diagram of brace deformation versus inter-storey drift angle relationship [15]

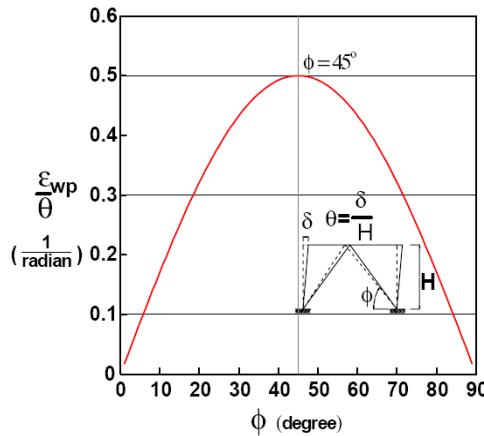


Figure 2.17 Brace strain to storey drift ratio versus brace angle relationship [15]

Thus, assuming that the strain outside the core segment is negligible, the BRB core inelastic upper bound strain  $\epsilon_c$  can be express as:

$$\epsilon_c \leq \frac{\epsilon_{wp}}{a} \tag{2.13}$$

From Equation 2.11 through 2.13, there can be found that, if the inter-storey drift demand is less than 0.02 rad, then the peak core strain would be close to 0.02 for a BRB with a length aspect ratio  $\alpha=0.5$  and oriented at a 45 degree

#### 40 Buckling restrained bracing systems for new and existing building structures - 2

angle. In addition, the following equation should be applied for estimating the maximum compressive strength possibly developed in a BRB:

$$P_{max} = \Omega \cdot \Omega_h \cdot \beta \cdot P_{yc} \quad (2.14)$$

where:

- $P_{yc} = \sigma_y A_c$  is the nominal yield strength of the core section,
- $\Omega$  and  $\Omega_h$  take into account the possible material over-strength and strain hardening factors of the core steel, respectively.

In addition, the bonding factor  $\beta$  represents the imperfect unbonding - the fact that the peak compressive strength is somewhat greater than the peak tensile strength observed during the large deformation cycles. Therefore, in [16] the required stiffness of the steel casing in order to prevent the BRB from a global flexural buckling is:

$$I_o \geq FS \cdot \frac{P_{max} L_f^2}{n^2 E_o} \quad (2.15)$$

As the flexural buckling of a single-cored BRB member under large compressive strains could occur (Tsai [17]) at a section where the steel tube terminates, it is recommended that the following stability criterion be met for the connection details shown in Figure 2.18.a and Figure 2.18.b:

$$P_{e\_trans} = \frac{n^2 EI_{trans}}{L_{fb}^2} \geq P_{max} \quad (2.16)$$

where:  $P_{max}$  is given in Equation [2.14] and  $EI_{trans}$  is the flexural stiffness of the core member at a section near the end of the steel tube.

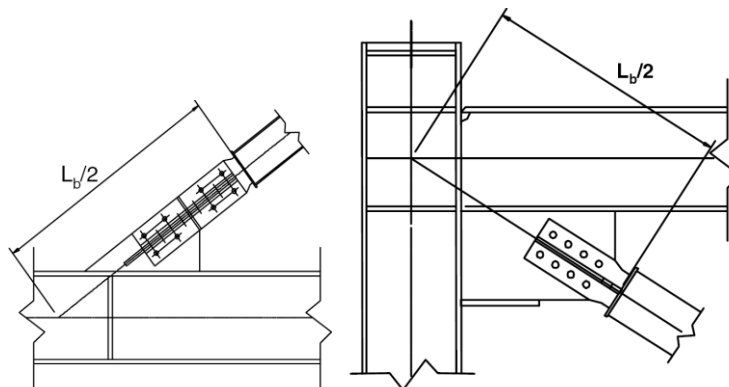


Figure 2.18: a) Splice plate details for single - cored BRB end connections; b) Double tee to gusset connection detail for double cored BRB end join [15]

#### **Design Code AISC2005 [17]**

According to AISC 2005 [17], the term Buckling-Restraining System describes those elements providing brace stability against overall buckling. This includes the casing as well as elements connecting the core. The adequacy of the buckling-restraining system must be demonstrated by testing.

According to AISC2005 [17], buckling-restrained braced frames (BRBF) are expected to withstand significant inelastic deformations when subjected to the

forces resulting from the motions of the design earthquake. The steel core shall be designed so as to resist the entire axial force in the brace.

The brace design axial strength,  $\Phi P_{y_{sc}}$  and the brace allowable axial strength,  $P_{y_{sc}}/\Omega$ , in tension and compression, according to the limit state of yielding, shall be determined as follows:

$$P_{y_{sc}} = F_{y_{sc}} A_{sc} \tag{2.17}$$

$$\Phi = 0.90 \text{ (LRFD) and } \Omega = 1.67 \text{ (ASD)}$$

where:

- $F_{y_{sc}}$  is the specified minimum yield stress of the steel core, or actual yield stress of the steel core as determined from a coupon test, (MPa)
- $A_{sc}$  is the net area of the steel core, (mm<sup>2</sup>)

Where required by these provisions, bracing connections and adjoining members shall be designed so as to resist the forces calculated based on the adjusted brace strength. The adjusted brace strength in compression shall be  $\beta \omega R_y P_{y_{sc}}$ . The adjusted brace strength in tension shall be  $\omega R_y P_{y_{sc}}$ .

Exception: The factor  $R_y$  needs not be applied if  $P_{y_{sc}}$  is established by using yield stress determined from a coupon test.

$$\beta = \frac{\omega F_{y_{sc}} A}{\omega F_{y_{sc}} A} = \frac{P_{max}}{T_{max}} \tag{2.18}$$

$$\omega = \frac{\omega F_{y_{sc}} A}{F_{y_{sc}} A} = \frac{T_{max}}{F_{y_{sc}} A} \tag{2.19}$$

where:

$P_{max}$  = maximum compression force, kips (N)

$T_{max}$  = maximum tension force within deformations corresponding to 200 percent of the design storey drift

$F_{y_{sc}}$  = measured yield strength of the steel core, MPa

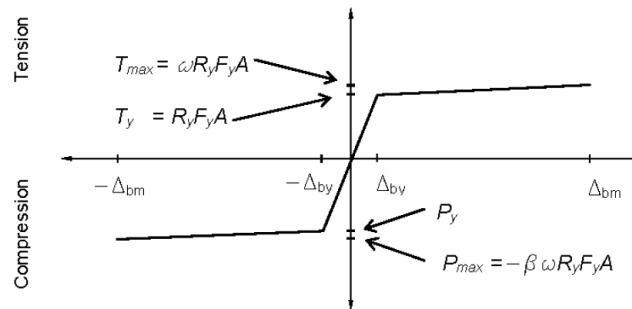


Figure 2.19 Diagram of the brace force displacement [18]

The Provisions are based on the use of brace designs qualified by testing. They are intended to ensure that braces be used only within their proven range of deformation capacity, and that yield and failure modes other than stable brace yielding be precluded at the maximum inelastic drifts corresponding to the design earthquake. These Provisions also offer information about:

- Bracing Members (Steel Core, Buckling-Restraining System, Testing, Bracing Connections)
- Special Requirements Related to Bracing Configuration
- Beams and Columns

## 2.3. Comparison with other removable passive hysteretic devices installed within the framed structure

### 2.3.1 INERD devices

Innovative dissipative (INERD) connections are used in seismic resistant braced steel frames for the connection of the braces to the adjacent members (columns or beams) [19]. Two types of INERD connections were developed:

a) Pin connections (Figure 2.20): they consist in two external eye-bars welded or bolted to the adjacent member (column or beam), two internal eye-bars welded to the brace and a pin running through the eye-bars. In this type of connection, the pin exhibits inelastic bending deformations and dissipates energy due to the fact that the eye-bars are placed at some distance between each other.

b) U-connections (Figure 2.21): the U-connections consist in one or two bent U-shaped thick plates that connect the brace to the adjacent member. Here again, energy dissipation takes place in the bent plate(s). The advantage of these connections is that, by appropriate sizing, inelastic deformations are limited within exactly predetermined zones, the pins or the U-plates, whereas the adjacent parts remain elastic. Consequently, braces are protected from buckling and damage is restricted in the pins or the U-plates. These are small parts that may be easily replaced if they are seriously deformed, after an unusually strong earthquake.

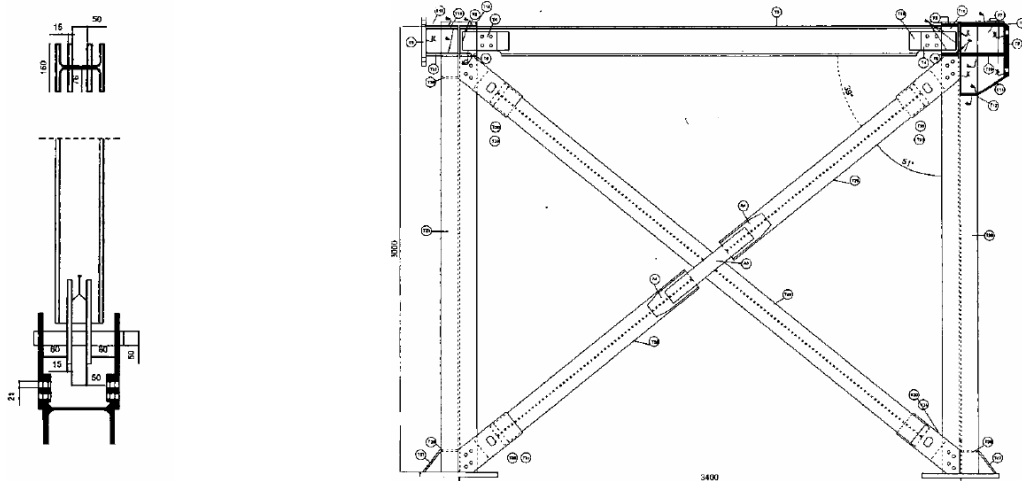


Figure 2.20 INERD pin connection in test frame [19]

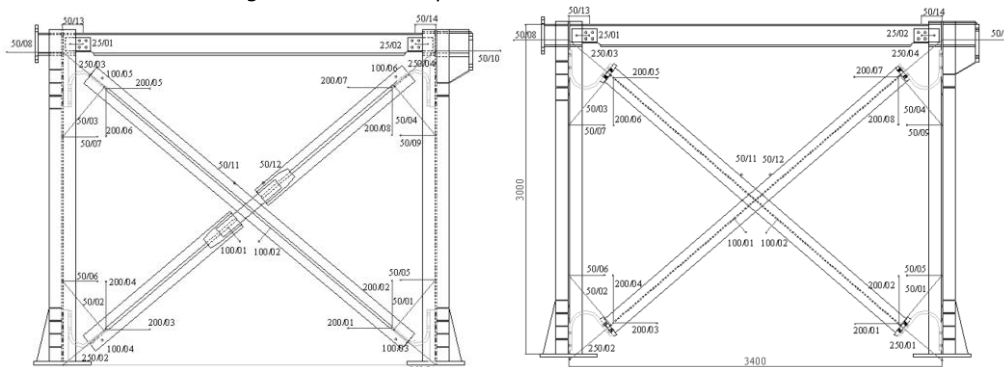
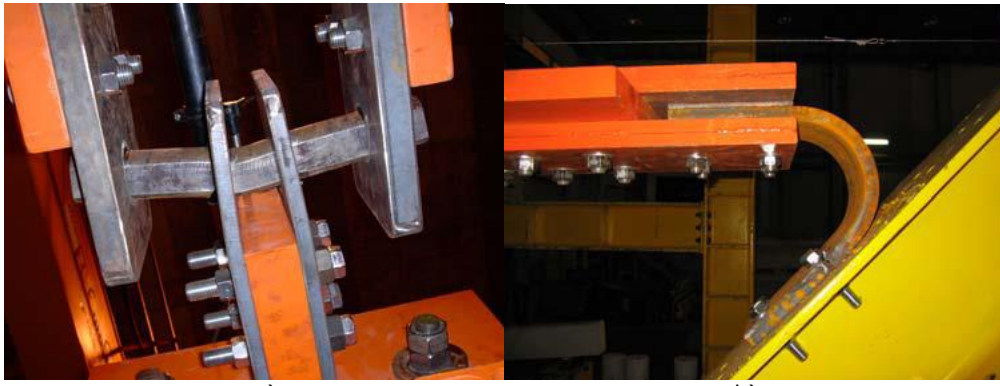


Figure 2.21 INERD U connection in test frame [19]



a) Pin device; b) U device [19]

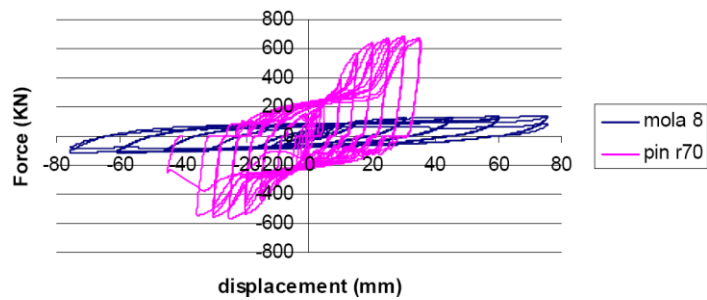


Figure 2.23 Comparisons U-device vs. Pin device [19]



Figure 2.24 Deformed pin connections after test [19]

### 2.3.2 EBF with removable link

Eccentrically braced frames with removable links connected to the beams using flush-end plate bolted connections are investigated as a practical way of implementing this design concept. High strength steel is used for members outside the links in order to enhance the global seismic performance of the structure, by constraining plastic deformations to removable links and reducing the permanent drifts of the structure [20].



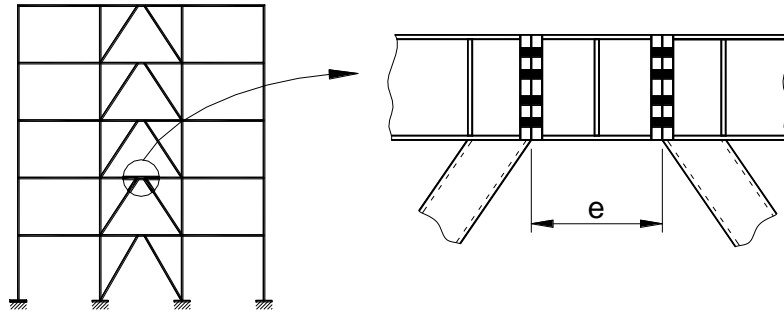


Figure 2.25 Bolted link concepts

Table 2.1 Yield and maximum forces evaluated for nominal and measured characteristics [20]

	specimen	$W_{pl}$ , cm <sup>3</sup>	$W_{plw}$ , cm <sup>3</sup>	$W_{pl}^*$ , cm <sup>3</sup>	$V_y$ , kN	$M_y$ , kNm	$1.6M_y/V_y$ , mm	$V_{max}$ , kN	$M_{max}$ , kNm
nominal	LH7, LL7	366.6	75.29	291.31	185.4	86.2	743	278.1	83.4
	LH6, LL6	366.6	75.29	291.31	185.4	86.2	743	278.1	69.5
	LH5, LL5	366.6	75.29	291.31	185.4	86.2	743	278.1	55.6
	LH4, LL4	366.6	75.29	291.31	185.4	86.2	743	278.1	41.7
measured	LH7, LL7	366.6	75.43	291.2	266.7	103.5	621	400.1	120.0
	LH6, LL6	366.6	75.43	291.2	266.7	103.5	621	400.1	100.0
	LH5, LL5	366.6	75.43	291.2	266.7	103.5	621	400.1	80.0
	LH4, LL4	366.6	75.43	291.2	266.7	103.5	621	400.1	60.0

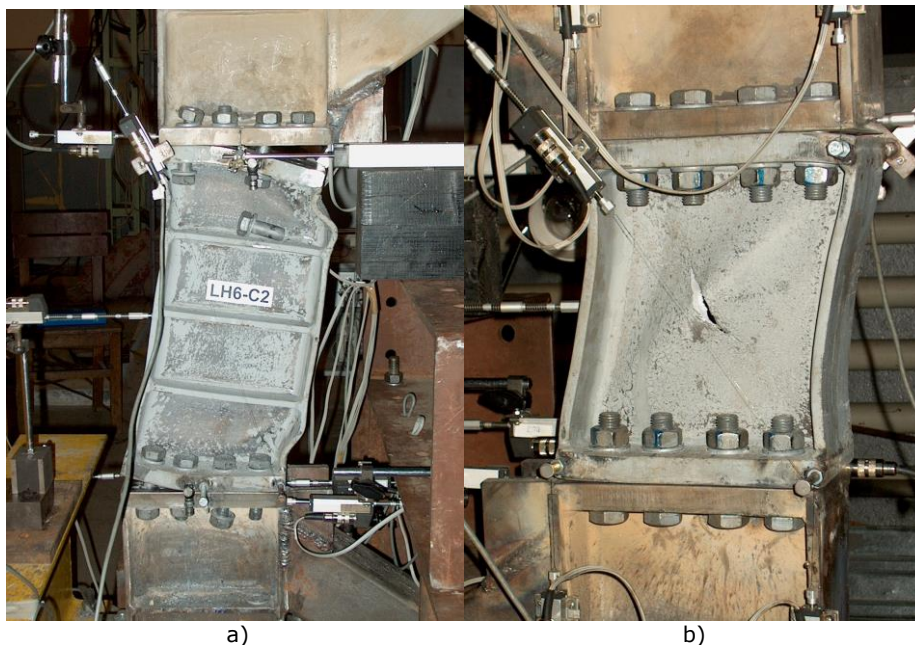


Figure 2.26 a) Failure by connection degradation at the LH6-c2 specimen plastic; b) web buckling at the LL4-c1 specimen [20]



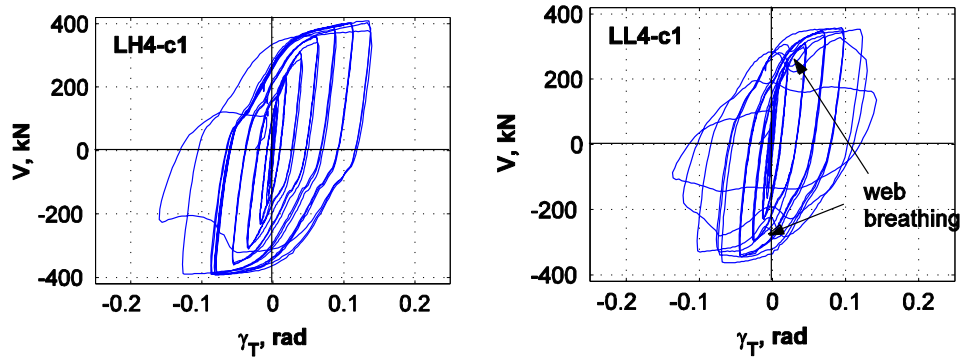
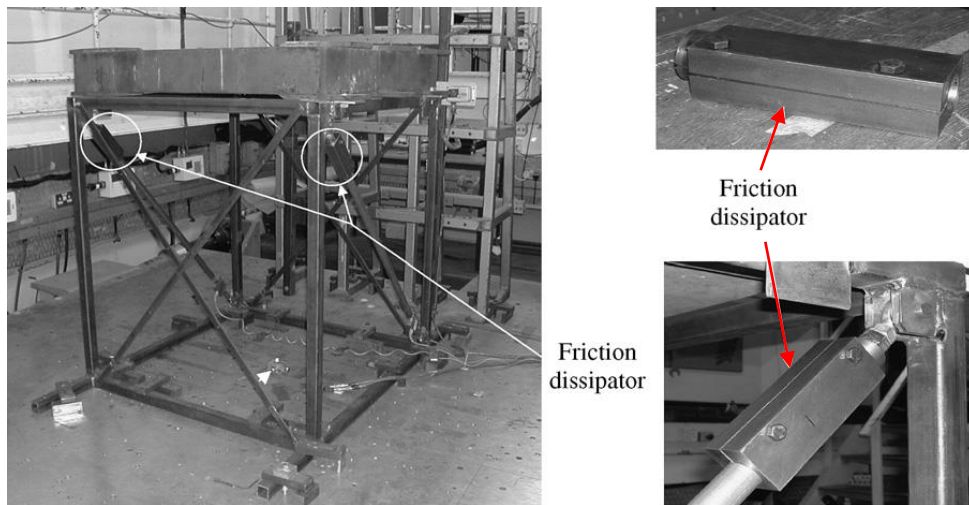
Figure 2.27 Force-total deformation relationships  $V$ - $\gamma_T$  for specimens LL4-c1 and LH4-c1

Figure 2.28 Test on full-scale frame with bolted links [21]

### **2.3.3 Hysteretic Dampers (CV+hysteretic dampers)**

This innovative system is based on a new algorithm intended to simulate the seismic response of N-story building frames that incorporate friction energy dissipators; there is considered a device per floor. The frames with the dissipative elements are described by 2D lumped masses models with two degrees of freedom per floor, namely the horizontal displacements of the main structure and of the dissipative elements. The proposed algorithm consists in a modification of the linear acceleration method. The main innovation consists in checking at each calculation instant the sliding or sticking condition at each floor, hence, the number of "active" degrees of freedom changes continuously, ranging between N (there is sticking condition at every dissipator) and 2N (there is sliding condition at every dissipator). Some results given by this algorithm are compared to the experimental results from ad-hoc testing and to the numerical results obtained with the ADINA software package. In both cases, the agreement is satisfactory while the proposed method is more computationally efficient [22].



Single-storey tested frame [22]

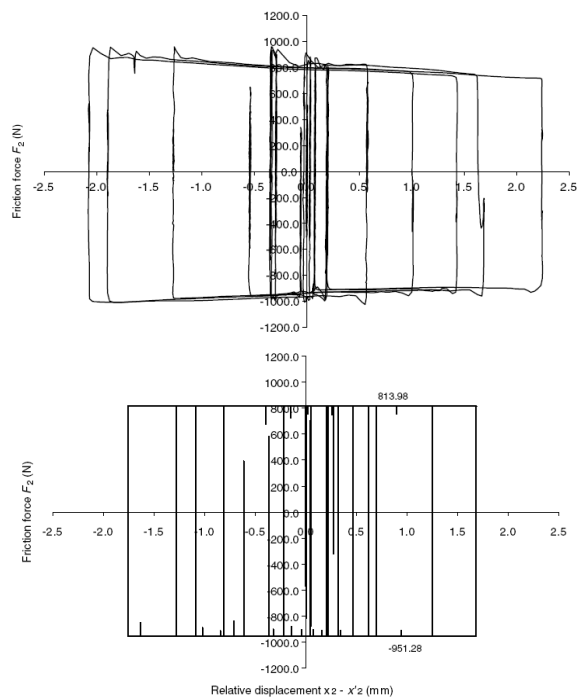


Figure 2.29 Comparison between numerical and experimental second floor hysteresis loops: (a) Second floor (test), (b) second floor (numerical) [22]

### **2.3.4 Shear walls of low yield steel (AISC2005 [17])**

Low yield point (LYP) steel shear walls can be used for steel panels. A series of experimental studies were carried out to examine the stiffness, strength and energy dissipation capacity of the LYP steel shear wall under cyclic load. The effect of width-to-thickness ratio of steel plate, the continuity of the shear wall, and the design of beam-to-column connections on the boundary frame were examined.

Good energy dissipation capacities were obtained for all the studied specimens. Excellent deformation capacities were obtained from both rigid frame–shear wall system and simple frame–shear wall system. The LYP steel shear wall is able to maintain stable up to 3–6% of the storey drift angle. A two-force strip model was also proposed in order to simulate the elastic and inelastic behavior of the shear wall system. Good correlations were found between the experimental and the analytical studies. Based on these research findings, suggestions are made for the design of LYP steel shear wall systems. An application of this system for seismic retrofitting of RC structures has been developed within the ILVA-IDEM project. In this project, shear panels have been applied for the seismic upgrading of an existing two-storey RC structure, which has been subjected to a cyclic push-over test [23].



Figure 2.30 Typical photographs showing specimen at the ultimate stage [23]

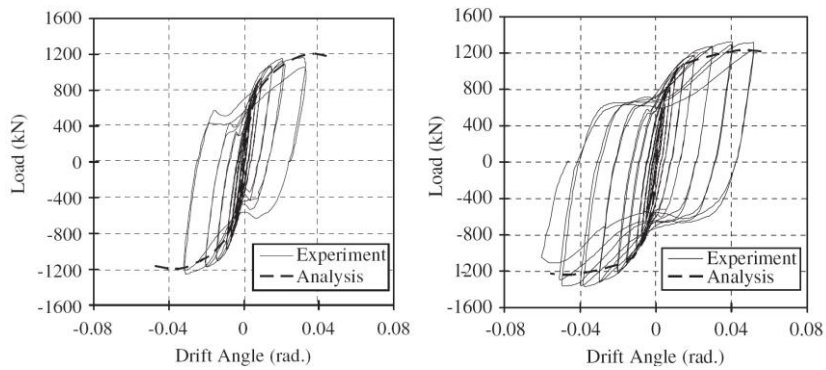


Figure 2.31 Hysteretic behavior of the specimens [23]



Figure 2.32 Global view of the structure retrofitted by means of: a) steel shear panels; b) aluminum shear panels [10]

**2.3.5 Self-centering devices**

Self-centering moment connections consist in post-tensioned steel beams, a reinforced concrete column, and a dissipative element placed only below the beam bottom flange for the simplicity of construction, the ease of replacement, and no interference with the composite slab. Two types of steel dissipative elements are proposed: one includes a reduced section plate restrained by two flat plates, and the other uses cross-shaped steel plates. Cyclic tests are conducted on three full-scale post-tensioned connection subassemblies and six dissipative elements. A finite element analysis is performed in order to investigate the cyclic performance and likelihood of fracture in critical regions within the dissipative element. Cyclic test results show that (1) the energy dissipation, the moment, and the flexural stiffness of the beam in positive bending are larger than those of the beam in negative bending, (2) the location of the compression toe at the end of the beam stabilizes at the junction between the beam flange and web after an inter-storey drift of 1.5%, in which the gap opening angles of the beams are similar on both bending directions, and (3) the shoulder radius equal to 2.5 times plate thickness results in a premature fracture along the shape transition of the reduced section plate. This study also develops an iterative analytical procedure for predicting un-symmetrical cyclic responses of post-tensioned connection subassemblies [24].

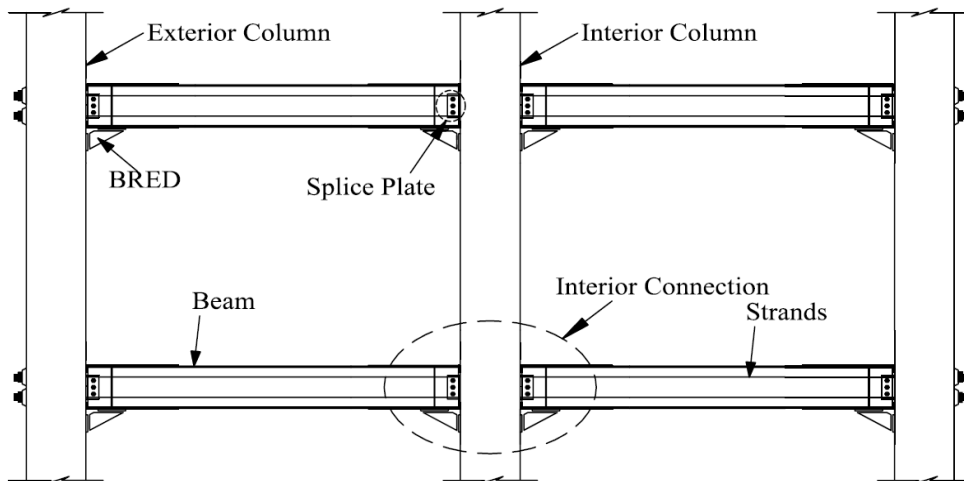


Figure 2.33 Post-tensioned RCS frame [24]

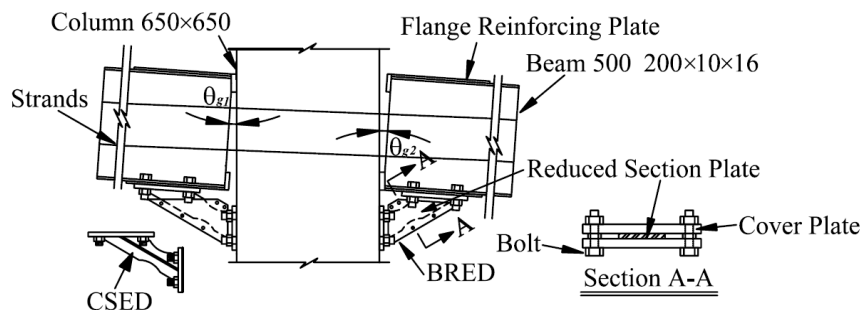


Figure 2.34 Connection details [24]

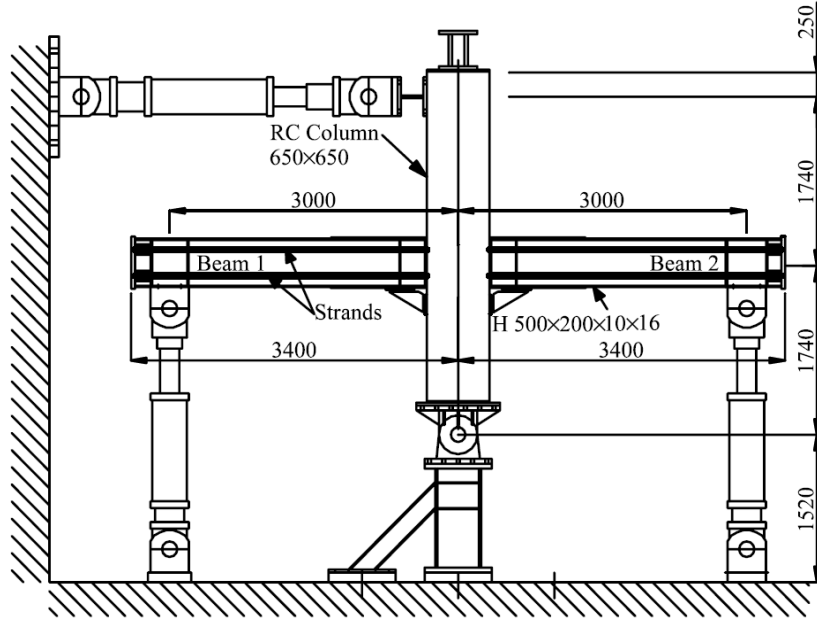


Figure 2.35 Test set-up [24]

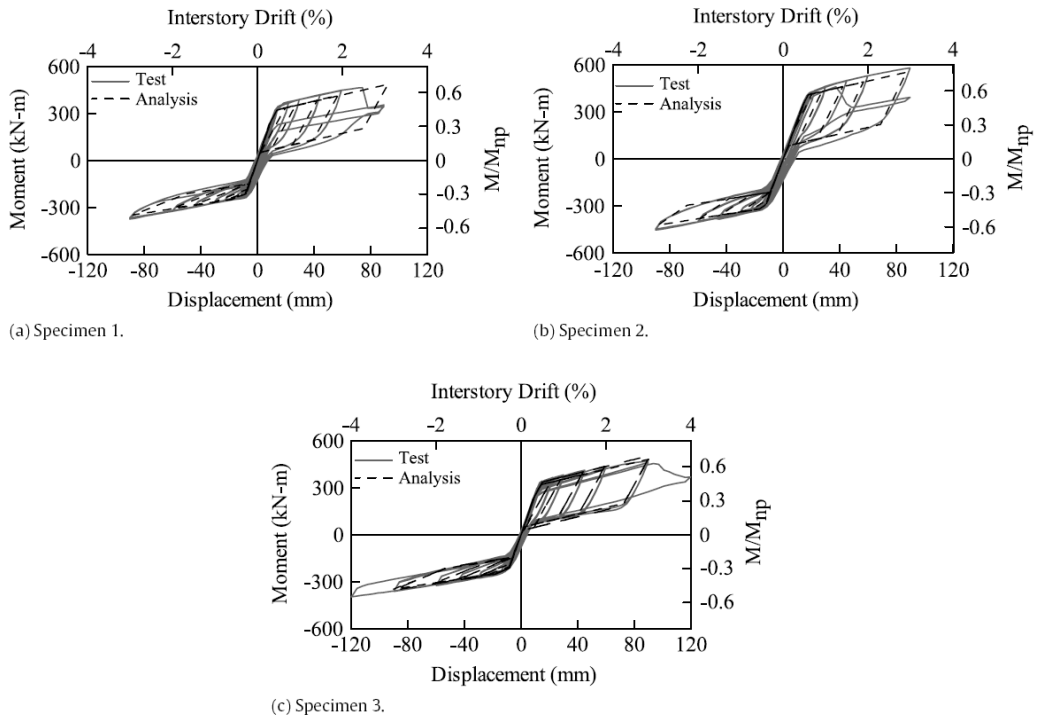


Figure 2.36 Beam moment versus drift relationship [24]



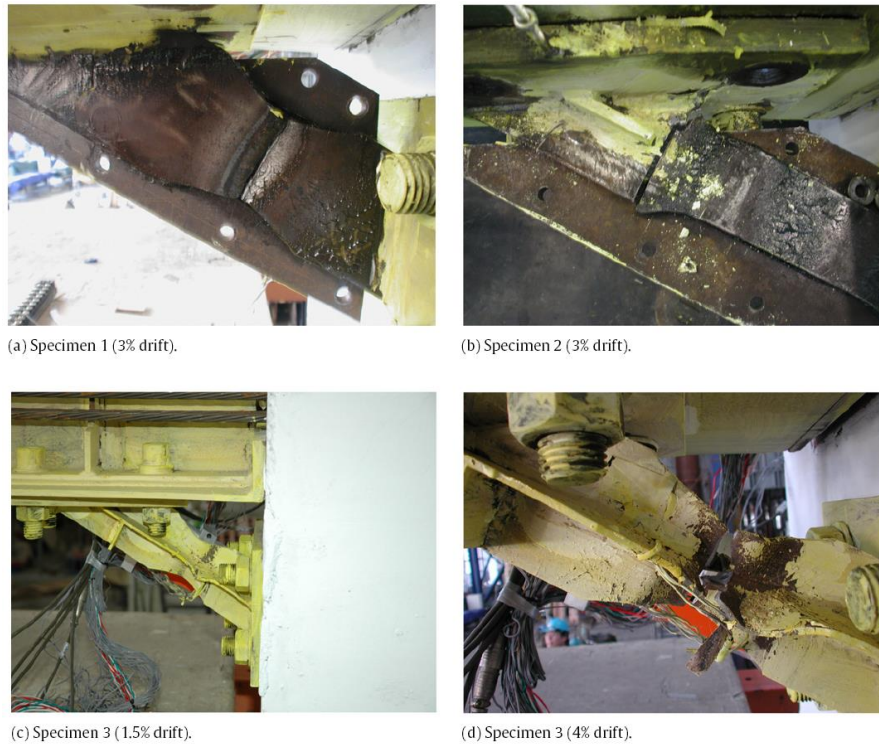


Figure 2.37 Specimen failure modes [24]

### 2.3.6 Shape Memory Alloy Systems

Shape memory alloy (SMA) is a new functional material which has found increasing applications in many areas. Recently, research efforts have been extended to using SMA for the control of civil structures. In the literature, there is a specific type of application of superelastic SMA wires for structural control purposes different from the aforementioned examples. This application uses the shape restoration property of superelastic SMA wires. For example, Sakai researched self-restoration of a concrete beam using superelastic SMA wires. The experimental results revealed that the mortar beam with SMA wires recovers almost completely after suffering an extremely large crack [25].

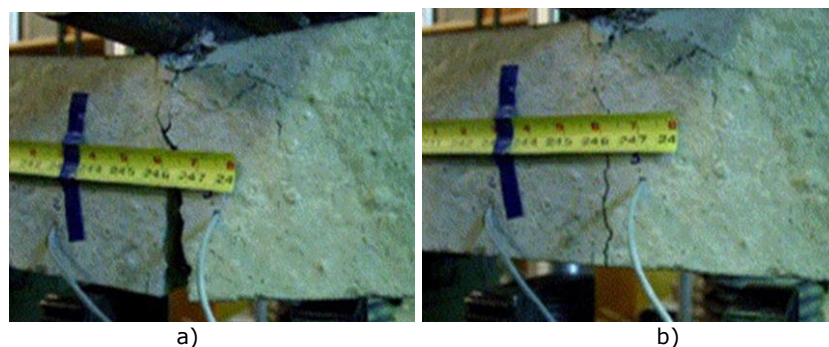


Figure 2.38 A large crack during a loading test. The crack closes after the loading test [25]

### 2.4. The advantages of using a BRBS

Compared to either moment frames or braced frames, BRB frames BRBF offer the following advantages [26]:

1. Compared to moment frames, BRBFs exhibit highly-elastic lateral stiffness at low-level seismic input motions, making it easy to satisfy the code drift requirements;

2. BRBFs eliminate the undesirable buckling of conventional CBFs by yielding under both tension and compression, thereby providing larger and stable energy dissipation at high-level seismic input motions;

3. BRBFs provide economical installation through a bolted or pinned connection to gusset plates, which eliminates costly field welding and inspection;

4. Braces act as a replaceable structural fuse, which minimizes the damage to other elements and it is possible to replace damaged braces after major seismic events;

5. BRBFs offer design flexibility because both the strength and stiffness of the braces can easily be tuned. Furthermore, it is easy to model the cyclic behavior of BRBs for inelastic analysis;

6. For seismic rehabilitation, BRBFs can be more advantageous than the conventional bracing system because the capacity design provisions for the latter system may require expensive foundation and floor diaphragm strengthening.

According to AISC 2005 [17], BRBF's display more ductility and energy absorption than CBF because of the overall brace buckling, and its associated strength degradation is precluded at forces and deformations corresponding to the design story drift.

In contrast with conventional bracing systems, the Unbonded Brace [27]:

1. Does not buckle;

2. Behaves symmetrically in tension and compression;

3. Very predictable tension and compression yield and post-yield behavior:

- No gusset plate yielding and buckling (CBFs);

- No cumulative damage to gravity members (EBFs);

- Allows reliable capacity design of connections, adjacent elements

and foundations;

4. Easily modeled and amenable to analysis;

5. Avoids substantial field welding (EBFs);

6. Allows more compact brace sizes, longer braces possible;

7. Braces replaceable, if necessary.

By contrast, buckling-restrained braces (BRBs) do not exhibit any of the unfavorable behavior characteristics of conventional braces [28]. Buckling-restrained braces have full, balanced hysteretic behavior, with compression yielding similar to tension yielding behavior. According to Sabelli [8], they achieve this through the decoupling of the stress-resisting and flexural-buckling-resisting aspects of compression strength. Axial stresses are resisted by a shaped steel core. Buckling resistance is provided to that core by a sleeve, which may be made of steel, concrete, composite, or other construction. Because the steel core is restrained from buckling, it develops almost uniform axial strains across the section. The plastic hinges associated with buckling do not form in properly designed and detailed BRBs. This also permits BRB's to be designed as to develop very high compression strength; as there is no reduction in the available material strength due to instability, the effective length of the core can be considered zero.

The following are among BRBF's desirable characteristics [28]:

1. High response modification factor, "R" (q in European format);

2. Braces are able to yield in compression;
3. Well-defined energy-dissipating elements (braces); limited damage to other structural elements;
4. Stable, fairly symmetric hysteretic loops;
5. The geometric properties (i.e., stiffness and area) of the load-resisting core plate increase only slightly for long slender braces;
6. Bolted end connections;
7. A brace element can be easily replaced after exhausting its service life.

According to (Uang and Nakashima 2004), BRB's offer the following advantages [29]:

- Simple modeling of their cyclic behavior for inelastic analysis;
- Ease of incorporating them into the structural system by means of a bolted or pinned connection to gusset plates;
- Stable hysteretic behavior without buckling with high energy dissipation capacity;
- Limited sensitivity to environmental condition changes;
- Design flexibility in the selection of both stiffness and strength of the whole structural system of a building;
- Ease of replacement when damaged after major seismic event;

In summary, BRB's can be used for [29]:

- frame buildings:
  - Reduction of structural response under seismic actions;
  - Reduction of inter-storey drift;
  - Damage reduction of the structural elements due to energy dissipation.
- masonry buildings
  - Reduction of structural response under seismic actions;
  - Increase of in-structure damping and energy dissipation.
- bridge structures
  - Reduction of top-pier displacement;
  - Reduction of damage in structural elements due to energy dissipation.

## **2.5. Research Development regarding Buckling Restrained Brace Systems and their use in Seismic Resistant Building Frames [11]**

A variety of BRB's systems, including various materials, geometries and technologies have been proposed and studied for more than 30 years. Variations of BRB's were subsequently developed in several other countries. A summary state of the art review of selected studies, following the research development in different countries is presented below.

### **Japan**

The concept of BRBs was first developed in two forms in Japan; to avoid buckling, the yielding steel element can be either sandwiched between precast concrete panels or encased in concrete-filled steel sections.



### Steel Core Sandwiched between Concrete Panels

The pioneering work on BRB's was started by Wakabayashi [30] in 1973 by developing a system in which braces made of steel flat plates were sandwiched between a pair of precast reinforced concrete panels. The research included the following: (1) pull-out tests in order to explore the methods of debonding, (2) compression tests of plates sandwiched between precast panels in order to examine the required stiffness and strength for the panels, (3) sub-assembly tests to examine the effectiveness of end connection details and (4) two-storey frame tests for system verification.

In the pull-out tests, epoxy resin, silicon resin, vinyl tapes, etc. were experimented as the debonding material. A total of 11 specimens were tested, and it was concluded that a layer of epoxy resin covered by silicon resin was most effective as the debonding material in terms of debonding effect, constructability and durability. In the compression tests, in which 21 specimens were tested, various reinforcing details were adopted for the precast concrete panels, and a special emphasis was placed on the reinforcement along the edges of the panels.

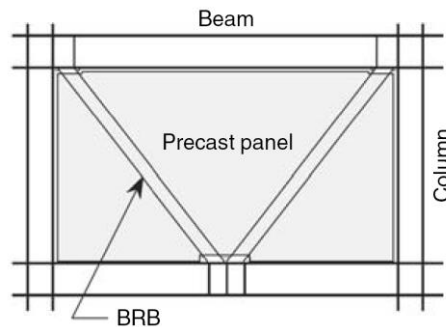


Figure 2.39 Buckling Restrained Braces sandwiched between precast concrete panels [30]

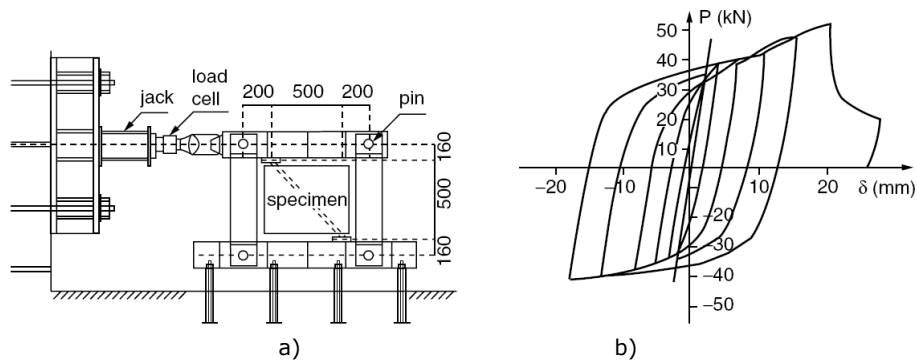


Figure 2.40 Sub-assembly test of BRB sandwiched between precast concrete panels a) Test setup; b) hysteretic behavior [30]

Inadequate reinforcement at these locations was found to cause damage earlier in the loading cycles because of the transverse forces that were produced by the out-of-plane deflection of braces. In the sub-assembly test, a pair of flat plates, arranged in either a diagonal or chevron pattern, was connected to a pin-connected steel frame and encased by precast concrete panels; the specimens were about 1/5 in scale (a). An example of hysteretic behavior is shown in (Figure 2.41b). From the

strain gage measurements it was confirmed that the embedded flat plates were uniformly strained. At higher deformation levels, the strength of the brace in compression is higher than that in tension. In the system verification tests, 2 two-storey and 2 two-bay frames of about a half scale, one with braces arranged diagonally and the other with braces arranged in a chevron pattern, were cyclically tested (Figure 2.41.a). Although the compressive strength of an individual brace is higher than the tensile strength at higher deformation levels, Figure 2.41.b shows that a symmetric response would result when braces are placed in pairs in each storey.

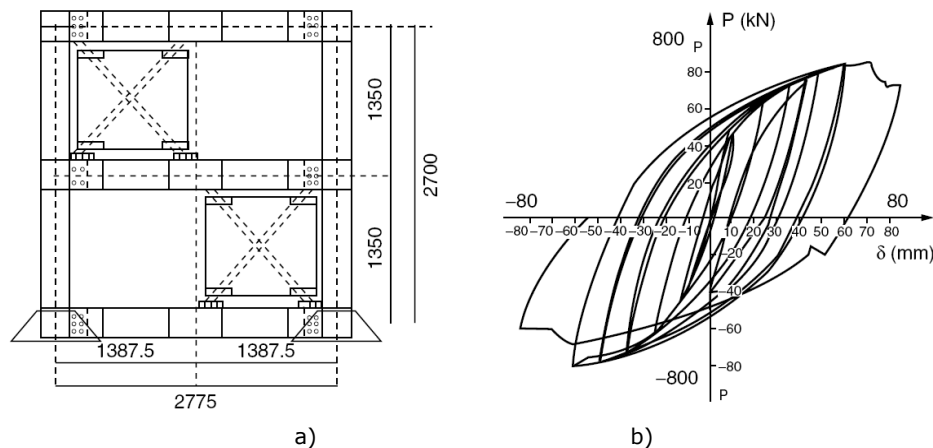


Figure 2.41 System test of BRB Subassemblies test of BRB sandwiched between precast concrete panels a) Test setup; b) hysteretic behavior [30]

Inoue and Sawaisumi extended in 1992 the work of Wakabayashi. On the basis of both analytical and experimental studies that directly measured the interaction forces between the brace and the panels, the researchers developed both stiffness and strength requirements for the design of precast concrete panels.

### Steel Core Encased in Concrete-Filled Steel Shape

Extending the concept of Wakabayashi [30], various developments on BRB's with a steel core confined by a steel casing were made in Japan in the 1980's to 1990's. Fujimoto in 1988 [31] studied the behavior of a type of BRB with a steel core encased in a steel casing filled with mortar (the end connection is shown in Figure 2.42.a). Tests were conducted with different steel casing sizes, and design criteria for both stiffness and strength of the casing were developed.

Nagao and Takahashi [32] developed in 1990 a BRB composed of a wide flange section encased in a reinforced concrete member. The end connection detail is shown in Figure 2.42.b, in which the wide flange section in the projected portion is stiffened by welded plates. The experimental study evaluated the reinforcing, stiffness and strength requirements of the concrete casing.

A study on the global buckling behavior of BRBs, with either square or rectangular HSS was conducted by Watanabe in 1988 [30]. A total of five specimens were tested; see Table 2.2 for the  $P_e/P_y$  ratios. The last two specimens were designed so as to have the ratio of  $P_e/P_y$  below 1. Each specimen was loaded cyclically up to 2% storey drift. Test results showed that specimen 4 and 5 buckled globally in compression, while the first three specimens exhibited stable and symmetric hysteresis under both tension and compression. This study confirmed

that Equation ( $P_e/P_y > 1$ ) needed to be satisfied in order to avoid global buckling. Although specimen 3, with a  $P_e/P_y$  ratio of 1.03, satisfied Equation ( $P_e/P_y > 1$ ), Watanabe showed from a numerical study that global buckling could still occur if the initial geometric imperfection is large. Watanabe suggested that for practical applications the  $P_e/P_y$  ratio be at least equal to 1.5.

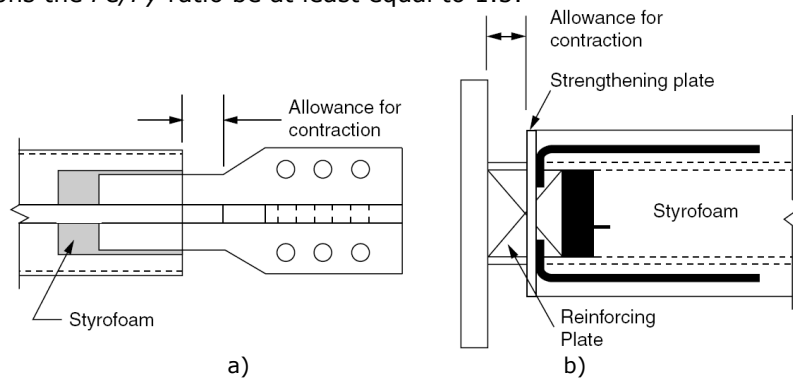


Figure 2.42 BRB end details [31] and [32]

Table 2.2  $P_e/P_y$  Ratios (by Watanabe et al., 1988) [30]

Specimen No.	$P_e/P_y$
1	3.53
2	1.39
3	1.03
4	0.72
5	0.55

Iwata et al. (2000) [33] reviewed the cyclic performance of four commercially available BRB's in Japan. Figure 2.43 shows the cross section of these four products. Note that an unbonding material was not used in either Type 2 or 4 specimens [30]. The buckling-restraining mechanism of specimen 3 was composed of two channels and two plates connected with high-strength bolts. Soft rubber sheets (1-mm thick) were provided between the core plate and the buckling-restraining mechanism for specimens 1 and 3 [11].

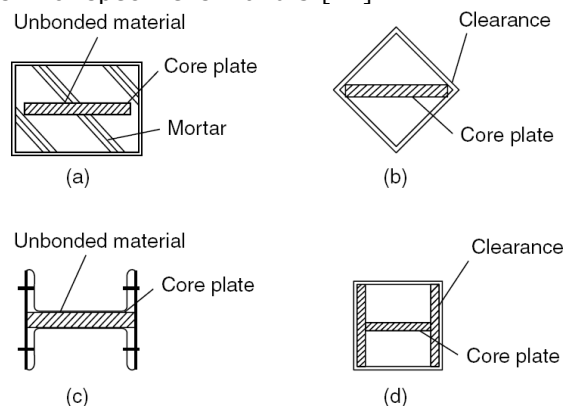


Figure 2.43 Section of four test specimens, a) Type 1; b) type 2; c) type 3; d) type 4 [33]

Figure 2.43 shows the cyclic responses of all test specimens. Note that specimens 2 and 4 did not perform well, probably because no mortar was used in order to limit local buckling. The restraining effect of specimen 3 was not as effective as that provided by the mortar and steel tube in specimen 1. As the gap between the core plate and channels grew larger at high-deformation levels, the high-strength bolts in specimen 3 eventually failed in shear. Specimen 1, which sustained 14 cycles at 3% strain, outperformed the other three braces. The failure mode was associated with mortar crushing and local buckling of the core plate.

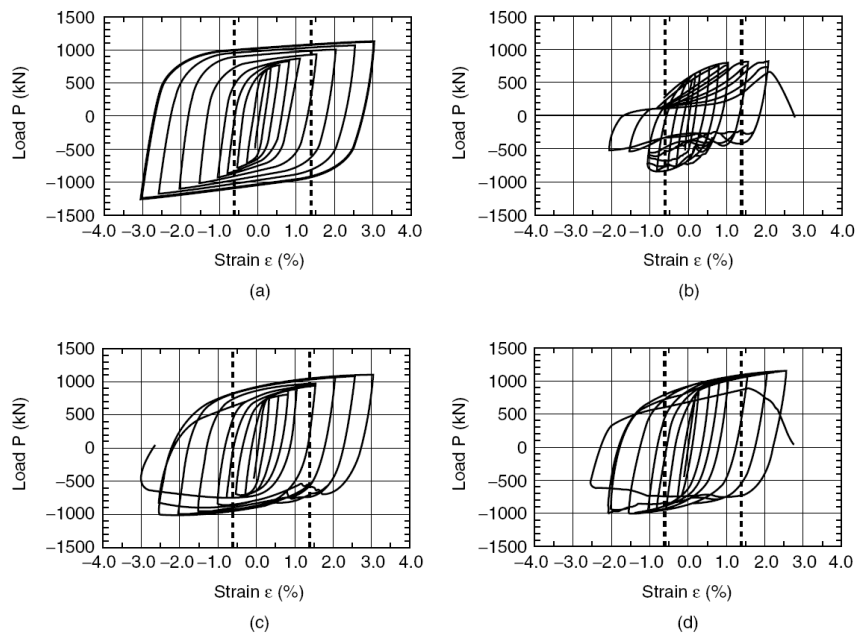


Figure 2.44 Cyclic response of four test specimen a) Type 1; b) type 2; c) type 3; d) type 4 [33]

In Japan, low-yield steels were introduced in the early 1990's and have been used as materials for hysteretic dampers; the yield strengths of such steels are about 1/3 to 1/2 those of commonly used mild steels. Research and implementation of BRB's made of low-yield steels have also been made [11].

### **United States [11]**

Three large-scale unbonded braces were tested at the University of Berkeley, California, to support the design and construction of the first building that utilized such BRBs in the United States (Clark, 1999 [3]). The first two specimens had a rectangular yielding cross section and the third specimen had a cruciform cross section. Japanese Industrial Standard Grade SM490A, which is equivalent to A572 Grade 50 steel, was used for the core plate. The measured yield and tensile strengths were 60.7 and 79.2 ksi, respectively. (Most projects that use Unbonded Braces in the United States specify either SN400B or SN490B steel for a better control of the upper limit of the yield strength. Low-yield strength steel has also been used.) In addition to testing the specimens with the SAC loading protocols (Clark 1997 [34]) or a simulated earthquake displacement record, constant-

amplitude low-cycle fatigue tests were also conducted. The target storey drift was 3%; the corresponding brace strain was approximately 2%.

Typical response of the braces is shown in Figure 2.45. Although bolt slip is evident from the sudden drops in the load of specimen 3, all specimens exhibited stable hysteresis. After specimen 2 was tested with the SAC loading history (Figure 2.45.a), a low-cycle fatigue test with an axial strain of 2% followed. The specimen was able to sustain 17 cycles before the core plate fractured. Several analyses including stability against global buckling, buckling of the inner core in higher modes and plastic torsional buckling of the inner core were also conducted by Black, 2002 [35].

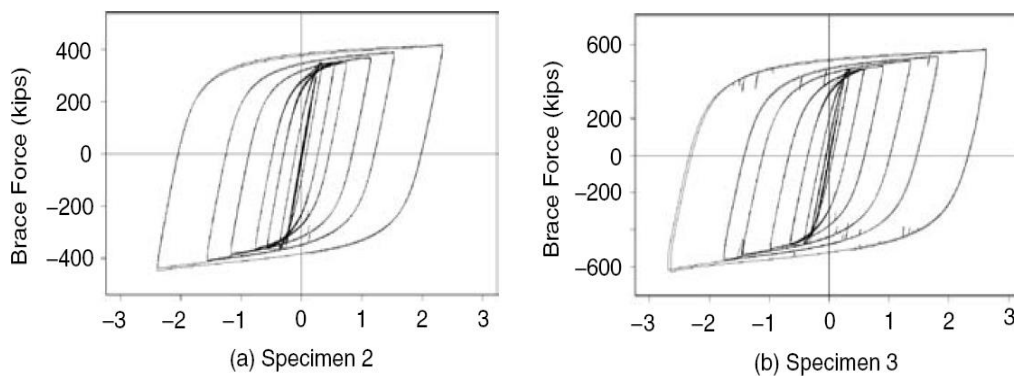


Figure 2.45 Cyclic response of Unbonded Braces s) Specimen 2; b) specimen 3 [3]

Higgins and Newell (2002) [36] studied a type of BRB that uses a steel pipe filled with non-cohesive media as the buckling-restraint mechanism; graded aggregates are used as the non-cohesive media. Yielding was confined to the central portion of the A36 steel core.

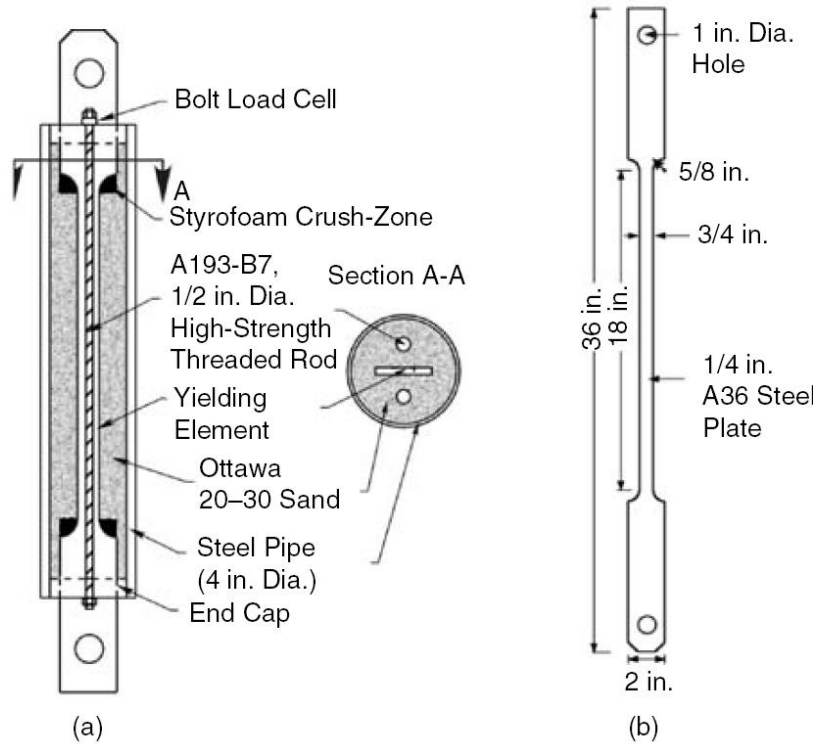


Figure 2.46 Composite confined hysteretic damper. a) Test specimen; b) steel core [36]

The non-cohesive media was ASTM 20-30 Ottawa Sand with 97% being retained between the numbers 20 and 30 sieve sizes. Normal force was applied to the sand with steel end caps and 1/2 in. diameter high-strength threaded rods. The observed hysteretic response under reversed cyclic loading shows stable and reliable energy dissipation to approximately 2% strain). The dampers also exhibit a small amount of friction damping (as seen in the material elastic range) that may be beneficial for wind response mitigation. An examination of the deformed configuration along the length of the steel core after testing indicates the plate buckled primarily in the 18th mode, indicating excellent confinement provided by the non-cohesive materials.

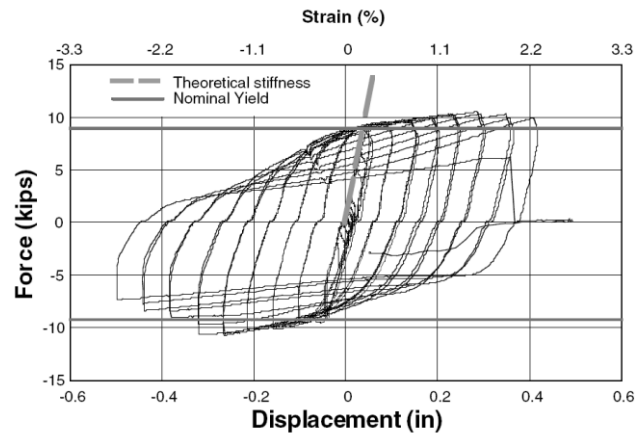


Figure 2.47 Hysteresis response of composite confined hysteretic damper [36]

At least three technical solutions BRBs have been or are being developed in the United States. These BRB's feature a steel core encased in a concrete-filled steel HSS.

The first study uses flat or cruciform steel core of A572 Grade 50 and A36 steel with bolted end splice connections. In order to facilitate erection, holes on the gusset plate and brace are oversized; faying surfaces of the gusset and connection plates were also sandblasted so as to reduce the number of high-strength bolts, and hence the length of gusset connection. Satisfactory performance has been showed by both uniaxial testing (Staker and Reaveley, 2002 [37]) and subassembly testing (Merritt et al., 2003 [38]).

The second study uses a steel core of A36 material and a pin-and-collar assembly at each end of the brace (a). The use of a pin connection at the gusset plate isolates the brace from any moment or shear that could be transmitted as a result of frame drift. Also by directly connecting the brace to the gusset by using a pin, the overall connection length is reduced, resulting in a long yielding core that reduces the axial strain. The pin also reduces the number of pieces being connected. The collar assembly adds to the overall stability of the brace by preventing out-of-plane buckling of the core section extending beyond the confining shell. If a collar were not in place, the section of the core that extends beyond the confining HSS can buckle and rotate. The use of pin and collar assembly also allows the use of ganging multiple braces together to make large capacity braces (b) [11].

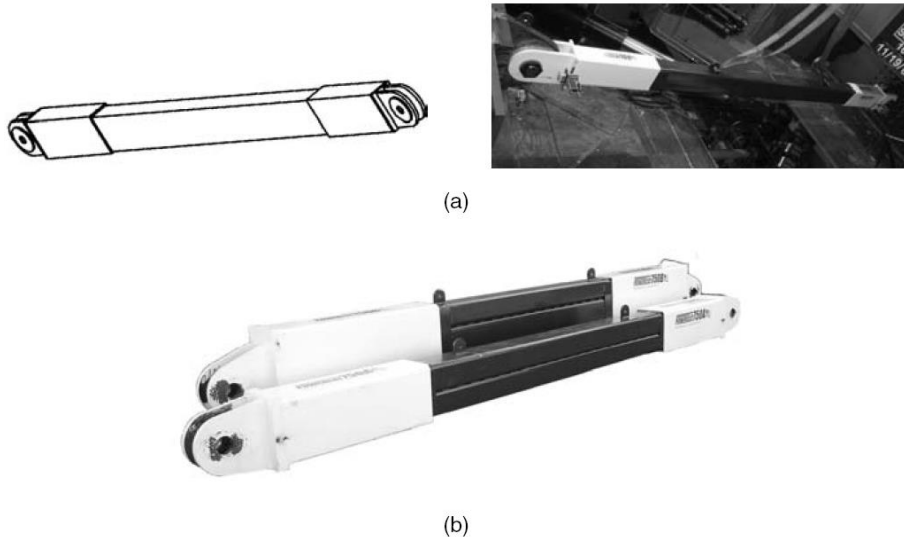


Figure 2.48 Star Seismic buckling – restrained brace, a) Single tube configuration; b) multitube configuration [11]

The third study uses a prismatic steel core along the entire length of the brace; each end is reinforced with welded stiffeners for the bolted splice connection with oversized holes for ease of erection. Figure 2.49.a shows the end details of the brace. Uniaxial testing (Merritt et al., 2003 [39]) has also been conducted in order to verify the cyclic performance (Figure 2.49.b) [11].

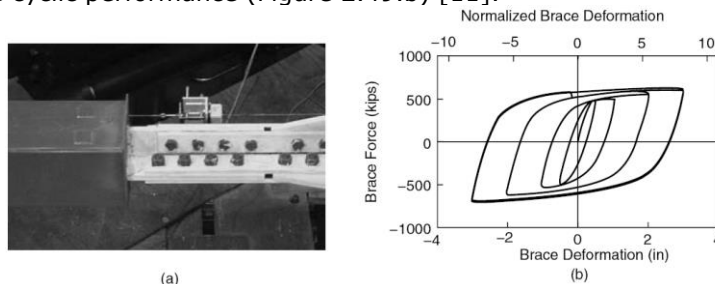


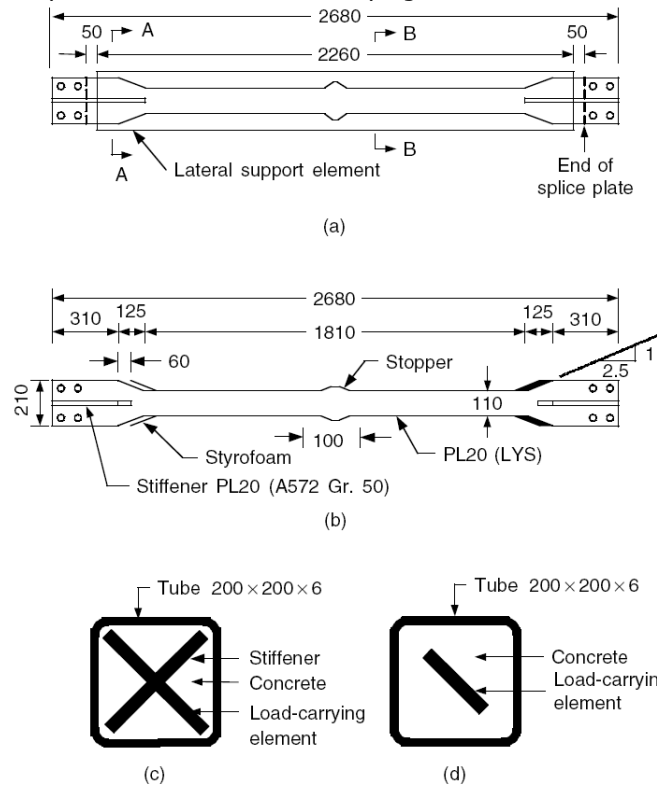
Figure 2.49 End details and typical hysteresis response. a) End details; b) hysteresis response [11]

### **Taiwan [11]**

Chen 2001 [40] studied the cyclic behavior of a type of BRB with low-yield strength steel (nominal  $F_y = 14.5$  ksi or 100 MPa). The brace, called buckling-inhibiting brace (BIB), used a concrete-filled tube to confine the steel plate (Figure 2.50). A layer of silicon grease was applied to the surface of the steel plate before the concrete was cast, in order to reduce the bonding force. Thus, very little space was provided for the load-carrying steel plate to expand under compression. The low-yield steel did not have a well-defined yield plateau, but the ultimate strain was very high (>50%). Note that low-yield steel would result in a reduced yield deformation, making the brace start yield at a much smaller drift level. Figure 2.50.b also shows a stopper at the center of the load-carrying element that was provided to prevent the buckling restrained system from slipping down. Figure 2.51



shows the typical response of this type of BRB. Note that the maximum compressive strength was much higher than the maximum tensile strength. As a result, Chen suggested that this type of bracing be used in a diagonal configuration, not V or inverted-V configuration. Chen also investigated the steel-only BRB's with built-up steel sections as the buckling-restraining mechanism. Figure 2.52 shows one example with low-yield steel as the load carrying steel core.



Unit = mm

Figure 2.50 Details of buckling inhibiting brace a) Overall view; b) load carrying element; c) A-A section; d) B-B section from [40]

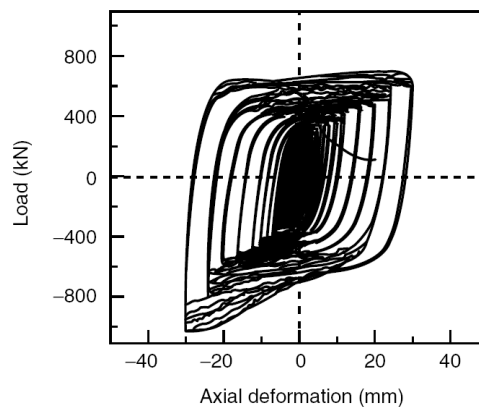


Figure 2.51 Typical response of buckling – inhibiting brace [41]

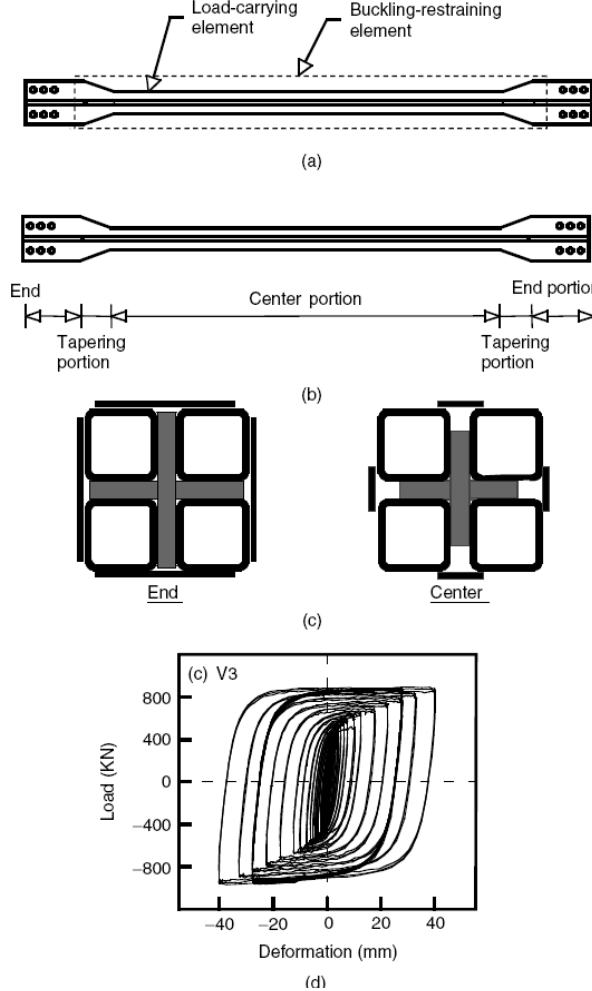


Figure 2.52 Steel – only buckling inhibiting brace: a) Components; b) load – carrying core steel; c) cross sections; d) hysteresis response

Tsai and Lai (2002) [16] studied the effect of the unbonding material on the cyclic response of BRB's. A total of 10 identical braces were tested, the only difference being the unbonding materials used. Figure 2.53 shows the geometry of the test specimens. The A36 steel yielding elements were cruciform in cross section; the measured strength was 50 ksi.

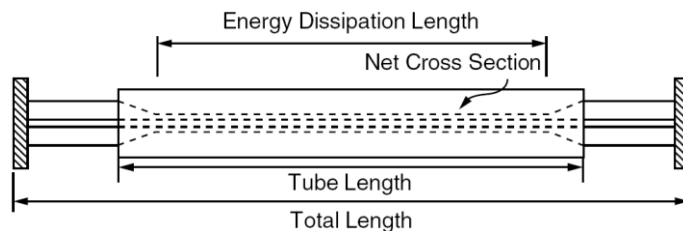


Figure 2.53 Geometry of buckling – restrained brace test specimens [16]

A typical hysteresis response is shown in Figure 2.54.a. Defining the axial load difference as  $\Gamma = (C_{max} - T_{max})/T_{max}$ , where  $C_{max}$  and  $T_{max}$  are the maximum compressive and tensile brace strengths at a given axial deformation level, the test results of all specimens are shown in Figure 2.54.b. The figure shows that the silicone rubber sheet produces the least axial load difference. Note that the hysteresis behavior shown in Figure 2.54.a was asymmetrical, with the compressive cycles showing higher force levels. Assuming that the Poisson ratio is equal to 0.5 in the inelastic range, the volume of the yielding steel segment remains constant.

$$A_0 L_0 = AL \tag{2.20}$$

where:

- $A_0$  and  $L_0$  refer to the original area and length
- $A$  and  $L$  refer to area and length where the brace is in either tension or compression.

It can be shown that the axial strain is:

$$\epsilon = 1 - \frac{L_0}{L} = 1 - \frac{A}{A_0} \tag{2.21}$$

Therefore,

$$A = A_0(1 - \epsilon) \tag{2.22}$$

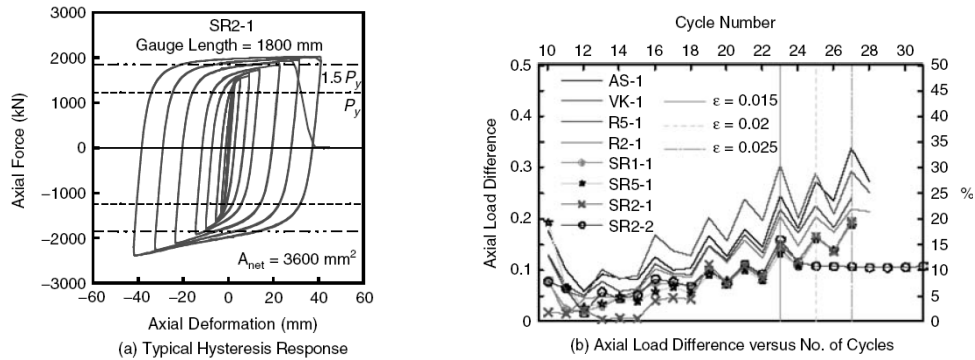


Figure 2.54 Buckling restrained brace effect of unbonding materials on axial load difference [16]

Table 2.3 Test Specimens [16]

Specimen	Unbonding Material	Thickness (mm)	Loading History
AS-1	Asphalt paint	NA	Standard
VF-1	Vinyl sheet + foaming tape	2	Standard
VK-1	Vinyl sheet + kraft tape	2	Standard
R2-1	Rubber sheet	2	Standard
R5-1	Rubber sheet	5	Standard
SR1-1	Silicone rubber sheet	1	Standard
SR2-1	Silicone rubber sheet	2	Standard
SR2-2	Silicone rubber sheet	2	Low-cycle fatigue
SR2-3	Silicone rubber sheet	2	Near-fault
SR5-1	Silicone rubber sheet	5	Standard

The ratio between compressive and tensile brace forces for a given (absolute) strain level is (Tsai and Lai, 2002):

$$\Gamma = \frac{C_{max} - T_{max}}{T_{max}} = \frac{A_c - A_t}{A_t} = \frac{A_0(1 - \varepsilon) - A_0(1 - \varepsilon)}{A_0(1 - \varepsilon)} = \frac{2e}{1 - \varepsilon} \approx 2e \quad (2.23)$$

The above equation shows that  $\Gamma$  is about 4% for  $\varepsilon = 2\%$ . But the test results in Figure 2.55.b shows much higher  $\Gamma$  values. Other than Poisson's effect, factors such as the friction between the steel core yielding element and mortar also contribute to the higher brace strength in compression cycles.

The most common applications of BRB's require two sets of bolts and eight splice plates at each brace-to-gusset connection. To reduce the size of the connections and to improve the constructability in the field, double-tube BRB's have been developed and extensively tested by Tsai and Lai (2002) [16]. The details of the double-tube BRB are shown in Figure 2.55.a. Each brace is composed of two identical parts. Each part comprises a steel core, which is either a plate or a structural tee, encased in a rectangular steel tube. Both ends of the steel core are tee-shaped, thus each part of the brace can be conveniently connected in the field to the gusset in the same manner as the conventional double-T brace is connected to gusset plate connections (Figure 2.55.b). After the two parts are installed, tab plates (see Figure 2.55.a) are then used in order to connect the two parts together. In addition to facilitating field installation, a reduced gusset connection length for improved stability in the connection region is another advantage of this type of brace. A typical response of the double-tube BRB is shown in Figure 2.55.c and Figure 2.55.d.

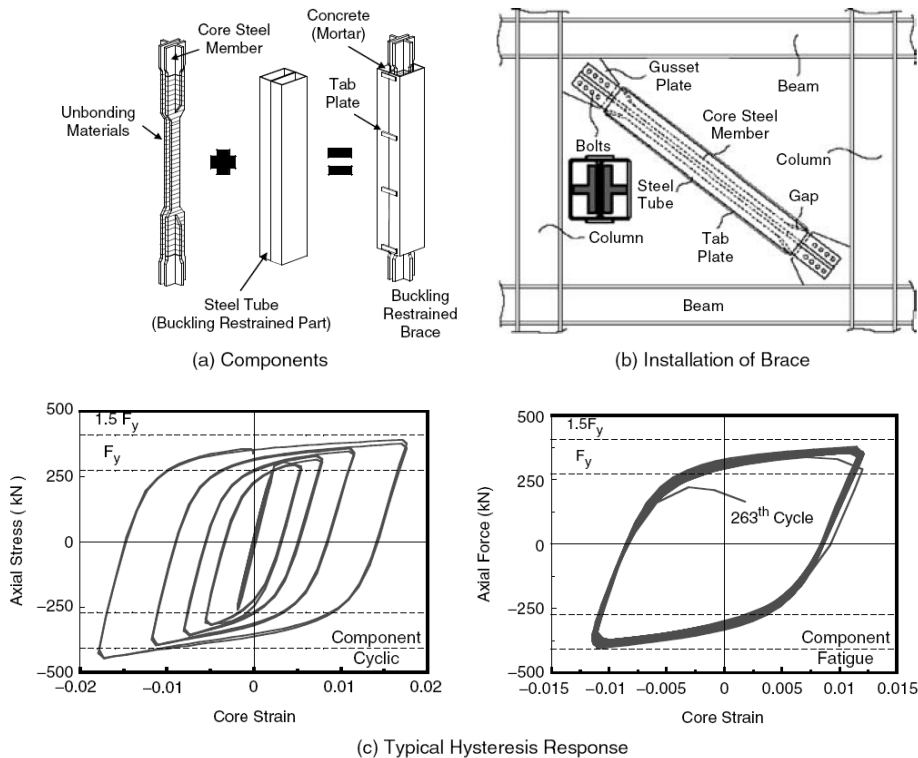


Figure 2.55 Double tube buckling restrained brace [16]

**Europe**

The BRB system was studied in Italy in 2005 by Mazzolani as a detachable "only steel BRB". This system was tested on a real scale RC MRF GLD frame, having only one span on both directions and two floors height. The BRB system was applied as a diagonal system.

**2.6.BRB application on new and existing buildings**

Examples of BRB applications which may be considered as relevant for the seismic protection of buildings, are stated by Isao Kimura from Nippon Steel Corporation Tokyo, Japan (2002) [26].



Figure 2.56 Osaka International Convention Center ("damage tolerant" structural design, \$420 million project, completed in 1999, 721000 s.f., 13+2 storeys, h=300 ft, 370 braces, largest 73 ft with  $P_y = 1200$  kips) [26]

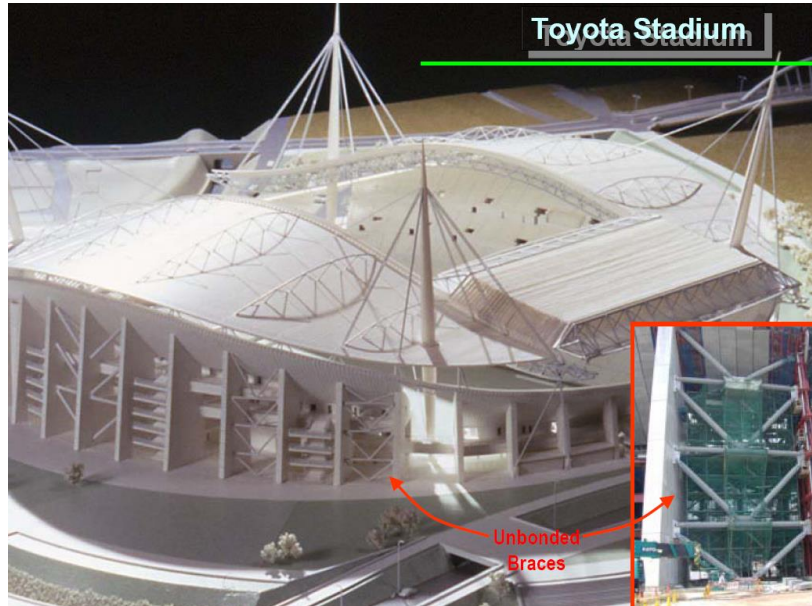


Figure 2.57 Toyota stadium [26]



Figure 2.58 Nippon TV Headquarters, Tokyo (1.4 million s.f., 32+2 storeys, h=630 ft, 68 braces, L=60 ft.,  $P_y = 2400$  kips) [26]





Figure 2.59 Hewlett Packard Co. – Building 5, Corvallis Campus [26]



Figure 2.60 Exterior exposition system, rectangular tube type: (upper left) SANKYO New Tokyo Headquarter Building (Tokyo, 1997); Nippon Television Tower (Tokyo, 2003) (lower left); Roppongi Hills (Tokyo, 2002); Seismic reinforcement of US Federal Government Building (Salt Lake, U.S., 2001) [4]

The Unbonded Brace™ has been used on nearly 200 buildings in Japan since 1987. ARUP used the Unbonded Brace™ on a number of Japanese projects, the first of which was the Osaka International Convention Centre in 1996, shown in Figure 2.61 [2].

ARUP San Francisco recognized the benefit this could bring to the Californian Construction Industry and looked for an opportunity to transfer this technology from Japan to California. This opportunity arose on the UC Davis Plant and Environmental Science Facility in 1999, shown in Figure 2.61.b [2].



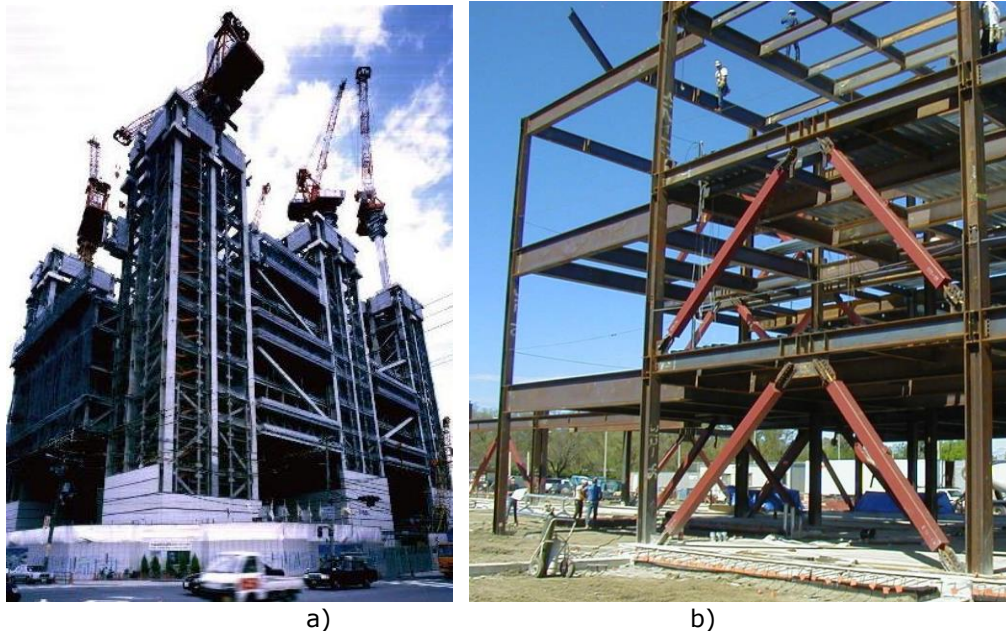


Figure 2.61 a) Osaka International Convention Centre, Japan b) UC Davis Plant & Environmental Facility, California [2]

On January 17<sup>th</sup> 2000, the first Unbonded Brace™ was installed in the United States at UC Davis. Actual field installation proved to be so simple and efficient that it reduced a month off the steel erection schedule for this building [2].

The next challenge was to implement this technology on a hospital project, as these are reviewed and approved by the Office of Statewide Health Planning and Development (OSHPD) in California. Arup applied this technology at Kaiser Santa Clara Medical Center project (Figure 2.62) [2].



Figure 2.62 Kaiser Santa Clara under construction [2]

The Wallace F. Bennett Federal Building stands prominently at the Southeast corner of 100 South and State Streets in the city center of Salt Lake City, Utah. This 8-storey, 300,000 sq. ft. office building has been a community landmark since it was built in the early 1960's. The reinforced concrete structure is built of eight-inch thick two-way flat plate floors, spirally-reinforced rectangular columns and pile





Shear transfer assembly and brace connection during construction



Brace connection assembly ready for installation at Grid Q'-2'

Figure 2.65 Joint detail of the braced frame elevation at Grid Line C at Wallace F. Bennett Federal Building [42]

#### **Applications and Cost Comparisons [42]**

Upon completion of the Schematic Design, Big-D Construction, Salt Lake City, Utah, was brought on board as a construction manager/general contractor with a guaranteed maximum cost of construction contract. Big-D prepared direct cost comparisons of two detailed braced frame designs: a conventional Concentrically Braced Frame and a scheme using buckling-restrained braces. The \$1.96 million cost to import the Unbonded Braces was mostly offset by direct reductions in the tonnage of the structural steel framework possible due to the better post-yield and energy dissipating characteristics of braces. Extensive modifications to the existing pile foundations that would have been required for the Concentrically Braced Frame scheme were essentially eliminated with the buckling-restrained brace system. Including savings achieved in the foundations, Big-D's estimates indicated a net savings to the structural system in excess of \$2 million. Also, the bolt-in-place Unbonded Braces saved about two months of construction time compared with field-welded conventional braces, making it possible to meet the GSA's extremely tight 14-month construction schedule requirement.

Buckling-restrained brace technology was a perfect fit for the Bennett Federal Building seismic upgrade project, and it allowed the project to exceed the defined seismic performance goals while meeting strict budget constraints. The benefits of improved seismic performance, reliability, and lower costs resulted in a win-win solution [42].





Figure 2.66 Wallace F. Bennett Federal Building Before Retrofitting and After Retrofitting [42]

Keh-Chyuan TSAI [43] presented some applications of BRB technologies in Taiwan, as it is presented Figure 2.67 and Figure 2.68:



Figure 2.67 Application of BRB to Constructions of the Tzu-Chi Culture Building ( TV Station ) [43]



Figure 2.68 Connection detail for application of BRB to Constructions of the Tzu-Chi Culture Building ( TV Station ) [43]

The BRB has been successfully adopted in Italy for the seismic upgrading of the University of Marche. In this application (Figure 2.69) BRB's were placed around the external perimeter of the RC structure, in order to both regularize the global response under lateral loads and enliven the architectural appearance.



Figure 2.69 University of Marche (Italy) [1]

As it may be seen, in Asia (Japan, Taiwan) BRBS experienced a large development both in research and application; also, this dissipative system spread across the ocean in USA and finally in Europe (Italy). All studies showed very good and predictable behavior also in the case of existing buildings, as in the case of new buildings.

### 2.7. Specific provisions in design codes

From late 1999 to 2001 an AISC and SEAOC [44] joint task group developed a document called Recommended Provisions for Buckling-Restrained Braced Frames. The Recommended Provisions were subsequently updated in July 2003. Since this development, buckling-restrained braces have been included in Section 8 of the NEHRP Recommended Provisions for Seismic Regulations for New Buildings and Other Structures (FEMA 450), and in Section 16 of the 2005 AISC Seismic Provisions for Structural Steel Buildings. These documents provide guidelines for the design of buckling-restrained brace elements, connections, and make recommendations for brace testing, when it is required [44].

Although American standard AISC 2005 [17] contain provisions about BRB's, this norm also considers that „a small amount of test data on BRBF system is available to structural engineers, it is also recommended that engineers refer to the following documents to gain further understanding of this system i.e. Uang and Nakashima (2003) [45], Watanabe and others (1988) [30], Clark and others (1999) [3], Tremblay and others (1999) [31] and Kalyanaraman [46] – AISC 2005.

The AISC [17] provisions contain:

- Requirements about BRB design/modeling (force-displacement diagram strength adjustment parameters)
- Basic requirements about experimental tests to certify BRB's (possible subassemblies, loading protocol).

Regarding the European guidelines or provisions about BRB's, there are no such dates. The same situation is in the Romanian seismic standard P100-1/2006 [47].

In order to have a control on BRB’s modeling and analysis, the following parameters should be established:

- **Seismic reduction factor (q)** for spectral analysis:

BRB frames and eccentrically braced frames are expected to possess similar structural ductility and they are assigned same values of force reduction factor R in AISC 2005 [17]. Therefore, in the case of steel frame buildings, the seismic reduction factor q to be used for BRB system was considered equal to the one assigned by Eurocode 8 [48] for eccentrically braced frames (q=6).

- **BRBS acceptance criteria** (needed in order to establish a PBSA (Performance Based Seismic Analysis) for retrofitting a RC MRF GLD building:

Performance criteria for BRB’s are generally difficult to define; in fact, BRB’s are rather manufactured than built. That is, they are typically made by a specialty manufacturer, rather than by a contractor or steel fabricator (although such a method of producing BRB’s is possible). Specifications should address the furnishing of the braces, including the associated brace-design calculations and quality-control procedures, and the documentation of successful tests that qualify the furnished braces for use in the project. In fact, the purpose of acceptance criteria for an element (BRB in our case), is to establish some “points” on force-deformation relation (Figure 2.70) where the element is considered to be in IO, LS or CP stage. Thus the acceptance criteria are based on the American FEMA356/ASCE41 [49]/[50], which is presented in more details in chapter 3.

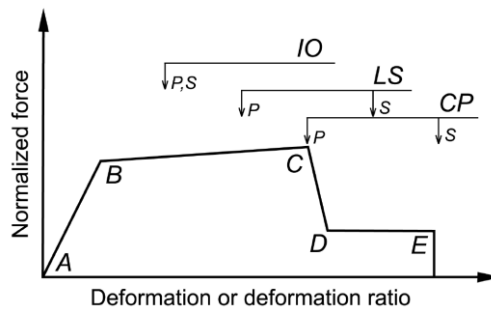


Figure 2.70 Generalized Force-Deformation Relation for Steel Elements or Components (FEMA356/ASCE41 [49]/[50])

To have some starting indicative values, another option is to use the values for braces in tension, recommended by FEMA (Table 2.4).

Table 2.4 Steel Braces in Tension Acceptance Criteria for Nonlinear Procedures—Structural Steel Components (FEMA356/ASCE41 [49]/[50])

Component/Action	Modeling Parameters			Acceptance Criteria				
	Plastic Deformation		Residual Strength Ratio	Plastic Deformation				
				IO	Primary		Secondary	
	a	b	c		LS	CP	LS	CP
Braces in Tension (except EBF braces) <sup>2</sup>	11Δ <sub>T</sub>	14Δ <sub>T</sub>	0.8	0.25Δ <sub>T</sub>	7Δ <sub>T</sub>	9Δ <sub>T</sub>	11Δ <sub>T</sub>	13Δ <sub>T</sub>

According to Mazzolani [51], in the case of the design of BRB’s for seismic upgrading of RC structures, the performance criteria of this device depend on the RC

lateral displacement response. RC frames generally yield for an interstorey-drift of about 1%, while the performance criterion for Collapse Prevention corresponds to 2.5% for a seismic event with a 10% probability of occurrence in 50 years (10/50).

Then, assuming a brace ductility capacity in the range of  $\mu = \varepsilon_{max}/\varepsilon_y = 4 \div 8$ , BRB's should be designed as to yield for an interstorey-drift of 0.25% (obtained by dividing an interstorey drift of 1% per the ductility capacity  $\mu$ ) in a 10/50 seismic event. In this way, the maximum displacement demand corresponds to the first RC damaging. While, in case of a 2/50 seismic event (i.e. with a 2% probability of occurrence in 50 years), it seems conservative not to exceed twice the ductility capacity considered for a life safety design.

In Table 2.5 are reported some indicative values of core plastic deformation ratio  $\varepsilon_{max}/\varepsilon_y$  that may be appropriate to a performance based design. The symbols IO, LS and CP are in the place of Immediate Occupancy, Life Safety and Collapse Prevention, respectively.

Table 2.5 Acceptance Criteria for BRB's [51]

Core Plastic deformation ( $\varepsilon_{max}/\varepsilon_y$ )		
IO	LS	CP
0.5	4	8

- **BRB main modeling parameters** (ductility ( $\mu$ ), strain hardening adjustment factor ( $\omega$ ) and compression adjustment factor ( $\beta$ ))

As it concern the modeling, the design and the acceptance criteria of a BRBS for new/existing buildings, it should be mentioned that there is no "public" standard, in order to assure their functionality; this is made only based on experimental tests and the "good" experience of people involved in this domain.

However, in USA, the American Institution of Steel Structures (AISC [17]) has conceived a series of provisions which should be respected in order to assure the basic design and modeling and to have an experimental check of their functionality. Thus, the provisions are divided in two chapters: in the first chapter, C16. BUCKLING-RESTRAINED BRACED FRAMES (BRBF), there is presented a description of the main components and some references in order to have a more detailed understanding about the main components of a BRB element (steel core, the restrain system, the importance of experimental tests, strength adjustment parameters), structural elements – BRB connection, provisions about BRB system configuration, provisions about the structural elements (beams and columns) from the frame portal in which the BRB element is inserted. The second chapter, „APPENDIX T QUALIFYING CYCLIC TESTS OF BUCKLING-RESTRAINED BRACES“, is tackling with the experimental testing mode, necessary for the validation of the BRB system or elements, as it follows: subassembly test, BRB element test and loading protocol history [52].

## 2.8. Research objectives of the Thesis

Starting from the state-of-the-art, previously reviewed and taking into account the research objectives of the thesis, the following objectives will be undertaken by numerical and experimental investigations:

- to define and perform nonlinear (static/dynamic/incremental dynamic) analysis on both RC frame building GLD and on retrofitted one;

## 76 Buckling restrained bracing systems for new and existing building structures - 2

- based on American FEMA356, to propose and apply a PBSE method on RC frame building and a PBSB on RC frame building global retrofitted by BRB system;
- to propose an acceptance criteria regarding the BRB performance levels i.e. Immediate Occupancy, Life Safety and Collapse Prevention, based on steel braces in tension acceptance criteria for nonlinear procedure from FEMA356;
- to obtain a reference value for the seismic reduction factor ( $q$ ) in the case of RC frames GLD retrofitted by BRB system;
- to propose and design a proper and functional detail for BRB-RC elements connections
- to propose and manufacture a BRB element configuration;
- to validate the proposed BRB element configuration, the unbonded material and the restraining device (for the sleeve and the infill material);
- based on the BRB element tests, to find the modeling parameters i.e. ductility ( $\mu$ ), strain hardening adjustment factor ( $\omega$ ) and compression adjustment factor ( $\beta$ );
- to validate experimentally the numerical results of inverted V BRB system pinned at the ends, inserted in a RC portal frame GLD at 1:1 scale (isolated from the considered analyzed RC building);
- to validate the pre-stressed tie connections between BRB-RC structural elements (beams/columns);
- to prove, experimentally, the BRB system efficiency on RC portal frame GLD, both monotonically and cyclically;
- to validate, the seismic reduction factor ( $q$ ) obtained in numerical analysis.



### **3. MODELS AND METHODS FOR PERFORMANCE BASED ANALYSIS AND DESIGN**

The main objective of this chapter is to describe the performance based seismic analysis and its application to the evaluation of an existing building, retrofitted by means of buckling restrained braces BRBs.

This chapter provides background information for the following topics: 1) general concept of the performance based seismic approach; 2) performance based evaluation of existing buildings before and after retrofitting: methodologies and general criteria; 3) models and performance criteria for materials; 4) models and performance criteria for elements; 5) global analysis: principles and methods; 6) selection of retrofitting technique and validation criteria; 7) case study: application of BRB to an existing RC building.

The results in terms of strength and ductility demands for the BRB's, obtained in the case study, will be compared against test results obtained in Chapter 4.

#### **3.1. General concept of the performance based seismic approach**

Building structures are designed so as to comply with the demands set up in the serviceability and ultimate limit states. For structures designed so as to resist seismic actions, the design criteria need to be extended, as yielding may occur during strong earthquakes. This extension refers to the requirement for provision of ductility, which corresponds to the capacity of certain parts of the structure to undergo large inelastic deformations under cyclic loading conditions, without considerable reduction in stiffness and strength. The criteria in respect to stiffness, strength and ductility may be complementary in design. It is therefore necessary to examine whether one of these criteria is prevailing, under what conditions and to what extent. For many years, the first goal of seismic design was the protection of people against serious injury or loss of lives and the avoidance of building collapse under a major earthquake. The second goal was the reduction of the damage level in the buildings. After each earthquake, more attention was paid to the structure performance than to the behavior of non-structural elements, which can produce more economic losses than the structural damages. This observation shows that is economically unacceptable solely the fulfillment of the condition of life protection. As a result, during the last fifteen years, a new philosophy for building evaluation and design has been developed.

Much of the development effort was done in USA, and envisaged the rehabilitation of existing buildings – FEMA 273 [53] and ATC-40 [54] or both the rehabilitation of existing buildings and the design of new ones - Vision 2000 [55]. Even if there were some differences between these methodologies, the basic framework was similar. In general, various performance levels are defined and associated to given levels of hazard (earthquake intensity). The objective is to evaluate/design the building structure so as to fulfill the performance levels.

Vision 2000 [55] was initiated and supported by the Structural Engineers Association of California SEAOC. The guideline was intended to be applicable to the rehabilitation of existing buildings as well as to the design of new ones. The main goal was to provide methods for evaluating, designing, constructing and maintaining buildings so that they be capable of providing predictable performance in the case of an earthquake-type ground motion. This framework explicitly addresses issues of functionality and damageability, which are more related to non-structural elements,

but also the issues of life-safety and prevention of collapse, which refer to structural elements. One of the key issues in a performance based analysis is the definition of multiple performance levels (damage levels) which are expected to be achieved – or at least not exceeded – when the structure is subjected to a given level of seismic intensity. Vision 2000 [55] defines four performance objectives (PO) for buildings of different importances. The PO's are defined in terms of performance levels and recommended hazard levels (earthquake design levels) (see Figure 3.1) and are assigned a specific class of importance, which varies from the “basic” objective to the “safety critical” objective.

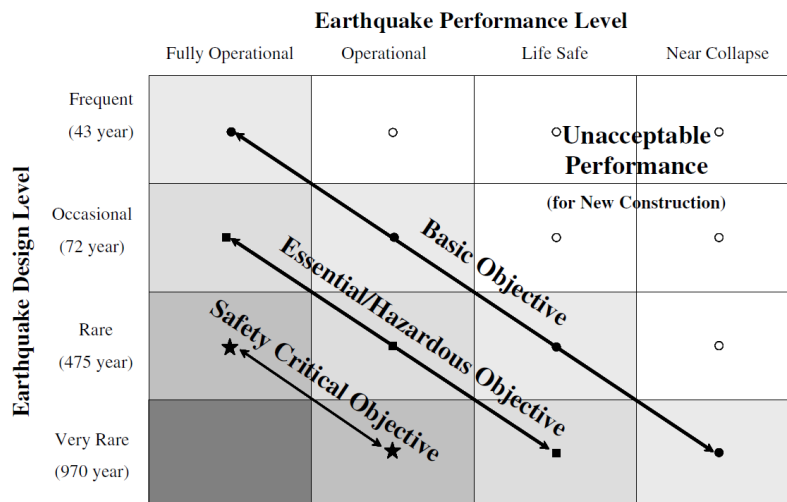


Figure 3.1. Matrix of performance objectives for buildings, recommended in Vision 2000

For each performance level, Vision 2000 guideline gives the description of the damage for various structural components and systems, architectural elements, equipments. Even the descriptions are mostly qualitative, quantitative limits on permissible transient, and there are also given permanent storey drifts at the various performance levels.

FEMA 273 was developed in parallel with the Vision 2000, by the U.S. Federal Emergency Management Agency FEMA and aimed at developing guidelines for the seismic rehabilitation of buildings. First report FEMA 273 was published in 1996, and was later modified and upgraded and then published in 2000 as FEMA 356 [49]. The framework is similar to that of Vision 2000, but differs in what concerns the hazard levels and definition of performance levels. The report address both structural and nonstructural performance levels and provides many quantitative rules compared to Vision 2000. An important contribution of FEMA 273/356 refers to the provisions for analysis procedures that can be used in order to assess the building performance. Both advanced and simplified analysis procedures are presented. Even if it recognizes that the nonlinear dynamic analysis (time history) is the most reliable, FEMA 273/356 also presents in details a simplified analysis procedure, including linear static and linear dynamic procedures, and the nonlinear static (pushover) procedure (Figure 3.2). Parameters shown in Figure 3.2 will be later on described in more details in this chapter.

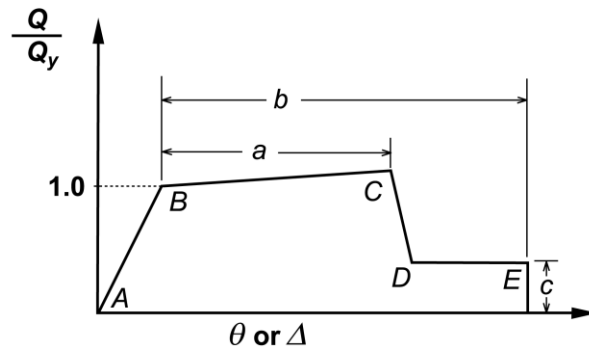


Figure 3.2. Normalized force versus deformation, FEMA 356

ATC-40 was developed in parallel with FEMA 273 and addressed the seismic evaluation and retrofit guidelines for existing reinforced concrete structures. The report ATC-40 was published in 1996. The framework is similar to that of Vision 2000. Similar to FEMA 273/356, the pushover analysis has become the preferred method for the evaluation of seismic demands, like storey drifts or plastic rotation. In this methodology, the evaluation of the target displacement is based on the capacity spectrum method. In the capacity spectrum method, the force displacement curve obtained from the pushover analysis is converted into an equivalent SDOF curve, and then intersected with a modified response spectrum to obtain the performance point (Figure 3.3). This method is similar to N2 method, developed by Fajfar [56] and introduced in Eurocode 8 for the evaluation of seismic performances of structures.

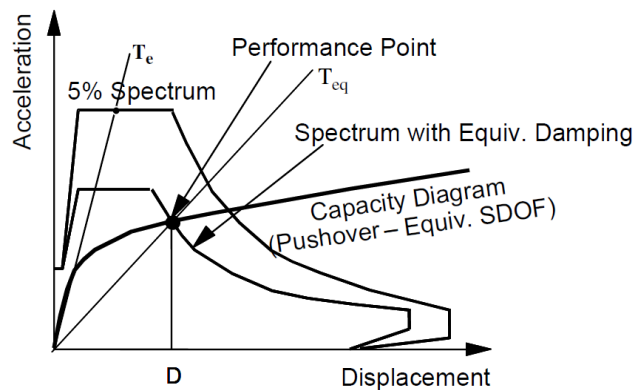


Figure 3.3. Capacity spectrum method, ATC-40

Similarly to the guidelines summarized in this paragraph, other developments efforts were initiated elsewhere. As a main characteristic, different documents use different performance levels and seismic hazard levels, showing that the scientific community did not come to a conclusion regarding these issues. There are also alternatives to the selection of discrete performance objectives (performance levels and associated seismic hazards). Figure 3.4 shows the expression of performance in terms of continuous variables, like percent

replacement costs, length of downtime and casualty rate [57]. The great advantage of the continuous variables is that they can be evaluated in probabilistic terms.

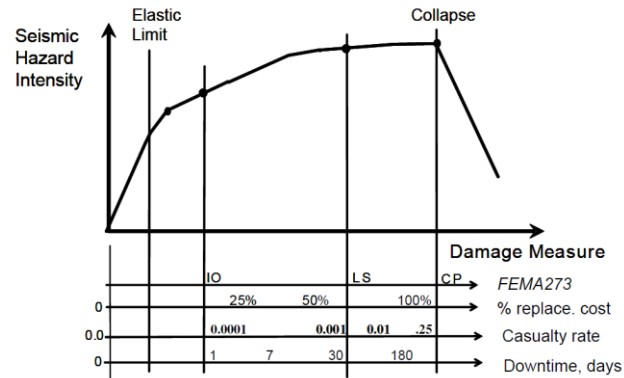


Figure 3.4. Relationship between the seismic hazard intensity and the structural performance

### 3.2. Performance based evaluation of existing buildings before and after retrofitting: methodologies and general criteria

The evaluation based on performance, introduced in the previous section, provides several advantages compared to the current seismic evaluation codes. Many existing buildings located in areas of seismic hazard, designed prior to the development of adequate seismic code provisions, are vulnerable to moderate and strong earthquake ground motions. Therefore, there is a strong demand for the coordination of efforts at national and international levels in order to reduce the seismic risk. The seismic retrofitting of existing building plays a very important role in reducing the seismic risk. But before selecting a specific rehabilitation strategy, the performance and effectiveness of the strategy should be carefully investigated. In order to prove its reliability, general methodology and general criteria should be defined.

If the vulnerability assessment indicates poor performance of the structure, an intervention strategy is adopted. The intervention strategy may refer to an increase of the strength, stiffness or ductility properties by local strengthening or by adding new structural systems, but also to reducing the seismic mass, partial demolition, removal of irregularities and discontinuities. If the first strategy is adopted, a retrofitting system is selected (e.g. buckling restrained braces). New performance objectives are defined, according to the expected behavior of the retrofitting technique. Performance criteria in terms of displacement or deformations are selected and/or calibrated using experimental tests. Modeling parameters can also be selected based on previous experience or can be defined based on experimental results. The assessment of structural global performance after the strengthening intervention can be performed by means of different analysis procedure. The analysis must be carefully selected, in order to identify those elements whose poor behavior (e.g. lack of ductility) may prevent the structure from reaching the targeted behavior.

### 3.3. Models and performance criteria for materials

Materials properties, like strength, deformability or toughness should be based on derived material properties and detailed component knowledge. They must be determined for two basic purposes: to allow the calculation of their ability to deliver load to other elements and components, and to allow the determination of their capacity to resist forces and deformations [49]. In the absence of material test records and quality assurance reports, the use of default material properties is permitted. This is particularly important for old buildings, where construction documents are rarely available.

For example, steel components of existing buildings may include columns, beams, braces, connections, link beams and diaphragms. They may be built up with plates, angles, and/or channels connected together with rivets, bolts, or welds. The material used in older construction is likely to be mild steel with the characteristics required by today regulations. The connectors in older constructions were usually mild steel rivets or bolts. The seismic performance of these components heavily depend on the condition of the in-place material.

The form, the function, the concrete strength, the concrete quality, the reinforcing steel strength, the quality and the detailing, the forming techniques and the concrete placement techniques have constantly evolved and have had a significant impact on the seismic resistance of a concrete building. Particularly with concrete materials, the date of the original building construction significantly influences the seismic performance. Early uses of concrete did not specify any design strength, and low-strength concrete was not uncommon. Also, the early use of concrete in buildings often employed reinforcing steel with relatively low strength and ductility, limited continuity, and reduced bond development. The continuity between specific existing components and elements (e.g., beams and columns, diaphragms and shear walls) is also particularly difficult to assess, given the presence of the concrete cover and other barriers to inspection. It is important that the personnel involved in the material property quantification and the condition assessment should have some experience in the proper implementation of testing practices and the interpretation of results. The following component and connection material properties shall be obtained for the as-built structure:

- concrete compressive strength.
- yield and ultimate strength of conventional and pre-stressing reinforcing steel and metal connection hardware.

Other material properties that may be of interest for concrete elements and components include:

- Tensile strength and modulus of elasticity,
- Ductility, toughness, and fatigue properties of concrete.
- Carbon equivalent present in the reinforcing steel.
- Presence of any degradation such as corrosion, bond with concrete, and

chemical composition.

Destructive and non-destructive test methods is used to obtain the in-place mechanical properties of materials. Materials testing is not required if material properties are available from the original construction documents that include material test records or material test reports.

Table 3.1. Numerical Acceptance Criteria for Linear Procedures—Reinforced Concrete Infilled Frames [49]

Conditions	m-factors <sup>3</sup>				
	Performance Level				
	IO	Component Type			
		Primary		Secondary	
	LS	CP	LS	CP	
<b>i. Columns modeled as compression chords<sup>2</sup></b>					
Columns confined along entire length <sup>1</sup>	1	3	4	4	5
All other cases	1	1	1	1	1
<b>ii. Columns modeled as tension chords<sup>2</sup></b>					
Columns with well-confined splices, or no splices	3	4	5	5	6
All other cases	1	2	2	3	4

1. A column may be considered to be confined along its entire length when the quantity of hoops along the entire storey height including the joint is equal to three-quarters of the one required for boundary elements of concrete shear walls. The maximum longitudinal spacing of sets of hoops shall not exceed either  $h/3$  or  $8db$ .

2. If load reversals result in both conditions i and ii applying to a single column, both conditions will be checked.

3. Interpolation will not be permitted.

Depending on the analysis procedure used for the evaluation of the performance, different modeling strategies may be adopted, with different complexity and refinement. Kent and Park [58] considered that the confined concrete has the same compressive strength as the non-confined concrete (Figure 3.5, Figure 3.6), while Paulay and Priestley [310] considered that there is a difference between the two strengths (the difference is given by a coefficient based on stirrups confinement capacity).

Other tests have shown that confinement by transversal reinforcement can considerably improve the stress and strain characteristics of concrete at high strains. Tests have also demonstrated that circular spirals are more effective than rectangular or square hoops in confining the concrete (Figure 3.7).

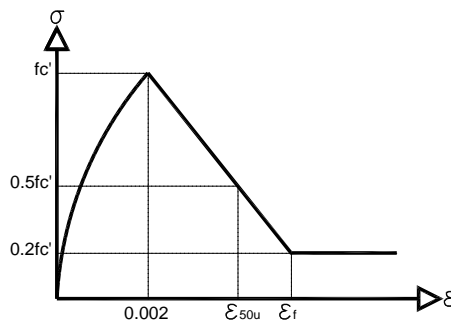


Figure 3.5. Kent & Park un-confined concrete definition [58]

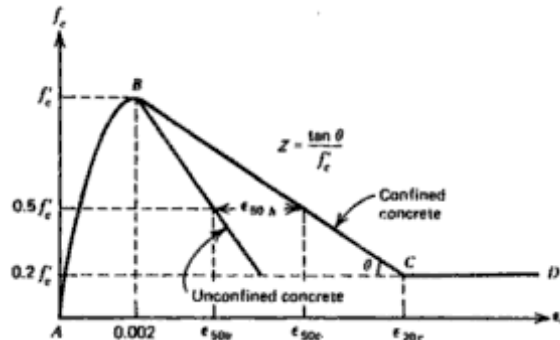


Figure 3.6. Stress-strain curve for concrete confined by rectangular hoops, Kent and Park [58]

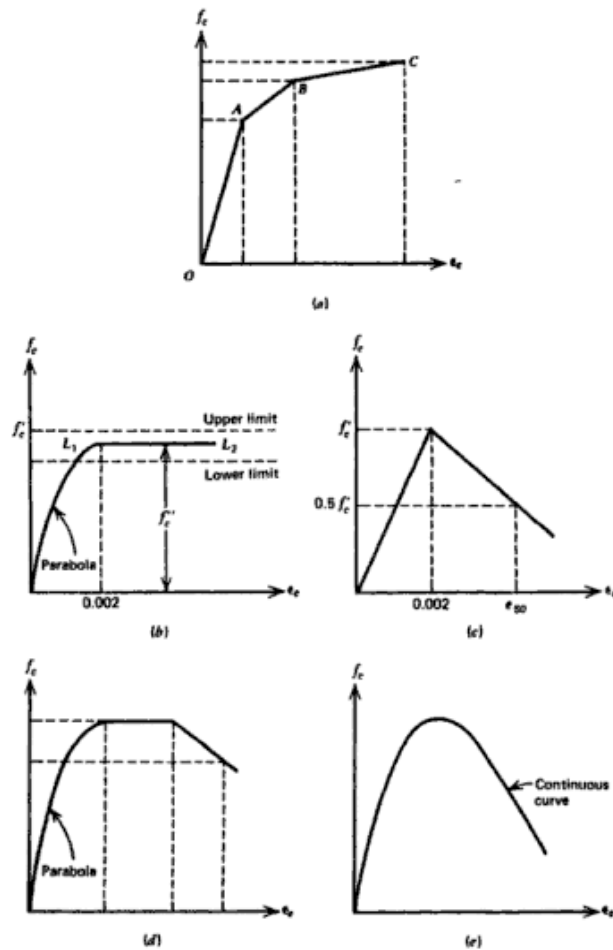


Figure 3.7. Some proposed stress-strain curves for concrete confined by rectangular hoops. (a) Chan and Blume et al., (b) Baker, (c) Roy and Sozen, (d) Soliman and Yu, (e) Sargin et al. [58]

The definition of regions A-B, B-C and C-D from Figure 3.6 are as follows [58]:

**Region AB:**

$$\varepsilon_c \leq 0.002$$

$$f_c = f_c' \left[ \frac{2\varepsilon_c}{0.002} - \left( \frac{\varepsilon_c}{0.002} \right)^2 \right] \quad (3.1)$$

This ascending part of the curve is represented by a second-degree parabola. It can be assumed that the confining steel has no effect on the shape of this part of the curve or the strain at maximum stress. It is also assumed that the maximum stress reached by the confined concrete is the cylinder strength  $f_c'$ . There is evidence that rectangular hoops will cause an increase in strength; however, this increase may be small. The maximum stress of  $f_c'$  will be conservative in most cases [58].

**Region BC:**

$$0.002 \leq \varepsilon_c \leq \varepsilon_{20c}$$

$$f_c = f_c' [1 - Z(\varepsilon_c - 0.002)] \quad (3.2)$$

$$Z = \frac{0.5}{\varepsilon_{50u} + \varepsilon_{50h} - 0.002} \quad (3.3)$$

$$\varepsilon_{50u} = \frac{3 + 0.002f_c'}{f_c' - 1000} \quad (3.4)$$

$$\varepsilon_{50h} = \frac{3}{4} \rho_s \sqrt{\frac{b''}{s_h}} \quad (3.5)$$

where:

$f_c'$  = concrete cylinder strength, in psi (1psi=0.00689 N/mm<sup>2</sup>)

$\rho_s$  = ratio between the volume of transversal reinforcement and the volume of the concrete core measured outside the hoops

$b''$  = width of the confined core measured outside the hoops

$s_h$  = spacing of hoops.

**Region CD:**

$$\varepsilon_c \geq \varepsilon_{20c}$$

$$f_c = 0.2f_c' \quad (3.6)$$

This equation accounts for the ability of concrete to sustain some stresses at very large strains.

In Eurocode 2, the stress-strain relation for nonlinear structural analysis is given by the following equation:

$$\frac{\sigma_c}{f_{cm}} = \frac{k\eta - \eta^2}{1 + (k-2)\eta} \quad (3.7)$$

where:

$$\eta = \varepsilon_c / \varepsilon_{c1}$$



-  $\epsilon_{c1}$  is the strain at peak stress

$$k = 1.05 E_{cm} |\epsilon_{c1}| / f_{cm}$$

-  $f_{cm}$  is the mean value of concrete cylinder compressive strength

Previous equation is valid for  $0 < |\epsilon_{c1}| < |\epsilon_{cu1}|$ , where  $|\epsilon_{cu1}|$  is the nominal ultimate strain.

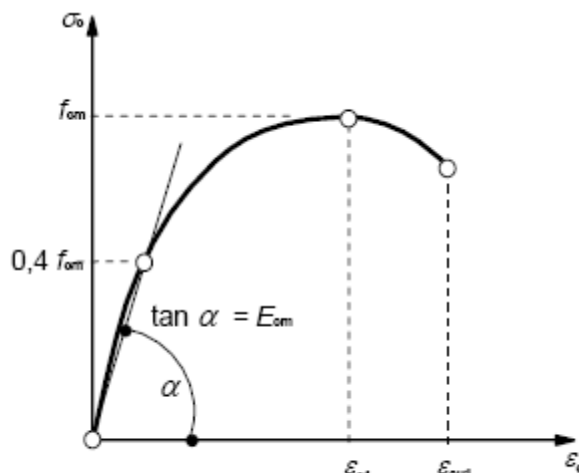


Figure 3.8 Stress-strain curve for nonlinear structural analysis, Eurocode 2 [59]

For the design of compressive strength, the following equations are used:

$$f_{cd} = \alpha_{cc} f_{ck} / \gamma_c \tag{3.8}$$

Where:

- $\gamma_c$  is the partial safety factor for concrete;
- $\alpha_{cc}$  is the coefficient that takes into account the long term effects on the compressive strength and unfavorable effects resulting from the manner in which the load is applied.

The value of the design tensile strength  $f_{ctd}$  is defined as:

$$f_{ctd} = \alpha_{ct} f_{ctk,0.5} / \gamma_c \tag{3.9}$$

where:

- $\alpha_{ct}$  is the coefficient taking into account the long term effects on the tensile strength and unfavorable effects resulting from the manner in which the load is applied.

Stress-strain curves for steel reinforcement may be defined by different laws (bilinear, tri-linear, parabolic) and may include or not a strengthening or softening domain (Figure 3.9). They can be defined with or without the compression capacity.

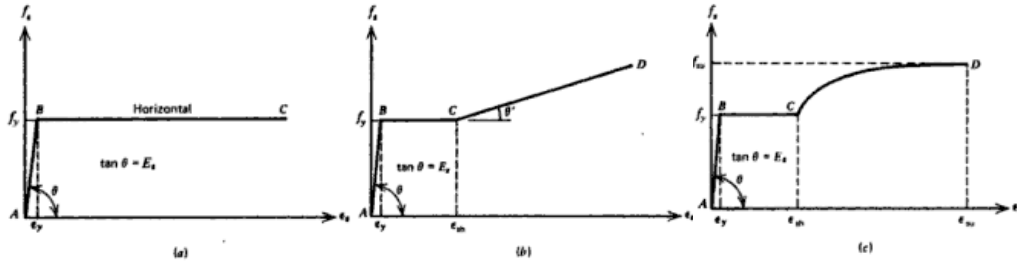


Figure 3.9 Idealisation of the stress-strain curve for steel reinforcements: (a) elastic perfectly plastic curve; (b) trilinear curve; (c) complete curve [58]

The specified yield strength normally refers to a guaranteed minimum strength. The actual yield strength of the bars is somewhat higher than the value considered in design.

Eurocode 2 only applies to ribbed reinforcements for yield strength  $f_{yk}$  ranging from 400 to 600 MPa. The behavior of reinforcing steel is characterised by the following properties:

- yield strength ( $f_{yk}$  or  $f_{0.2k}$ )
- maximum actual yield strength ( $f_{y,max}$ )
- tensile strength ( $f_t$ )
- ductility ( $\epsilon_{uk}$  and  $f_t/f_{yk}$ )
- blendability
- bond characteristics
- section sizes and tolerances
- fatigue strength
- weldability
- shear and weld strength for welded fabric and lattice girder

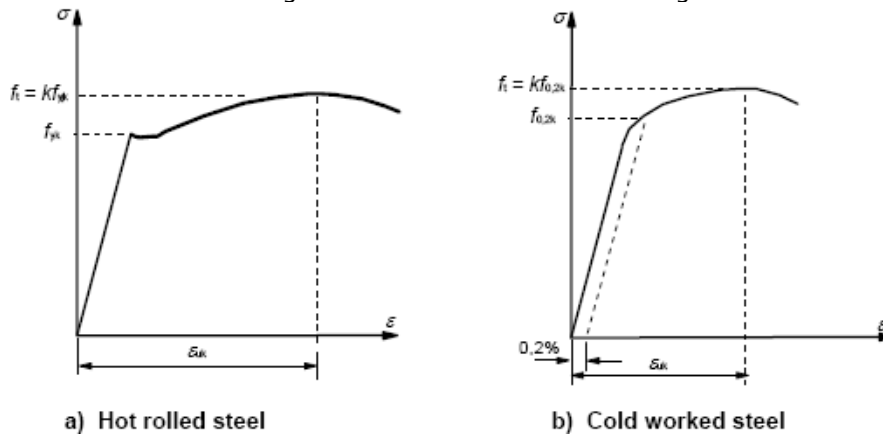


Figure 3.10 Stress-strain diagrams of typical reinforcing steel (absolute values are shown for tensile stress and strain) [59]

Design should be based on the nominal cross-section area of the reinforcement and the design values:

a) an inclined top branch with a strain limit of  $\epsilon_{ud}$  and a maximum stress of  $kf_{yk}/\gamma_s$ .

b) A horizontal top branch without the need to check the strain limit.

The mean value of the density may be considered  $7850 \text{ kg/m}^3$ .

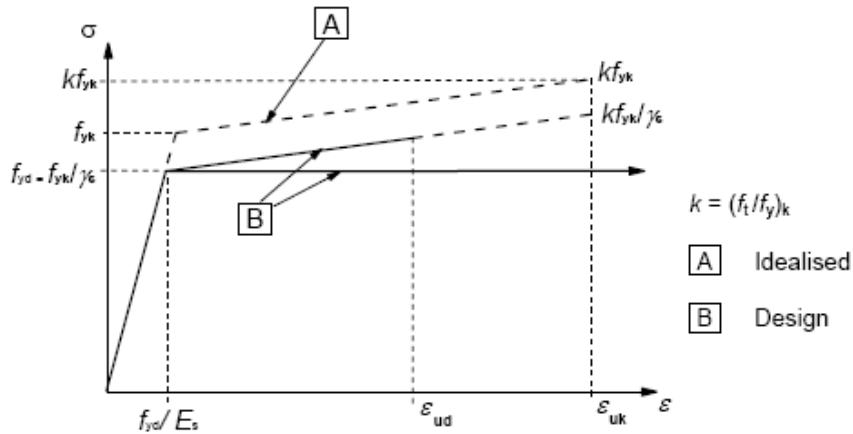


Figure 3.11 Idealised and design stress-strain diagrams for reinforcing steel (for tension and compression) [59]

### 3.4. Models and performance criteria for elements

#### 3.4.1. Type of models

Accurate models of elements and their connections are necessary for assessing reliable results. Models must be adapted to the real behavior of the elements and to the analysis procedure (Figure 3.12).

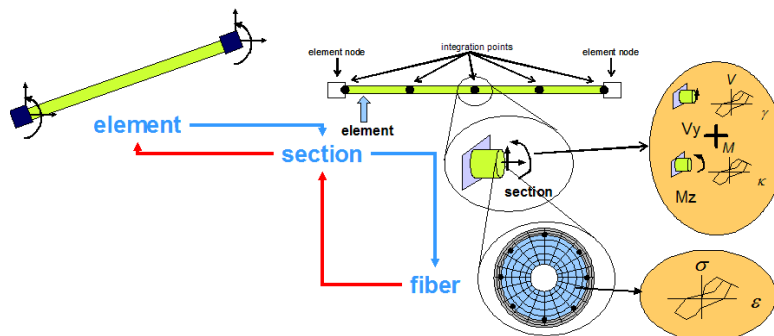


Figure 3.12 Structural element modeling (OpenSees [60])

These models may be classified into three main groups:

#### 1. Plastic zones model (plasticity distributed along the element)

This model allows for geometric instabilities and material non-linearities (plasticity), residual stresses and imperfections. It allows for the gradual plastification of the member, starting from the most stressed fiber of the most stressed cross section and spreading over the depth of the cross section and along the member longitudinal axis. Accordingly, the stiffness along the member changes with loading, as, at cross sections where yielding has occurred, the initial elastic stiffness ( $EI$ ) gradually reduces. However the deflection line is continuous over the entire loading, and unloading, process. and rotation takes place only at true, and not plastic, hinges. The plastic zones model is very accurate but more complex and time consuming than other models.

**2. The fiber modeling (distributed plasticity along the section)**

According to this method, the section is subdivided into  $n$  fibers and the stresses are integrated over the cross-sectional area so as to obtain stress resultants such as force or moment. There are several assumptions are used with this model:

- plane sections remain plane after bending;
- multiaxial stress states, such as those due to confinement effects, can be included by increasing the concrete strength and by modifying the concrete post-peak response.

Concrete cracking is generally accounted for the local buckling of the steel components and initial stresses resulting from either erection loads or thermal residual effects can be included.

The advantage of the fiber model analysis is that it can easily account for the presence of structural steel, reinforcing bars, and concrete (Figure 3.13).

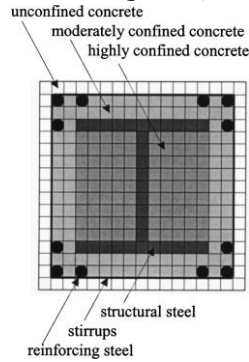


Figure 3.13 Fiber model for the discretization of a composite section [61]

**3. The elastic-plastic hinge (plasticity concentrated on the element)**

In the plastic hinge method, plasticity is supposed to concentrate in certain member locations, which, after the plastic moment of the section is reached, entirely lose their stiffness and behave like hinges (Figure 3.14).

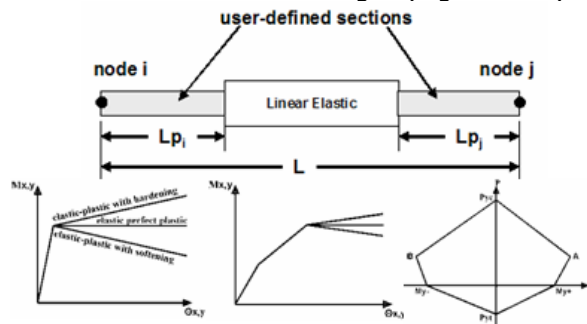


Figure 3.14 Elastic plastic hinge modeling [60]

The application of the plastic zones method allows for the observation of the gradual plastification in individual cross sections, in contrast to the plastic hinge method, where cross sections behave either fully elastic or plastic. The deformation diagrams in the plastic zones method are continuous, while, in the plastic hinge method, discontinuities appear at plastic hinges (Figure 3.15).

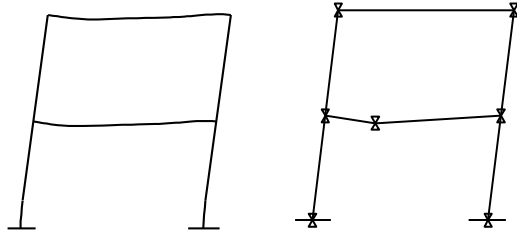


Figure 3.15 Deformed frames for the application of plastic zones and plastic hinges methods

The models used in the performance based evaluation of buildings must be in accordance with the analysis procedure and the acceptance criteria. Figure 3.16 [49] shows the generalized force versus the deformation curves used in order to specify the component modeling and the acceptance criteria for deformation-controlled actions in any of the four basic material types.

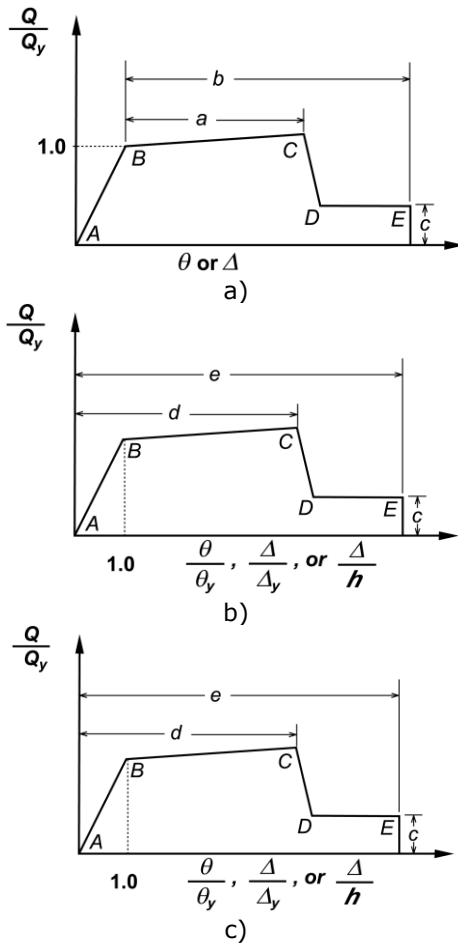


Figure 3.16 Generalized Component Force-Deformation relations for depicting modeling and acceptance criteria: a) deformation; b) deformation ratio; c) component or element deformation acceptance criteria [49]

The linear response is depicted between point A (unloaded component) and an effective yield point B. The slope from B to C is typically a small percentage (0-10%) of the elastic slope, and is included in order to represent phenomena such as the strain hardening. C has an ordinate that represents the strength of the component, and an abscissa value equal to the deformation at which significant strength degradation begins (line CD). Beyond point D, the component responds with substantially reduced strength to point E. At deformations greater than point E, the component strength is essentially zero.

For some components, it is convenient to prescribe acceptance criteria in terms of deformation (e.g.,  $\theta$  or  $\Delta$ ), while for others it is more convenient to give criteria in terms of deformation ratios. To accommodate this, two types of idealized force vs. deformation curves are used. Figure 3.16.a shows the normalized force ( $Q/Q_{CE}$ ) versus deformation ( $\theta$  or  $\Delta$ ) and the parameters  $a$ ,  $b$  and  $c$ . Figure 3.16.b shows the normalized force ( $Q/Q_{CE}$ ) versus the deformation ratio ( $\theta/\theta_y$ ,  $\Delta/\Delta_y$ , or  $\Delta/h$ ) and the parameters  $d$ ,  $e$ , and  $c$ . Elastic stiffnesses and the values of the parameters  $a$ ,  $b$ ,  $c$ ,  $d$ , and  $e$  that can be used for modeling components depend on the type of element. The acceptance criteria for deformation or deformation ratios for primary members (P) and secondary members (S) corresponding to the target Building Performance Levels of Collapse Prevention (CP), Life Safety (LS), and Immediate Occupancy (IO), as shown in Figure 3.16.c, also depend on the type of the structural element [49].

### 3.4.2. Performance criteria for elements

Performance Based Evaluation PBE can be performed on the global level and the member level. FEMA 356 [49] gives the acceptance criteria for elements and connections for the three performance levels (IO, LS and CP). There are also some acceptance criteria for the global level evaluation, but they can be used just as guidance.

For the seismic retrofitting of RC buildings with BRB's, it is of interest to analyze the acceptance criteria for the concrete frame (column and beams) and steel braces. As acceptance criteria for BRB are not specifically described in FEMA 356, a test program was developed and is presented in Chapter 4. So that, the values of acceptance limits provided by FEMA 356 refer to conventional centrically X steel braces and are presented as reference.

Table 3.2 FEMA 356 modeling parameters and numerical acceptance criteria for nonlinear procedures - RC beams [49]

Conditions		Modeling parameters <sup>3</sup>			Acceptance criteria <sup>3</sup>					
		Plastic rotation angle, radians	Residual strength ratio	c	Plastic rotation angle, radians					
a	b				IO	Performance level				
		Component type								
		Primary		Secondary						
		LS	CP	LS	CP					
i. Beams controlled by flexure <sup>1</sup>										
$\rho - \rho'$	Transverse Reinforcement <sup>2</sup>	$\frac{V}{b_w d \sqrt{f'_c}}$								
$\rho_{bal}$										
$\leq 0.0$	C	$\leq 3$	0.025	0.05	0.2	0.01	0.02	0.025	0.02	0.05
$\leq 0.0$	C	$\geq 6$	0.02	0.04	0.2	0.005	0.01	0.02	0.02	0.04
$\geq 0.5$	C	$\leq 3$	0.02	0.03	0.2	0.005	0.01	0.02	0.02	0.03
$\geq 0.5$	C	$\geq 6$	0.015	0.02	0.2	0.005	0.005	0.015	0.015	0.02
$\leq 0.0$	NC	$\leq 3$	0.02	0.03	0.2	0.005	0.01	0.02	0.02	0.03
$\leq 0.0$	NC	$\geq 6$	0.01	0.015	0.2	0.0015	0.005	0.01	0.01	0.015
$\geq 0.5$	NC	$\leq 3$	0.01	0.015	0.2	0.005	0.01	0.01	0.01	0.015
$\geq 0.5$	NC	$\geq 6$	0.005	0.01	0.2	0.0015	0.005	0.005	0.005	0.01
ii. Beams controlled by shear <sup>1</sup>										
Stirrup spacing $\leq d/2$			0.003	0.02	0.2	0.0015	0.002	0.003	0.1	0.02
Stirrup spacing $\geq d/2$			0.003	0.01	0.2	0.0015	0.002	0.003	0.005	0.01
iii. Beams controlled by inadequate development or splicing along the span <sup>1</sup>										
Stirrup spacing $\leq d/2$			0.003	0.02	0	0.0015	0.002	0.003	0.1	0.02
Stirrup spacing $\geq d/2$			0.003	0.01	0	0.0015	0.002	0.003	0.005	0.01
iv. Beams controlled by inadequate embedment into beam-column joint <sup>1</sup>										
			0.015	0.03	0.2	0.01	0.01	0.015	0.02	0.03

Notes:

1. When more than one of the conditions i, ii, iii, and iv occur for a given component, use the minimum appropriate numerical value from the table.
2. "C" and "NC" are abbreviations for conforming and nonconforming transverse reinforcement. A component is conforming if, within the flexural plastic hinge region, hoops are spaced at  $\leq d/3$ , and if, for components of moderate and high ductility demand, the strength provided by the hoops ( $V_s$ ) is at least three-fourths of the design shear. Otherwise, the component is considered nonconforming.
3. Linear interpolation between values listed in the table shall be permitted.

Table 3.3 FEMA 356 modeling parameters and numerical acceptance criteria for nonlinear procedures - RC columns [49]

Conditions			Modeling parameters <sup>4</sup>			Acceptance criteria <sup>4</sup>				
			Plastic rotation angle, radians	Residual strength ratio	Plastic rotation angle, radians					
Performance level										
					Component type					
					Primary		Secondary			
					IO	LS	CP	LS	CP	
a	b	c								
i. Columns controlled by flexure <sup>1</sup>										
$\frac{P}{A_g f'_c}$	Transverse Reinforcement <sup>2</sup>	$\frac{V}{b_w d \sqrt{f'_c}}$								
≤ 0.1	C	≤ 3	0.02	0.03	0.2	0.005	0.015	0.02	0.02	0.03
≤ 0.1	C	≥ 6	0.016	0.024	0.2	0.005	0.012	0.016	0.016	0.024
≥ 0.4	C	≤ 3	0.015	0.025	0.2	0.003	0.012	0.015	0.018	0.025
≥ 0.4	C	≥ 6	0.012	0.02	0.2	0.003	0.01	0.012	0.013	0.02
≤ 0.1	NC	≤ 3	0.006	0.015	0.2	0.005	0.005	0.006	0.01	0.015
≤ 0.1	NC	≥ 6	0.005	0.012	0.2	0.005	0.004	0.005	0.008	0.012
≥ 0.4	NC	≤ 3	0.003	0.01	0.2	0.002	0.002	0.003	0.006	0.01
≥ 0.4	NC	≥ 6	0.002	0.008	0.2	0.002	0.002	0.002	0.005	0.008
ii. Columns controlled by shear <sup>1,3</sup>										
All cases <sup>5</sup>			-	-	-	-	-	-	0.003	0.004
iii. Columns controlled by inadequate development or splicing along the clear height <sup>1,3</sup>										
Hoop spacing ≤ d/2			0.01	0.02	0.4	0.005	0.005	0.01	0.01	0.02
Hoop spacing ≥ d/2			0	0.01	0.2	0	0	0	0.005	0.01
iv. Columns with axial loads exceeding 0.70P <sub>o</sub> <sup>1,3</sup>										
Conforming hoops over the entire length			0.015	0.025	0.02	0	0.005	0.01	0.01	0.02
All other cases			0	0	0	0	0	0	0	0

Notes:

- When more than one of the conditions i, ii, iii, and iv occur for a given component, use the minimum appropriate numerical value from the table.
- "C" and "NC" are abbreviations for conforming and nonconforming transverse reinforcement. A component is conforming if, within the flexural plastic hinge region, hoops are spaced at ≤ d/3, and if, for components of moderate and high ductility demand, the strength provided by the hoops (V<sub>s</sub>) is at least three-fourths of the design shear. Otherwise, the component is considered nonconforming.
- To qualify, columns must have transverse reinforcement consisting of hoops. Otherwise, actions shall be treated as force-controlled.
- Linear interpolation between values listed in the table shall be permitted.
- For columns controlled by shear, acceptance criteria are different



Table 3.4 FEMA 356 modeling parameters and numerical acceptance criteria for nonlinear procedures - RC beam-column joints [49]

Conditions	Modeling parameters <sup>4</sup>			Acceptance criteria <sup>4</sup>				
	Plastic rotation angle, radians		Residual strength ratio	Plastic rotation angle, radians				
				Performance level				
			IO	Component type				
				Primary		Secondary		
a	b	c	LS	CP	LS	CP		

i. Interior joints<sup>2,3</sup>

$\frac{P}{A_g f'_c}$	Transverse Reinforcement	$\frac{V}{V_n}$ <sup>3</sup>								
≤ 0.1	C	≤ 1.2	0.015	0.03	0.2	0	0	0	0.02	0.03
≤ 0.1	C	≥ 1.5	0.015	0.03	0.2	0	0	0	0.015	0.02
≥ 0.4	C	≤ 1.2	0.015	0.025	0.2	0	0	0	0.015	0.025
≥ 0.4	C	≥ 1.5	0.015	0.02	0.2	0	0	0	0.015	0.02
≤ 0.1	NC	≤ 1.2	0.005	0.02	0.2	0	0	0	0.015	0.02
≤ 0.1	NC	≥ 1.5	0.005	0.015	0.2	0	0	0	0.01	0.015
≥ 0.4	NC	≤ 1.2	0.005	0.015	0.2	0	0	0	0.01	0.015
≥ 0.4	NC	≥ 1.5	0.005	0.015	0.2	0	0	0	0.01	0.015

ii. Other joints<sup>2,3</sup>

$\frac{P}{A_g f'_c}$	Transverse Reinforcement <sup>1</sup>	$\frac{V}{V_n}$								
≤ 0.1	C	≤ 1.2	0.01	0.02	0.2	0	0	0	0.015	0.02
≤ 0.1	C	≥ 1.5	0.01	0.015	0.2	0	0	0	0.01	0.015
≥ 0.4	C	≤ 1.2	0.01	0.02	0.2	0	0	0	0.015	0.02
≥ 0.4	C	≥ 1.5	0.01	0.015	0.2	0	0	0	0.01	0.015
≤ 0.1	NC	≤ 1.2	0.005	0.01	0.2	0	0	0	0.0075	0.01
≤ 0.1	NC	≥ 1.5	0.005	0.01	0.2	0	0	0	0.0075	0.01
≥ 0.4	NC	≤ 1.2	0	0	-	0	0	0	0.005	0.0075
≥ 0.4	NC	≥ 1.5	0	0	-	0	0	0	0.005	0.0075

Notes:

- "C" and "NC" are abbreviations for conforming and nonconforming transverse reinforcement. A joint is conforming if hoops are spaced at ≤ hc/3 within the joint. Otherwise, the component is considered nonconforming.
- P is the design axial force on the column above the joint and Ag is the gross cross-sectional area of the joint.
- V is the design shear force and Vn is the shear strength for the joint.
- Linear interpolation between values listed in the table shall be permitted.

Table 3.5 FEMA 356 modeling parameters and numerical acceptance criteria for nonlinear procedures – member controlled by flexure [49]

Conditions	Modeling Parameters			Acceptance Criteria			
	Plastic Rotation Angle, radians	Residual Strength Ratio	Plastic Rotation Angle, radians				
			Performance Level				
	a	b	c	IO	Component Type		
Primary					Secondary <sup>4</sup>		
				LS	CP	LS	CP

i. Shear walls and wall segments

$\frac{(A_s - A'_s)f_y + P}{t_w l_w f'_c}$	$\frac{Shear}{t_w l_w \sqrt{f'_c}}$	Confined Boundary <sup>1</sup>								
≤ 0.1	≤ 3	Yes	0.015	0.02	0.75	0.005	0.01	0.015	0.015	0.02
≤ 0.1	≥ 6	Yes	0.01	0.015	0.4	0.004	0.008	0.01	0.01	0.015
≥ 0.25	≤ 3	Yes	0.009	0.012	0.6	0.003	0.006	0.009	0.009	0.012
≥ 0.25	≥ 6	Yes	0.005	0.01	0.3	0.0015	0.003	0.005	0.005	0.01
≤ 0.1	≤ 3	No	0.008	0.015	0.6	0.002	0.004	0.008	0.008	0.015
≤ 0.1	≥ 6	No	0.006	0.01	0.3	0.002	0.004	0.006	0.006	0.01
≥ 0.25	≤ 3	No	0.003	0.005	0.25	0.001	0.002	0.003	0.003	0.005
≥ 0.25	≥ 6	No	0.002	0.004	0.2	0.001	0.001	0.002	0.002	0.004

ii. Columns supporting discontinuous shear walls

Transverse reinforcement <sup>2</sup>									
Conforming	0.01	0.015	0.2	0.003	0.007	0.01	n.a.	n.a.	
Nonconforming	0	0.01	0.2	0	0	0	n.a.	n.a.	

iii. Shear wall coupling beams

Longitudinal reinforcement and transverse reinforcement <sup>3</sup>	$\frac{Shear}{t_w l_w \sqrt{f'_c}}$								
Conventional longitudinal reinforcement with conforming transverse reinforcement	≤ 3	0.025	0.05	0.75	0.01	0.02	0.025	0.025	0.05
	≥ 6	0.02	0.04	0.5	0.005	0.01	0.02	0.02	0.04
Conventional longitudinal reinforcement with nonconforming transverse reinforcement	≤ 3	0.02	0.035	0.5	0.006	0.012	0.02	0.02	0.035
	≥ 6	0.01	0.025	0.25	0.005	0.008	0.01	0.01	0.025
Diagonal reinforcement	n.a.	0.03	0.05	0.8	0.006	0.018	0.03	0.03	0.05

Notes:

1. Requirements for a confined boundary are given in ACI 318.
2. Requirements for conforming transverse reinforcement in columns are: (a) hoops over the entire length of the column at a spacing ≤ d/2, and (b) strength of hoops  $V_s \geq$  required shear strength of column.
3. Conventional longitudinal reinforcement consists of top and bottom steel parallel to the longitudinal axis of the coupling beam. Conforming transverse reinforcement consists of: (a) closed stirrups over the entire length of the coupling beam at a spacing ≤ d/3, and (b) strength of closed stirrups  $V_s \geq 3/4$  of required shear strength of the coupling beam.
4. For secondary coupling beams spanning < 8'-0", with bottom reinforcement continuous into the supporting walls, secondary values shall be permitted to be doubled.

Table 3.6 FEMA 356 modeling parameters and numerical acceptance criteria for nonlinear procedures – member controlled by shear [49]

Conditions	Modeling Parameters			Acceptance Criteria					
	Total Drift Ratio (%) or Chord Rotation, radians <sup>1</sup>	Residual Strength Ratio		Acceptable Total Drift (%), or Chord Rotation, radians <sup>1</sup>					
				Performance Level					
	a	b	c	IO	Component Type				
Primary					Secondary				
				LS	CP	LS	CP		
i. Shear walls and wall segments									
All shear walls and wall segments <sup>2</sup>	0.75	2.0	0.40	0.40	0.60	0.75	0.75	1.5	
ii. Shear wall coupling beams <sup>4</sup>									
Longitudinal reinforcement and transverse reinforcement <sup>3</sup>	$\frac{Shear}{t_w l_w \sqrt{f'_c}}$								
Conventional longitudinal reinforcement with conforming transverse reinforcement	$\leq 3$	0.002	0.030	0.60	0.006	0.015	0.020	0.020	0.030
	$\geq 6$	0.016	0.024	0.30	0.005	0.012	0.016	0.016	0.024
Conventional longitudinal reinforcement with nonconforming transverse reinforcement	$\leq 3$	0.012	0.025	0.40	0.006	0.008	0.010	0.010	0.020
	$\geq 6$	0.008	0.014	0.20	0.004	0.006	0.007	0.007	0.012

Notes:

1. For shear walls and wall segments, use drift; for coupling beams, use chord rotation;
2. For shear walls and wall segments where inelastic behavior is governed by shear, the axial load on the member must be  $\leq 0.15A_g f'_c$ ; otherwise, the member must be treated as a force-controlled component.
3. Conventional longitudinal reinforcement consists of top and bottom steel parallel to the longitudinal axis of the coupling beam. Conforming transverse reinforcement consists of: (a) closed stirrups over the entire length of the coupling beam at a spacing  $\leq d/3$ , and (b) strength of closed stirrups  $V_s \geq 3/4$  of required shear strength of the coupling beam.
4. For secondary coupling beams spanning  $< 8'-0"$ , with bottom reinforcement continuous into the supporting walls, secondary values shall be permitted to be doubled.

Table 3.7 FEMA 356 modeling parameters and numerical acceptance criteria for nonlinear procedures – braces in tension [49]

Component/Action	Modeling Parameters			Acceptance Criteria				
	Plastic Deformation		Residual Strength Ratio	Plastic Deformation				
				IO	Primary		Secondary	
	a	b	c		LS	CP	LS	CP
Braces in Tension (except EBF braces) <sup>2</sup>	11 $\Delta_T$	14 $\Delta_T$	0.8	0.25 $\Delta_T$	7 $\Delta_T$	9 $\Delta_T$	11 $\Delta_T$	13 $\Delta_T$

Note:

1.  $\Delta_T$  is the axial deformation at expected tensile yielding load.

### 3.5. Global analysis: principles and methods

Several methodologies have been developed in order to analyze structural models so as to estimate the demand from a seismic action and to determine the level of seismic intensity that may cause a structure to exceed a certain limit state or performance level.

Most seismic codes define four basic analysis procedures. Two procedures are linear and two are nonlinear. The two linear procedures are the Linear Static Procedure (LSP) and the Linear Dynamic Procedure (LDP). The two nonlinear procedures are the Nonlinear Static Procedure (NSP) and Nonlinear Dynamic Procedure (NDP).

Linear procedures are appropriate when the expected level of nonlinearity is low. When higher mode effects are not significant, static procedures are appropriate. This is generally true for short, regular buildings. For tall buildings, buildings with torsional irregularities or non-orthogonal systems, dynamic procedures are required.

The nonlinear static or dynamic procedure is acceptable for most buildings.

The term “nonlinear” in nonlinear analysis procedures implies explicit material nonlinearity or inelastic material response, but geometric nonlinearity may also be included.

As the present thesis is concerned with the aspects of nonlinear behavior of existing and retrofitted buildings, only nonlinear static and dynamic procedures will be detailed.

#### 3.5.1. Nonlinear Static Procedure

Nonlinear static procedures have seen a growing interest in the seismic design of buildings. Several procedures have been developed, mainly as an alternative to more advanced nonlinear time history analysis. The static nonlinear procedures were also used by the Performance Based Evaluation or Design (PBE, PBD) guidelines [53] – [49]. The most known ones are the capacity spectrum method [54] and N2 method [56].

In these procedures, the comparison between the seismic demand and the capacity is made in terms of displacements by applying the equivalent single degree of freedom (SDOF) substitution approach and by plotting a force-displacement curve, namely the “capacity curve”, or a spectral acceleration-displacement curve, namely the “capacity spectrum”.

These methods may be used for any structure and any performance level with some limitations. The most important limitation refers to the influence of higher modes. The procedure should not be used for structures in which higher-mode

effects are significant. Higher-mode effects shall be considered significant if the shear in any storey calculated from the analysis with 90 percent mass participation exceeds 130 percent of the corresponding story shear from the analysis considering only the first mode response.

According to NSP, the model that incorporates the inelastic response is pushed to a certain displacement, called "target displacement", and the forces and deformations are evaluated. The target displacement represents the maximum displacement to be experienced during the design earthquake. Calculated displacements and internal forces are then compared to the allowable values. The NSP requires that at least two lateral load distributions be used, in order to identify the potential failure modes.

The general procedure for the NSP is as follows:

- An elastic model is developed and then loaded with gravity loads according to the definition of the load combination;
- The structure is subjected to a set of lateral loads, using one load pattern. For example Eurocode 8 [48] recommends two load patterns, one proportional to the storey inertia forces and one proportional to the fundamental load of vibration (eg. reversed triangular load).
- The intensity of the lateral load is increased until the weakest component reaches a deformation at which its stiffness changes significantly (a member reaches the yield load or member strength).
- Step 3 is continued as more elements reach their yield load or strength.
- The loading process is continued until the unacceptable performance is detected or a top displacement is obtained that is larger than the maximum displacement expected in the design earthquake at the control **node**.
- The displacement of the control **node** versus base shear at various loading stages is plotted as a representative nonlinear response diagram of the structure. The changes in slope of this curve indicate the yielding of various components.
- The control **node** displacement versus base shear curve is used in order to estimate the target displacement.
- Once the target displacement is known, the accumulated forces and deformations at this displacement of the control **node** should be used in order to evaluate the performance of components and elements.
- If either the force demand in force-controlled actions, components, or elements, or the deformation demand in deformation-controlled actions, components, or elements, exceeds permissible values, then the action, component, or element is deemed to violate the performance criterion.

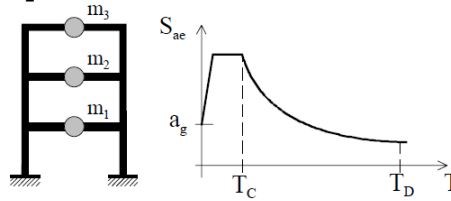
The recommendation to carry out the analysis to at least 150% of the target displacement is meant to encourage the engineer to investigate likely building performance under extreme load conditions that exceed the design values. The engineer should recognize that the target displacement represents a mean displacement value for the design earthquake loading, and that there is considerable scatter about the mean value. Estimates of the target displacement may be unconservative for buildings with low strength compared with the elastic spectral demands.

A short summary of N2 nonlinear static procedure is presented here. This method will be used in order to analyze an existing RC frame building, before and after retrofitting by means of the BRB technique [56].

**3.5.2. Summary of the N2 method [56]**

**I. DATA**

- a) Structure
- b) Elastic acceleration spectrum  $S_{ae}$



**II. DEMAND SPECTRA IN AD FORMAT**

- a) Determine elastic spectrum in AD format

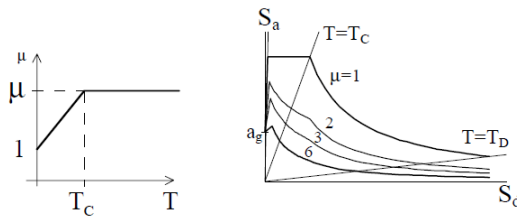
$$S_{de} = \frac{T^2}{4\pi^2} S_{ae}$$

- b) Determine inelastic spectra for constant ductilities

$$S_a = \frac{S_{ae}}{R_\mu}, \quad S_d = \frac{\mu}{R_\mu} S_{de}$$

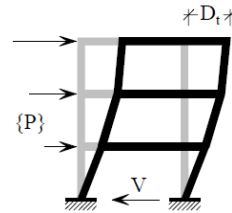
$$R_\mu = (\mu - 1) \frac{T}{T_c} + 1 \quad T < T_c$$

$$R_\mu = \mu \quad T \geq T_c$$



**III. PUSHOVER ANALYSIS**

- a) Assume displacement shape  $\{\Phi\}$
  - b) Determine vertical distribution of lateral forces
- $$\{P\} = [M] \{\Phi\}, \quad P_i = m_i \Phi_i$$
- c) Determine base shear ( $V$ ) – top displacement ( $D_t$ ) relationship



**IV. EQUIVALENT SDOF MODEL**

- a) Determine mass  $m^*$
- $$m^* = \sum m_i \Phi_i^2$$

Note:  $\Phi_n = 1.0$ ,  $n$  denotes roof level

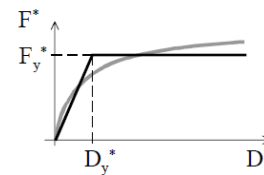
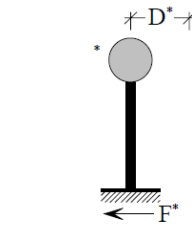
- b) Transform MDOF quantities ( $Q$ ) to SDOF quantities ( $Q^*$ )

$$Q^* = \frac{Q}{\Gamma}, \quad \Gamma = \frac{m^*}{\sum m_i \Phi_i^2}$$

- c) Determine an approximate elasto-plastic force – displacement relationship

- d) Determine strength  $F_y^*$ , yield displacement  $D_y^*$ , and period  $T^*$

$$T^* = 2\pi \sqrt{\frac{m^* D_y^*}{F_y^*}}$$



e) Determine capacity diagram (acceleration versus displacement)

$$S_a = \frac{F^*}{m^*}$$

**V. SEISMIC DEMAND FOR SDOF MODEL**

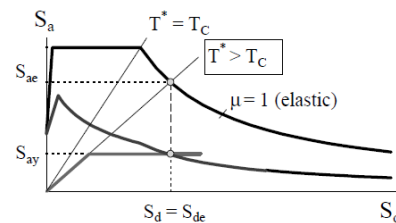
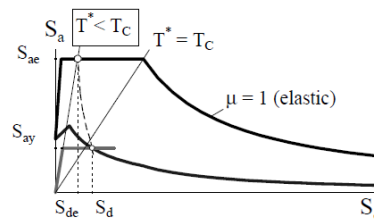
a) Determine reduction factor  $R_\mu$

$$R_\mu = \frac{S_{ae}}{S_{ay}}$$

b) Determine displacement demand  $S_d = D^*$

$$S_d = \frac{S_{de}}{R_\mu} \left( 1 + (R_\mu - 1) \frac{T_c}{T^*} \right) \quad T^* < T_c$$

$$S_d = S_{de} \quad T^* \geq T_c$$



**VI. GLOBAL SEISMIC DEMAND FOR MDOF MODEL**

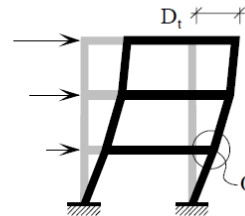
a) Transform SDOF displacement demand to the top displacement of the MDOF model

$$D_t = \Gamma S_d$$

**VII. LOCAL SEISMIC DEMANDS**

a) Perform pushover analysis of MDOF model up to the top displacement  $D_t$  (or to an amplified value of  $D_t$ )

b) Determine local quantities (e.g. story drifts, rotations  $\Theta$ ), corresponding to  $D_t$



**VIII. PERFORMANCE EVALUATION**

a) Compare local and global seismic demands with the capacities for the relevant performance level

**3.5.3. Nonlinear Dynamic Procedure NDP**

With the Nonlinear Dynamic Procedure, the design displacements and internal efforts are not established using a target displacement, but instead they are determined directly through dynamic analysis by using ground-motion histories. The basis, the modeling approaches, and the acceptance criteria for the Nonlinear Dynamic Procedure are similar to those of the Nonlinear Static Procedure.

One of the most promising NDP is the Incremental Dynamic Analysis (IDA). IDA involves the subjecting of a structural model to one (or more) ground motion



record(s), each scaled to multiple levels of intensity, thus producing one (or more) curve(s) of response parameterized versus the intensity level (Figure 3.17).

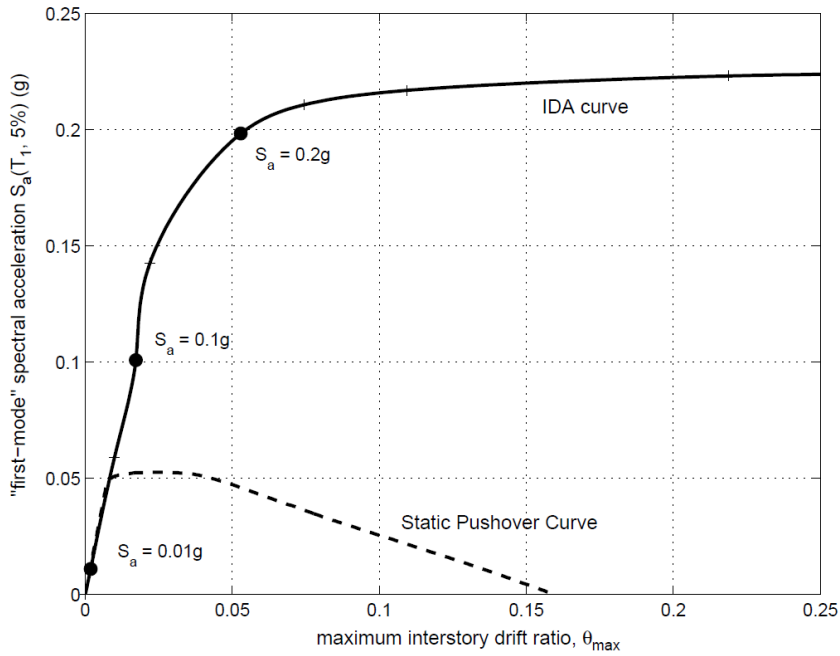


Figure 3.17 Comparison between the IDA curve and the pushover static pushover curve

The structural response is sensitive to the type of ground motion. Therefore, several ground motion records are recommended in order to increase the reliability of the method (Figure 3.18).

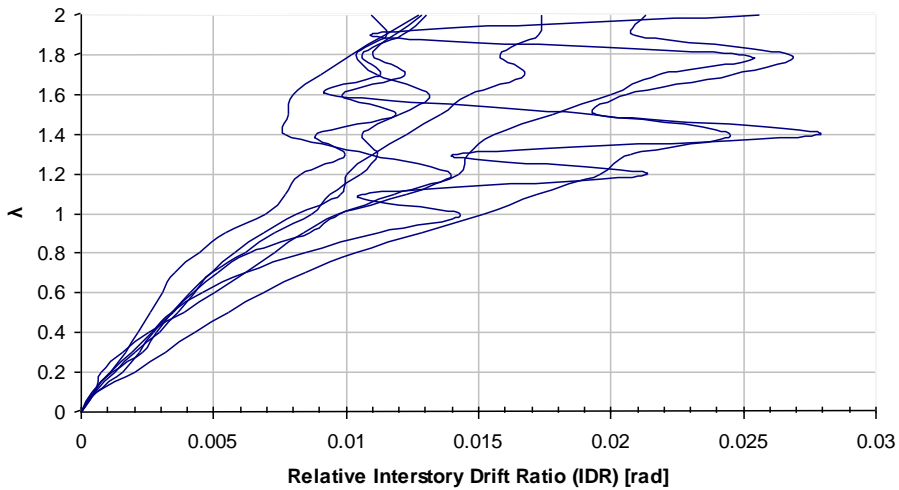


Figure 3.18 Relative interstorey drift vs. seismic multiplication factor  $\lambda$  for several records

Concern is often expressed about the reliability of the results obtained from records that have been scaled up or down. Nassar&Krawinkler [62] used for scaling the records the peak ground acceleration PGA, and the results were rather scattered. Apart from PGA, other scaling methods were used by different researchers:

- Effective peak acceleration (EPA)
- Effective peak velocity (EPV)

EPV and EPA values are effective peak values of velocity and accelerations Lungu & Cornea, 1995 [63]:

$$EPV = \frac{\max \overline{SV}_{0.4s}}{2.5}; \quad EPA = \frac{\max \overline{SA}_{0.4s}}{2.5} \quad (3.10)$$

The definition of the parameters EPA and EPV- invariant to the frequency content of the seismic motions - is obtained by averaging the response spectrum for absolute accelerations SA and the response spectrum for relative velocities SV on a period interval with a reference width of 0.4 s. The average interval is mobile and it is positioned on the axis of periods where the maximum of the average of the spectral values is obtained, respectively:

- Spectral acceleration corresponding to the fundamental mode of vibration;
- Mean spectral acceleration for a range of vibration periods.

### 3.6. Case study: application of BRB to an existing RC building

This study aims at the evaluation of the seismic vulnerability of an existing reinforced concrete frame building RC, designed for gravity loads GLD. The building was designed and constructed in the '60. As the results of the analysis showed very poor behavior, seismic upgrade was necessary. The retrofitting technique selected for this application was buckling restrained X braces BRB.

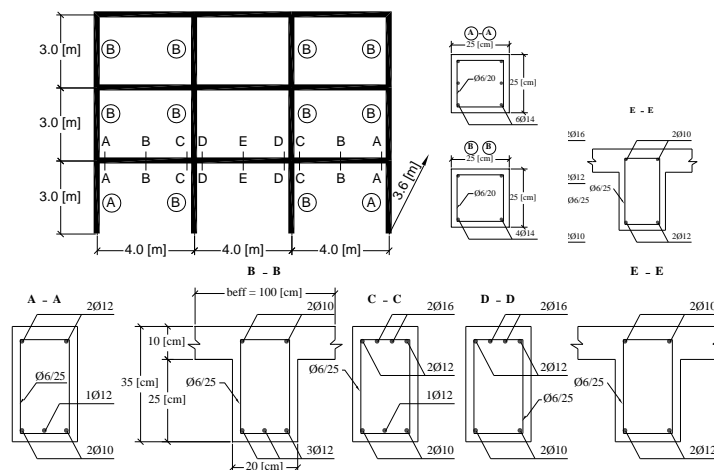


Figure 3.19 Frame geometry, characteristic beam and column cross-sections

Common materials used in the period of construction, like B200 concrete (corresponding to class C12/15 in Eurocode 2 [59]) and reinforcement steel OB37

(with a characteristic yield strength of 235 N/mm<sup>2</sup>) were considered for the structure.

### 3.6.1. Frame design and strengthening solution

The design of the RC frame for gravity loads was done according to the Romanian codes in force at that time. The building is located in Bucharest. The beam's effective width was considered only for sections at mid-span. Detailing of the reinforcement was characteristic for the design practice used in Romania in that period:

- poor anchorage length of bottom bars at the supports;
- inclined reinforcement used for shear force resistance;
- open stirrups, largely spaced (20 - 25 cm) in potential plastic zones.

External walls of the building are made of infill masonry 38 cm thick. In Table 3.8 are presented the loads and in Table 3.9 the combination of loads, both according to the original design and the modern code design.

Table 3.8 Type of gravity loads

Loads	original	modern
	design	code design
	[kN/m <sup>2</sup> ]	[kN/m <sup>2</sup> ]
Dead Load (DL)	3.08	3.08
Live Load* (LL) - roof level	3.00	2.00
Live Load (LL) - current level	1.50	1.50
Snow Load(SL)	1.00	1.60
Wind Load(WL)	0.70	0.52

Table 3.9 Load combinations

Fundamental Combinations	original design	modern code design
1	1.3(DL+LL1+SL)	1.35DL+1.5LL1+ +1.05(SL+WL)
2	1.3(DL+LL2+SL)	1.35DL+1.5LL2+ +1.05(SL+WL)
3	1.3(DL+LL3+SL)	1.35DL+1.5LL3+ +1.05(SL+WL)
4	1.2 (DL+LL1+SL+ +WL)	DL+LL1+ +0.7(WL+SL)

Table 3.10 Verification of beams

Beam Sections	Internal actions symbol	design	internal actions	
		strength	original code	modern code
A	M [kNm]	15.32	15.00	14.80
	Q [kN]	118.00	23.84	22.95
B	M [kNm]	23.00	22.83	21.47
C	M [kNm]	42.21	31.84	25.68
	Q [kN]	143.00	31.47	30.31
D	M [kNm]	42.36	27.58	26.02
	Q [kN]	144.30	28.40	26.02
E	M [kNm]	15.34	13.31	11.37

Beam Sections	Internal actions symbol	design* strength	internal actions	
			original code	modern code
A	M [KNm]	43	4.25	7.72
	N [KN]		399.35	390
B	M [KNm]	38	10.95	6.22
	N [KN]		371	368

\*the design strengths were determined to gravity axial load of the each column element

### 3.6.2. Strengthening solution

Three strengthening solutions were considered for seismic upgrade i.e. steel BRB's only, confinement of the ground and first floor columns using fiber reinforced polymers (FRP) and the combination of the previous two solutions.

The BRB's were introduced only in the middle span, as inverted V braces. The design of the BRB's was done according to Eurocode 3 [64], following the procedure described in AISC 2005 [17]. Design seismic forces were obtained by using spectral analysis with a reduction factor  $q$  equal to 6. The steel core of the buckling restrained brace was considered to be of rectangular shape. Cross-section areas of braces resulted from the design are:

- ground floor  $A=250 \text{ mm}^2$
- first floor  $A=230 \text{ mm}^2$
- second floor  $A=112 \text{ mm}^2$

### 3.7. Analysis procedure

A pushover analysis was applied in order to evaluate the performances of the frame building before and after retrofitting. Displacement demands were estimated according to the N2 method implemented in Eurocode 8 [48] (see previous section). Seismic action is characterized by an elastic response spectrum with a peak ground acceleration  $a_g=0.24g$  and a control period  $T_c=1.6s$ . The performance of the structure was evaluated in terms of inelastic deformation demand corresponding to the ultimate limit state. The development of the plastic mechanism was also monitored.

An inverse triangular distribution pattern of the lateral forces were considered in the analysis.

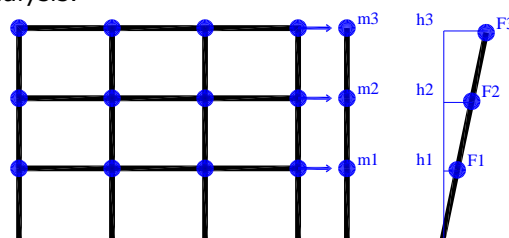


Figure 3.20 Lateral load pattern

The performance of structural elements at the ultimate limit state was defined in terms of:

- plastic rotations of beams and columns;
- axial plastic deformations for buckling restrained braces.

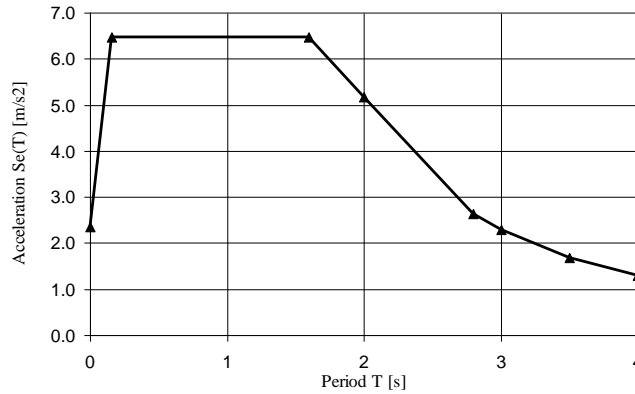


Figure 3.21 Elastic response spectrum for construction site

### 3.8. Modeling for pushover analysis

As the detailing of RC elements was considered insufficient, concrete was taken as unconfined. The material model was considered according to Kent & Park [58] (Figure 3.22), as an unconfined material with linear softening of the rigidity and no tension. The concrete compressive strength was considered equal to  $f'_c=12.5$  N/mm<sup>2</sup>, while the ultimate strain  $\epsilon_f=0.015$ .

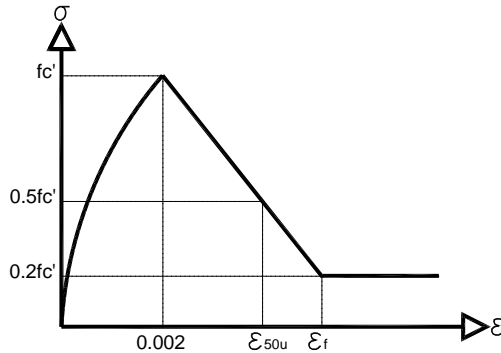


Figure 3.22 Kent & Park unconfined concrete definition [58]

Due to the poor anchorage length of the bottom longitudinal reinforcement in the beams, equivalent yield strength of the steel was used by applying the equation FEMA356 [49]:

$$f_{y,eq} = f_y \times \frac{L_{b,av}}{L_{b,req}} \quad (3.11)$$

where:

- $f_{y,eq}$  = equivalent yield strength;
- $f_y$  = steel reinforcement yield strength;
- $L_{b,av}$  = available anchorage length;
- $L_{b,req}$  = required anchorage length (according to Eurocode2).

Table 3.12 shows the sections where anchorage was insufficient and the yield strength needs to be corrected with  $f_{y,eq}$ . The reinforcing steel has the characteristic yield strength of 235 N/mm<sup>2</sup> and it was defined as a bilinear material with strain hardening.

Table 3.12 Equivalent yield strength of the reinforcements

Element	Section	Diameter [mm]	$L_{b,req}$ [mm]	$L_{b,av}$ [mm]	$f_{y,eq}$ [N/mm <sup>2</sup> ]
Beams	A	Φ12	505	225	104.70
		Φ10	421.2	225	125.53
	C	Φ10	421.2	250	139.48
		Φ12	505	250	116.34
	D	Φ10	421.2	250	139.48
Column	A, B	Φ14	589.7	560	223.16

Unlike the beams, where original effective width was considered only for the sections along the span, a 72 cm effective width, according to FEMA356 [49], was considered. Four rebars of 8 mm spaced at 18 cm, have been considered for the slab in the effective width. The effective stiffness of the members corresponding to cracked cross-section was reduced according to FEMA 356 [49] as follows (Table 3.13):

- beam flexural stiffness was reduced by 0.5;
- column flexural stiffness was reduced depending on the level of axial force.

Table 3.13 Column stiffness reduction according to FEMA356 [49]

Edge Columns	Floors	Stiffness reduction	Internal Columns	Floors	Stiffness reduction
	second	0.5		second	0.5
	first	0.5		first	0.525
	ground	0.7		ground	0.67

For plastic analysis, beams and columns were modeled by using concentrated plasticity at the ends, defined as rigid plastic bilinear moment-rotation relationship. The plastic hinge length was calculated with the relation [65]:

$$L_{pi} = 0.08 \times L_i + 0.022 \times d_i \times f_y \quad (3.12)$$

where:

$L_i$  = half of the span of the element,

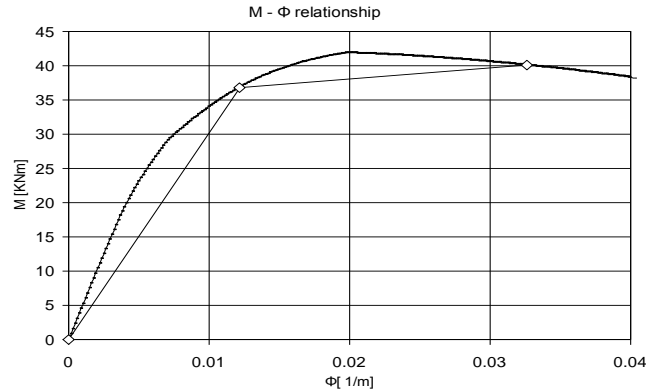
$d_i$  = the diameter of the longitudinal reinforcement and  $f_y$  = characteristic strength for steel.

The plastic hinge length resulted  $L_{p (column)} = 0.19$  m and  $L_{p (beam)} = 0.21$  m.

The bilinear idealization of moment curvature was obtained by considering:

- the yield point occurred when the rebars yield or concrete attains its compressive strength;
- the ultimate curvature calculated at the point when the materials reached their ultimate strains (e.g. 0.005 for concrete and 0.05 for steel);
- a 1% hardening applied to the initial stiffness was considered (Figure 3.23).

The M- $\Phi$  relationships for columns were obtained by using the axial force from the gravitational loads in the earthquake combination.

Figure 3.23 M- $\Phi$  relationship

Buckling restrained braces were considered pinned at the ends. The inelastic behavior was modeled by concentrated plasticity. The material used for BRB was S235 steel grade. For a length of 3.6 m, the yield displacement  $\Delta_y$  amounted 4 mm. The ultimate displacement  $\Delta_u$  was estimated based on experimental results presented in Newell tests [66]. Based on these results, ductility ratios  $\Delta_u/\Delta_y$  were estimated for tension and compression, amounting to 8.3 and 7.5 respectively. In order to obtain the adjustment of the design strengths (maximum compression strength  $C_{max}$  and maximum tension strength  $T_{max}$ ), the AISC formulas [17] were applied, see equations below:

$$T_{max} = \omega \cdot R_y \cdot f_y \cdot A \quad (3.13)$$

$$C_{max} = \omega \cdot \beta \cdot R_y \cdot f_y \cdot A \quad (3.14)$$

where:

$f_y$  is the yield strength;

$R_y$  is the ratio of the expected yield stress to the specified minimum yield stress  $f_y$  (considered equal to 1).

The experimental values of the compression adjustment factor  $\beta=1.05$  and strain hardening adjustment factor  $\omega=1.25$  were obtained using AISC formulas [17], see equation:

$$\beta = \frac{C_{max}}{T_{max}} \quad \text{and} \quad \omega = \frac{T_{max}}{f_{fysc} \cdot A} \quad (3.15)$$

where:

-  $f_{fysc}$  is the measured yield strength of the steel core.

Behavior of BRB members can be modeled with a bilinear force-deformation relationship with hardening. Figure 3.24 BRB behavior model shows the BRB behavior model for all 3 storeys.

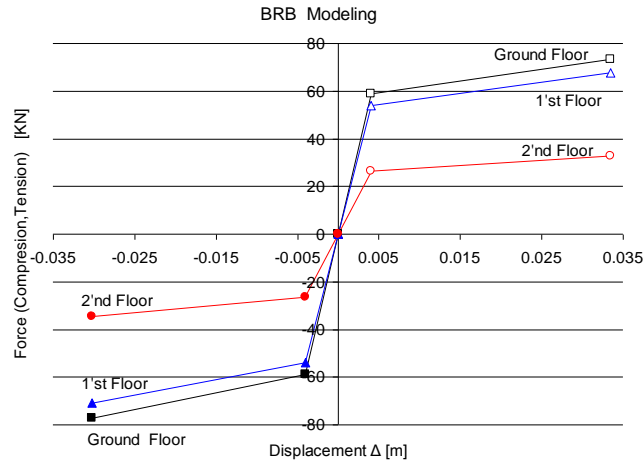


Figure 3.24 BRB behavior model

In order to enhance the ductility of reinforced concrete columns, they were strengthened with FRP [67]. The fabric was applied in horizontal layers, in order to increase the confinement of the concrete. The effect of confinement by FRP consisted in an increase of the concrete compression strength (from  $12.5 \text{ N/mm}^2$  to  $40.8 \text{ N/mm}^2$ ) and of the ultimate strain (from 0.005 to 0.02) (Figure 3.25) [67]. The strength increases 3 times for the design axial strength corresponding to the balance point (from 987 kN to 2771 kN for column section A) and about 20% of the the design moment resistance corresponding to an axial force of 389.6 kN from seismic combination (in the column section A).

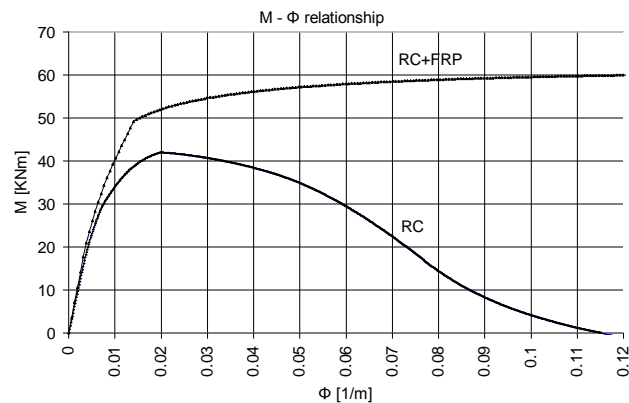


Figure 3.25 Effect of the confinement by FRP on the moment-curvature relationship corresponding to an axial force of 389.6 kN from seismic combination of column section A.

### 3.9. Performance assessment

#### 3.9.1. Initial RC frame (MRF)

Analysis of the original RC frame (MRF) showed an unsatisfactory seismic response. First plastic hinges developed in columns. Plastic mechanism involved columns from the first and second floors (Figure 3.26a), and also some beams from the first storey. Lateral drifts at the ultimate limit state indicated a concentration of



damage in the first two storeys. At ultimate limit states, columns failed due to the exhaustion of the rotation capacity. It can be observed that the structure has a limited global ductility, because columns attain ultimate plastic deformations at a top displacement four times smaller than the top displacement demand associated with the design earthquake. The fundamental period of vibration and the target displacements at the ultimate limit state for the original reinforced concrete frame and for the retrofitted structures are presented in Table 3.14. The fundamental period of vibration and the target displacements for the considered structures

### **3.9.2. Strengthening with buckling restrained braces**

When the frame is strengthened with buckling-restrained braces, the strength and the stiffness of the frame increase considerably (Figure 3.27). The top displacement demand at the ultimate limit state decreases by almost 50%. The first plastic hinges developed in the column, followed by plastic hinges in braces and beams. The plastic mechanism involves the first two storeys (Figure 3.26b and Figure 3.28). This strengthening solution reduces the overall damage in the structure, as less plastic hinges form in the reinforced concrete elements at the target displacement (Figure 3.26b). However, seismic performance is still unsatisfactory, as inelastic deformations in columns, braces and beams corresponding to the ultimate limit state are exhausted before reaching the target displacement.

### **3.9.3. Strengthening by fiber reinforced polymers**

As an alternative to strengthening by buckling restrained braces, the possibility to improve seismic performance by confining the columns with FRP was investigated. FRP was applied only for columns from the ground floor and the first floor. The FRP fabric was considered as applied on the horizontal direction only, which ensures a confinement of the concrete, but does not act as supplementary reinforcement. The application of FRP resulted in an increase of the axial force capacity and the ductility of the columns, and a slight increase of the bending moment capacity.

The overall structural response did not change significantly (Figure 3.27) but the ultimate deformation in columns (corresponding to the ultimate limit state) was increased. Consequently the first plastic hinge developed in the beam element. The ultimate deformation in the column was attained at larger top displacement demands than in the case of the original frame (Figure 3.26c and Figure 3.27). Also, the top displacement and the interstorey drift demands at the ultimate limit state did not change significantly, as compared to the initial frame.

### **3.9.4. Strengthening by BRB and FRP**

Strengthening of the RC frame by means of BRB's only did not eliminate the failure of RC members. Therefore, a consolidation by both FRP and BRB systems was considered. The main beneficial effect of the BRB system is the improvement of global force-deformation characteristic (increased strength and stiffness), which results in lower top displacement demands at the ultimate limit state (Figure 3.27). On the other hand, FRP technique enhances the local behaviour of columns by increasing their ductility. Also, it must be specified that the first plastic hinge in column elements is attained in the unconfined column from the second floor. Consequently, less damage is observed in columns (Figure 3.26d and Figure 3.27). Inelastic demands in beams and buckling restrained braces are still large. Ultimate

plastic deformations in bracings and beams are attained at top displacements lower than the displacement demand at the ultimate limit state.

The structure was also studied as moderately dissipative using a behavior factor  $q=3$  in order to design buckling restrained braces. Consequently the cross-section of BRB's was doubled, resulting in a more rigid system and the displacement demand was reduced by 35% with respect to the ductile system (designed with  $q=6$ ).

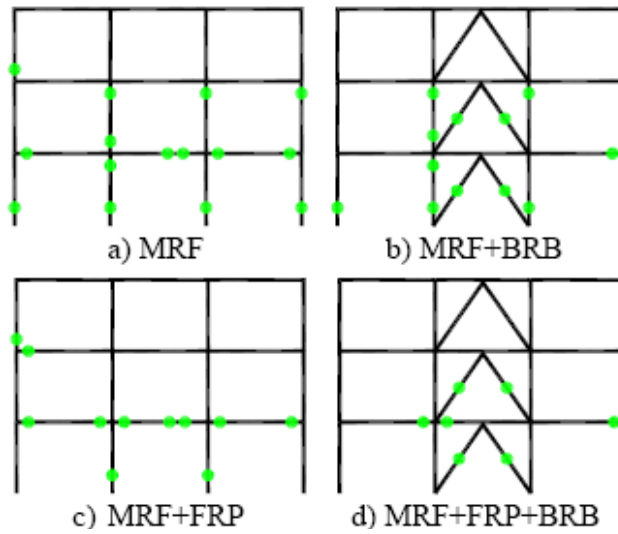


Figure 3.26 Plastic hinges with inelastic deformations larger than the ULS capacity at the target displacement

Table 3.14 The fundamental period of vibration and the target displacements for the considered structures

Structure	Period T [s]	Target displacement $d_t$ [m]
MRF + FRP + BRB	0.64	0.222
MRF + BRB	0.64	0.224
MRF+FRP	1.0	0.395
MRF	1.0	0.39

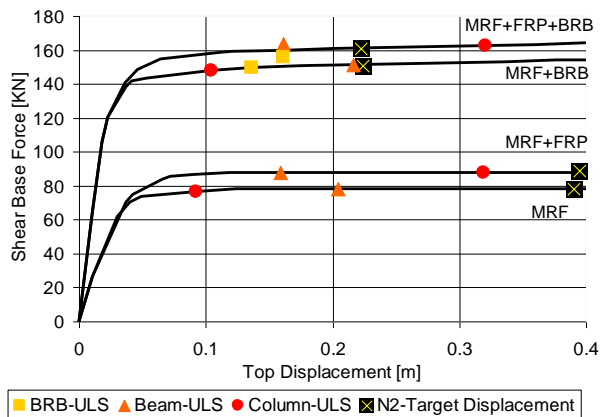


Figure 3.27 Pushover curves of the analyzed frames

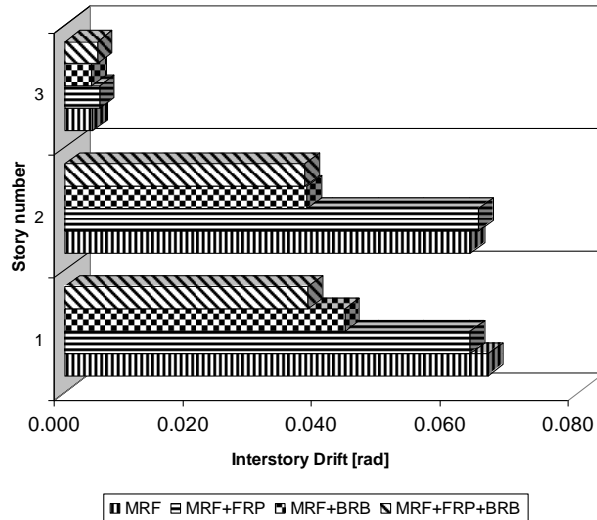


Figure 3.28 Interstorey drift demands at the target displacement

Displacement Demand		
BRB displacement inside RC frame with/without FRP contribution	Pushover analysis target demand	FEMA 356 criteria
	(ULS*)	(LS**)
(-)FRP	62.0	28
(+)FRP	56.0	28

\* ULS – corresponding to LS (life safety)  
 \*\* LS – CBF braces in tension – plastic deformation

Table 3.15 Displacement demand and acceptance criteria (FEMA), in mm

### 3.10. Conclusions

RC frames designed for gravity loads GLD are vulnerable to seismic actions and need seismic rehabilitation in order to comply with modern seismic design requirements. The seismic upgrade of this structure by means of buckling restrained braces was investigated. The main effect of the dissipative bracing system is the improvement of overall strength and stiffness. However, the application of the dissipative bracing system alone is not sufficient for an appropriate seismic performance. Additionally, the existing RC members should be strengthened locally. The most convenient solution seems to be the application of FRP on beams and columns. The analysis showed that the seismic rehabilitation of RC GLD frames cannot be accomplished by means of very ductile dissipative bracing systems without a proper strengthening of RC members.

In the present study, only the columns have been confined (not strengthened!) with FRP. A better response capacity of a BRB strengthened moment-resisting frame is expected if both RC columns and beams are properly reinforced with FRP. In fact, if FRP reinforcement is effective, the beams and columns will work mainly in the elastic domain, while ductile steel BRB will be responsible for the dissipative behavior. Therefore a Performance Based Design approach could be more effective.

## **4. CHARACTERIZATION AND EVALUATION OF BUCKLING RESTRAINED BRACES: EXPERIMENTAL PROGRAM.**

### **4.1. BRB experimental program**

#### **4.1.1. Introduction**

In Chapter 3, a three-storey three-bay RC frame, designed and built in accordance with the technical regulation in service during the '60s, was evaluated and then strengthened with a BRB system. The strengthening system was applied at the inner span of the concrete frame. Nonlinear static analyses were performed in order to evaluate the contribution of the BRB system. The introduction of BRBs aims at strengthening the frame but also at providing additional ductility.

In order to check the effectiveness of the strengthening system, tested numerically in Chapter 3, the BRB elements have been tested experimentally. This chapter mainly focuses on the experimental results but also on the comparisons with the numerical values obtained in Chapter 3. The experimental program comprised twelve specimens, tested monotonically and cyclically. Different types of unbonding materials were used.

The main objectives of the experimental program developed at the Politehnica University of Timisoara, Laboratory of Steel Structures, were as follows:

- Confirmation of the modeling technique and parameters used in the numerical analysis in Chapter 3;
- Evaluation of the influence of the unbonding material. Three materials, i.e. rubber with 3 mm thickness, 2 mm thick asphalt bitumen and 1 mm thick PVC film were used;
- Evaluation of the influence of the loading protocol in the case of cyclic loading
- Comparison of plastic deformation demand with the acceptance parameters.

#### **4.1.2. Test Arrangements**

A typical BRB specimen consisted of a steel core and a steel tube filled with concrete, see Figure 4.1. Twelve BRB specimens were tested, four specimens for each unbonding material. Testing protocol included two monotonic tests, one in tension and one in compression, and two cyclic tests. For cyclic tests, both AISC 2005 [42] and modified ECCS [60] cyclic loading protocols were used.

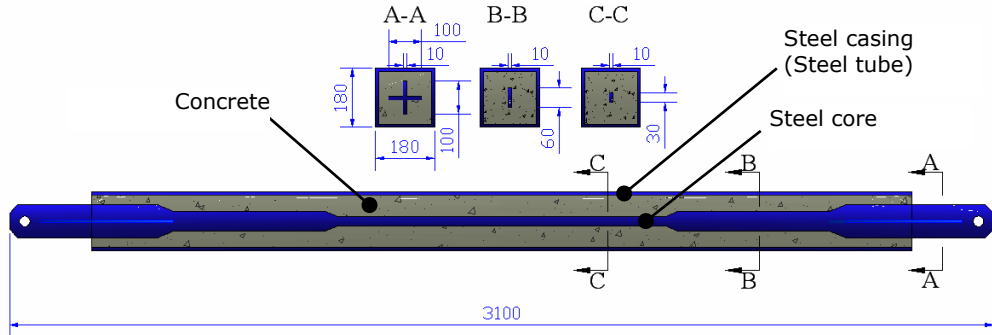


Figure 4.1 Geometry of the tested BRB element

According to AISC 2005 [42] testing protocol, apart from tests on materials and connections, a subassembly test (see Figure 4.2 ) and a uniaxial test shall be performed. The purpose of the subassembly test is to provide evidence that the brace design can satisfactorily accommodate the deformation and rotational demands associated with the design and further, to demonstrate that the hysteretic behavior of the brace in the subassembly is consistent with that of the individual brace elements tested uniaxially. The uniaxial test is used so as to obtain the design parameters of the BRB.

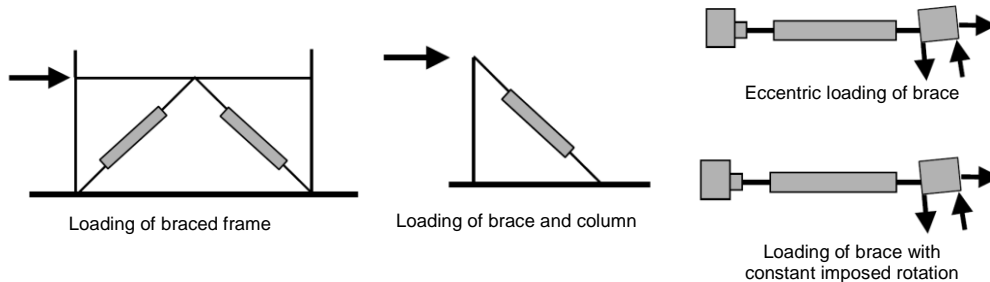


Figure 4.2 Subassembly BRB test, according to AISC 2005 [42]

The scheme of the unit test for BRB conformity test (Type I) is shown in Figure 4.3 , where the span and the height of the model represent the half span of the regular RC frame and the storey height of the RC frame that is subjected to retrofitting with BRB, respectively.

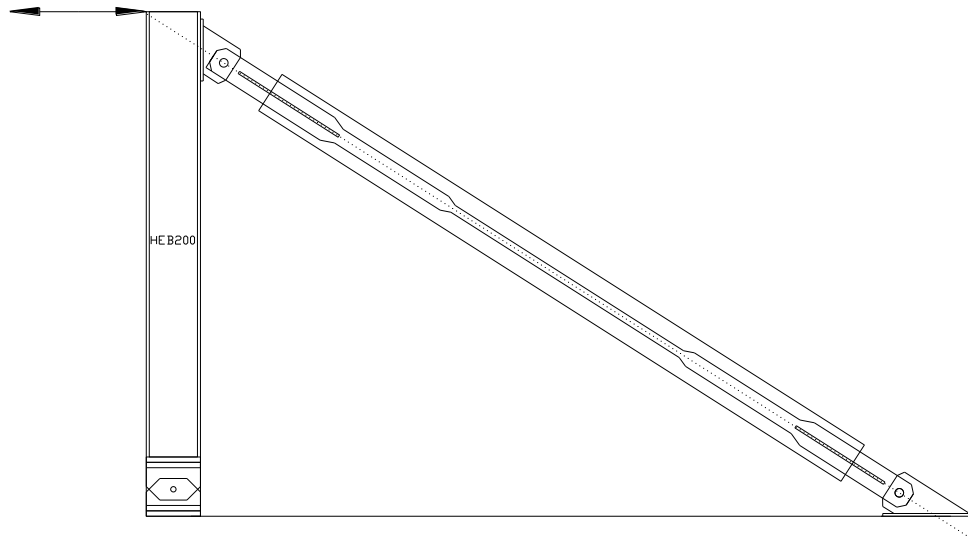


Figure 4.3 Type I subassembly

A second unit test on a braced portal frame (Figure 4.4 ) is aimed to check the behavior of the RC frame under monotonic loading (in tension and in compression) and cyclic loading. This test, which will be described in more details in chapter VI, also aims at validating the retrofitting solution applied in chapter V for an existing RC building frame.

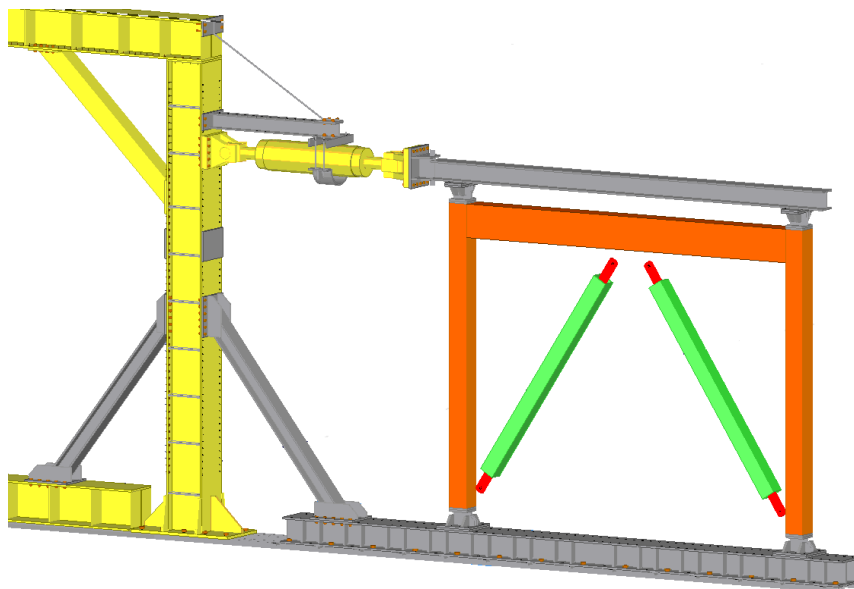


Figure 4.4 Test setup for Type II subassembly

## 4.2. Experimental setup, proposed BRB system and loading protocol

### 4.2.1. BRB specimens

The specimens tested in the experimental program were isolated from the inner span of the first floor of the analyzed frame (see Figure 4.5 ).

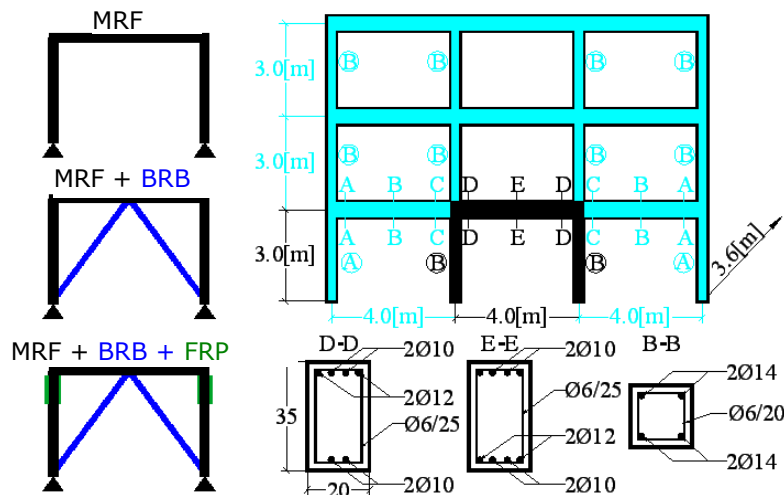


Figure 4.5 Reinforced concrete frame considered in the experimental program

The BRB design follows the provisions of EN 1998-1 for centrally braced steel frames and also the provisions of AISC 2005 [42]. The BRB system is represented by a steel core plate and a steel casing (steel tube) filled with concrete. The steel core plate is designed to resist the loads and dissipate seismic energy by yielding, while the steel casing filled with concrete inside resists overall brace buckling and restrains high-mode steel core buckling.

The manufacture of the BRB elements was conducted at the Steel Structure Laboratory within the Politehnica University of Timisoara (see Figure 4.6 ) and was composed of:

- wrapping of steel core (material characteristics S275 -  $f_y = 275 \text{ N/mm}^2$ ,  $f_u = 400 \text{ N/mm}^2$ ,  $A\% = 34\%$ ),
- insertion of the wrapped core in the steel tube (S275 steel, 4mm thick)
- centering and fixing of the wrapped steel core inside the tube
- fixing the tube in vertical position
- pouring the concrete inside the tube (C40/50 concrete)

As it may be observed in Figure 4.1, the definition of the steel core is based on three sections: active segment (or yielding segment), transition segment and end connection segment. In order to avoid the out-of-plane buckling of the connection segment, which is outside of the restraining steel tube, it was stiffened with two transversal plates.





Figure 4.6 Manufacturing of BRB elements: wrapped BRB elements; centering and fixing inside the tubes; pouring the concrete in vertical position

#### 4.2.2. Test setup

In order to study the behavior of the BRB element, a unit test has been performed. The test was carried out according to AISC 2005 [42] recommendations. Figure 4.7 shows the test setup. The materials used for the test specimen were as follows: for the steel core - S275 steel ( $f_y = 275 \text{ N/mm}^2$ ,  $f_u = 400 \text{ N/mm}^2$ ,  $A\% = 34\%$ ); three types of unbonding materials (i.e. PVC transparent film, rubber and asphalt bitumen) and, as infill material, concrete C40/50.

Two monotonic tests (one in tension and one in compression) and two cyclic tests have been performed for each type of BRB.

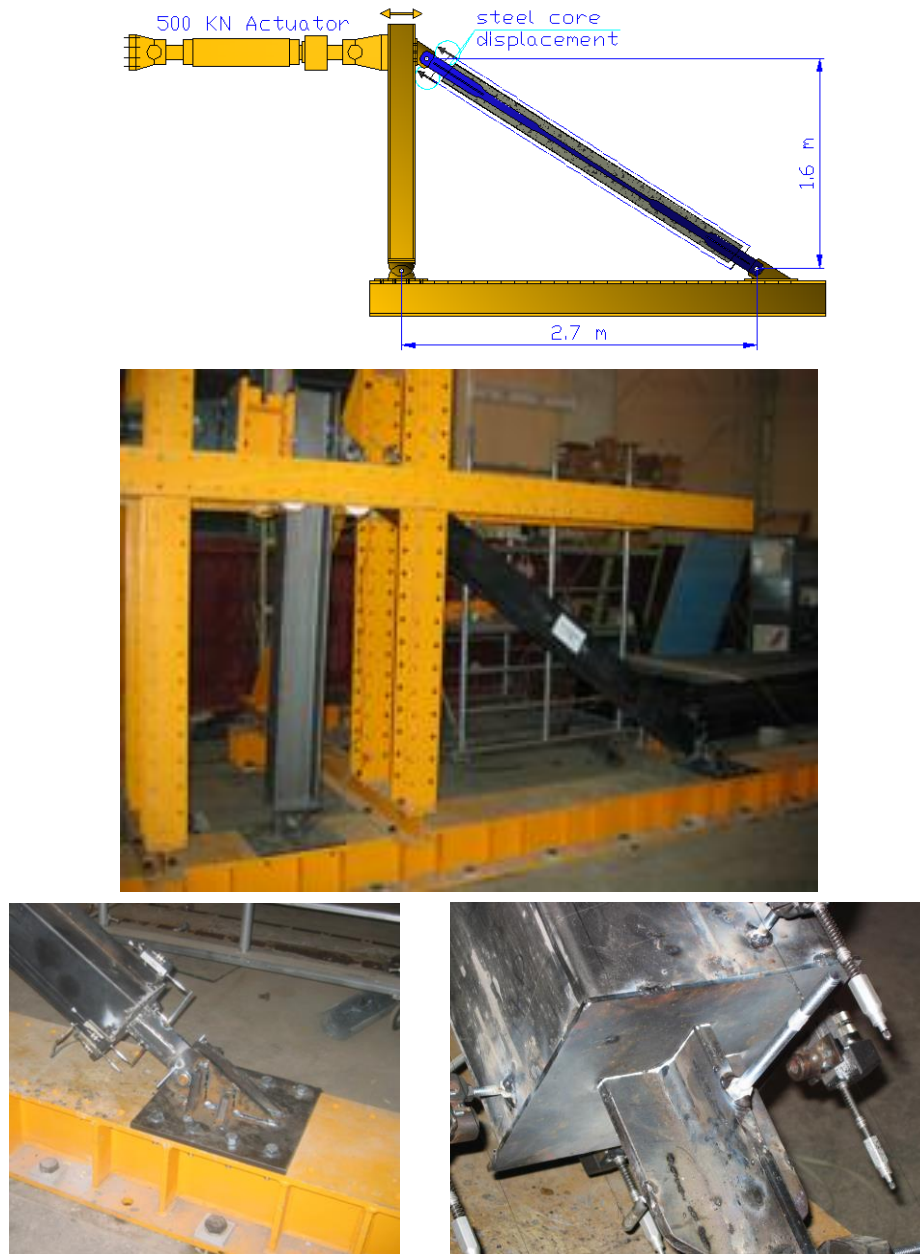


Figure 4.7 Test setup

The test was conducted by controlling the displacement and the following parameters have been measured during the tests: the steel core displacement, the pin-ended connection displacement (to check the steel plate in bearing) and the global rotation of the BRB.

**4.2.3. Test results**

The yielding displacement ( $D_y$ ) and the corresponding yielding force ( $F_y$ ) from the monotonic tests are summarized in Table 4.1.

Table 4.1 Yielding displacements and yielding forces for BRB, for different unbonding materials

Unbonding material		Dy	Fy
		mm	kN
PVC (transparent) film (t = 1 mm)	C*	1.89	124.73
	T**	1.87	126.79
Asphaltic Bitumen (t = 2 mm)	C	2.11	129.72
	T	NA	NA
Rubber (t = 3 mm)	C	2.24	129.85
	T	1.44	128.66

\*C – compression; \*\*T - tension.

Figure 4.8 shows the force-displacement diagrams for the monotonic tests. The tests have shown that the particular unbonding material can significantly influence the deformation capacity. The difference between the deformation capacity in tension and in compression is reduced. The reference values of  $F_y$  and  $D_y$  reached 1.91mm and 128 kN, respectively, and were determined as the mean values of the individual tests.

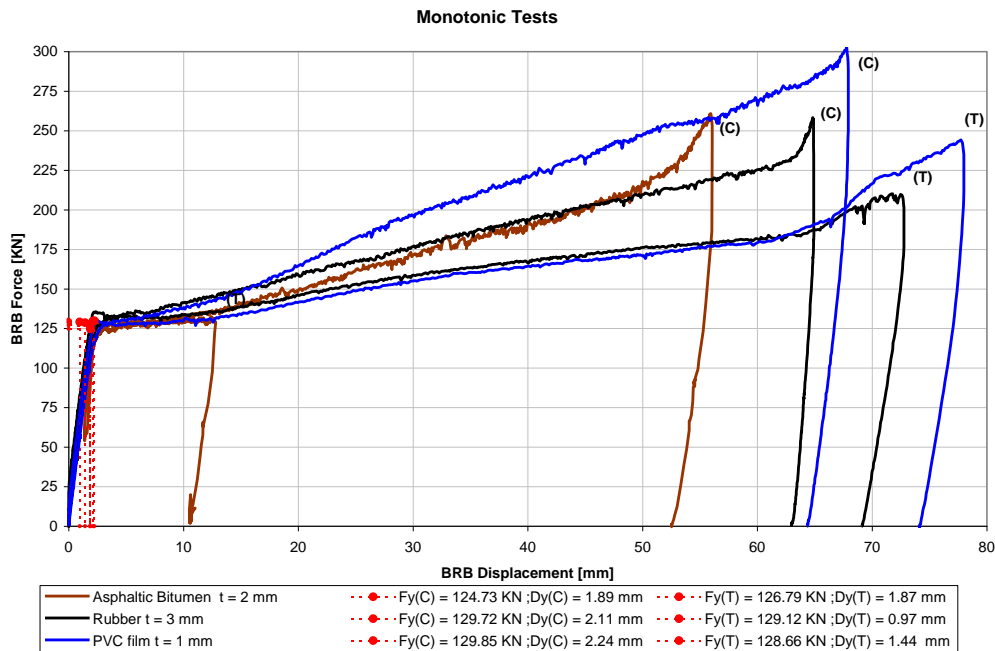


Figure 4.8 The monotonic behavior of the BRB tests (compression vs. tension)

For the cyclic tests, two loading protocols were applied. For the 1<sup>st</sup> specimen, the cyclic loading was applied according to AISC 2005 [42].

According to AISC 2005 [42], the loading sequence shall be applied to the test specimen to produce the following deformations:

- 2 cycles of loading at the deformation corresponding to  $\Delta_b = \Delta_{by}$

- 2 cycles of loading at the deformation corresponding to  $\Delta_b = 0.50\Delta_{bm}$
- 2 cycles of loading at the deformation corresponding to  $\Delta_b = 1\Delta_{bm}$
- 2 cycles of loading at the deformation corresponding to  $\Delta_b = 1.5\Delta_{bm}$
- 2 cycles of loading at the deformation corresponding to  $\Delta_b = 2.0\Delta_{bm}$ .
- Additional complete cycles of loading at the deformation corresponding to  $\Delta_b = 1.5\Delta_{bm}$  as required for the brace test specimen, so as to achieve a cumulative inelastic axial deformation of at least 200 times the yield deformation (not required for the unit test specimen). The design storey drift shall not be taken as less than 0.01 times the storey height for the purposes of calculating  $\Delta_{bm}$ .

A characteristic of this loading protocol is the repetition of two cycles at  $D_y$ , followed by groups of two cycles with increments of  $0.5D_{bm}$ , until the cumulative inelastic deformation reaches at least 200 times  $D_y$ . For the 2<sup>nd</sup> specimen, the modified ECCS [60] cyclic loading protocol was applied. This loading protocol is characterized by a single loading at  $D_{y/4}$ ,  $2D_{y/4}$ ,  $3D_{y/4}$  and  $D_y$ , followed by three repetitions at  $4D_y$ ,  $8D_y$ , the end of the protocol being at 200 times  $D_y$ . As a remark, the cumulative plastic displacement of 200 times  $D_y$  was used in both protocols, as a reference value. The two loading protocols are plotted in Figure 4.9 .

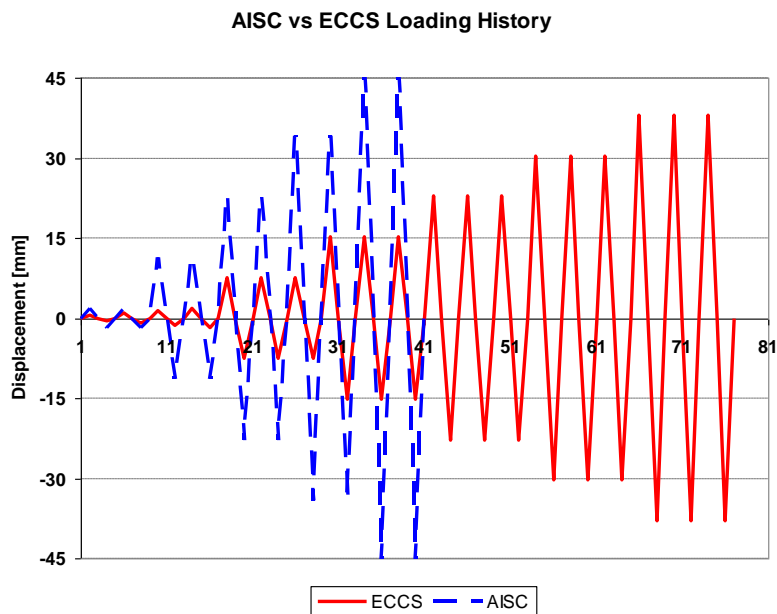


Figure 4.9 The AISC [42] and ECCS [60] loading protocols for cyclic tests

It can be seen from Figure 4.9 that the specimens tested under ECCS [60] loading protocol are more prone to fail due to low cycle fatigue compared to AISC [42], due to the larger number of cycles (Table 4.2). The hysteretic behavior of the BRB with PVC transparent film unbonding material is presented in Figure 4.10 . These bracing elements exhibited symmetrical and stable hysteretic behavior under tensile and compressive forces, through significant inelastic deformations.

Table 4.2 Summary of cyclic tests

BRB Type function of unbonding materials	D <sub>y</sub> mm	F <sub>y</sub> kN	AISC			ECCS					
			no. of cycles	D <sub>u</sub> (+)* mm	D <sub>u</sub> (-)* mm	D <sub>cum</sub> ** mm	no. of cycles	D <sub>u</sub> (+)* mm	D <sub>u</sub> (-)* mm	D <sub>cum</sub> ** mm	
PVC (transparent) film (t = 1 mm)	C*	1.89	124.73	10	45.8	46.1	448	16	30.5	31.4	432
	T**	1.87	126.79								
Asphaltic Bitumen (t = 2 mm)	C	2.11	129.72	7	35.0	34.3	196	13	22.8	22.9	252
	T	NA	NA								
Rubber (t = 3 mm)	C	2.24	129.85	9	45.6	45.6	356	14	30.4	30.4	312
	T	1.44	128.66								

\* D<sub>u</sub> (+) – max/min plastic displacement  
 \*\* D<sub>cum</sub> – cumulative displacement

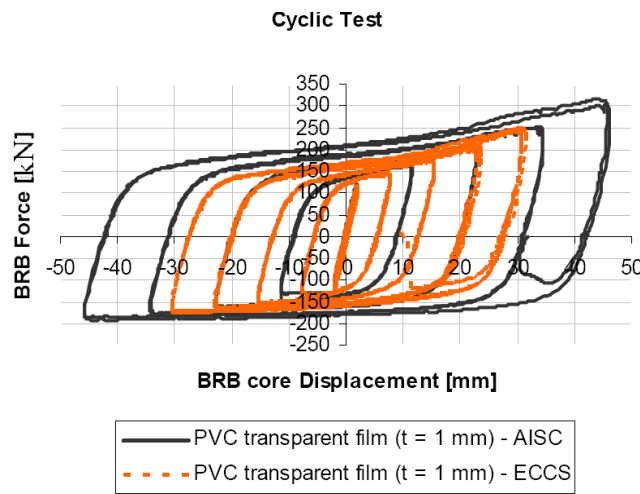


Figure 4.10 Hysteretic behavior of the BRB with PVC transparent film unbonding material, AISC [42] and ECCS [60] loading protocols

In Figure 4.11 , the envelopes of BRBs with PVC transparent film unbonding material are displayed for ECCS [60] and AISC [42] loading protocols, in comparison with monotonic tension and compression curves. A similar behavior can be observed under cycling loading for the two cyclic loading protocols, except for the reduction of the ultimate displacement due to low cycle fatigue in the case of the ECCS [60] one. There is also a good agreement between cyclic envelopes and monotonic curves.

Figure 4.12 shows one specimen after the test. There can be seen the sine wave shape after plastic buckling, which enabled for stable and highly dissipative loops during cyclic test.

The ductility capacity of the BRB elements can be characterized by means of the energy based ductility index ( $\mu_{\%}$ ). This index was used in order to compute the ductility for all types of unbonding materials, based on the experimental results obtained in the cyclic tests. The results are summarized in Table 4. 3 and show that the ductility capacity is very much affected by the type of unbonding material. The testing protocol may also affect the ductility. Smaller ductility indices were obtained in the case of the ECCS [60] protocol.

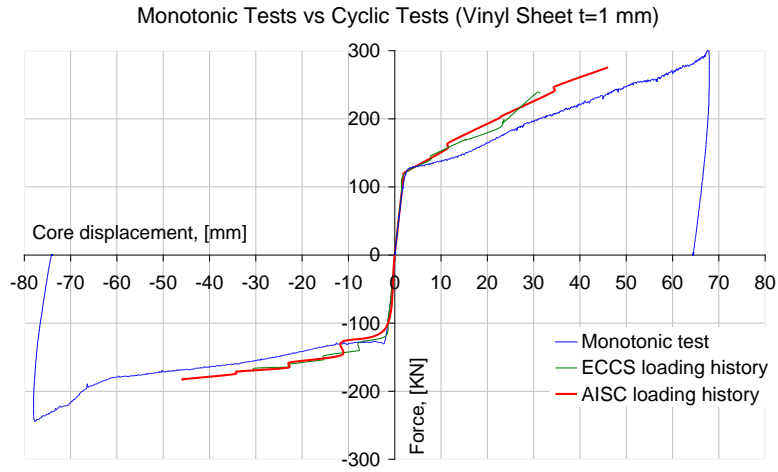


Figure 4.11 Monotonic tests vs. the envelopes from AISC [42] and ECCS [60] loading protocols for PVC transparent film

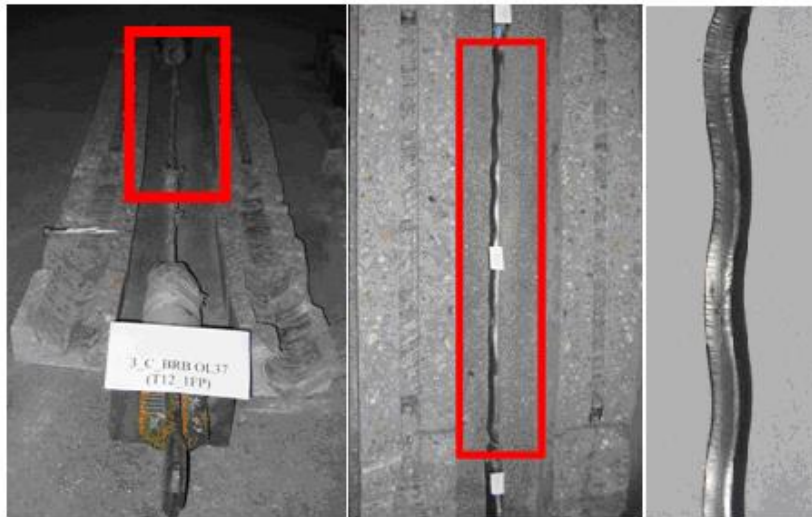


Figure 4.12 Steel core deformations (local buckling)

Table 4. 3 Dissipative energy of the BRBs

BRB Type function of unbonding materials		$\mu$ %*	
		AISC	ECCS
PVC (transparent) film (t = 1 mm)	C	78.15	39.38
	T	61.47	31.25
Asphaltic Bitumen (t = 2 mm)	C	39.32	25.7
	T	23.48	23.66
Rubber (t = 3 mm)	C	57.65	27.00
	T	77.66	35.45

$$* \mu \% = \frac{(E_{pl} - E_y)}{E_y} \cdot 100,$$



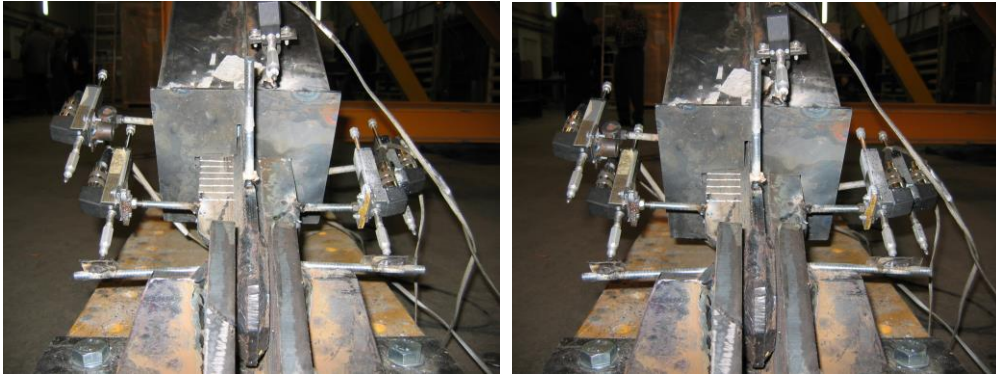


Figure 4.13. The elongation of the steel core plate is visible using scale marks on the transversal stiffeners of the end connection segment

Table 4.4 shows the ultimate displacements obtained from the cyclic tests for all types of unbonding materials and the acceptance criteria Nonlinear Procedures provided by FEMA 356. If the AISC [42] protocol is considered, all BRB types fulfill the FEMA requirements. For PVC and Rubber unbonding materials, the deformation capacity is roughly double than the demand. The lowest deformation capacity is recorded for Asphalt Bitumen unbonding materials. In the case of ECCS [60] protocol, the deformation capacity is lower and satisfies the requirements for PVC and Rubber unbonding materials, only. In the case of the Asphalt Bitumen material, the deformation capacity cannot fulfill the demand and therefore should be avoided, as low cycle fatigue phenomena may occur.

Table 4.4 Ultimate displacement of BRB from cyclic test vs. acceptance criteria (in mm)

BRB elements (function of unbonding materials)	Ultimate deformation		Acceptance criteria (plastic deformation) FEMA 356, LS*
	AISC mm	ECCS	
PVC film (t = 1 mm)	+/- 46	+/- 31	
Asphaltic Bitumen (t = 2 mm)	+/- 34	+/- 22	28
Rubber (t = 3 mm)	+/- 45	+/- 30	

\* LS - plastic deformation at life safety for braces in tension

### 4.3. Conclusions

Buckling restrained braces BRBs are expected to withstand significant plastic inelastic deformations when subjected to axial forces. In this chapter, the effectiveness of BRB systems used for strengthening existing RC frames has been investigated experimentally. BRB specimens have been designed as to fulfill the acceptance criteria provided by FEMA 356. The plate used in the steel core was made from S275 steel and was protected with unbonding material. The steel core was inserted in a steel tube made of S275 steel and C40/50 concrete was then poured inside the tube. In order to investigate the influence of the unbonding material, three types of BRB have been manufactured, based on three different unbonding materials (i.e. PVC transparent film, asphalt bitumen and rubber). Both monotonic and cyclic tests have been performed. Monotonic tests were conducted



until the failure of the specimens, both in tension and in compression. Cyclic tests have been carried out according to the specifications of AISC 2005 [42] and ECCS [60]. All three BRB solutions satisfied the demand, however the one using PVC transparent film showed a better behavior.

The main conclusions of the experimental program on BRB specimens are summarized below:

- BRBs show good performance and large deformation capacity
- The values of the deformation capacity under monotonic tests show similar results in tension and in compression.
- Cyclic tests show very stable and repeatable behavior.
- In the case of cyclic tests, the deformation capacity is affected by the loading protocol. When more cycles are used (eg. ECCS [60] procedure), the low cycle fatigue phenomenon reduces the deformation capacity
- Cyclic tests are consistent with the monotonic tests, but the deformation capacity is lower
- The unbonding material may have an important influence on the deformation capacity of the BRBs. Specimens with PVC material show better behavior, while the use of bitumen would greatly reduce the deformation capacity.
- The compression-strength adjustment factor,  $\beta$ , that accounts for the compression over-strength (with respect to the tension strength), obtained as a mean value of the two loading protocols, amounts to 1.3
- The tension strength adjustment factor,  $\omega$ , that accounts for strain hardening, obtained as a mean value of the two loading protocols, amounts to 2.2
- For minimum values from the cyclic tests, the compression adjustment factor  $\beta$  amounts to 1.2, while the tension adjustment factor  $\omega$  amounts to 1.9.

Based on the results of the experimental program, a case study of performance of BRBs for retrofitting existing RC frame building is developed in Chapter 5. The performance of the RC building will be analyzed before and after the retrofitting intervention.

## **5. PERFORMANCE BASED EVALUATION AND RETROFITTING OF REINFORCED CONCRETE BUILDING FRAMES: A CASE STUDY**

### **5.1 Building description**

#### **5.1.1. Geometry**

The case study is represented by a historical building erected in Toscana, Italy in the first half of the XX<sup>th</sup> century. The building has a reinforced concrete structure. The structure was regarded as a "benchmark structure", and different retrofitting systems based on steel material were applied. The investigation was done within the framework of the STEELRETRO international project.

The reinforced concrete building was designed according to the Italian design code in force at the time, issued in 1939. The decision was to adopt this old design code as it was used for the design of many reinforced concrete buildings from the '50 to early '70 in Italy [70].

Common construction materials used in that period were concrete with characteristic compressive strength  $f_{ck}=20\text{N/mm}^2$  and reinforcements with a characteristic yield strength  $f_{sk}=230\text{N/mm}^2$ . The detailing of the reinforcement is also characteristic for the design practice of the time, with poor anchorage length of the rebars at the external beam-column joint, the use of plane rebars (not ribbed), inclined reinforcement used for shear force resistance and large spaced stirrups (15 cm for columns and 25 cm for beams) in potential plastic zones. A 3 storey RC frame was selected for the analysis. The dimensions of the whole building in plane are 23.4 x 18.4 m and the height is 11.95 m.

Due to its high seismic vulnerability, it was decided to retrofit the building by means of a centrally inverted V braced system (CBF). The disadvantages of conventional CBF systems consist in a reduced dissipation capacity and large unbalanced seismic forces in the beams connected to the V braces. These disadvantages can be overcome if the braces can yield both in tension and compression without buckling. Therefore, the BRB system was considered more advantageous than a conventional CBF system. A 3D view of the building model is presented in Figure 5.1. Figure 5.2 shows transversal and longitudinal sections through the building. The heights of the storeys are 3.9m for the ground floor, 3.4m for the first floor, 3.35 m for the second floor and 0.9m and 1.8m, respectively, for the rafters' eave. More details about the geometry and the elements cross sections are presented in Annex 1.

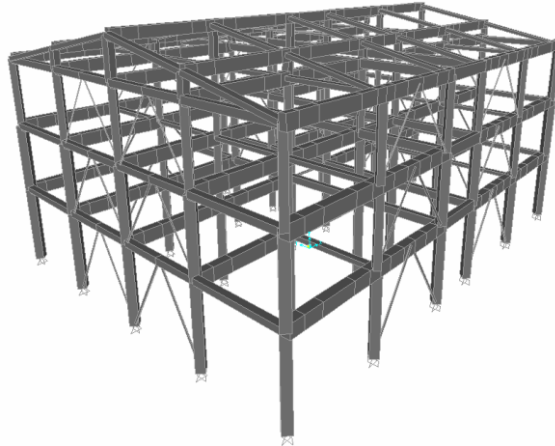


Figure 5.1 STEELRETRO reference benchmark RC building model and BRB system distribution

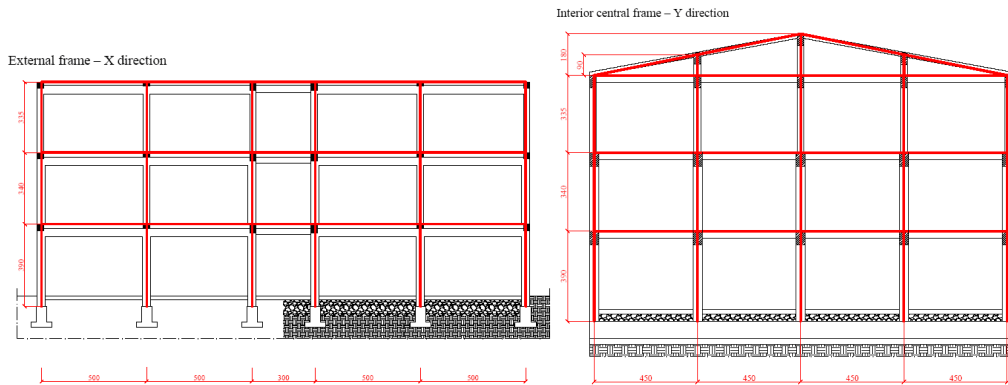


Figure 5.2 External frame on X direction and interior central frame on Y direction

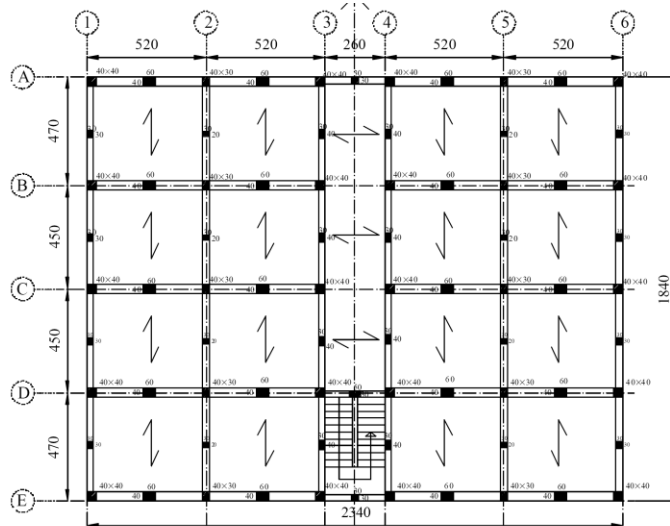


Figure 5.3: Plan view of the first and second floor and direction of ribs in the floor

### 5.1.2. Loads

As a first step, the existing RC building was verified for ULS condition using dead load (DL), live load (LL), snow load (SL) and wind load (WL) but also seismic load (EQ) in accordance with European codes ([59], [64], [71] and [72]). In order to evaluate the self weight of the concrete elements, a  $25 \text{ KN/m}^3$  was considered for the reinforced concrete specific weight. The concrete floor consists of concrete in-situ cast parallel ribs (15 cm ribs + 5 cm slab) with 15 cm thick bricks (see Figure 5.4).

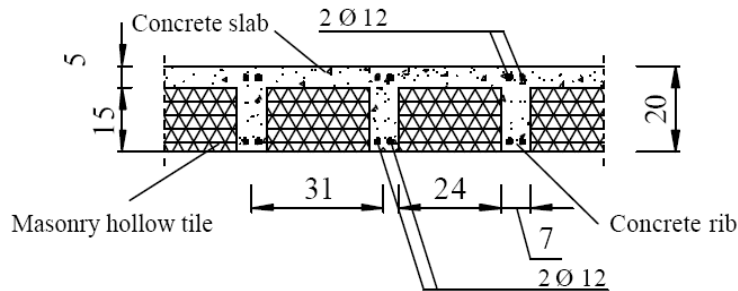


Figure 5.4 Floor structure

A  $0.8 \text{ KN/m}^2$  load was considered for the weight of the partition walls. The weight of the exterior walls/cladding was considered  $2.5 \text{ KN/m}^2$  and the action was transmitted only to the columns, by the arch effect.

The building is classified into category C1, and therefore the live load amounts to  $3 \text{ KN/m}^2$  (office areas). The roof is classified into category H (inaccessible roofs), with a live load of  $0.4 \text{ KN/m}^2$ .

The snow load amounts to  $0.8 \text{ KN/m}^2$ . The wind load is distributed perpendicularly on the columns on both directions ( $0.69 \text{ KN/m}^2$  and  $-0.29 \text{ KN/m}^2$  on X direction, respectively  $0.74 \text{ KN/m}^2$  and  $-0.40 \text{ KN/m}^2$  on Y direction).

Global imperfections on both X and Y directions were considered in the analysis.

The seismic load was defined by using the elastic spectrum, with the peak ground acceleration (PGA) of  $0.23g$ ,  $\gamma_I=1.0$ ,  $T_B=0.15s$ ,  $T_C=0.5s$ ,  $T_D=2.0s$ ,  $S = 1.2$ . For the original reinforced concrete structure, a seismic behavior factor  $q = 1.5$  was used. For the reinforced concrete structure retrofitted with BRB system, the seismic behavior factor  $q$  amounted to 4 (see Figure 5.5). An accidental torsional effect for the eccentricity  $e_{ai}=\pm 0.05$  was also considered.

The combination of actions for fundamental and special combinations followed the format from Eurocode.

The lateral forces for the pushover analysis were considered according to 1<sup>st</sup> eigen mode as follows [48]:

$$F_i = \frac{m_i \cdot h_i}{\sum m_i \cdot h_i} \quad (5.1)$$

where:

$h_i$  = the height of level  $i$  relatively to the base of the frame and  $m_i$  = the mass at level  $i$  computed from the fundamental combination  $DL+0.6 \times 0.8 \times LL$  and distributed in the main nodes.

The floors and roof were modeled as rigid diaphragms.

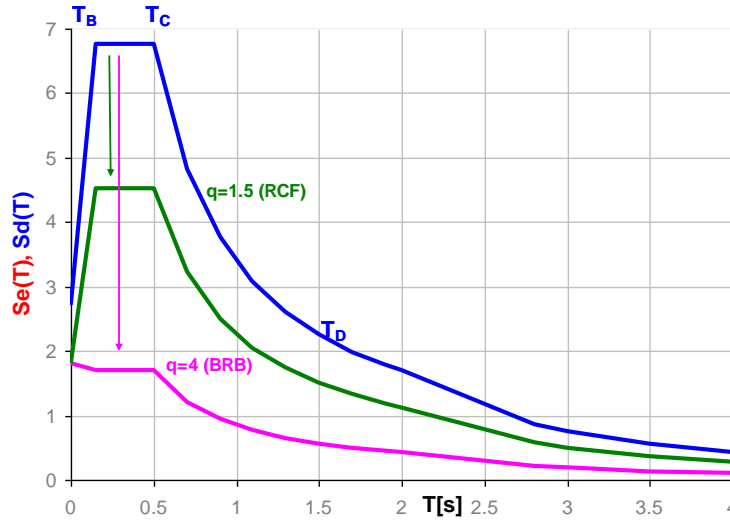


Figure 5.5 Elastic and design response spectrum

### 5.1.3. Materials

The concrete material was modeled using nonlinear model of Kent and Park [58] (see Figure 5.6a) with no tension. If the hoops are spaced at distances  $> d/3$ , the component should be considered unconfined, where  $d$  is the distance from the extreme compression fiber to the center of the tension reinforcement. As a result, the concrete was considered unconfined. For the type of concrete used for the structure, a Young modulus of 29000 MPa was used.

The reinforcement was modeled by using a modified Park model, a yield strain of 0.015 and an ultimate strain ranging from 0.2 to 0.3. A yield strength of 230 MPa and an ultimate strength of 350 MPa were considered (see Figure 5.6b).

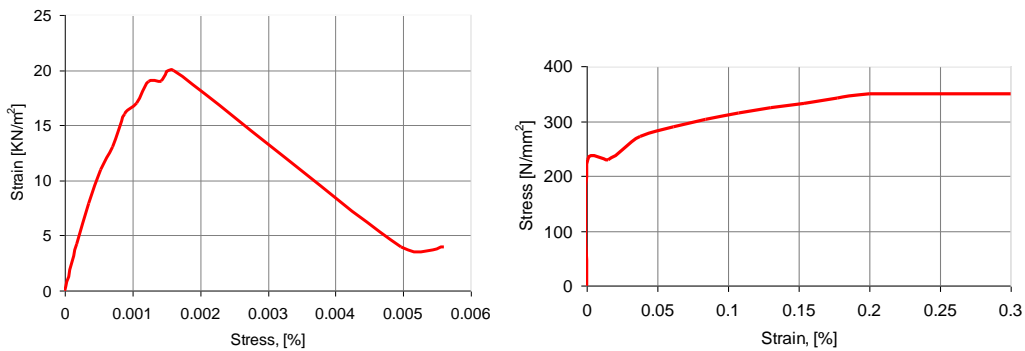


Figure 5.6: a) Reinforced concrete nonlinear model based on Kent and Park [58]; b) modified Park nonlinear model for steel reinforcement [58]

### 5.1.4. Members

Reinforced concrete members were modeled with plastic hinges concentrated at the ends. In the case of beams, plastic hinges were concentrated in

all points where the number of rebars changed from the upper part to the lower part of the cross section and on the reverse direction (see Figure 5.7).

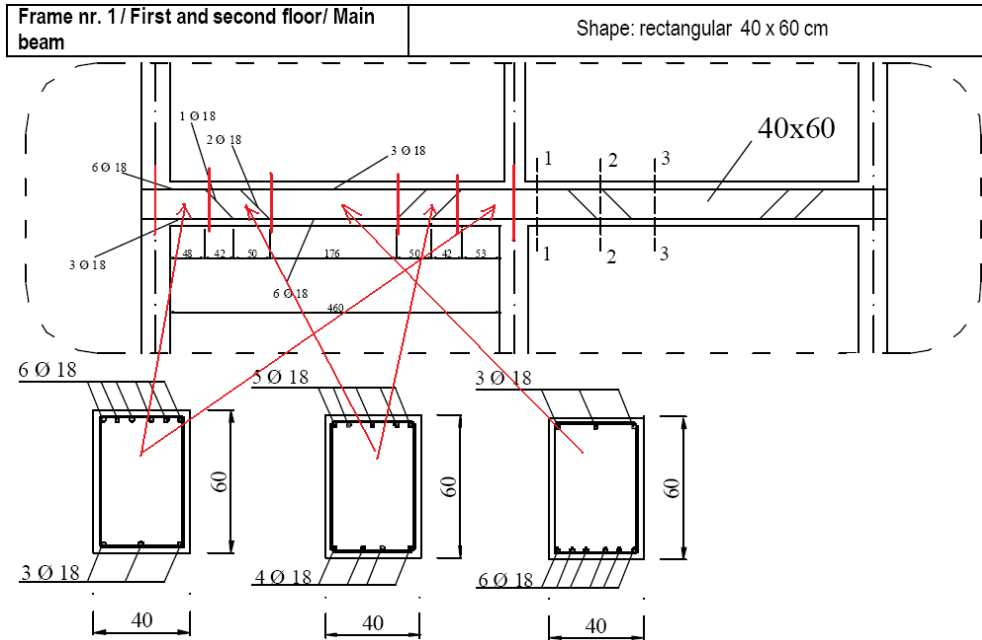


Figure 5.7 Definition of the reinforced concrete beam elements

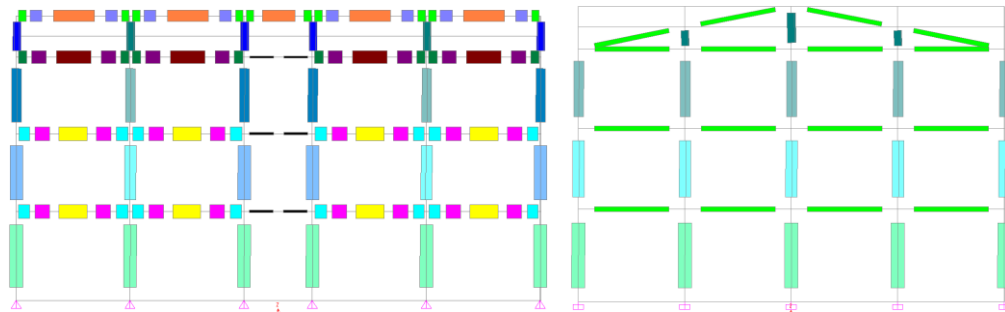


Figure 5.8 Splitting of elements on RC elements on X direction and Y direction (plastic hinges modeled at the end of each element)

Plastic hinges were defined as load-deformation relationship, with a deformation controlled typology (ductile).

In the case of beams, the moment-rotation relationship for unconfined concrete was described following the acceptance criteria from (see Figure 5.9a). It should be precise that after the insertion of the inverted V BRB system, the plastic hinges defined in beams at their intersection with braces elements, were defined as moment – rotation curves at different stages of the axial force (P-M-M) see Figure 5.9b. In the same way were defined all plastic hinges for the columns, but the moment – rotation relation was defined differently for each direction of column cross section.



Figure 5.9: a) Moment – rotation relation based on FEMA procedure; b) P-M-M surface interaction

The evaluation of the seismic performance of the RC frames was made by using a PBSE methodology. Due to the presence of a linear modeling of the plastic hinges (from point A to point B) in terms of the moment-rotation curve, the effective stiffness corresponds to the secant stiffness from the origin to the yield point of the component. In the case of the analyzed RC frame structure, beams and columns stiffness should be reduced by 50%, due to the fact beams are not pre-stressed and columns have axial compression due to design gravity load  $< 0.3A_gf_c'$  [49]/[50].

#### 5.1.5. BRB seismic upgrade of RC frames

The BRB's, pinned at the ends, are installed in the external frames of the RC building, as it can be seen in Figure 5.1. As it was presented in the previous chapter, the BRB element is characterized by the same behavior in compression as in tension because of the core plate which absorbs the loads and by yielding its dissipating seismic energy while the steel tube and the infill material restrain the buckling of the core plate.

##### The seismic reduction factor ( $q$ )

The American standards AISC 2005 [17] and NEHRP 2003 [73] recommend a force reduction factor  $R=8$  (where  $R$  is the equivalent of the  $q$  factor in Eurocode 8 [48]) for Buckling Restrained Braced Frames BRBF, Moment Resisting Frames MRF and Eccentrically Braced Frames EBF. As in Eurocode 8 there is no reference for BRB systems, a  $q$  factor equal to 6 was initially adopted for BRB framing, similar to that of MRF and EBF systems. However, the  $q$  factor defined according to previous codes is valid for the design of new steel buildings. Romanian Seismic Evaluation standard [74] recommends for existing RC buildings a  $q$  factor equal to 2.5 and a  $q$  factor equal to 4 for existing EBF. Therefore, it was considered more appropriate to take an average value of the  $q$  factor,  $2.5 < q < 4$ . Thus, considering that BRBS has an adequate contribution to the system, a  $q$  factor of 4 was considered.

The BRB design was made using a  $q = 4$  and started with a steel core cross section of  $3 \text{ cm}^2$  (1 cm thickness and 3 cm wide). Table 5.1 shows the  $\Omega_i$  values for the initial design.

Table 5.1:  $\Omega$  values in the case of constant BRB steel core plates for all levels

	$N_{Ed} X[\text{KN}]$	$\Omega X$	$N_{Ed} Y[\text{KN}]$	$\Omega Y$
<b>ground floor</b>	60	1.18	59	1.19
<b>1'st level</b>	34	2.07	47	1.50
<b>2'nd level</b>	24	2.94	27	2.61
<b>25%&lt;&lt;&lt;&lt;&lt;</b>	$\Omega_{final} = 150$		$\Omega_{final} = 119$	



In order to assure a homogeneous dissipative behavior of the diagonals, it should be checked that the maximum overstrength  $\Omega_i$  does not differ from the minimum value  $\Omega$  by more than 25% [48]. In

Table 5.2, new  $\Omega_i$  values have been calculated for the new values of BRB steel core sections.

BRB core plate cross section, X direction:

ground floor = 2 cm x 4 cm

1<sup>st</sup> level = 1 cm x 4 cm

2<sup>nd</sup> level = 1 cm x 3 cm

BRB core plate cross section, Y direction:

ground floor = 2 cm x 3 cm

1<sup>st</sup> level = 1 cm x 5 cm

2<sup>nd</sup> level = 1 cm x 3 cm

Table 5.2:  $\Omega$  values in the case of variable BRB steel core plates cross section

	$N_{Ed}$ X [KN]	$\Omega$ X	$N_{Ed}$ Y [KN]	$\Omega$ Y
<b>ground floor</b>	60	3.13	59	2.39
<b>1<sup>st</sup> level</b>	34	2.76	47	2.50
<b>2<sup>nd</sup> level</b>	24	2.94	27	2.61
<b>25%&gt;</b>	$\Omega_{final} = 13$		$\Omega_{final} = 9$	

The BRB cross section is represented in the model as constant along the length. Therefore, a reduction of the axial stiffness  $K$  [KN/m] is applied (Table 5.3).

Table 5.3: modeled stiffness and real stiffness ratio

Direction	BRB	cs [cm <sup>2</sup> ]	$K_e$ [KN/m]	$K$ [KN/m]	$K/K_e$
X	<b>ground floor</b>	2x4	72368	36285	0.50
	<b>first floor</b>	1x4	36184	19952	0.55
	<b>second floor</b>	1x3	27138	15072	0.56
Y	<b>ground floor</b>	2x3	54276	27938	0.51
	<b>first floor</b>	1x5	45230	25735	0.57
	<b>second floor</b>	1x3	27138	15633	0.58

For this particular case and a BRB cross section made of S235 steel, the geometry of the core was defined so that all braces have the same active length of 1.7 m. Thus, for this active length and the end restraints, the yield displacement amounts to  $\Delta_y = 1.9$  mm. The estimation of the ultimate displacement  $\Delta_u$  was based on the results of the experimental tests presented in Chapter 4. Based on these results, ductility ratios  $\Delta_u/\Delta_y$  were estimated for tension and compression amounted to 22, as the average of the values obtained from AISC cyclic loading protocol. In order to obtain the adjustment of the design strengths (maximum compression strength  $C_{max}$  and maximum tension strength  $T_{max}$ ), the following formulas from [17] were applied:

$$T_{max} = \omega \times R_y \times f_y \times A \quad (5.2)$$

$$C_{max} = \omega \times \beta \times R_y \times f_y \times A \quad (5.3)$$

where,  $f_y$  is the yield strength,  $R_y$  is the ratio of the expected yield stress to the specified minimum yield stress  $f_y$  (may be considered equal to 1).

The values of the compression adjustment factor  $\beta=1.2$  and a strain hardening adjustment factor  $\omega=1.9$  was obtained from the experimental tests, using the following formulas from [17]:

$$\beta = \frac{C_{\max}}{T_{\max}} \quad (5.4)$$

$$\omega = \frac{T_{\max}}{f_{\text{fysc}} \cdot A} \quad (5.5)$$

where:

$f_{\text{fysc}}$  is the measured yield strength of the steel core.

The inelastic behavior of BRB system was modeled considering the concentrated tri-linear plasticity curve with strain hardening and strength degradation of 0.8 from maximum capacity, according to FEMA356 [49] (see Figure 5.10)

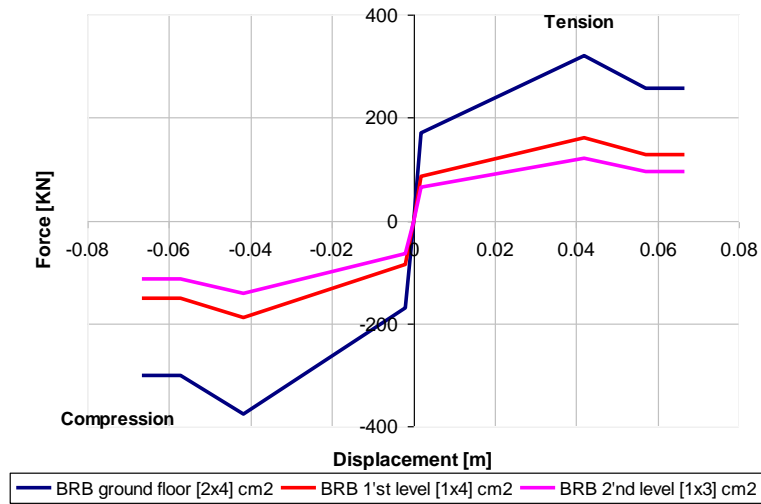


Figure 5.10 BRB tri-linear model on X direction

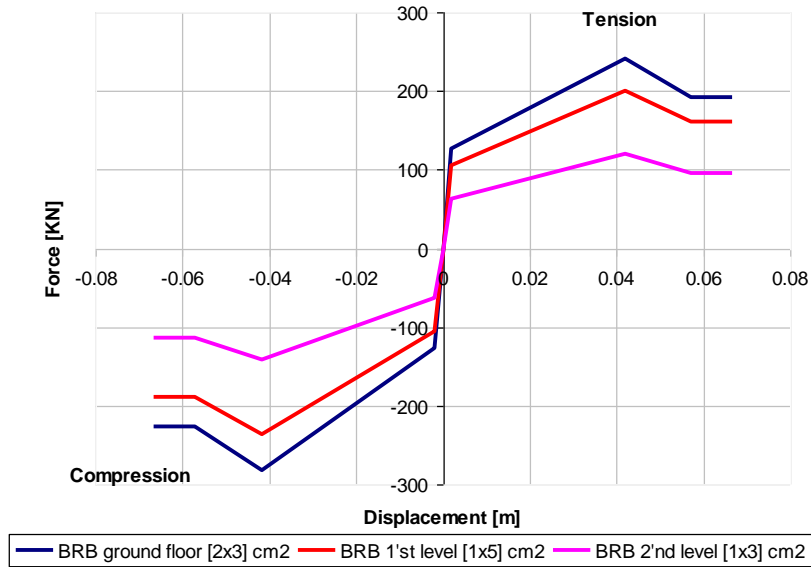


Figure 5.11 BRB trilinear model in Y direction

The modeling parameters and the acceptance criteria given by FEMA 356 [49], for steel braces in tension, were used in the evaluation of the performance of BRB elements. The results of the experimental tests on BRB specimens, presented in Chapter 4, showed an available ductility of around  $22D_t$ , which is twice the value given by FEMA 356, i.e.  $11D_t$ .

The BRB tri-linear model used in the present analysis is characterized by the following parameters:

Table 5.4: BRB modeling parameters for the final benchmark analysis

BRB properties		Final Benchmark analysis
Modeling Curve	type	trilinear (FEMA/ASCE model)
Material	steel	S235
Aria-core c.s.	$A_c$ [cm <sup>2</sup> ]	1x3 (tested cross section)
Core length	$L_c$ [m]	1.7
Yielding displacement	$\Delta_y$ [mm]	1.9
Ductility displacement	$\mu$	22 (cyclic AISC)
Strain hardening adjustment factor	$\omega$	1.9 (minimum from cyclic ECCS+AISC)
Compression adjustment factor	$\beta$	1.2 (minimum from cyclic ECCS+AISC)
Acceptance criteria (modified FEMA356/ASCE41 acceptance criteria for braces in tension)	IO	0.5 $\Delta_t$
	LS	14 $\Delta_t$
	CP	18 $\Delta_t$
BRB effective stiffness	$K_e$	considered

Table 5.5: BRB modeling parameters for the final benchmark analysis

BRB properties		BRB element test
Material	steel	S275
Aria-core c.s.	Ac [cm <sup>2</sup> ]	1x3
Core length	Lc [m]	1
ductility displacement	$\mu$	32 (monotonic test)
		22 (cyclic AISC)
		14.7 (cyclic ECCS)
strain hardening adjustment factor	$\omega$	2.2 (average from cyclic ECCS+AISC)
		1.9 (minimum from cyclic ECCS+AISC)
compression adjustment factor	$\beta$	1.3 (average from cyclic ECCS+AISC)
		1.2 (minimum from cyclic ECCS+AISC)

As it can be seen, the displacement ductility factor,  $\mu$ , depends on the loading program. Therefore, it may be concluded that a good estimation of BRB displacement ductility  $\mu$  for the pushover analysis can be made by applying the value from monotonically compression tests, i.e.  $\mu=32$ . Meanwhile, for nonlinear dynamic (time history) analysis, a good estimation of displacement ductility  $\mu$  can be made if the value from cyclic tests according to ECCS [68] loading protocol is applied, i.e.  $\mu=14.7$ . If the AISC [17] loading protocol is considered, the ductility displacement  $\mu$  amounts to 22.

## 5.2. Performance based seismic evaluation of the initial and the retrofitted reinforced concrete frame

### 5.2.1 Preliminary considerations

In order to assess the performance of the RC frame structure by means of a PBSE, it is necessary to define the plastic deformation of the elements for each performance level (Immediate Occupancy IO, Life Safety LS and Collapse Prevention CP).

#### 5.2.1.1. Elements controlled by flexure

According to the performance based evaluation PBE procedure [49] described in Chapter 3, it can be assumed a deformation-controlled action of the RC elements, represented by the Type 1 curve. The type 1 curve needs to be adapted to the model of the backbone curve. Considering that the elements are controlled by flexure, four parameters should be clear for each of beams and columns:

#### **a) Conforming C and nonconforming NC transversal reinforcement**

This condition must be applied for beams and columns. According to FEMA 356 [49], a component is conforming if within the flexural plastic hinge region, hoops are spaced at distances smaller than one third of the measured distance from the fiber of the cross section in compression to the middle of rebar in tension, and if, for components of moderate and high ductility demand, the strength provided by the hoops ( $V_s$ ) is at least three quarters of the design shear capacity, or otherwise, the component is considered nonconforming.

According to these rules, all the elements can be considered nonconforming (NC)

**b) ratio  $(\rho - \rho') / \rho_{bal}$  (ratio between the difference of the reinforcement in tension ( $\rho$ ) and in compression ( $\rho'$ ) and the reinforcement ratio that produces balanced strain conditions ( $\rho_{bal}$ ))**

This condition is applied only for beams and for the calculation of the reinforcement ratio that produces strain conditions ( $\rho_{bal}$ ). Also, the condition was considered for both cases, i.e. when the reinforcement in tension is located in the upper part of the cross section and when the reinforcement in tension is located in the lower part of the cross section:

$$\rho_{bal} = \frac{0.85 \cdot f_c' \cdot \beta_1}{f_y} \cdot \frac{0.003 \cdot E_s}{0.003 \cdot E_s + f_y} \quad (5.6)$$

When  $\rho < \rho_{bal}$ , reinforcement fails in tension. In all cases,  $\rho < 0.01 < \rho_{bal} = 0.046$ ). When  $\rho > \rho_{bal}$ , reinforcement fails in compression [58].

**c) Ratio between the axial force (P) and the axial strength of the cross section  $A_g \cdot f_c'$  for columns**

As a result of the preliminary pushover analysis on two orthogonal directions X and Y, the maximum axial force (P) in each column cross section was extracted. As it can be observed (see Annex 1), the ratio between the axial force and the axial strength of the cross section is predominantly smaller than 0.1. There are also cases when  $0.1 < P/(A_g \cdot f_c') < 0.4$ , and linear interpolation is necessary.

**d) Ratio between the shear force (V) and the shear strength of the cross section for beams and columns**

In the case of beams, in order to verify the ratio  $V/(b_w \cdot d \cdot \sqrt{f_c'})$ , elements were divided in function of the number of the rebars in the upper or the lower parts of the cross section.

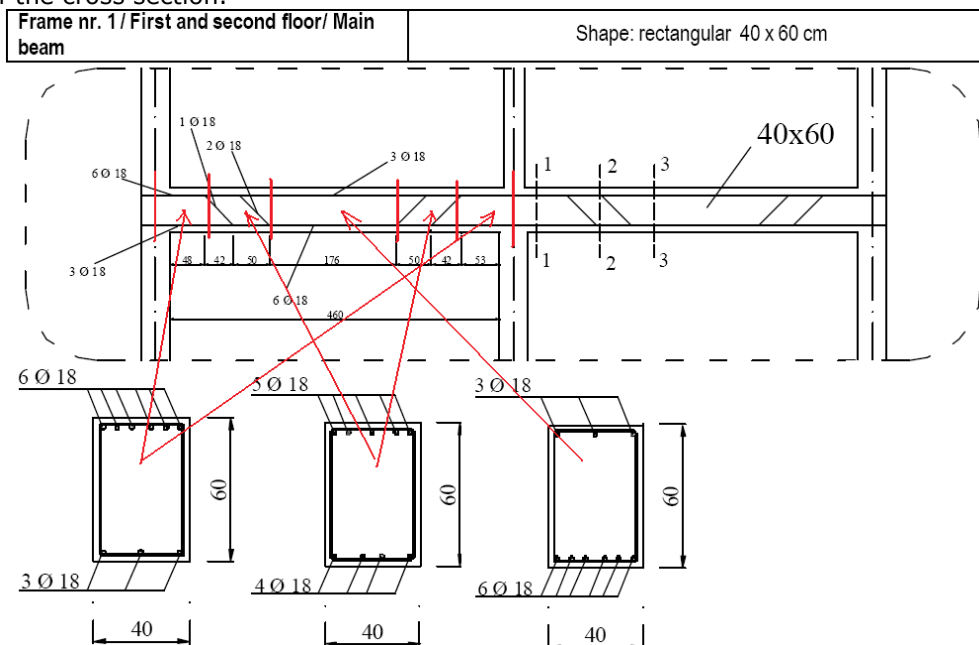


Figure 5.12 Definition of the reinforced concrete cross section

The maximum shear force  $V$  was extracted from the result of the preliminary pushover analysis on X and Y directions of the building and on each different cross section (see Annex 1). As it can be observed, the ratios between the shear force and the shear capacity of all beams cross sections are smaller than 30%. The same results were obtained for the columns.

### 5.2.1.2. Elements controlled by shearing

For the shearing verification of beam elements, the detailed procedure was applied [75]. In this case, the shear strength  $Q_{cap}$  is determined by summing the shear strength of the concrete  $Q_b$ , the shear strength of stirrups  $Q_e$  and the shear strength of inclined rebars  $Q_i$ . In Annex 1 all the formulas and parameters used in verifications are presented. During an earthquake ground motion, due to the load reversal, the negative moment (top in tension) under gravity loads at the end of the beam may change to positive moment. Therefore, the cracks may develop both at the top and the bottom of the cross section. As the number of longitudinal reinforcements is different (6 bars at the top and only 3 at the bottom), there is a strong difference in terms of  $Q_b$  for the two situations. A contribution to this difference is also due to the lack of effect from the inclined rebars when the moment changes the sign.

Based on the procedure detailed above [75], it was determined that none of beams were controlled by shearing (see Annex 1 for more details).

For shearing verification of column elements, the detailed procedure from [75] was applied. Compared to the beams, the only difference is the contribution of the inclined bars. In this case, the shear strength  $Q_{cap}$  is determined by summing up the shear strength of concrete  $Q_b$  and the shear strength of stirrups  $Q_e$ .

Results have shown that none of the columns are controlled by shearing. The results are presented in more details in Annex 1.

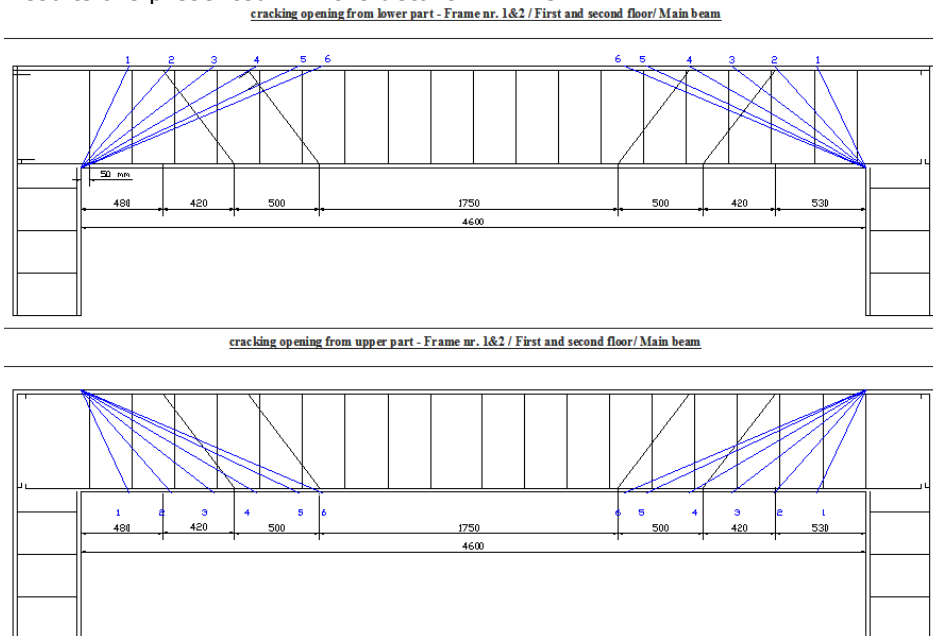


Figure 5.13 Cracks distribution in a beam element with opening from lower/upper part of the element [75]

### 5.2.1.3. Rebars overlapping along the elements

Both beams and columns were investigated in order to control the overlapping of longitudinal reinforcements. According to the construction details (Figure 5.14), it was considered that the overlapping of the rebars in beams and columns was at least 40 times the diameter  $\Phi$ . Complete results are presented in Annex 1 and show that the overlapping is sufficient both for beams and for columns.

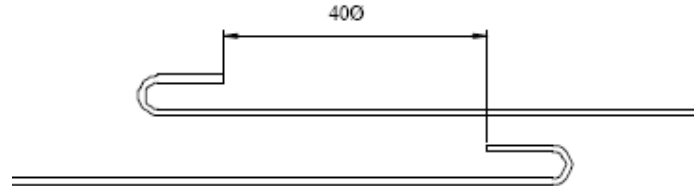


Figure 5.14 Steel-Retro Benchmark building – overlapping of longitudinal reinforcements

### 5.2.1.4. Beams controlled by inadequate anchorage of reinforcement into the beam-column joint

It is important for beam and column longitudinal reinforcement to be anchored adequately so that the joint could resist beam and column moments. For interior joints, the reinforcement typically extended through the joint and is anchored in the beam. For exterior joints, the longitudinal reinforcement terminates with hooks and is anchored in the joint. According to RC building detailing (Figure 5.15), the existing anchorage length in exterior beam-columns joints is the difference between the height of the column cross section and the minimum cover  $a$ . The results are presented in more details in Annex 1.

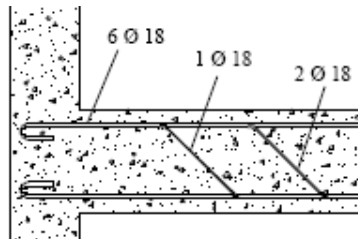


Figure 5.15 Steel-Retro Benchmark building – Anchorage of the reinforcing bars in the exterior joint

With the exception of  $l_{b,min}$ , all the other parameters are computed as described above. The results show that there are beams where the anchoring length is not sufficient  $l_{b,min} < l_{b,req}$ , and therefore in order to take into account in the verifications, an equivalent yield strength of the rebars needs to be computed, as follows [49]/[50]:

$$f_{y,eq} = f_y \cdot \frac{l_{b,av}}{l_{b,req}} \quad (5.7)$$

where:

- $f_y$  – is  $\sigma_{sd}$  (defined above)
- $l_{b,av}$  – is  $l_{b,min}$  (define above)
- $l_{b,req}$  – is  $l_{b,req}$  (define above)

### 5.2.1.5. Columns with axial loads exceeding $0.7P_o$

The preliminary results of the pushover analysis indicate that the axial force in columns ( $P_{max}$  – obtained from pushover analysis) does not exceed 70% of the nominal axial load strength at zero eccentricity ( $P_o$ ) (more details in Annex 1). Therefore, the definition of plastic deformation for different Performance Levels (Immediate Occupancy – IO, Life Safety – LS, Collapse Prevention – CP) can be done according to FEMA356/ASCE41 [49]/[50].

### 5.2.1.6. Earthquake Hazard Level EHL - Conversion coefficients of PGA for different EHL (according to national standard)

The seismic hazard in terms of horizontal acceleration response spectra needs to be defined according to the national standard and according to the location of the building (in this case, the Italian seismic standard NTC [76]). The acceleration for each performance level is then obtained by multiplying the PGA with the conversion coefficients, which are 0.5 for IO, 1.0 for LS and 1.5 for CP.

Table 5.6 presents the earthquake levels in terms of Probability of Exceedence PE and Return Periods MRI for each performance level and the conversion coefficients for scaling the accelerograms.

Table 5.6: Earthquake hazard levels

Earthquake Hazard Level	Frequency	BPL	FEMA 356		NTC-2008		Conversion coefficients
			MRI	PE	MRI	PE	
			<i>Occasional</i>	<i>IO</i>	<b>225</b>	20%/50	
<i>Rare</i>	<i>LS</i>	<b>474</b>	10%/50	<b>475</b>	10%/50	1.0	
<i>Very Rare</i>	<i>CP</i>	<b>2475</b>	2%/50	<b>2475</b>	2%/50	1.5	

Considering that the case study refers to a RC building designed for gravity loads GLD during the '60, it was considered that a rehabilitation objective as BSO/Enhanced Objectives is acceptable. According to FEMA356 methodology, for an earthquake hazard with MRI of 225 years (occasional), the building performance level should be IO, for a rare earthquake (MRI = 474 years), the building performance level should be LS and for a very rare earthquake (MRI = 2475 years) the building performance should be CP. Once the Building Performance Level is selected, the Performance Levels for Structural and Nonstructural elements need to be defined. According to FEMA356 [49], for all three Building Performance Levels (IO, LS and CP) the same performance levels are selected for structural elements (Figure 5.16).



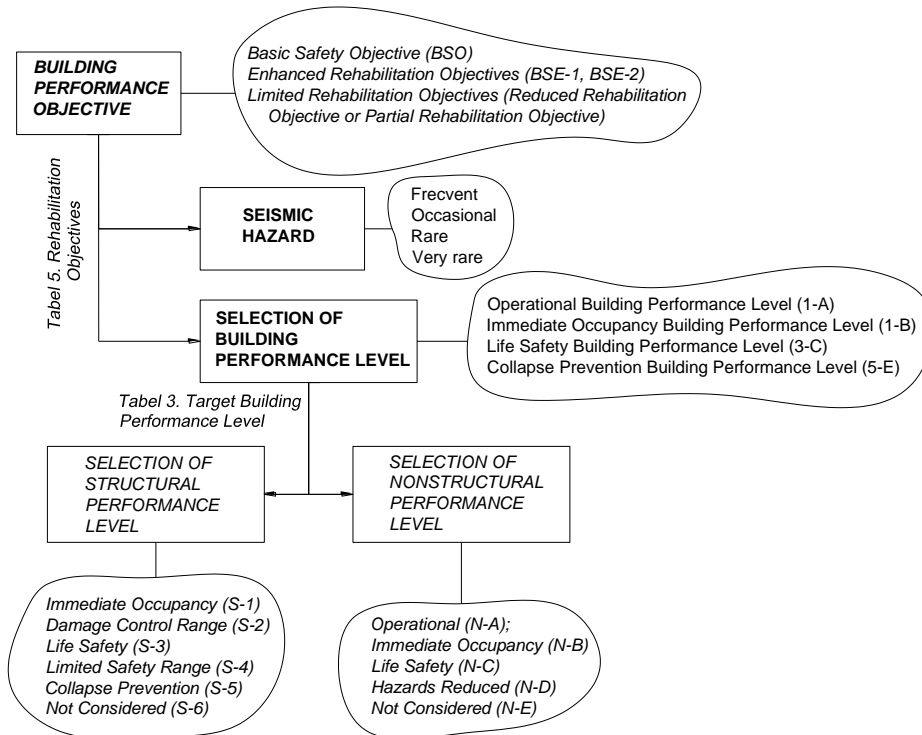


Figure 5.16 Selection of seismic hazard and performance levels for structural and nonstructural members.

### 5.2.1.7. Evaluation of performance with nonlinear pushover analyses (N2 method) [48]

Seismic performance of RC structure is computed by means of static nonlinear (pushover) and compared to the preliminary results obtained using a simplified response spectra analysis. In order to assess whether the building can achieve the rehabilitation objectives, the following methodology is applied:

- A non-retrofitted frame is analyzed in order to determine the history of plastic hinges;
- If necessary, a local retrofitting of the elements (beams, columns) is adopted until a favorable plastic mechanism is obtained;
- A Global Retrofitted frame is analyzed in order to determine the history of plastic hinges;
- If necessary, a local retrofitting of the elements (beams, columns) is adopted until a favorable plastic mechanism is obtained. It is also checked that the dissipative system (i.e. BRB) be properly designed. If not, the system is adjusted so as to meet the requirements of a favorable plastic mechanism.
- Static nonlinear analysis using N2 method is employed for the evaluation of performance for each case.

### 5.2.1.8. Time History analysis

Time history analyses are also employed for the evaluation of seismic performances. The seismic hazard will be defined by means of a set of ground

motions records, characteristic for the building location. Ground motions records are scaled by using the conversion coefficients evaluated in the previous section for each performance level.

### 5.2.2 Pushover analysis

Pushover analysis were performed on 3D models for the initial structure and for the retrofitted structures (local, global and both) (Figure 5.17 - Figure 5.26). More details are presented in Annex 1.

The results of the pushover analysis on X direction are presented in Figure 5.17. It may be seen that the initial structure MRF and the initial structure with local retrofitting MRF + FRP have a limited ductility and do not attain the displacement demands for LS and CP levels. The benefit of local retrofitting is reduced.

When the global retrofitting is accomplished MRF+BRB, the behavior is much improved. The stiffness and the strength increase, and the structure attains the LS performance. The structure cannot attain the CP level, due to the failure of the concrete structure. The contribution of the local retrofitting is again very limited (MRF+BRB+FRP).

The results of the pushover analysis on Y direction are presented in Figure 5.18. It may be seen that the initial structure MRF has limited ductility and does not attain the displacement demand for LS level. When the initial structure is retrofitted with FRP (MRF + FRP), the strength and the stiffness do not change but the ductility increases. The structure attains the displacement demand for LS but not for CP level.

When the global retrofitting is accomplished MRF+BRB, the behaviour is much improved. The stiffness and the strength increase, and the structure attains the LS performance. The structure cannot attain the CP level, due to the failure of the concrete structure. The contribution of the local retrofitting is limited (MRF+BRB+FRP).

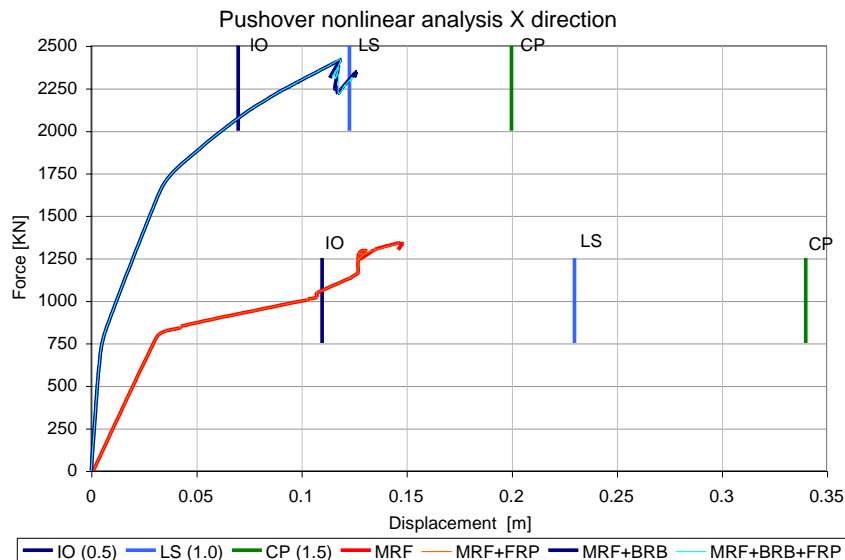


Figure 5.17 Pushover curves in X direction

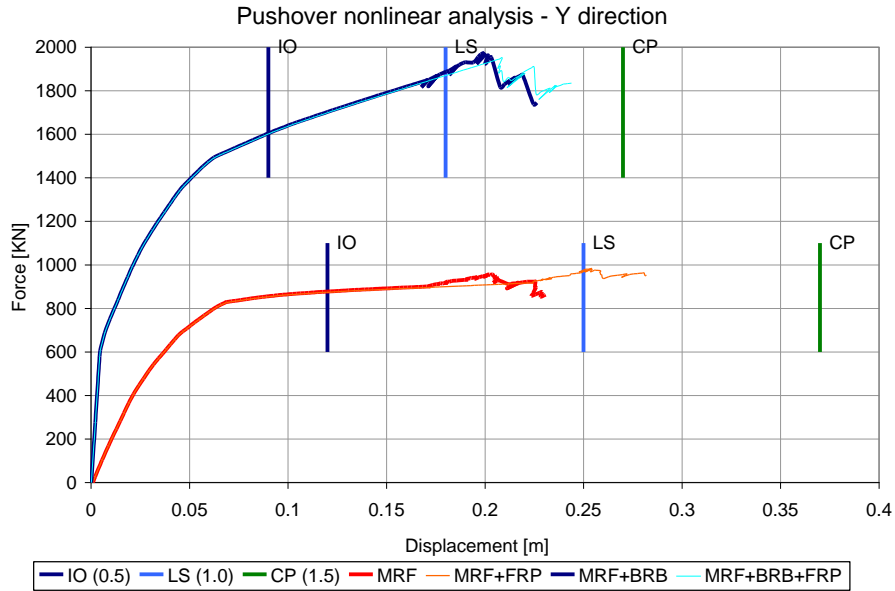


Figure 5.18 Pushover curves on Y direction

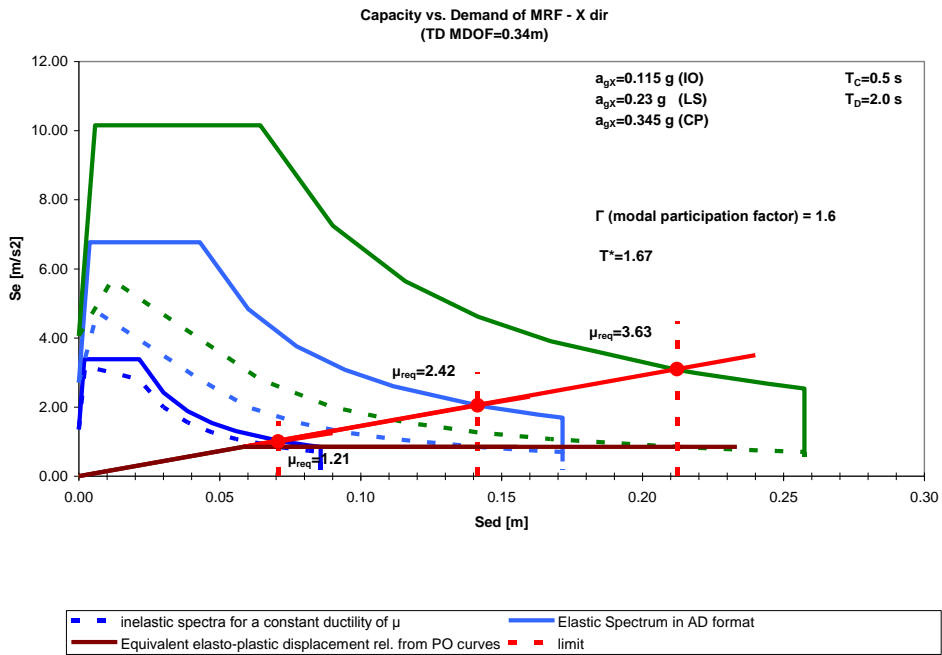


Figure 5.19 Demand and capacity diagram of the equivalent SDOF system MRF - X direction

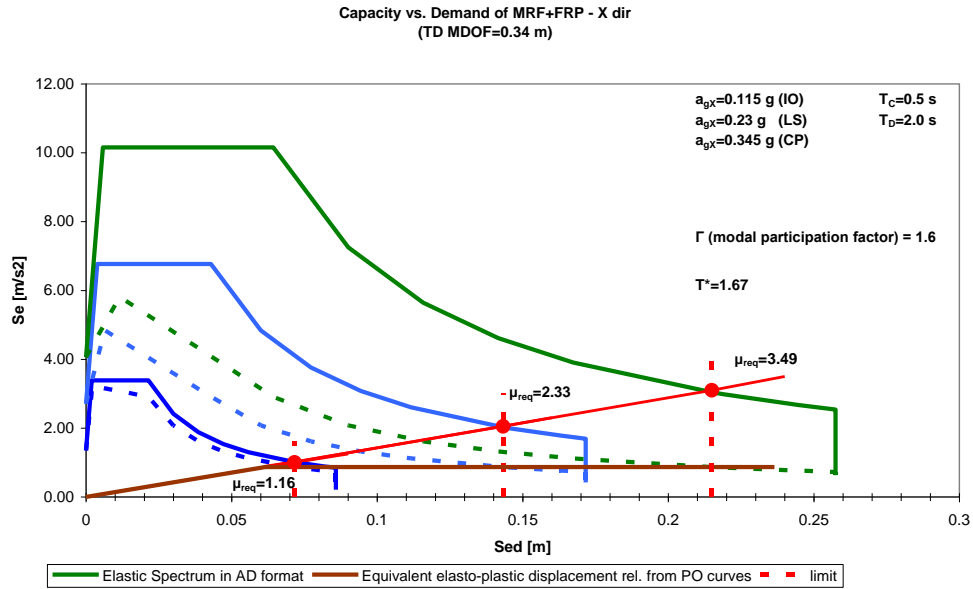


Figure 5.20 Demand and capacity diagram of the equivalent SDOF system MRF+FRP - X direction

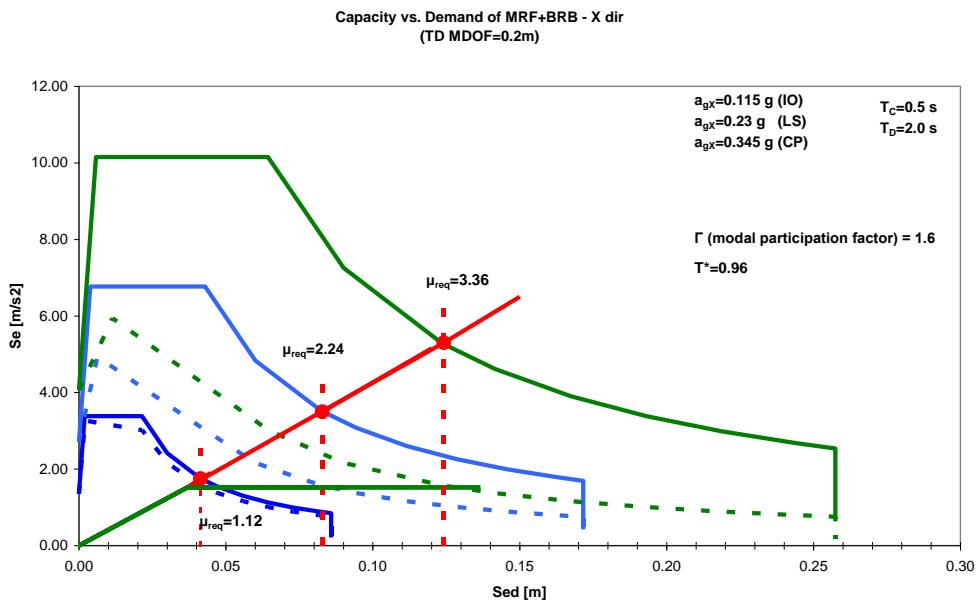


Figure 5.21 Demand and capacity diagram of the equivalent SDOF system MRF+BRB - X direction

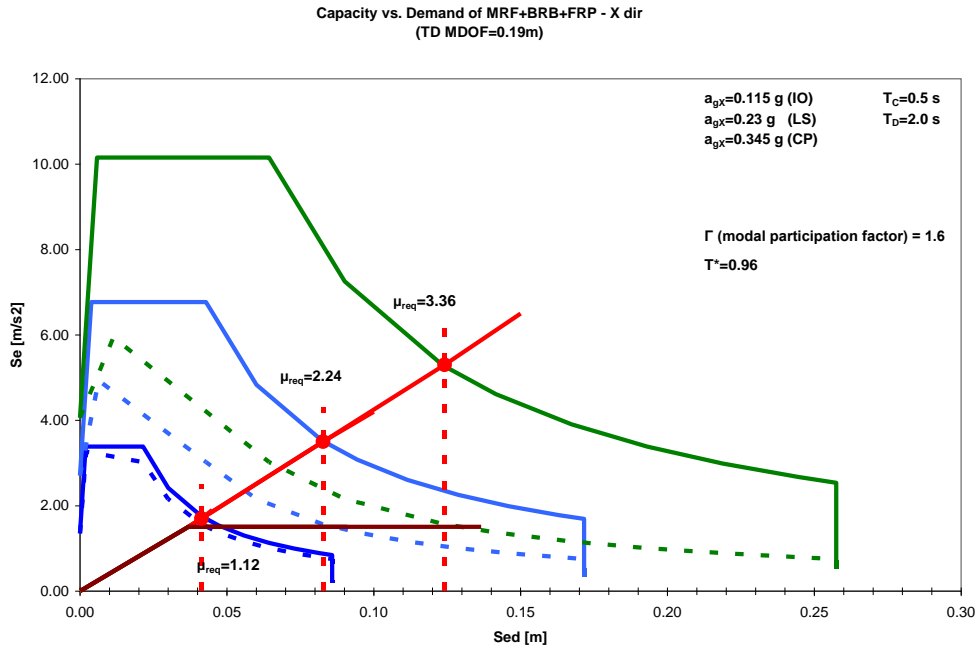


Figure 5.22 Demand and capacity diagram of the equivalent SDOF system MRF+FRP+BRB - X direction

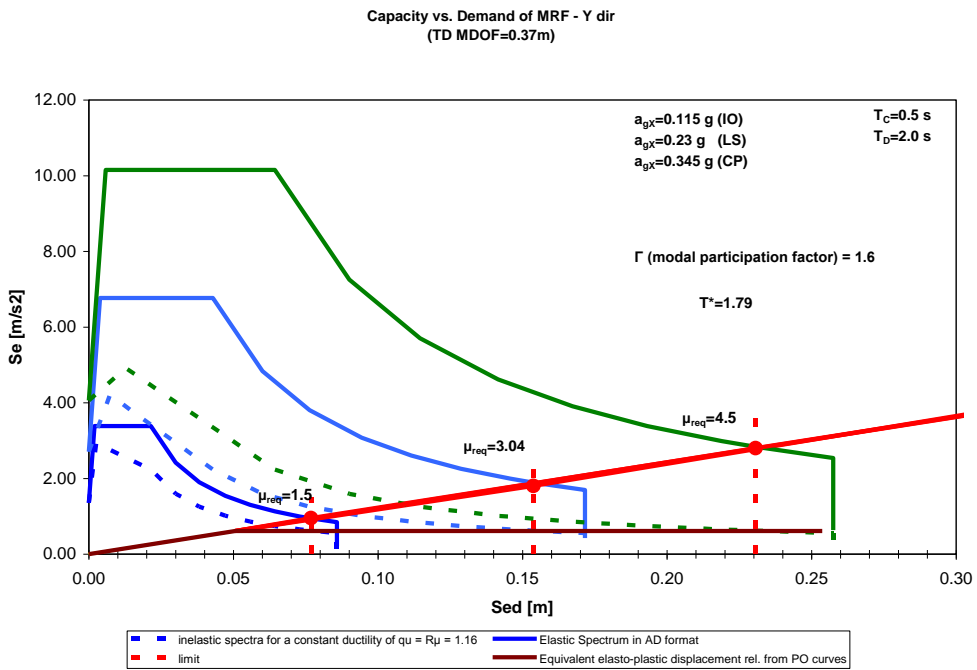


Figure 5.23 Demand and capacity diagram of the equivalent SDOF system MRF - Y direction

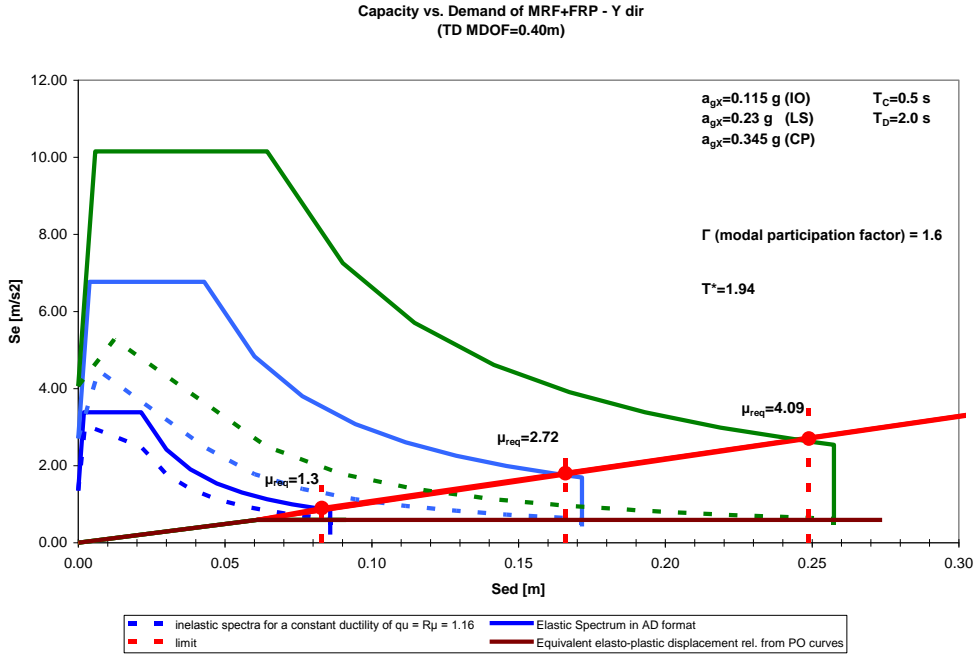


Figure 5.24 Demand and capacity diagram of the equivalent SDOF system MRF+FRP - Y direction

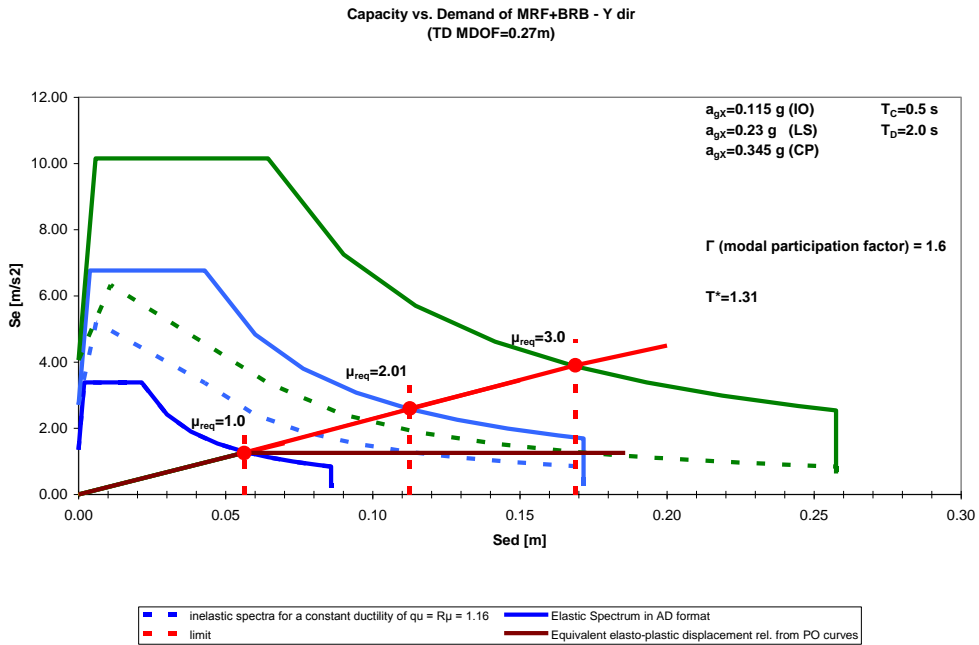


Figure 5.25 Demand and capacity diagram of the equivalent SDOF system MRF+BRB - Y direction

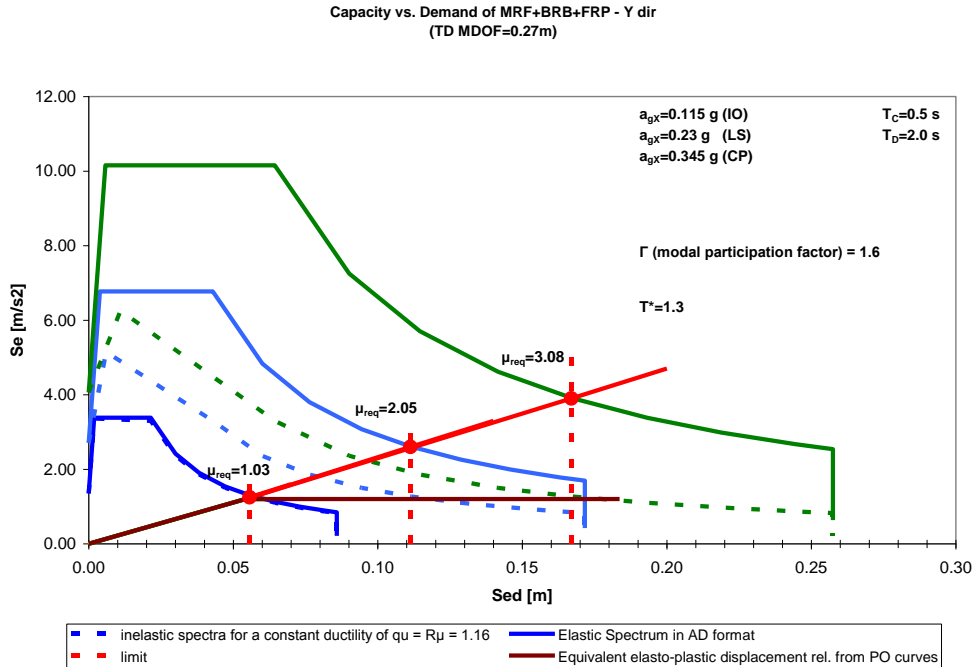


Figure 5.26 Demand and capacity diagram of the equivalent SDOF system MRF+FRP+BRB - Y direction

### 5.2.3 Nonlinear Dynamic Analysis

As the results of the static nonlinear analysis were partially favorable, it was decided to investigate the seismic performances of the structure before and after the retrofitting by means of nonlinear dynamic analysis. Seven artificial accelerograms were generated (Figure 5.27), whose response spectra are compatible with the design spectra from Eurocode 8 (PGA = 0.23g and  $T_c=0.5$  s).

Each artificial accelerogram was scaled so as to attain the hazard level of IO, LS and CP performance levels. For IO, the PGA was scaled down by 0.5 and CP was scaled up by a factor of 1.5. For LS the PGA corresponded to the design situation (PGA = 0.23g). The results of the nonlinear dynamic analysis are detailed in Annex 1.

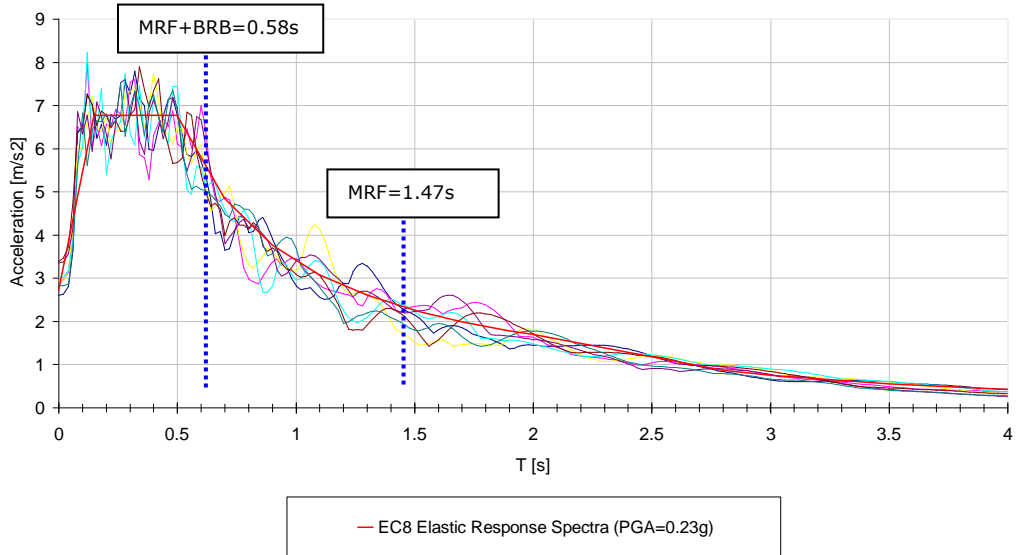


Figure 5.27 Artificial elastic response spectra of the artificial accelerograms vs. elastic response spectra, 5% damping

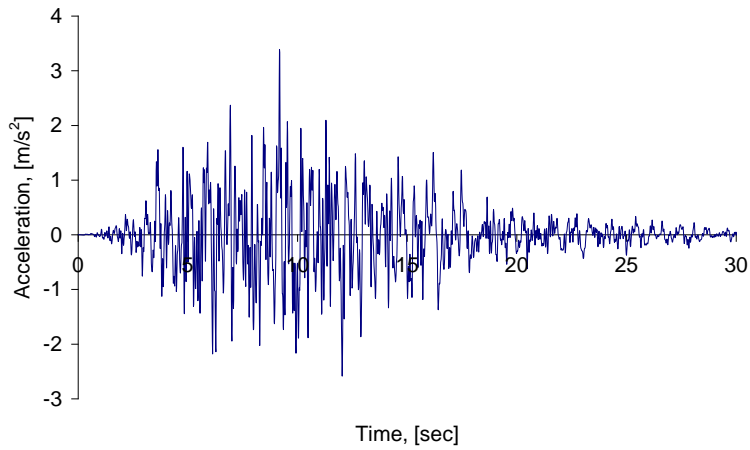


Figure 5.28 Example of an artificial accelerogram used in the time history analysis

The location of the corresponding point for the top displacement is presented in Figure 5.29.

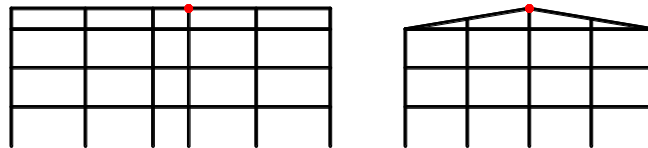


Figure 5.29 Position of the reference point for top displacement



Figure 5.30 and Figure 5.31 show the history of the top displacement for the initial structure MRF and the initial structure with local retrofitting MRF+FRP, on X direction. Similarly to the results of the static nonlinear analysis, it can be seen that the contribution of local retrofitting is reduced.

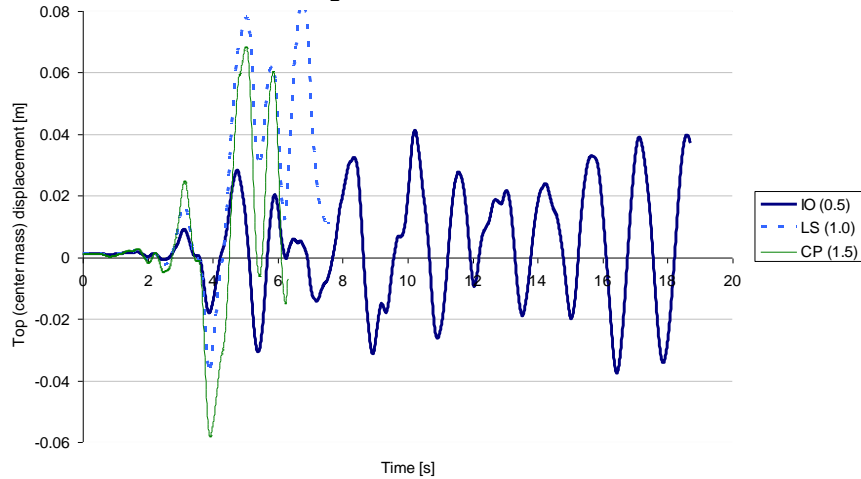


Figure 5.30. History of the top displacement on X direction for MRF, at IO, LS and CP, 2<sup>nd</sup> accelerogram

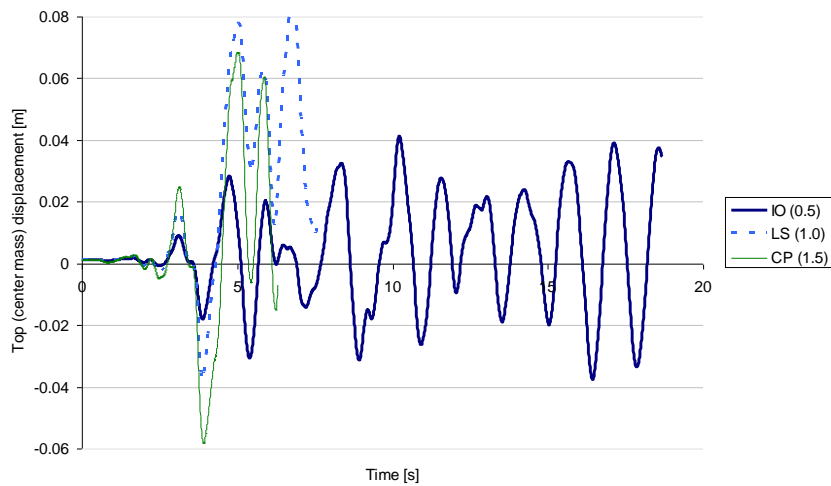


Figure 5.31. History of the top displacement on X direction for MRF+FRP, at IO, LS and CP, 2<sup>nd</sup> accelerogram

The structure fails under a ground motion scaled to LS and CP due to the development of plastic hinges in the columns of the ground floor. The initial RC frame structure (MRF) has limited ductility and does not attain the displacement demands for LS and CP levels. The benefit of local retrofitting is reduced.

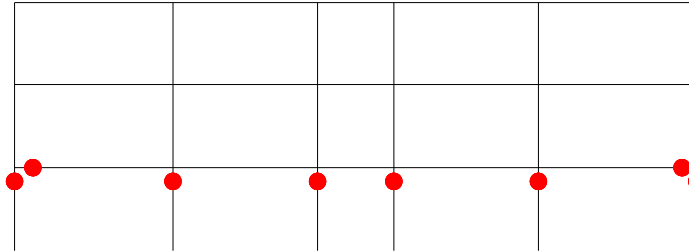


Figure 5.32. Location of plastic hinges (elements at CP level), frame in X direction, MRF structure in LS stage, 2<sup>nd</sup> accelerogram

Figure 5.33 and Figure 5.34 show the history of the top displacement of the structure with global retrofitting system MRF+BRB and for the structure with global retrofitting system and local retrofitting MRF+FRP+BRB, on X direction. The structure has a favorable behavior until LS, with the initiation of plastic deformations in the concrete elements (Figure 5.36). Concerning the development of plastic hinges in columns, this can be avoided if the columns are strengthened locally. The application of FRP served also to increase the local confinement but it can be applied also to local strengthening. Another option is to reduce the ductility demand by reducing the behavior factor  $q$  of the bracing system. The structure does not meet the requirements for CP and fails prematurely under a ground motion scaled between LS and CP, due to the exhaustion of the plastic deformation capacity in concrete columns.

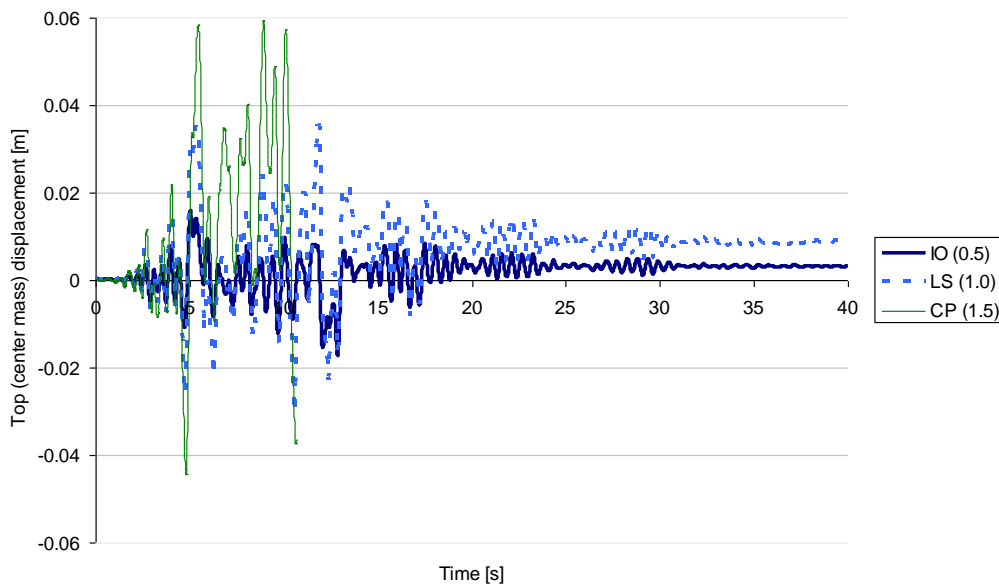


Figure 5.33. History of the top displacement on X direction for MRF+BRB, at IO, LS and CP, 2<sup>nd</sup> accelerogram

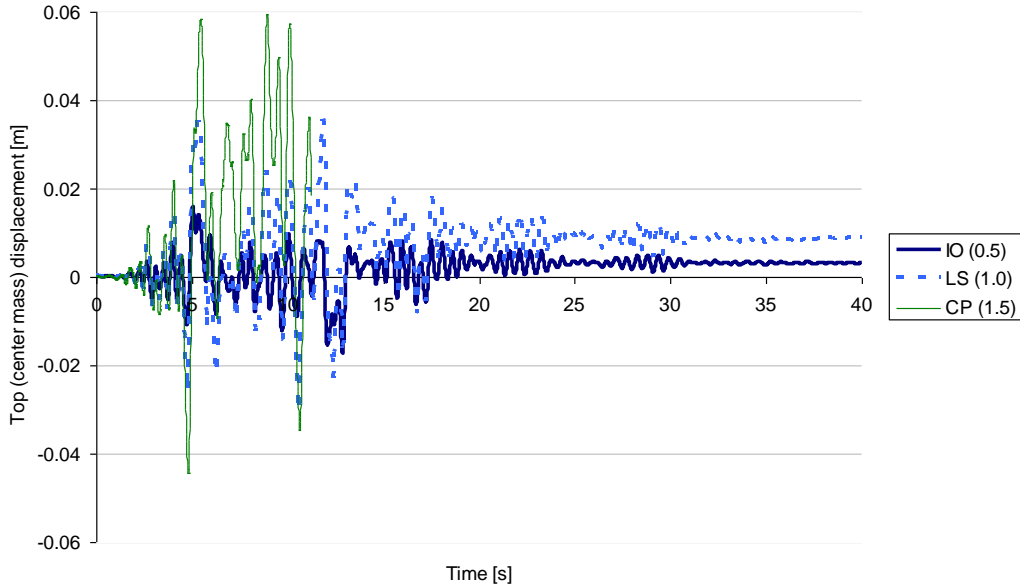


Figure 5.34. History of the top displacement on X direction for MRF+BRB+FRP, at IO, LS and CP, 2<sup>nd</sup> accelerogram

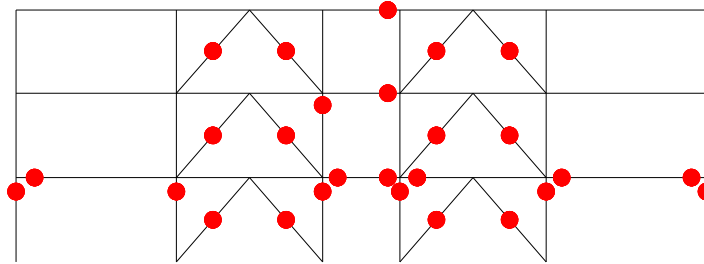


Figure 5.35 Location of plastic hinges (elements at IO level), frame in X direction, MRF+BRB+FRP structure in LS stage, 2<sup>nd</sup> accelerogram

Table 5.7 shows the values of plastic rotations in beams and columns and plastic deformations in braces.

The initial RC structure shows poor performances, and even for the IO level there are elements that fail due to the exhaustion of the deformation capacity. No benefit is observed when concrete elements are locally confined by using FRP.

When the structure is retrofitted with BRB's, the structure attains the IO and LS levels, but it fails in attaining the CP level, due to the failure of the concrete columns. Therefore, it is necessary to strengthen the columns and not only to confine them, in order to fulfill the requirements for the three performance levels.

Table 5.7. Plastic rotations and deformations in elements for static and dynamic nonlinear analysis

Analysis	PL	Elements	MRF	MRF+FRP	MRF+BRB	MRF+FRP+BRB
TH, X direction	IO	Beams[rad]	0.0014	0.0014	0	0
		Columns [rad]	LF	LF	0	0
		BRBs [m]			0.007	0.007
	LS	Beams [rad]	NA	NA	0.0014	0.0014
		Columns [rad]	NA	NA	0.0033	0.0033
		BRBs [m]			0.016	0.016
PO, X direction	IO	Beams [rad]	0.003	0.003	0.0028	0.0028
		Columns [rad]	LF	LF	0.0049	0.0056
		BRBs [m]			0.028	0.028
	LS	Beams [rad]	NA	NA	0.01	0.0098
		Columns [rad]	NA	NA	LF	LF
		BRBs [m]			LF	LF

Notes:

TH – nonlinear dynamic analysis

PO – nonlinear static analysis

PL – performance level

NA – not attained

LF – local failure due to the exhaustion of the plastic deformation capacity

### 5.2.4 Incremental Dynamic Analysis (IDA)

Current seismic codes are based on the force-controlled design, by using the base shear approach. The parameter related to the degradation of the structure is the behavior factor  $q$ , based on the maximum capacity of the structure to dissipate energy in the ultimate limit state (ULS). The  $q$  factor is composed of two main factors, which are the ductility factor,  $R_{\mu}$ , that accounts for the ductility of the structure and the overstrength factor  $R_s$  that accounts for the reserve of strength in the structure. There are several factors that lead to the system overstrength, like structural redundancy, material overstrength, member oversize due to design, other non seismic load combinations and serviceability requirements [77]. The behavior factor  $q$  may be evaluated with the following equation:

$$q = \frac{\lambda_u}{\lambda_1} \quad (5.8)$$

where:

- $\lambda_u$  is the acceleration multiplier for the ultimate limit state
- $\lambda_1$  is the acceleration multiplier for first yielding

In order to evaluate multipliers  $\lambda_u$  and  $\lambda_e$ , incremental dynamic analysis IDA was employed. IDA was applied only for structure retrofitted with BRB system - MRF+BRB. In order to quantify the contribution of ductility to the  $q$  factor, a partial behavior factor was considered, by using the following formula:

$$R = R_{\mu} \cdot R_R = V_e / V_1 = \lambda_u / \lambda_1 \tag{5.9}$$

$R_R$  represents the contribution of structural redundancy. For the evaluation of the interstorey drift in the dynamic analysis, the following nodes were followed (see Figure 5.37). The same artificial accelerograms were used as in the previous section. Accelerograms were scaled up to a factor  $\lambda = 2$ .

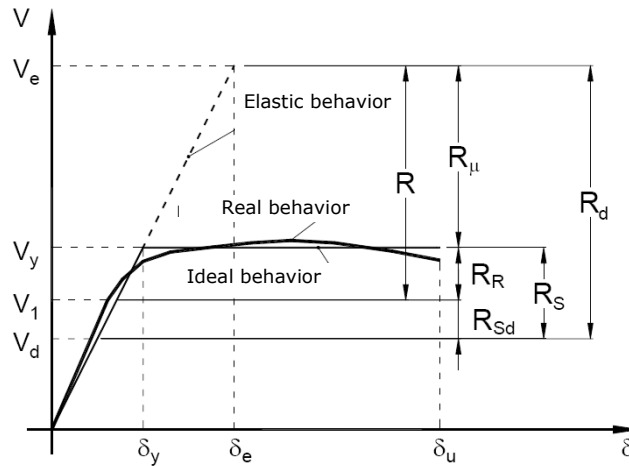


Figure 5.36 Definition of behavior factor

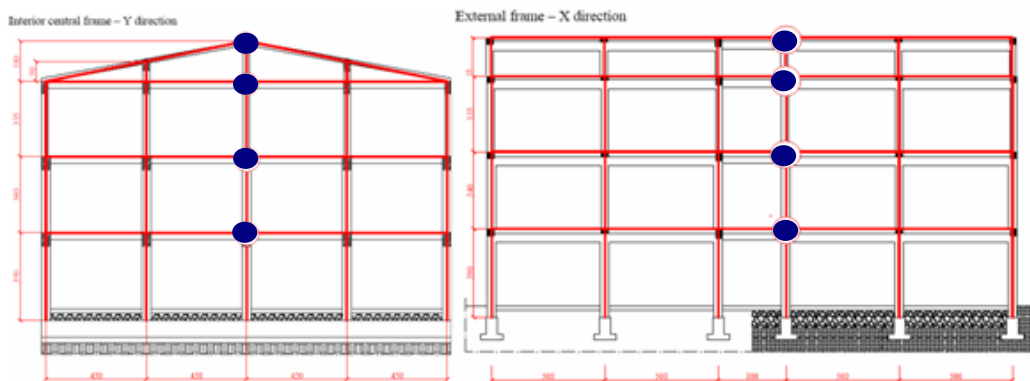


Figure 5.37 Nodes followed in IDA

The values of the partial behavior factor  $q$  obtained by using equation  $q = \frac{\lambda_u}{\lambda_1}$  (5.8), on X and Y directions, are summarized in Table 5.8. The mean

value of the  $q$  factor on X direction is larger than the value considered in the analysis of the structure, which was  $q = 4$ . On Y direction, the  $q$  factor is close to the value used for design and amounts to 3.9. It is important to note that even the accelerograms were scaled so as to fit the response spectra given by the code, the results are scattered, ranging from 3.0 to 5.5 on X direction and from 3.5 to 4.3 on Y direction. The values of  $q$  factors presented in Table 5.8 represent only the contribution of ductility. It is expected that these values could be enlarged if the

overstrength (see 1st paragraph) of the system is large. However, the value of this overstrength can be very different from one structure to another, and therefore the values of the  $q$  factor may be different.

**Incremental Dynamic Analysis (IDA) - MRF+BRB - X direction**

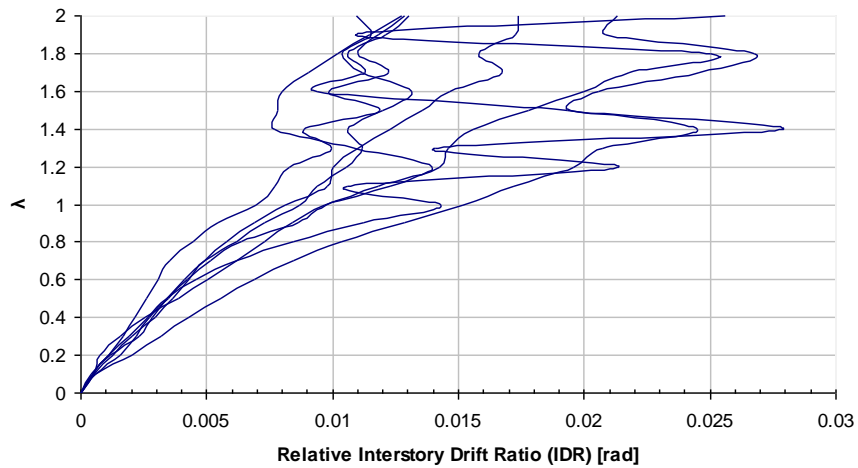


Figure 5.38 Relative interstorey drift vs. seismic multiplication factor  $\lambda$  on X direction

**Incremental Dynamic Analysis (IDA) - MRF+BRB - Y direction**

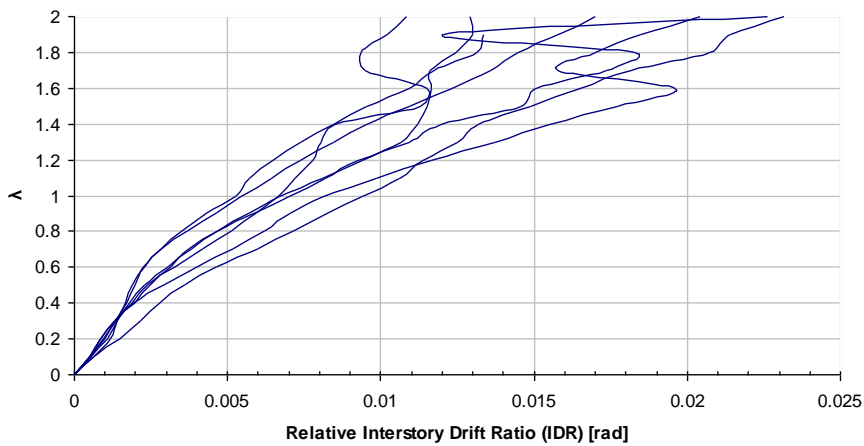


Figure 5.39 Relative interstorey drift vs. seismic multiplication factor  $\lambda$  on Y direction

Table 5.8: Values of the partial behavior factor  $q$ 

Artificial Accelerogram	X direction			Y direction		
	$\lambda_1 (IO)$	$\lambda_u (LS)$	$q = \lambda_u / \lambda_1$	$\lambda_1 (IO)$	$\lambda_u (LS)$	$q = \lambda_u / \lambda_1$
Accelerogram 1	0.3	1.3	<b>4.3</b>	0.4	1.6	<b>4.0</b>
Accelerogram 2	0.3	1.2	<b>4.0</b>	0.4	1.6	<b>4.0</b>
Accelerogram 3	0.3	1.3	<b>4.3</b>	0.4	1.6	<b>4.0</b>
Accelerogram 4	0.2	1.0	<b>5.0</b>	0.3	1.3	<b>4.3</b>
Accelerogram 5	0.3	1.2	<b>4.0</b>	0.4	1.5	<b>3.8</b>
Accelerogram 6	0.2	1.1	<b>5.5</b>	0.4	1.4	<b>3.5</b>
Accelerogram 7	0.3	0.9	<b>3.0</b>	0.4	1.4	<b>3.5</b>
<b>Average on X</b>			<b>4.3</b>	<b>Average on Y</b>		<b>3.9</b>

### 5.3. Conclusions

The static and dynamic nonlinear analysis was performed in order to evaluate the performances of an existing RC frame building. The preliminary results have shown that the structure is vulnerable and does not meet the seismic requirements. Therefore, it was decided to retrofit the structure by means of a BRB system. Additionally, a local confinement of the concrete elements by means of FRP was envisaged.

The results have shown that the initial structure MRF and the initial structure with local retrofitting MRF + FRP have a limited ductility and do not attain the displacement demands for LS and CP levels. The benefit of local retrofitting is reduced. When the global retrofitting is accomplished MRF+BRB, the behavior is much improved. The stiffness and strength increase, and the structure attains the LS performance. The structure cannot attain the CP level, due to the failure of the concrete structure. The contribution of the local retrofitting is again very limited. Therefore, it is necessary to strengthen the columns, and not only to confine them in order to fulfill the requirements for the three performance levels.

The analysis focused also on the evaluation of the behavior factor  $q$ . The mean value of the  $q$  factor was larger than the initial value considered in the analysis. Even so, the use of a high  $q$  factor may not be recommended, as the deformation capacity supply of RC elements is reduced. Therefore, the retrofitting of existing RC frames with buckling restrained steel braces can be based on  $q$  factors amounting to 3 – 3.5. If larger  $q$  factors are used, the strengthening of the concrete elements is necessary.

## 6. EXPERIMENTAL QUALIFICATION OF BRB SYSTEMS FOR THE SEISMIC RETROFITTING OF REINFORCED CONCRETE FRAMED STRUCTURES

### 6.1 Introduction

A large proportion of the existing Reinforced Concrete Frame Buildings designed for gravity loads RC GLD proved their vulnerability during recent earthquakes. Most of these RC building were designed and constructed without considering the seismic action.

In Chapter 5, the seismic performance of an existing RC building was analyzed by using nonlinear static and dynamic analysis. The structure showed very poor ductility and failed in a brittle manner. The structure was retrofitted by means of Buckling Restrained Braces. The application of the retrofitting technique showed an important improvement, especially in strength and stiffness, but also in ductility. Based on the good results obtained in Chapter 5, a testing program was developed in Chapter 6, in order to prove the efficiency of the retrofitting system based on BRB. The retrofitting system is applied to a RC portal frame, selected from the RC building.

The experimental program aims at evaluating the performances of the retrofitted structure. The performances of the BRB system are evaluated in terms of acceptance criteria. The connection of the BRB to the existing concrete frame structure is very important, both in terms of performance and workability.

### 6.2 Frame model

#### 6.2.1 RC frame

The RC frame extracted from the RC building is located at the second floor on Y direction. The main reason for selecting the frame from this floor comes from the limitation of the testing capacity in the Laboratory. Concrete elements of this floor are reduced, compared to the elements of the lower floors.

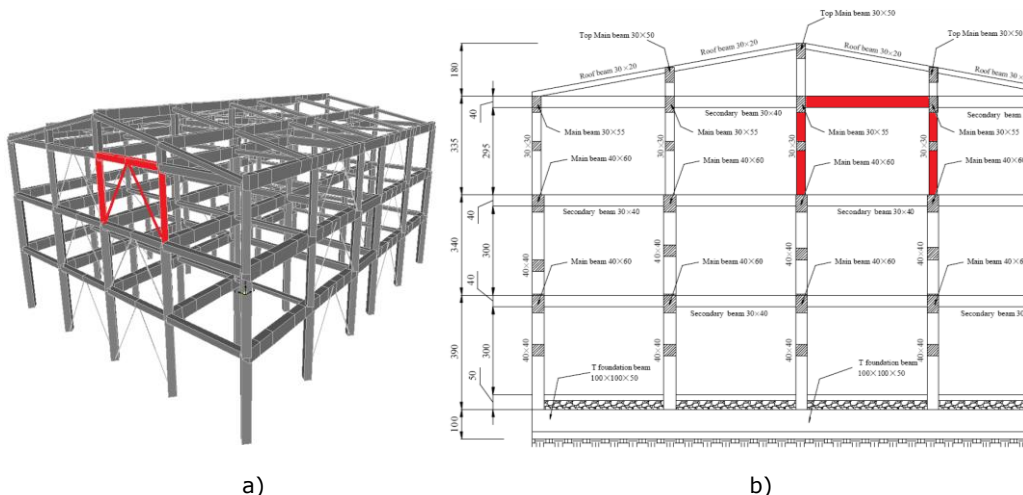


Figure 6.1 RC frame location: a) 3D view; b) plan view of the third floor



### 6.2.2 Details of the concrete frame

All details regarding the number of rebars, the distribution of rebars in element cross section, the distance between stirrups (15 cm for columns and 25 cm for beams) and diameters were similar to those from the Benchmark structure [70], see Chapter 5. The cover concrete was considered 2.5 cm.

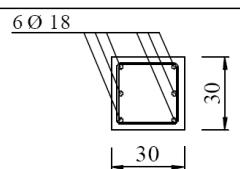
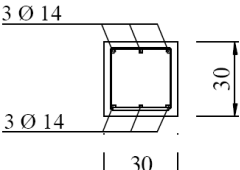
<p><b>Second floor / columns C1, D1</b></p> <p>Cross section Longitudinal reinforcing bars: - 2 position of nr. 3 bars, diameter 18 mm Stirrup: nr. 1 bar, diameter 6 mm, spacing 15 cm</p>	<p>Shape: rectangular 30 x 30 cm</p> 
<p><b>Frame nr. 4 / First, second and third floor / Secondary beam</b></p> <p>Cross section Longitudinal reinforcing bars: - upper position nr. 3 bars, diameter 14 mm - bottom position nr. 3 bars, diameter 14 mm Stirrup: nr. 1 bar, diameter 6 mm, spacing 25 cm</p>	<p>Shape: rectangular 30 x 30 cm</p> 

Figure 6.2 RC elements cross sections (columns and beam)

As the frame selected for the experimental program is an interior frame, the longitudinal reinforcements from the columns and beam need to be anchored appropriately. In order to assure a sufficient anchorage length, the rebars were bent so as to assure a sufficient anchorage length. In order to limit the influence on the strength capacity of beams and columns, the bent was made inside the beam-column joint.

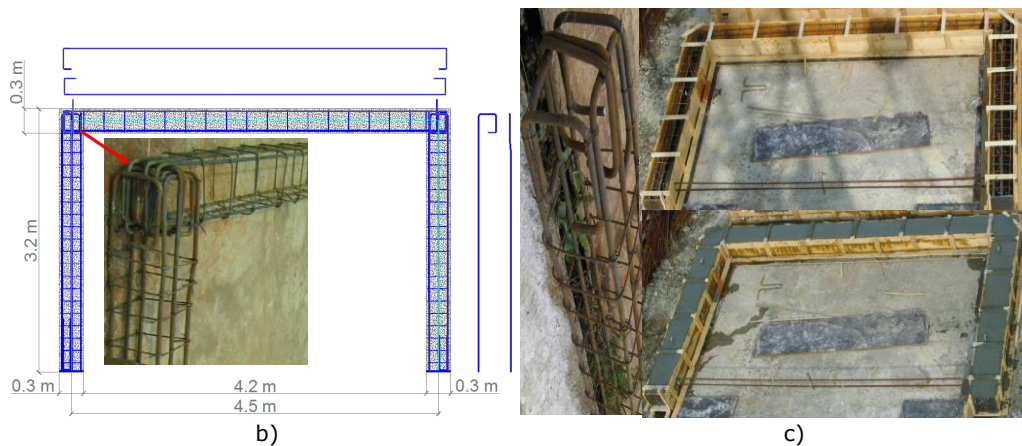


Figure 6.3 RC frame and node details: a) rebars bent in the joints; b) formwork of the concrete frame

In order to keep the same construction details, plane rebars were used for all reinforcements.

Table 6.1).

Table 6.1 Theoretical vs. quality certificate vs. experimental rebars samples material characteristics

Materials used for RC Frame	Theoretical	Quality Certificate	Experimental
Standard	STAS 438/1-89		
<b>Stirrups <math>\Phi 6</math></b>	OB37	OB37	Specimen Test
Minimum Yield strength Re [N/mm <sup>2</sup> ]	235	289 - 303	NA
Tensile strength Rm [N/mm <sup>2</sup> ]	360	402 - 424	NA
Minimum Elongation %	25	38.0 - 41.5	NA

Materials used for RC Frame	Theoretical	Quality Certificate	Experimental
Standard	STAS 438/1-89 & ST 009 - 2005		
<b>Beam rebars <math>\Phi 14</math></b>	OB37	OB37	Specimen Test
Minimum Yield strength Re [N/mm <sup>2</sup> ]	235	312	497
Tensile strength Rm [N/mm <sup>2</sup> ]	360	448	623
Minimum Elongation %	25	36	31

Materials used for RC Frame	Theoretical	Quality Certificate	Experimental
Standard	STAS 438/1-89 & ST 009 - 2005		
<b>Column rebars <math>\Phi 18</math></b>	OB37	OB37	Specimen Test
Minimum Yield strength Re [N/mm <sup>2</sup> ]	235	287	402
Tensile strength Rm [N/mm <sup>2</sup> ]	360	402	537
Minimum Elongation %	25	38	25


	
<p>Concrete material for RC frame (1m<sup>3</sup>): (C20/25 =&gt; Rc = 20.5 N/mm<sup>2</sup>)</p> <ul style="list-style-type: none"> <li>- aggregates: 1708 Kg               <ul style="list-style-type: none"> <li>type I: (0-4) mm – 632 Kg</li> <li>type I: (4-8) mm – 427 Kg</li> <li>type I: (8-16) mm – 649 Kg</li> </ul> </li> <li>- cement: II BM(S-V)32.5R - 400Kg</li> <li>- additive: BV3M (2l)</li> <li>- water: 195l</li> </ul> <p>=&gt; Rc = 35.5 N/mm<sup>2</sup> (28 days)</p> <p style="text-align: center;">a)</p>	<p>Concrete material for BRB infill (1m<sup>3</sup>): (C25/30 =&gt; Rc = 24.3 N/mm<sup>2</sup>)</p> <ul style="list-style-type: none"> <li>- aggregates: 1660 Kg               <ul style="list-style-type: none"> <li>type I: (0-4) mm – 614 Kg</li> <li>type I: (4-8) mm – 415 Kg</li> <li>type I: (8-16) mm – 631 Kg</li> </ul> </li> <li>- cement: II BM(S-V)32.5R - 430Kg</li> <li>- additive: BV3M (1%-from cement)</li> <li>- water: 195l + 10l</li> </ul> <p>=&gt; Rc = 35.1 N/mm<sup>2</sup> (22 days)</p> <p style="text-align: center;">b)</p>

Figure 6.4 Characteristics of the concrete used for: a) RC frame; b) BRB infill material

### 6.2.3 Characteristics of the BRB system

In the first step, the analysis of the concrete frame retrofitted with the BRB system was based on the material characteristics of the Benchmark building, detailed in Chapter 5. In order to take into account the real characteristics of the materials from the specimens that were to be tested experimentally, a new analysis was performed.

As presented in details in Chapter 5, a BRB steel core plate can be divided into three main segments: the end segment (connection), the transition segment and the yielding segment (where all plastic deformation develop). Based on the

experimental results obtained in Chapter 4, polyethylene foil of 1 mm thickness was used as the unbonding material. Table 6.2 presents the geometrical characteristics and modeling parameters. Figure 6.6 shows the bilinear force-displacement relation used in the analysis.

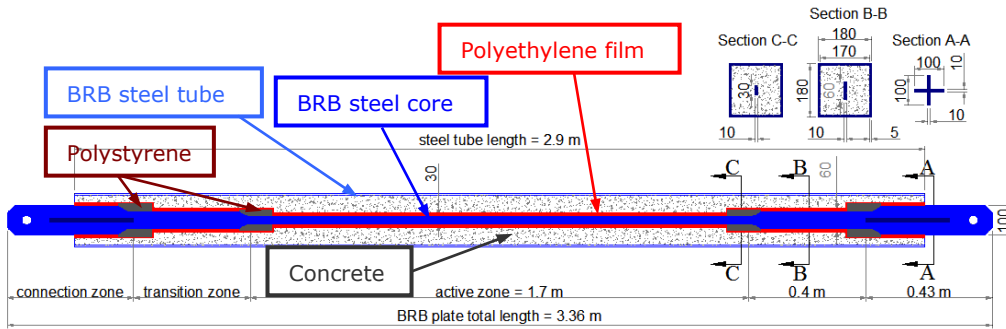


Figure 6.5 BRB composition and geometry (unbonding material – polyethylene foil, 1mm thick)

Table 6.2 Theoretical vs. experimental BRB characteristics and parameters

BRB steel plate parameters	Theoretical
Yield strength, $f_y$ [ $N/mm^2$ ]	S355
Geometry - Core Length [m]	1.7
Geometry - Core cross section [cmxcm]	1x3
Ductility parameters - in tension $\mu_T$	14.6
Ductility parameters - in compression $\mu_C$	14.8
Compression-strength adjustment factor $\beta$	1.3
Tension-strength adjustment factor $\omega$	2.2

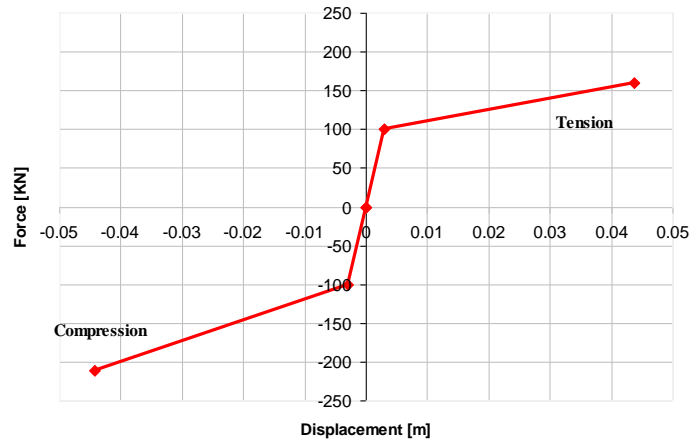


Figure 6.6 Modeling parameters for the BRB element (bilinear force-displacement relation)

The results of the coupon test on the steel from the BRB core plate are presented in Table 6.3.

Figure 6.7 shows details of the test specimens and Figure 6.8 presents the stress-strain curves for BRB steel core plates.

Table 6.3 Material characteristics of the BRB steel core plates

Material influence in BRB modeling	Theoretical	Quality Certificate	Experimental
Standard	EN10025:1993	EN10051 Class A	EN 10002-1
BRB steel plate grade	S235JRG2	S235JRG2	Specimen Test
Minimum Yield strength Re [N/mm <sup>2</sup> ]	235	255	335
Tensile strength Rm [N/mm <sup>2</sup> ]	340 - 470	360	439
Minimum Elongation %	26	39	28

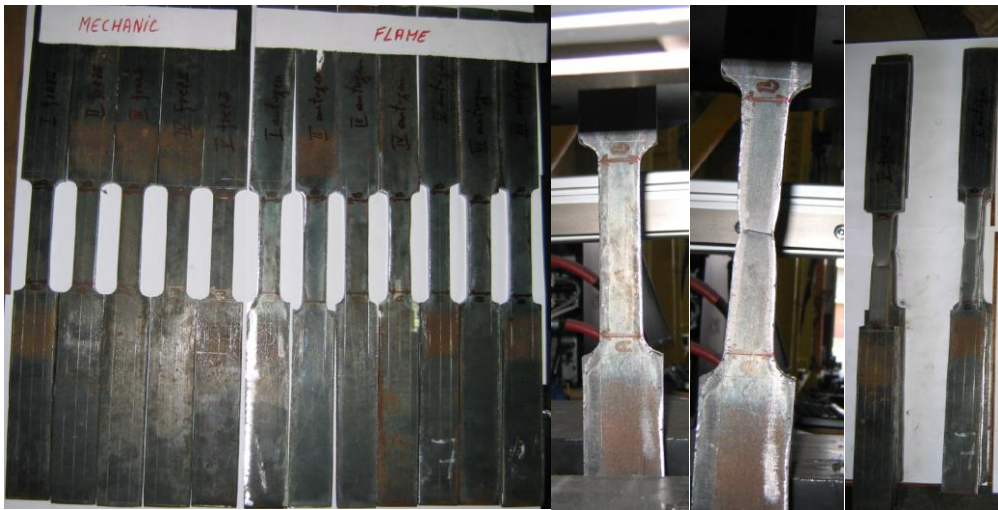


Figure 6.7 BRB steel plate specimens (5 for mechanical cut and 6 for flame cut)

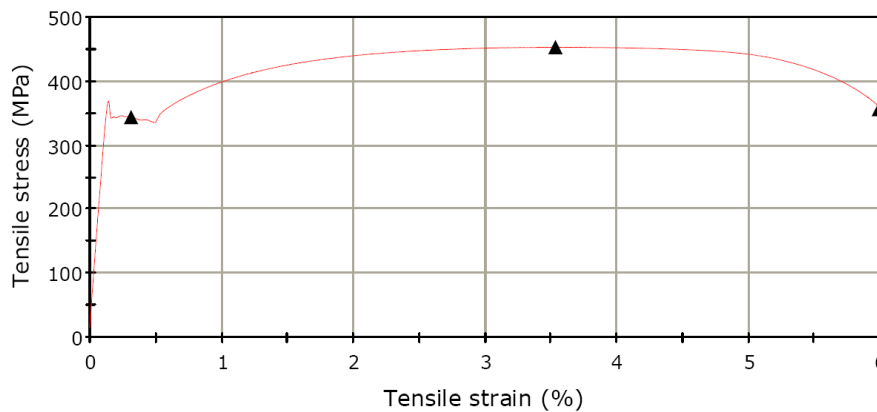


Figure 6.8 Stress-strain curves for BRB steel core material

The BRB elements were manufactured and tested in the Laboratory of Steel Structures from the "Politehnica" University of Timisoara. The following operations were performed:

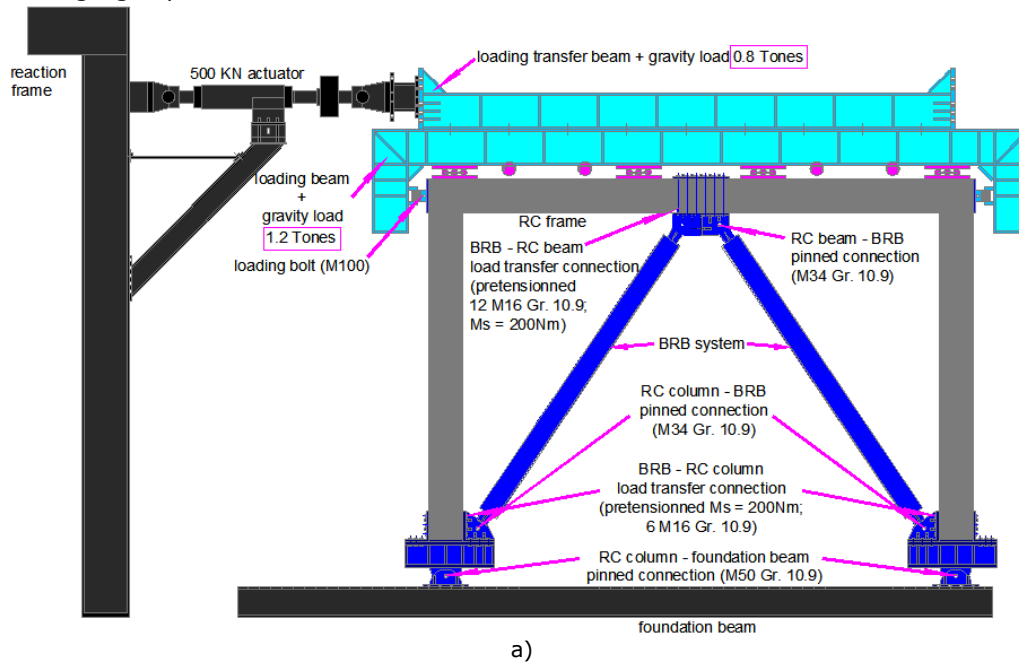
- mechanical cut
- welding of the web stiffeners
- positioning of the polystyrene
- wrapping of the unbonding material (PVC transparent foil, 1mm thick)

- insertion and calibration of the wrapped steel core into restraining steel tube
- the filling up of the infill material (concrete)

### 6.3 Testing set-up

#### 6.3.1. Testing rig and connection between BRB and RC Frame

The scheme with the testing rig and the loading system Figure 6.9.a, while in Figure 6.9.b and Figure 6.9.c, the RC frame and RC frame+BRB installed in testing rig is presented.





b)



c)

Figure 6.9 Testing rig and the loading system: a) scheme of the testing rig; b) RC portal frame (MRF); c) RC portal frame and BRB system (MRF+BRB)

Pinned connections have been used between the BRB elements and the beam and at the base of the columns (Figure 6.10 and Figure 6.11).



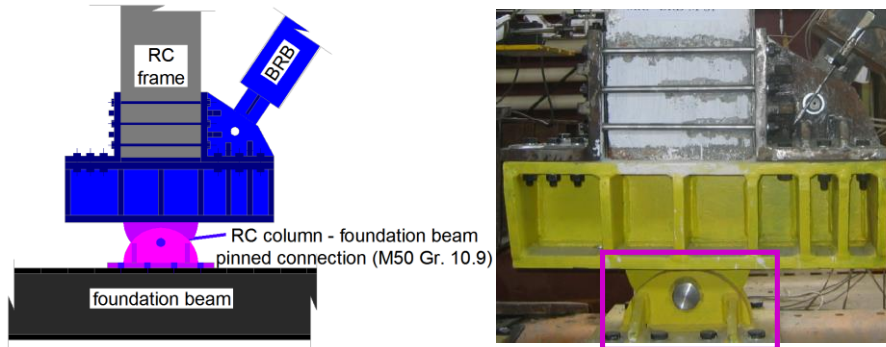


Figure 6.10 Column base connection

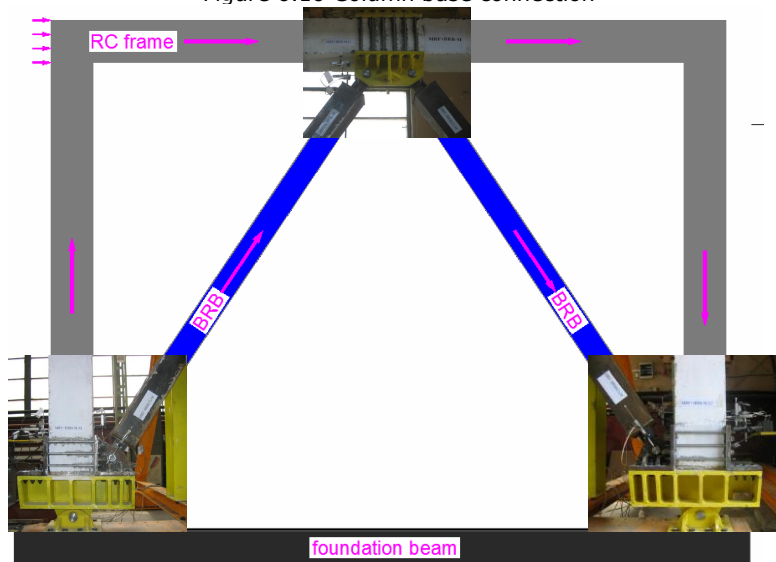


Figure 6.11 Column base and BRB connections

In order to prevent the slip of the connection between the BRB and the RC beam, high strength preloaded ties have been used. The effectiveness of the connecting device has been preliminary checked by FEM simulation. The maximum force applied to all bolts ( $F_t \times n_{bolts}$ ) by bolt pretension ( $M_s = 200Nm$ ), creates a pressure ( $\sigma_{pl}$ ) which is smaller than the compressive strength of the RC beam. Consequently, the friction force ( $F_f$ ) between the steel plate and the concrete element should be larger than the cumulated horizontal  $BRB_H$  force (Figure 6.13).

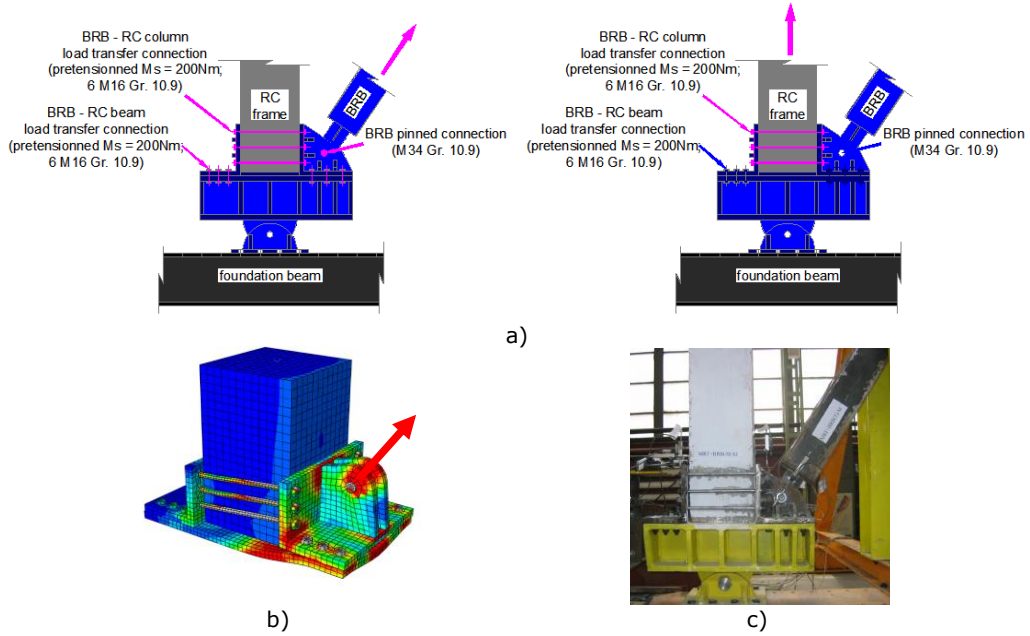


Figure 6.12 Column base and BRB to column connections: a) BRB and RC column; c) FEM modeling; d) detail of the BRB - RC connection

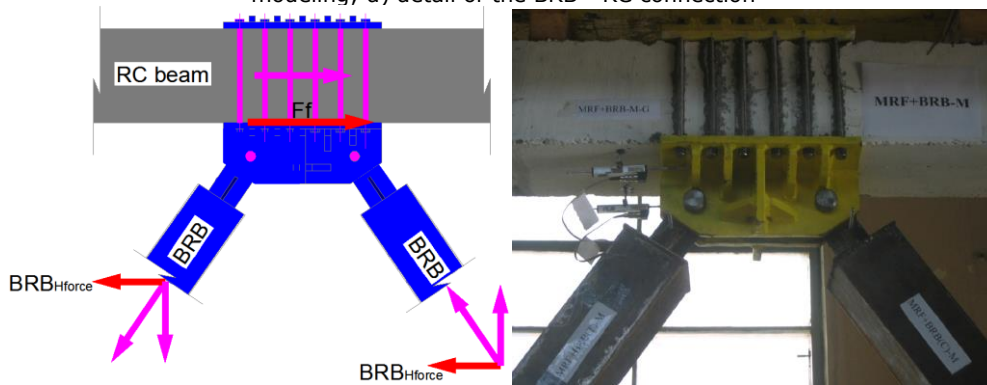


Figure 6.13 Friction between BRB connection and the beam

The numerical simulation aimed to calibrating the level of pre-stressing forces in the ties in order to avoid the slippage of the connection. Local pressure on the concrete was also checked, in order to keep the connection "elastic" (Figure 6.14).



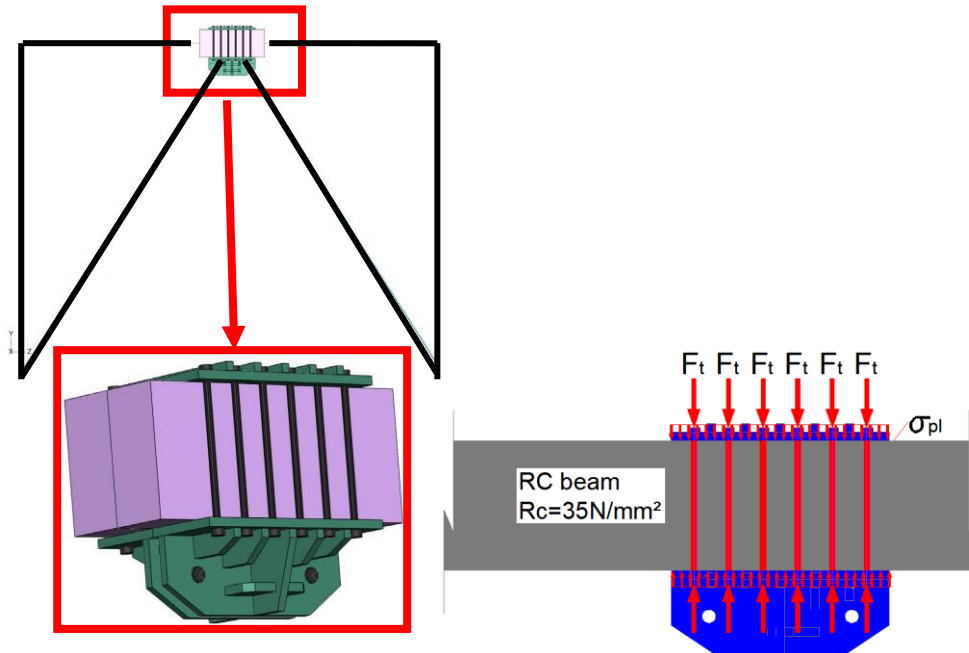
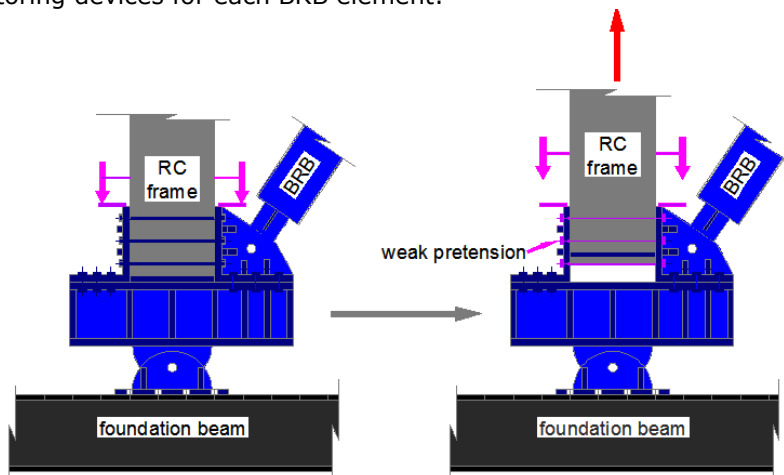


Figure 6.14 Numerical simulation: a) RC beam – BRB connection; b) RC beam – BRB connection: pressure under the steel plate due to bolts pre-stressing

### 6.3.2. Monitoring devices and measurements

In order to monitor the connection between BRB's and the RC columns, four measurement devices were applied on the bottom of each column. Two of them measured the vertical displacement of the connection (Figure 6.15), and the other two measured the horizontal displacement of the connection (Figure 6.16). In order to monitor the slippage of the connection between the BRB and the RC beam, two monitoring devices were installed on the RC beam (Figure 6.17). Figure 6.18 shows the monitoring devices for each BRB element.



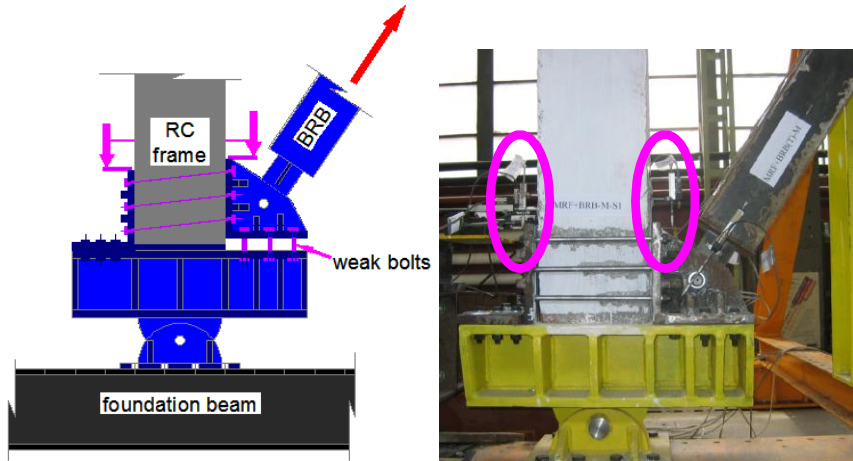


Figure 6.15 Measurement of the vertical displacement of the connection between the BRB and the column

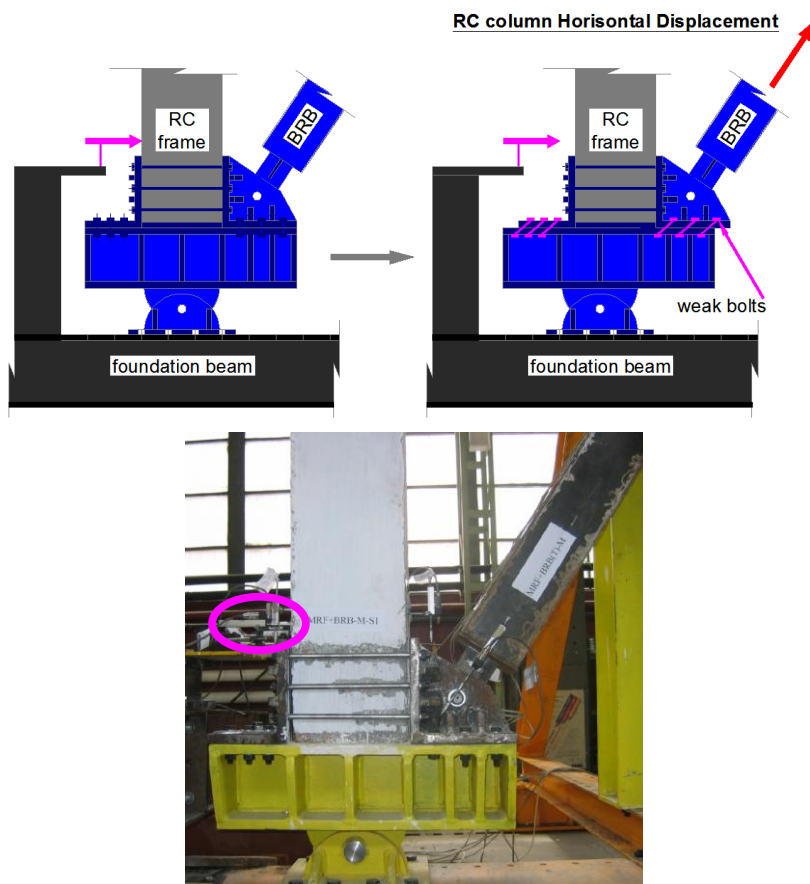


Figure 6.16 Measurement of the horizontal displacement of the connection between the BRB and the column

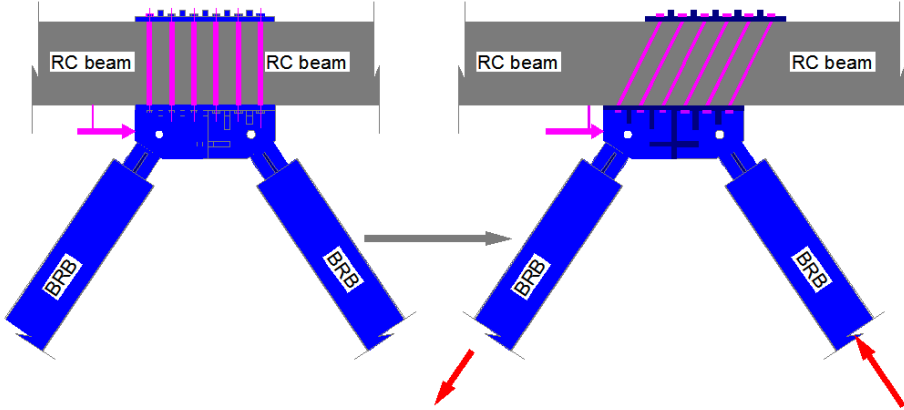
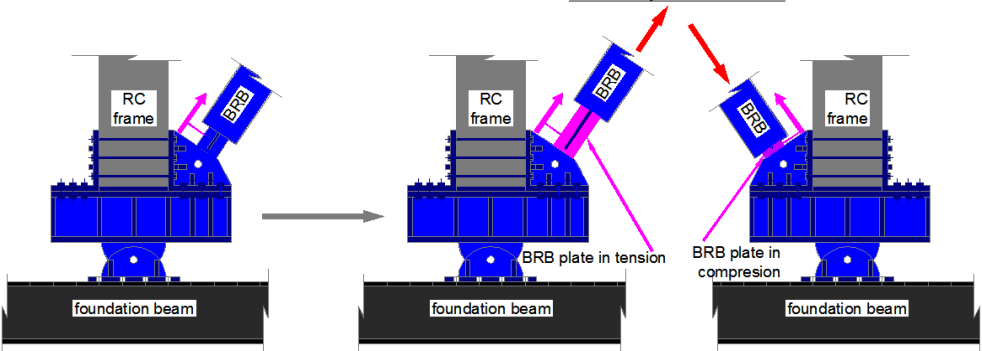


Figure 6.17 Measurement devices distribution: Horizontal on the RC beam

BRB steel plate deformation



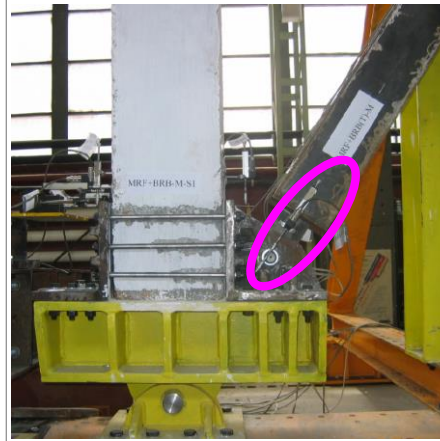


Figure 6.18 Measurement devices distribution: on BRB elements

To measure the top displacement of the RC frame, two measurement devices were positioned on the RC beam (Figure 6.19).

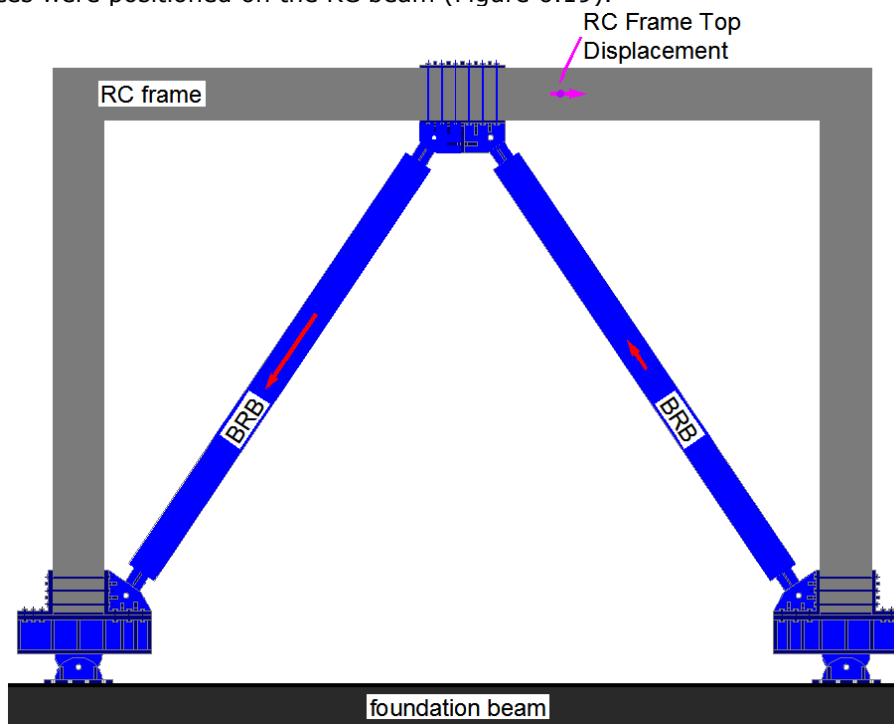




Figure 6.19 Measurement devices distribution: on RC frame

## 6.4 Loading protocol

Monotonic tests were also conducted on the frame in order to evaluate the yield point. The results from monotonic tests are also used as reference values when comparing to the cyclic tests. The quasi-static cyclic testing was carried out according to a loading protocol based on the ECCS Recommendations [68]. The loading protocol used for the test was described in detail in Chapter 4. Apart from the evaluation of the effectiveness of BRB retrofitting technique, the experimental program also aimed at evaluating the reduction factor  $q$ .

### 6.4.1. Monotonic tests

Figure 6.20 shows the force–displacement curves for the initial RC frame MRF and for the retrofitted frame MRF+BRB. The effectiveness of the seismic strengthening of the RCF frame by means of a BRB system is confirmed by the increase of the stiffness and strength. The ultimate load increases from almost 40kN to 200 kN.

In order to evaluate the yield displacement ( $D_y$ ) and the yield force ( $F_y$ ), two methods proposed by ECCS [68] were used. According to the first method, the yield load  $F_y$  is defined as the interception between the initial stiffness line at the origin of the force-displacement curve evaluated from monotonic test and the tangent line to the force-displacement curve having a slope of 10% of the initial stiffness (Figure 6.21).

According to the second method (Figure 6.22), the yield displacement is the value corresponding a certain time the deformation which would have been obtained in a purely elastic behavior. In this case, this factor was considered equal to 2.

The strain rate in the monotonic tests was 5mm/min, so that the application of the load was considered quasi-static.

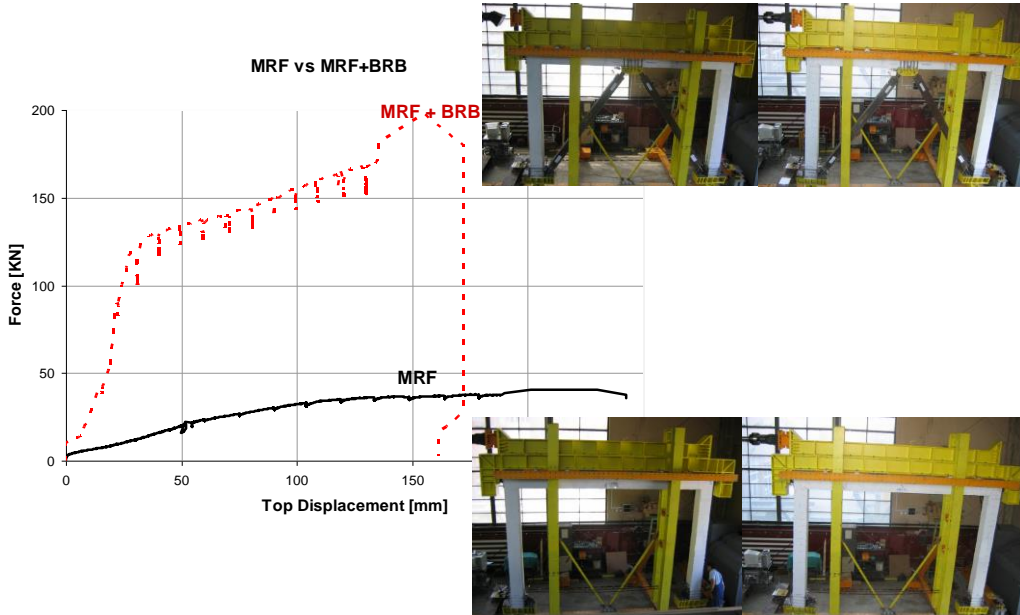


Figure 6.20 Experimental results of MRF vs. MRF+BRB: Monotonic Test

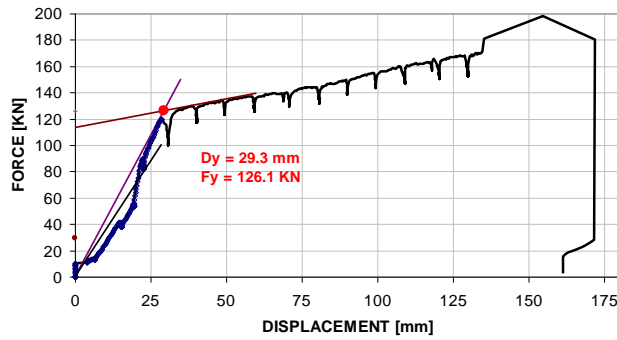


Figure 6.21 Evaluation of  $D_y$  from MRF monotonic test - method 1

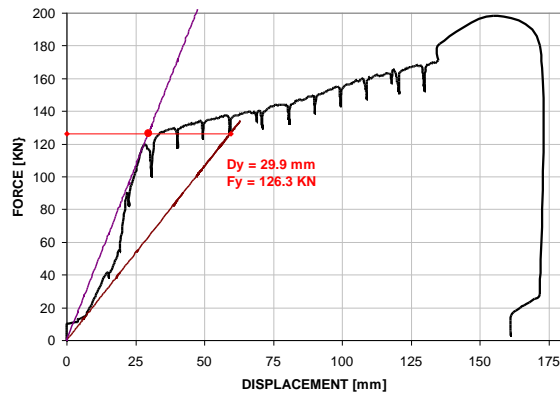


Figure 6.22 Evaluation of  $D_y$  from MRF monotonic test - method 2



### 6.4.2. Cyclic Tests

The modified ECCS loading protocol was applied in cyclic tests. This modified procedure is characterized by a single loading at  $D_y/4$ ,  $2D_y/4$ ,  $3D_y/4$  and  $D_y$ , followed by three repetitions of the cycles increased by  $0.5 D_y$  ( $1.5D_y$ ,  $2D_y$ ). Figure 6.23 presents both the original ECCS loading protocol and the modified procedure.

The strain rate in the cyclic tests was 5mm/min, so that the application of the load was considered quasi-static.

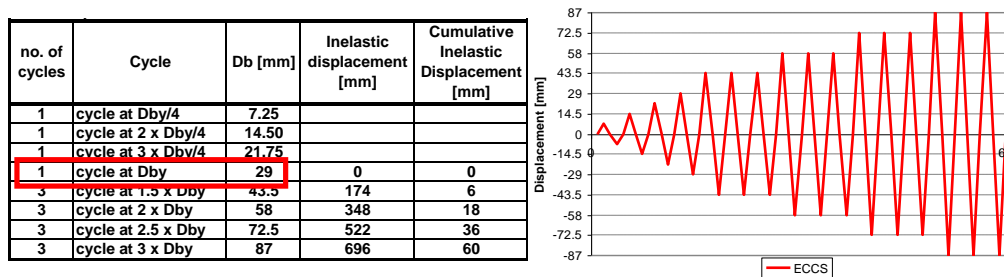


Figure 6.23 ECCS loading history for cyclic test

## 6.5 Experimental Results

### 6.5.1. Observations and direct measurements

Figure 6.24 to Figure 6.27 show the initial RC frame under cyclic loading test. The distribution of the cracks from bending and shear are presented in Figure 6.25 and Figure 6.26. Bending cracks occurred first and were followed by shear cracks. The development of shear cracks is mainly due to the inadequate distribution of stirrups. Figure 6.27 shows the failure of the beam-to-column joint.



Figure 6.24 RC frame under cyclic load



Figure 6.25 RC frame under cyclic load – development of bending cracks

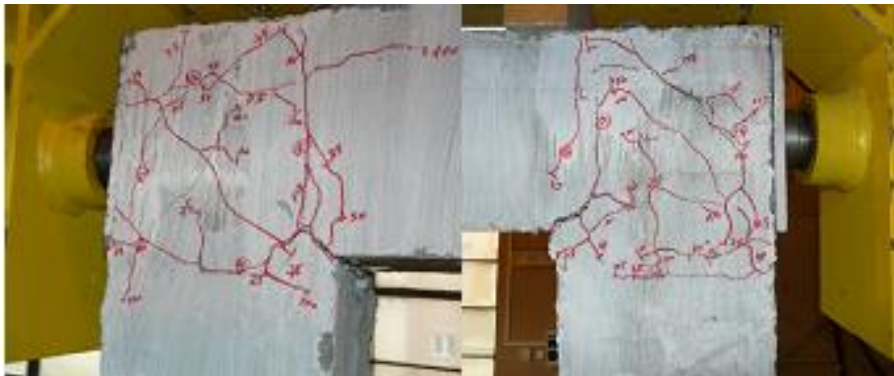


Figure 6.26 RC frame under cyclic load – development of shear cracks



Figure 6.27 RC frame under cyclic load – failure of the node

Figure 6.28 to Figure 6.30 show the retrofitted RC frame (MRF + BRB) under cyclic loading test. The distribution of the cracks from bending and shear are presented in Figure 6.29 and Figure 6.30. Bending cracks occurred first and were followed by shear cracks. The development of shear cracks is mainly due to the inadequate distribution of stirrups.





Figure 6.28 MRF + BRB under cyclic load



Figure 6.29 MRF+BRB under cyclic load – bending moment cracks



Figure 6.30 MRF+BRB under cyclic load – shear cracks at ultimate stage

In Figure 6.31 shows the force – displacement curves for RC frame before and after retrofitting. It may be noticed the contribution of the retrofitting system in terms of strength, stiffness and ductility. The behavior of the frame after retrofitting shows similar performances in tension and compression and a large strain hardening.

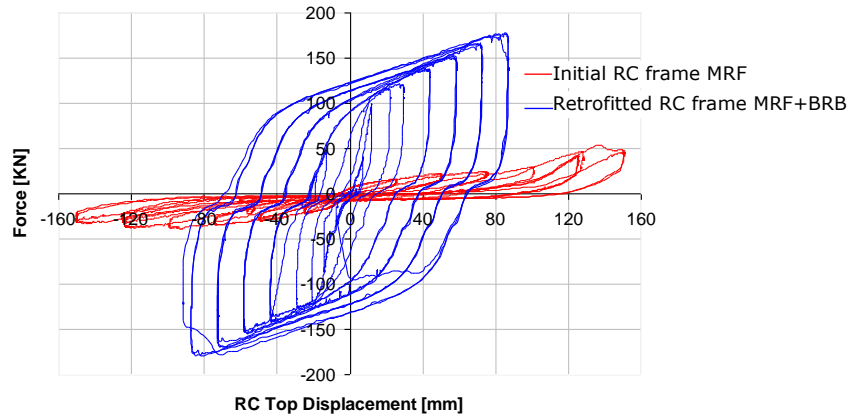


Figure 6.31 The initial RC frame vs. the retrofitted frame

Figure 6.32 and Figure 6.33 show the force–displacement curves for the left and the right braces. The two hysteretic curves show similar behavior in tension and compression, a stable plastic behavior and a very large ductility.

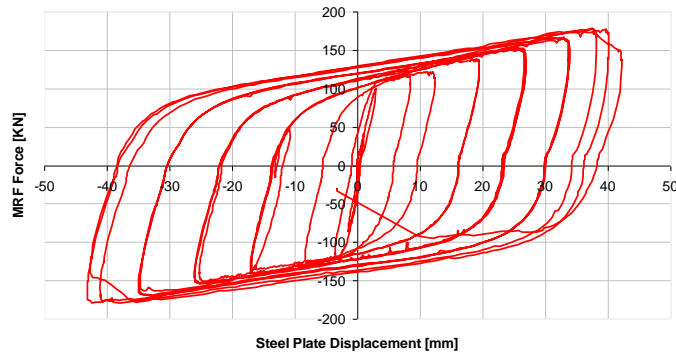


Figure 6.32 Left BRB during cyclic test

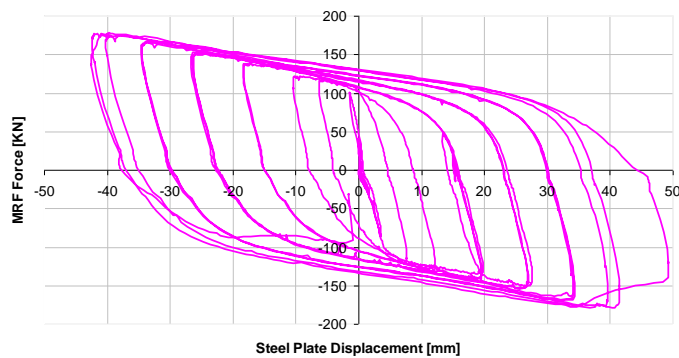


Figure 6.33 Right BRB during cyclic test

Figure 6.34 show the steel core plates after the test (left brace BRB-C-L and right brace BRB-C-R). The failure of the BRB took place before the failure of the concrete elements.



Figure 6.34 BRB steel core plates during cyclic test

All the connections between BRB system and RC frame (BRB to column and BRB to beam showed a very good behavior and no slippage was recorded).



Figure 6.35 BRB to column connection after cyclic test

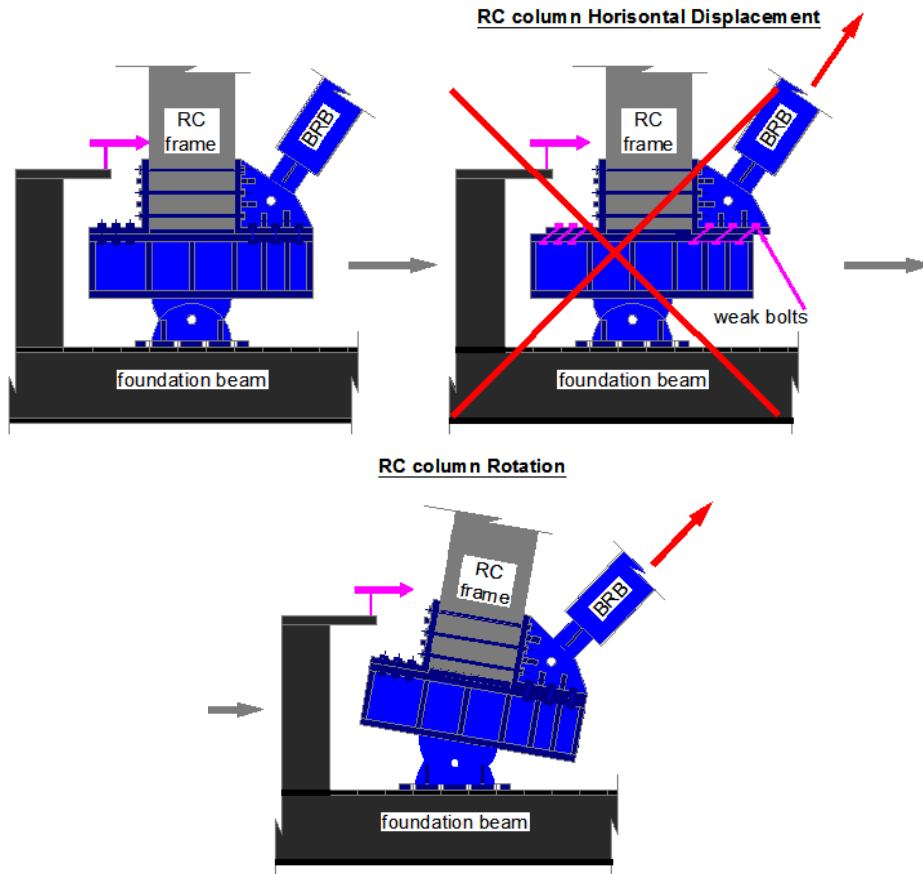
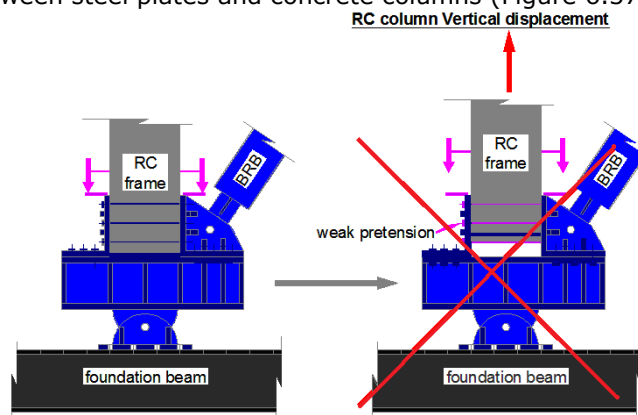


Figure 6.36 Connection between RC column and BRB - influence of horizontal displacement

From a close inspection of connection of RC columns, there was no evidence of slippage between steel plates and concrete columns (Figure 6.37 to Figure 6.39).



**BRB connection Vertical displacement**

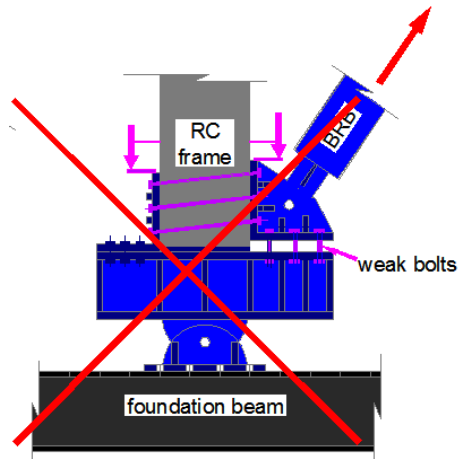
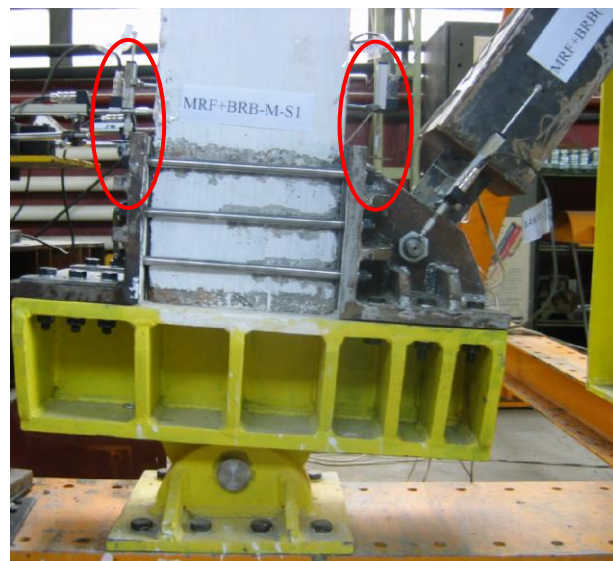


Figure 6.37 Connection between RC column and BRB – influence of vertical displacement





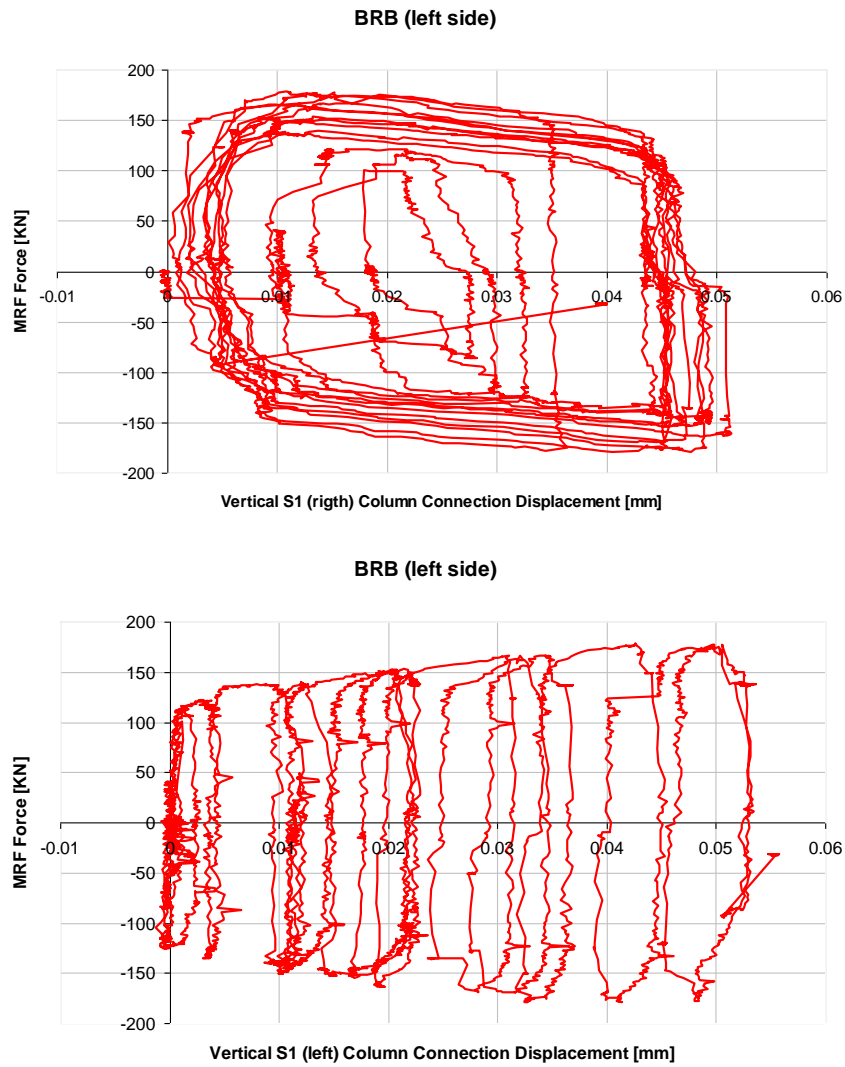
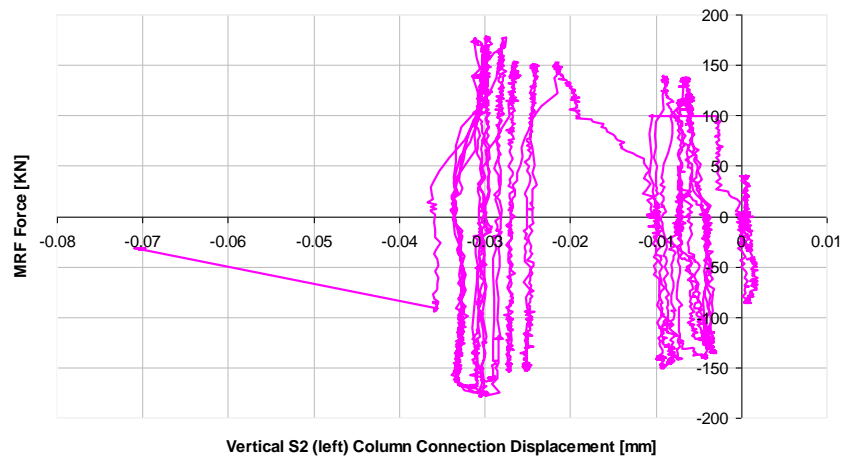


Figure 6.38 Behavior of connection between BRB and left RC column during cyclic test



BRB (right side)



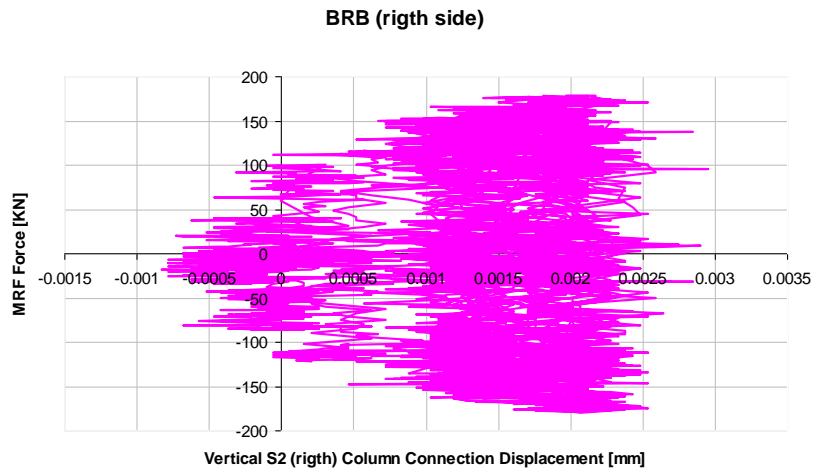


Figure 6.39 Behavior of connection between BRB and right RC column during cyclic test

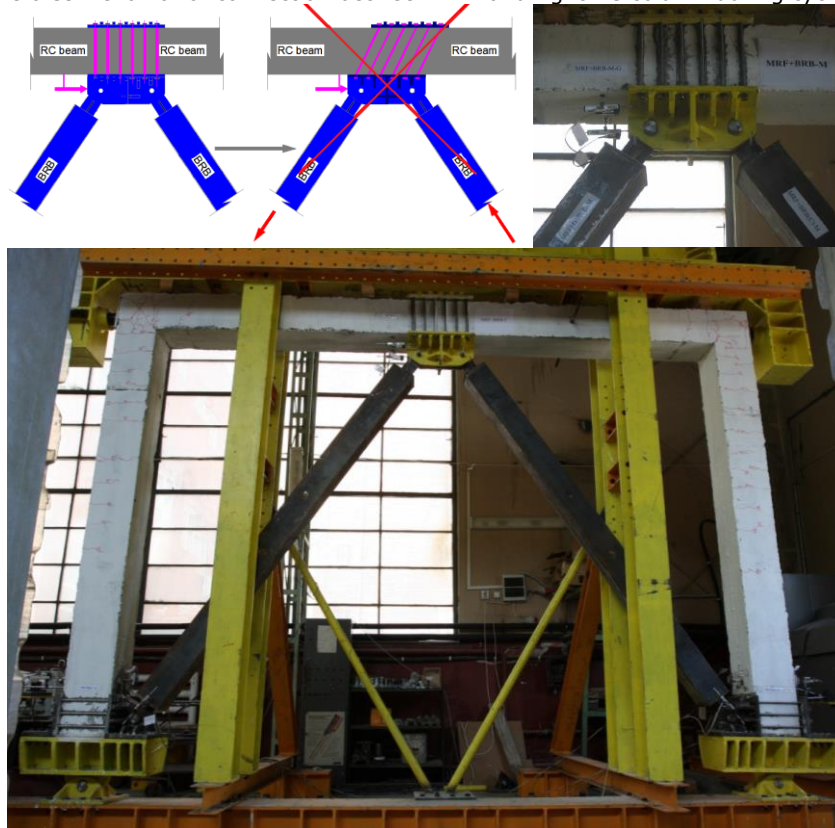


Figure 6.40 Connection between BRB and beam during the cyclic test – influence of horizontal action



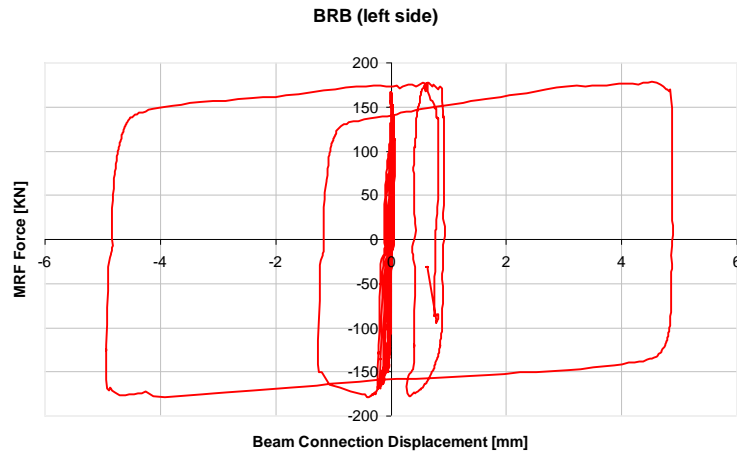


Figure 6.41 Connection between the BRB and the beam during cyclic test – hysteretic curve

When the left side BRB failed in tension, the horizontal displacements recorded at the connection between BRB and the RC beam amounted to 5 mm, only (Figure 6.40).

### 6.5.2. Evaluation of the results

Monotonic and cyclic tests were conducted on a RC frame, before and after retrofitting with a BRB system. The results were used in order to evaluate the effectiveness of the retrofitting technique and the performance criteria used in design (acceptance criteria,  $q$  factor). The influence of the type of loading was also evaluated (monotonic vs. cyclic, type of cyclic loading protocol).

Test results were compared to the results of the numerical study performed in Chapter 4 (Figure 6.42, Figure 6.43). Figure 6.42 shows the comparison between the results obtained in the monotonic tests and the results obtained using a static nonlinear analysis for initial frame (MRF) and retrofitted frame (MRF+BRB).

Based on the experimental results obtained in Chapter 6, the following parameters have been upgraded in the analysis:

- the bilinear model was transformed into a trilinear model
- FEMA356 acceptance criteria, as described in chapter 5, were modified
- ductility ratios  $\Delta_u/\Delta_y$  were estimated for tension and compression, amounting to 22 (the average value obtained from AISC cyclic loading protocol)
- the experimental values of the compression adjustment factor  $\beta=1.3$  changed to  $\beta=1.2$  and the strain hardening adjustment factor  $\omega=2.2$  changed to  $\omega=1.9$ .
- effective stiffness was applied ( $K_e$ )

This effective stiffness takes into account the variation of the cross section of the steel core along the length of the steel brace.

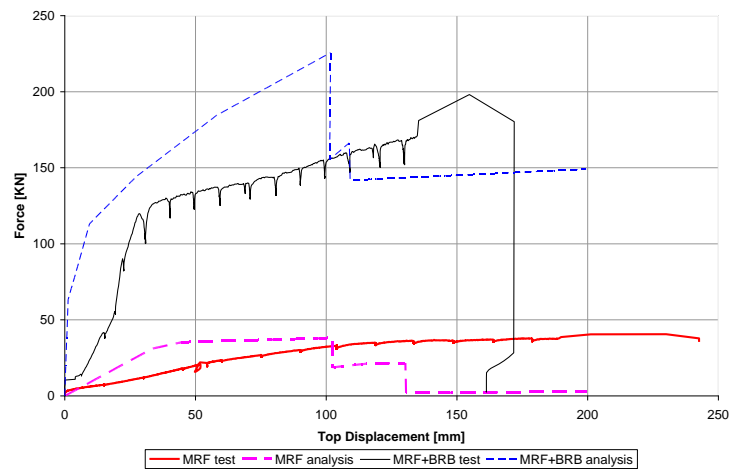


Figure 6.42: a) Numerical vs. experimental Results (Pushover Analysis vs. Monotonic test)

Figure 6.43 shows the push-over curve and the results of the monotonic and cyclic tests. It may be seen that the analysis overestimates the results obtained in the monotonic test, especially the stiffness. Numerical results are close to the results of the cyclic test. The ductility from the cyclic test is very close to the analytical one.

An important objective of the experimental program was the evaluation of the behavior factor  $q$  for RC frames, before and after retrofitting with BRB systems. For the initial RC frame - MRF, the parameter  $D_u$  corresponds to the attainment of the ultimate strength (shear strength), see Figure 6.27. For the retrofitted frame MRF+BRB,  $D_u$  corresponds to the failure of the BRB in tension (see Figure 6.30 and Figure 6.34). Figure 6.44 shows the envelopes of the MRF and MRF+BRB cyclic tests.

The yield displacement  $D_y$  can be considered when the elastic stiffness changes the slope. In the case of MRF, the displacement  $D_y$  amounts to 50 mm, while in the case of MRF+BRB, it amounts to 11 mm and 20 mm, respectively (Figure 6.45). Based on the values of yield and ultimate displacements calculated above, the behavior factor  $q$  for MRF amounts to 3, while for MRF+BRB, the  $q$  factor amounts to 4.2.

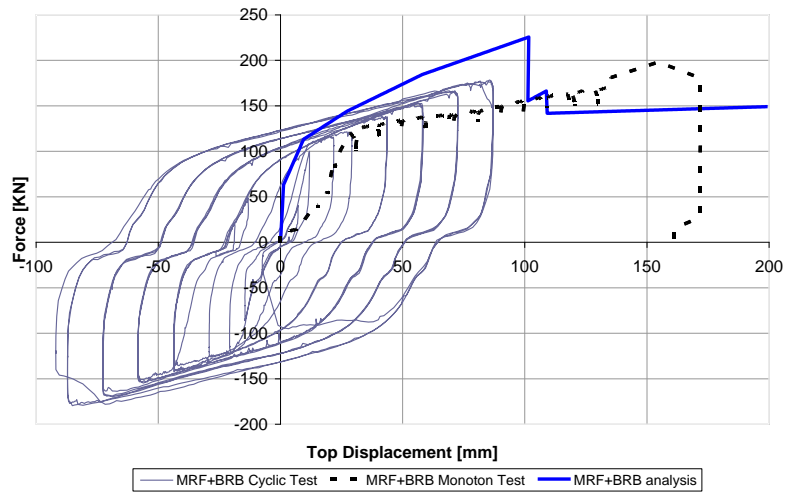


Figure 6.43 Analytical vs. Experimental Results (Pushover Analysis vs. Monotonic & Cyclic Test)

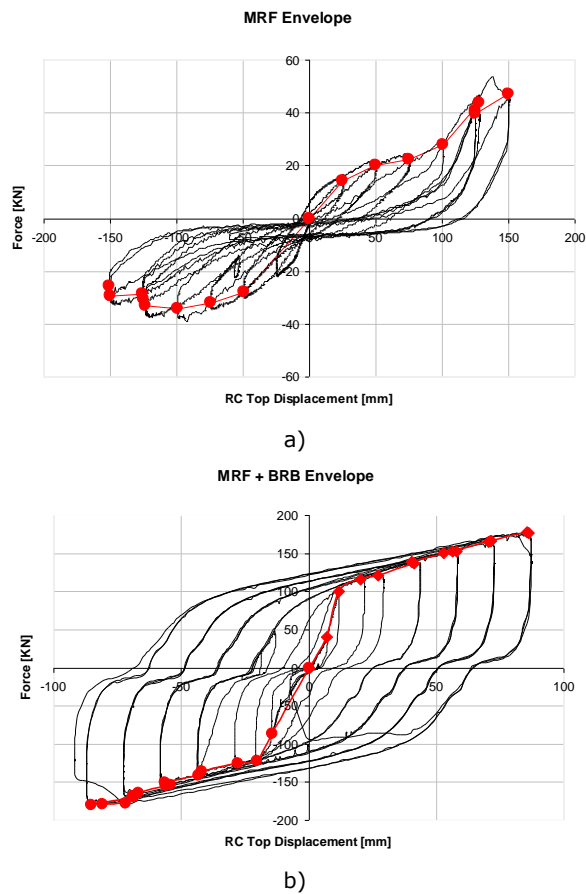


Figure 6.44: a) Envelope of the MRF cyclic test; b) Envelope of the MRF+BRB cyclic test

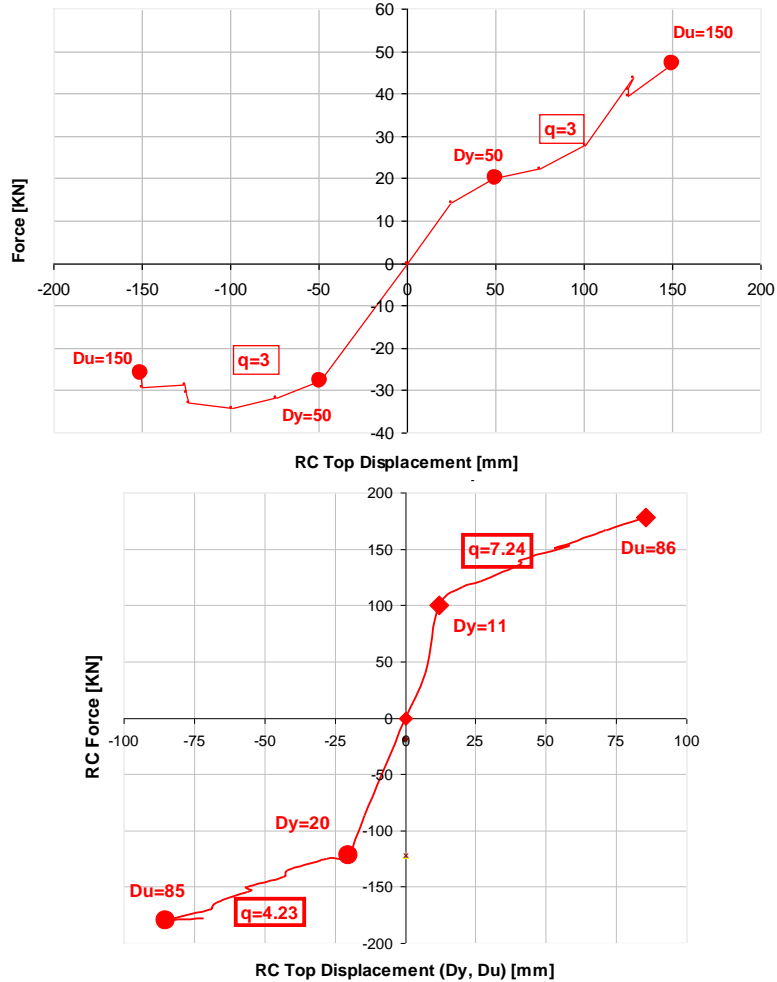


Figure 6.45 a) Preliminary value of the seismic reduction factor  $q$  based on envelopes of MRF and MRF+BRB hysteretic curves

In order to have a better estimation of the  $q$  factor, the method of evaluating the yield displacement recommended by ECCS was considered (Figure 6.46, Figure 6.47, Figure 6.48, Figure 6.49). For the definition of envelope curves, the results from each third cycle of a certain step were considered. Figure 6.46 shows the evaluation of the yield point from the positive envelope of MRF cyclic test and Figure 6.47 shows the evaluation of the yield point from the negative envelope of MRF cyclic test. The ultimate displacements  $D_u$  were calculated similarly to the previous case. Based on these values of the yield and the ultimate displacements, the behavior factor  $q$  for MRF amounts to 2.2, while for MRF+BRB, the  $q$  factor amounts to 3.7.

Table 6.4 summarizes the values of the  $q$  factor based on the test results. In the bottom line of the table, the values of the  $q$  factor obtained in Chapter 5 by means of time history analysis is also presented for comparison. The first method, called "the stiffness method", refers to the evaluation of the yield displacement

based on the change of the slope of the initial stiffness. The second method, called the "ECCS method", refers to the evaluation of the yield displacements by means of the ECCS recommendations. In both cases, the ultimate displacement corresponds to the failure of the concrete element (MRF) and the failure of BRB in tension (MRF+BRB).

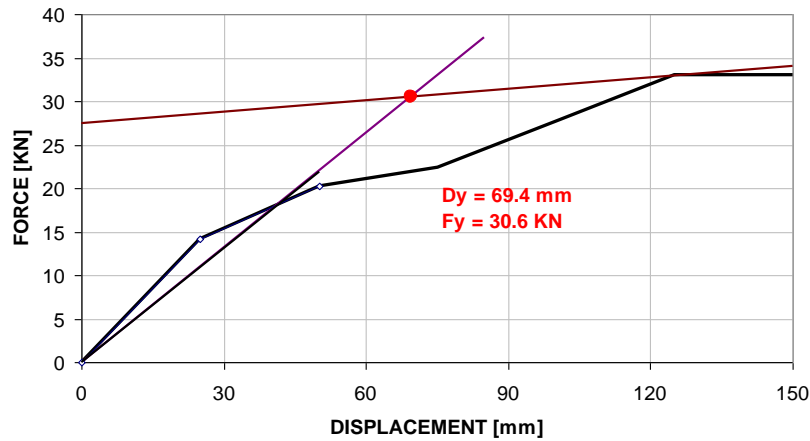


Figure 6.46 Evaluation of  $D_y$  from the positive envelope of MRF cyclic test

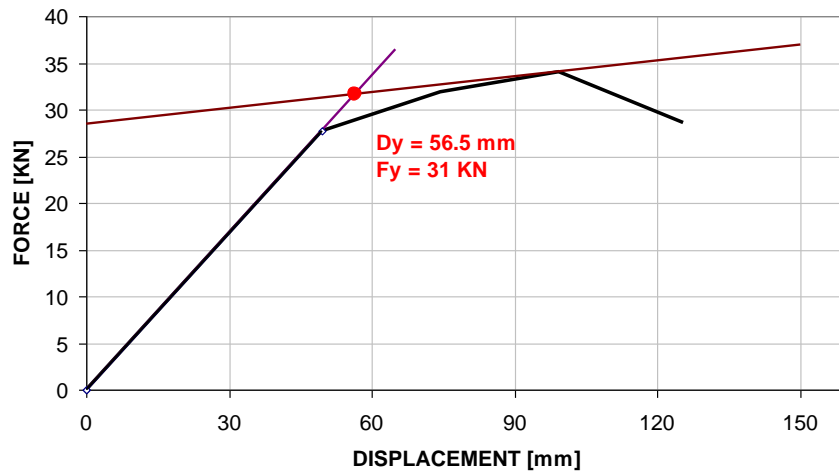


Figure 6.47 Evaluation of  $D_y$  from the negative envelope of MRF cyclic test

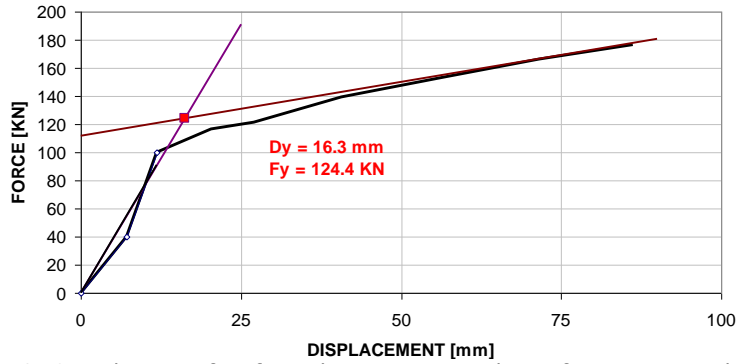


Figure 6.48 Evaluation of  $D_y$  from the positive envelope of MRF+BRB cyclic test

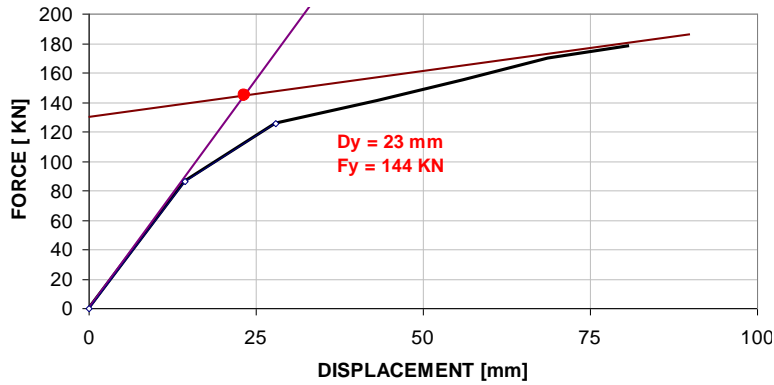


Figure 6.49 Evaluation of  $D_y$  from the negative envelope of MRF+BRB cyclic test

Comparing the results of the  $q$  factor presented in Table 6.4, there are important differences among the methods. In the case of the retrofitted frame MRM+BRB, the values of the  $q$  factor from negative envelopes are close to the values obtained in the numerical analysis. It is important to underline the difference between the envelopes on the positive and negative directions and the implications in the elements modeling.

Table 6.4. The  $q$  factor values for the RC frame structure, before and after retrofitting

Method	MRF							
	Positive Envelope				Negative Envelope			
	$D_y$ [mm]	$D_u$ [mm]	$F_y$ [kN]	$q$	$D_y$ [mm]	$D_u$ [mm]	$F_y$ [kN]	$q$
Stiffness	50	150	-	3.0	50	150	-	3.0
ECCS	69.4	150	-	2.2	56.5	150	-	2.7
Method	MRF+BRB							
	Positive Envelope				Negative Envelope			
	$D_y$ [mm]	$D_u$ [mm]	$F_y$ [kN]	$q$	$D_y$ [mm]	$D_u$ [mm]	$F_y$ [kN]	$q$
Stiffness	11	86	-	7.8	20	85	-	4.3
ECCS	16.3	86	-	5.3	23	85	-	3.7

	MRF+BRB		
Numerical (mean values)	X direction	4.3	
	Y direction	3.9	

## 6.6 Conclusions

In this chapter, a RC frame designed for gravity loads was tested with and without the BRB retrofitting system. The frame was isolated from the benchmark structure analyzed in chapter 5. The two types of frames were tested monotonically and cyclically. Tests showed a very good behavior of the retrofitted structure. The ductility of the structure was very much improved and the failure was caused by the failure of the steel brace in tension. The connections between the BRB and the RC elements performed very well. The workability of the system with pre-stressed ties was also tested. The connection devices used for installing BRB's within the frame took benefit from the friction resistant forces induced by the ties pretension and showed a very good behavior. In fact, reduced slips were observed, with very small influence on the hysteretic loops of BRB system. The results recommend the application of this connecting system for such interventions. Moreover, in the case of multi-storey frames, such connecting systems also provide a beneficial confining effect at the frame joints, enhancing both strength and ductility of the MRF+BRB system. The portal frame tested experimentally couldn't take such benefit.

The  $q$  factor values for frames were evaluated and then compared to the theoretical values obtained in Chapter 5. There is a good agreement between the values used for the design and the values based on the test. The difference between the  $q$  factor values corresponding to the positive and negative branches of the envelope curves can be explained by the fact that the negative direction corresponds to the reversed cycle, after the damages have already occurred in the positive cycle. There are several factors that may affect the behavior factor, including the system overstrength. Therefore, in order to validate these values of the  $q$  factor, parametrical studies on different frame typologies are necessary. The values of the  $q$  factor between 3 and 4 seem to be reasonable for such types of retrofitted structures. Compared with the initial RC frames, the values of the  $q$  factor are higher by approximately 50% for retrofitted frames. Surprisingly, the values of the  $q$  factor for the initial RC frame amounted between 2 and 3. One reason for this could be the strength of the concrete and of the reinforcement steel, which was higher than the nominal values used for design. Thus, this overstrength and not the ductility may be responsible for these unexpectedly large  $q$  factor values, since during the test the cracks initiated at early stages.

## **7. PROPOSED DESIGN METHOD FOR THE RETROFITTING OF REINFORCED CONCRETE BUILDING FRAMES WITH BUCKLING RESTRAINED BRACE SYSTEM**

On the basis of previous chapters, a general methodology used for the performance based seismic design of BRB seismic upgrade of reinforced concrete building frames, is suggested.

This methodology is based on the FEMA 356/ASCE 41 approach. It uses the definitions and reference values of performance parameters provided by these documents and it involves compulsory nonlinear analyses (at least one pushover analysis according to the N2 method). For buildings of higher importance, an inelastic time-history analysis is recommended.

Starting from the initial evaluation of existing buildings, a strengthening scheme using BRB system is suggested and preliminary assessed by applying current design codes methodology (spectral analysis, capacity design, SLS and ULS criteria,  $q$  factor). We suggest in this thesis a behavior  $q$  factor value of 3, according to the results; this value corresponds to a moderate ductility which enables the protection of the concrete structure, particularly the columns. Considering the results of the evaluation of existing buildings, BRB intervention can be applied alone or accompanied by the local strengthening of some RC members, either columns or beams or both.

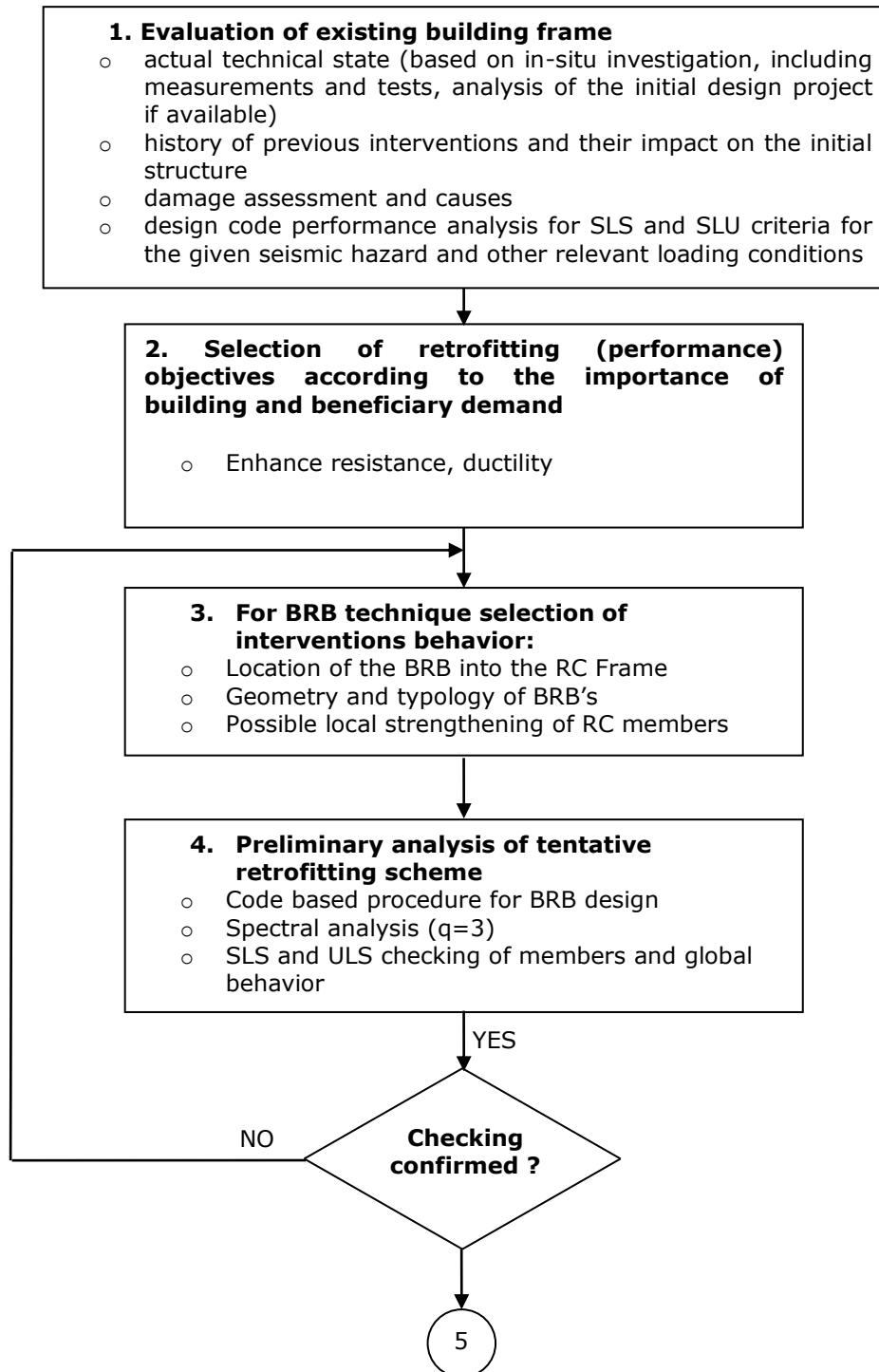
In the preliminary design of the intervention, BRB members are designed according to AISC 2005 code provisions. In the next phase of the procedure, a push-over analysis will be applied. For this purpose, refined models have to be proposed for BRB members which have to be defined either by test (home solutions) or by relevant technical specifications provided by specialized supplies of such devices.

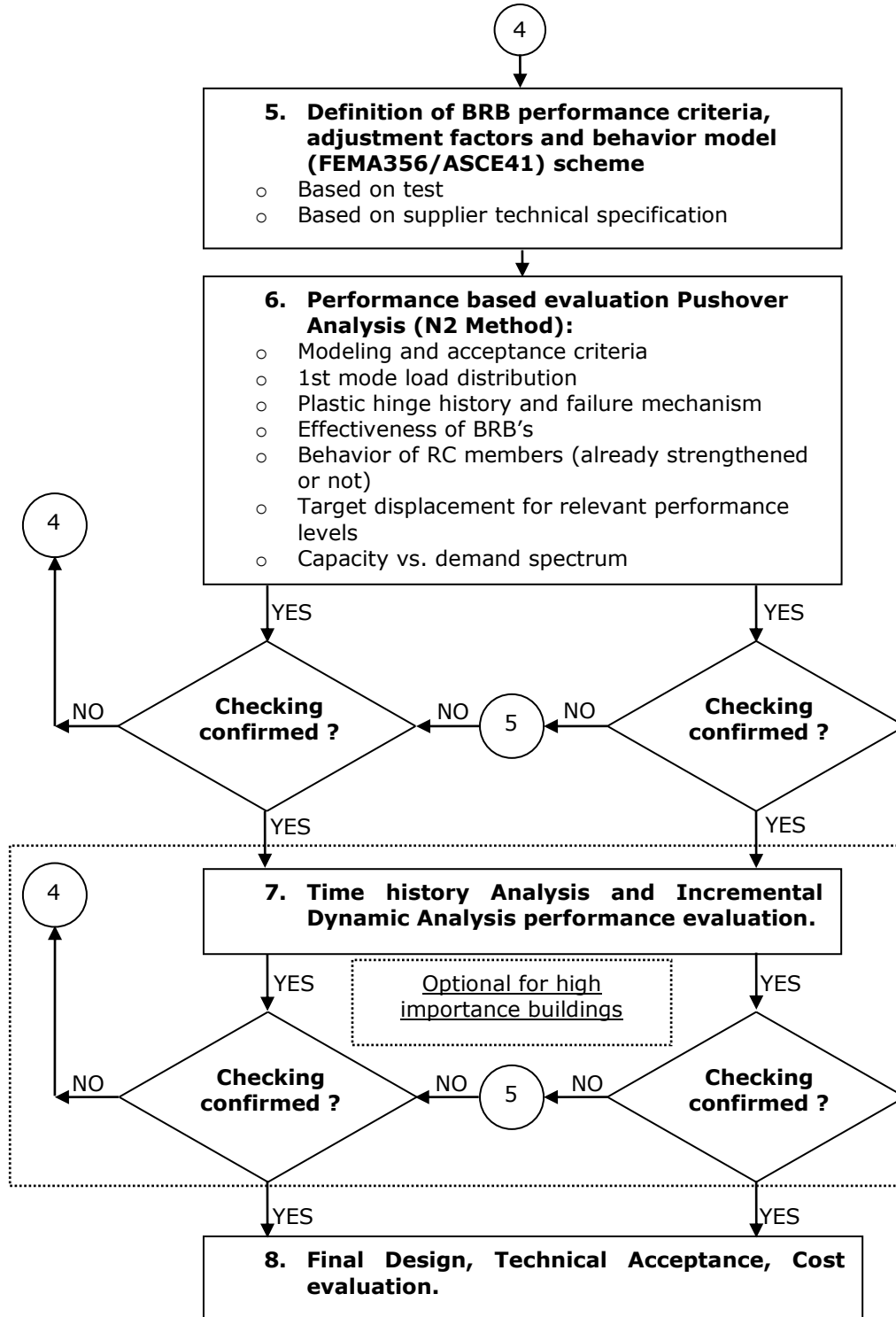
When the nonlinear PBE validates the intervention technique, the final design can be completed.

The flowchart of all methodologies is presented below:



## General Methodology for Performance Based Design of BRB Seismic upgrade of RC Building Frames





## 8. CONCLUSIONS AND PERSONAL CONTRIBUTIONS

The thesis addresses the subject of dual (MRF+CBF) building frames equipped with BRB systems, in general, but the specific research was focused on the application of BRBs strengthening MRFs reinforced concrete frames. Particularly, non-seismic resistant or poor seismic design based on such frames are addressed. Usually these frames cannot carry the horizontal forces induced by seismic actions, even if they are located in moderated seismic zones, due to the fact that both the concrete grade and the reinforcement quality are poor. A quite convenient intervention technique is the one based on introducing steel braces, centric or eccentric system, accompanied by locally reinforcing the reinforced concrete members (jacketing, FRP techniques).

Due to the fact that EBF systems with vertical links have the disadvantage of reducing the free height of the frame, CBF systems are preferred in most cases. However, in the case of CBF systems the main problem is that they provide enhanced stiffness to the framing systems and also theoretically enhance the resistance to horizontal loading, but they induce very high axial stresses in the columns and transverse stresses in the beams that these poor reinforced concrete members are not prepared to carry. That is why the BRB technique seems to be appropriate for use as a passive dissipative system in such cases.

After the introduction in the first chapter, where the objective of the thesis was defined, chapter 2 presents a summary state-of-art of the research in the field, based on the literature review, and chapter 3 presents the PBE/PBD methodology for frame structures according to FEMA 356/ASCE41 and illustrates the application of these provisions by means of a simple study case.

The specific research investigation is treated in chapter 4, 5 and 6.

The conclusions of the "research chapters" are summarized below:

### Chapter IV

Buckling restrained braces BRB's are expected to withstand significant plastic inelastic deformations when subjected to axial forces. In this chapter, the effectiveness of BRB systems used for strengthening existing RC frames has been investigated experimentally. BRB specimens have been designed as to fulfill the acceptance criteria provided by FEMA 356. The plate used in the steel core was made from S275 steel and was protected with unbonding material. The steel core was inserted in a steel tube made of S275 steel and C40/50 concrete was then poured inside the tube. In order to investigate the influence of the unbonding material, three types of BRB's have been manufactured, based on three different unbonding materials (i.e. PVC transparent film, asphalt bitumen and rubber). Both monotonic and cyclic tests have been performed. Monotonic tests were conducted until the failure of the specimens, both in tension and in compression. Cyclic tests have been carried out according to the specifications of AISC 2005 [42] and ECCS [60]. All three BRB solutions satisfied the demand, however the one using PVC transparent film showed better behavior.

The main conclusions of the experimental program on BRB specimens are summarized below:

- BRB's show good performance and large deformation capacity

- The values of the deformation capacity under monotonic tests show similar results in tension and in compression;
- Cyclic tests show very stable and repeatable behavior;
- In the case of cyclic tests, the deformation capacity is affected by the loading protocol. When more cycles are used (eg. ECCS [60] procedure), the low cycle fatigue phenomenon reduces the deformation capacity;
- Cyclic tests are consistent with the monotonic tests, but the deformation capacity is lower;
- The unbonding material may have an important influence on the deformation capacity of the BRB's. Specimens with PVC material show better behavior, while the use of bitumen may greatly reduce the deformation capacity;
- The compression-strength adjustment factor,  $\beta$ , that accounts for the compression over-strength (with respect to the tension strength), obtained as a mean value of the two loading protocols, amounts to 1.3;
- The tension strength adjustment factor,  $\omega$ , that accounts for strain hardening, obtained as a mean value of the two loading protocols, amounts to 2.2;
- For the minimum values obtained from the cyclic tests, the compression adjustment factor  $\beta$  amounts to 1.2, while the tension adjustment factor  $\omega$  amounts to 1.9.

Based on the results of the experimental program, a case study of performance of BRB's for retrofitting existing RC frame building is developed in Chapter 5. The performance of the RC building will be analyzed before and after the retrofitting intervention.

## **Chapter V**

Static and dynamic nonlinear analysis was performed in order to evaluate the performances of an existing RC frame building. The preliminary results have shown that the structure is vulnerable and does not attain the seismic requirements. Therefore, it was decided to retrofit the structure by means of a BRB system. Additionally, a local confinement of concrete elements by means of FRP was envisaged.

Results have shown that the initial structure MRF and the initial structure with local retrofitting MRF + FRP have limited ductility and does not attain the displacement demands for LS and CP levels. The benefit of local retrofitting is reduced. When the global retrofitting is accomplished MRF+BRB, the behavior is much improved. The stiffness and the strength increase and the structure attains the LS performance. The structure cannot attain the CP level, due to the failure of the concrete structure. The contribution of the local retrofitting is again very limited. Therefore, it is necessary to strengthen the columns and not only to confine them in order to fulfill the requirements for the three performance levels.

The analysis focused also on the evaluation of the behavior factor  $q$ . The mean value of  $q$  factor was larger than the initial value considered in the analysis. Even so, the use of a high  $q$  factor is not recommended, as the deformation capacity supply of RC elements is reduced. Therefore, the retrofitting of existing RC frames with buckling restrained steel braces can be based on  $q$  factors amounting from 3 to 3.5. If higher  $q$  factors are used, the strengthening of the concrete elements is necessary.

## Chapter VI

In this chapter, a RC frame designed for gravity loads was tested with and without the BRB retrofitting system. The frame was isolated from the benchmark structure analyzed in chapter 5. The two types of frames were tested monotonically and cyclically. Tests showed very good behavior of the retrofitted structure. The ductility of the structure was very much improved and the failure was caused by the failure of the steel brace in tension. The connections between BRB and RC elements performed very well. The workability of the system with pre-stressed ties was also tested. The connection devices used for installing BRB's within the frame took benefit from the friction resistant forces induced by the ties pretension and showed a very good behavior. In fact, reduced slips were observed, with very small influence on the hysteretic loops of the BRB system. Results recommend the application of this connecting system for such interventions. Moreover, in the case of multi-storey frames, such connecting systems also provide a beneficial confining effect at the frame joints, enhancing both strength and ductility of the MRF+BRB system. The portal frame tested experimentally couldn't take such benefit.

The q factor values for frames were evaluated and then compared to the theoretical values obtained in Chapter 5. There is a good agreement between the values used in design and the values based on test. The difference between the q factor values corresponding to the positive and negative branches of envelope curves can be explained by the fact that the negative direction corresponds to the reversal cycle, after the damages have already occurred in the positive cycle. There are several factors that may affect the behavior factor, including system overstrength. Therefore, in order to validate these values of the q factor, parametrical studies on different frame typologies are necessary. Values of the q factor between 3 and 4 seem to be reasonable for such types of retrofitted structures. Compared with initial RC frames, the values of the q factor are higher by approximately 50% for retrofitted frames. Surprisingly, the values of the q factor for the initial RC frame amounted between 2 and 3. One reason for this could be the strength of the concrete and of the reinforcement steel, which was larger than the nominal values used in design. Thus, the value responsible for these unexpected large q factors is probably this overstrength and not the ductility, since during the test the cracks initiated at early stages.

In chapter 7, a general methodology for PBD of BRB strengthening of existing MRF reinforced concrete frames is suggested.

The main personal contributions of the author within the frame of this thesis can be summarized as follows:

- 1) Experimental program for BRB specimens which have been built following the design realized by the author, which enabled the calibration of the design parameters and the calculation model to be used in global analyses.
- 2) Performance Based Analysis on the building frame of real building strengthened with BRB system designed by the author and conducted according to FEMA356 by means of push-over and time-history analyses. The q factor value was evaluated for this structure by means of IDA's.
- 3) The experimental program for the validation of the BRB system applied for the retrofitting of an RC frame. For this purpose, a portal frame unit extracted from the multistorey structure with/without the BRB's was tested under monotonic and cyclic loadings. Experimental q factor values have

been obtained; these values confirmed the ones obtained by IDA on the whole structure.

4) A connecting system for BRB to existing frame has been proposed and tested, being confirmed.

5) A general flowchart for a general methodology to apply PBSE/PBSD to the retrofitting of RC MRFs with BRB systems has been proposed.

The test on BRB's and on the portal frame are the first ones of this type achieved in Romania, while the experimental evaluation of the q factor of RC MRF's strengthened with BRB's are, to the knowledge of the author, a first attempt in the field.

During the research period, the contributions in the thesis have been published and disseminated by means of scientific articles and within research project as follows:

PN – II – RU – TD – 2008 – 3 „Proiecte de Cercetare pentru Tineri Doctoranzi” TD 55/2008 “Studiul sistemelor cu cadre duale cu contravântuiri metalice comprimate cu flambaj împiedecat” – project manager (2008/2009)

UE/RFSR-CT-2007-00050 „Steel Solutions for Seismic Retrofit and Upgrade of Existing Constructions” STEEL RETRO – research assistant (2008 – present)

PROHITECH FP6 INCO-CT-2004-509119/2004 Earthquake Protection of Historical Buildings by Reversible Mixed Technologies – member in team research

COST C26 – COST Action C26 – Urban Habitat Constructions under Catastrophic Events – program participant

PROACTEX 31042/2007 „Sisteme structurale si solutii tehnologice inovative pentru protectia cladirilor la actiuni extreme in contextul cerintelor pentru dezvoltare durabila” - member in team research

**Bordea, S.**, Dubina, D., 2009, “*Retrofitting/upgrading of reinforced concrete elements with buckling restrained bracing elements*”, Conference on SUSTAINABILITY in SCIENCE ENGINEERING, Timisoara, pp. 407-412 (Thomson ISI).

Dubina, D., **Bordea, S.**, Stratan, A., 2009, “*Performance Based Evaluation of a RC Frame strengthened with BRB Steel Braces*”, International Conference PROHITECH, Roma, Italia, [WWW.PROHITECH09.COM](http://WWW.PROHITECH09.COM), ISBN 978-0-415-55803-7, pp. 1009-1014.

**Bordea, S.**, Dubina, D., 2009, “*Retrofitting/upgrading of reinforced concrete elements with buckling restrained bracing elements*”, Zilele Academice Timisene, Timisoara, Romania (CNCSIS categoria D).

**Bordea, S.**, Stratan, A., Dubina, D., 2008, “*Performance based evaluation of a non –seismic RC frame strengthened with Buckling Restrained Braces*” – in Urban Habitat Constructions under catastrophic events, COST Action C26, Ed. Mazzolani F. et all, Malta.

Dinu, F., **Bordea S.**, Dubina, D., 2008, “*High strength steel dual frames with Buckling Restrained Braces*”, Proc. of the 5th European Conference on Steel and Composite Structures EUROSTEEL 2008, 3-5 September, Graz, Austria. R. Ofner, D. Beg, J. Fink, R. Greiner, H. Unterweger (Eds), 3-5.09.

Dubina, D., **Bordea, S.**, Stratan, A., 2008, „*Seismic Upgrade of Reinforced Concrete Moment Resisting Frame with Dissipative Buckling Restrained Steel Braces*”, Conferința „Construcții 2008 in ACTA TECHNICA NAPOCENSIS, Section Civil Engineering-Architecture, 51, vol I, Ed. Prof. Adrian Ioani si Prof. Calin Mircea, Napoca STAR, Cluj Napoca, Romania, 2008, pp. 353-360.(CNCSIS categoria B).

**Bordea, S.**, 2008, „*Strengthening of MRF RC frames located in seismic areas with BRB & FRP*”, 3rd International PhD Symposium, Pollak Periodica, Vol 3, pp. 45-56, Pecs, Hungary. (BDI SCOPUS).

**Bordea, S.**, 2008, „*Seismic upgrade of RC MR Frames with dissipative BR Steel Braces*” at 7<sup>th</sup> International PhD Symposium in Civil Engineering, Stuttgart, Germany.

**Bordea, S.**, Stratan, A., Dogariu, A., Dubina, D., 2007, „*Seismic upgrade of non-seismic r.c. frames using steel dissipative braces*” COST Action C26 – European Cooperation in the Field of Scientific and Technical Research – Urban Habitat Construction Under Catastrophic Events – Proceedings of Workshop in Prague, 30-31 March, pp. 211-220. (www.cost.esf.org).

Dogariu, A., Munteanu, N., **Bordea, S.**, Daescu, C., Diaconu, D., Demeter, I., Florut, C., 2007, Special Prize at “Sesiunea Națională de Comunicări Științifice Studentești” with article: *Studiu Experimental a unei soluții de consolidare a zidăriei*, Cluj Napoca, Romania.

Dubina, D., Stratan, A., **Bordea, S.**, 2007, „*Seismic Retrofit of r.c. frames with hysteretic bracing*”, Steel and Composite Structures, Ed. Y.C. Wang and C.K. Choi, Taylor and Francis, London, UK, 2007, pp. 833 – 840 (BDI SCOPUS).

Grecea, D., **Bordea, S.**, Stratan, A., Dogariu, A., Dubina, D., 2007, „*Soluții moderne pentru consolidarea și reabilitarea clădirilor amplasate în zone seismice*”, editia X a Zilelor Academice Timisene, in Lucrarile simpozionului „Structuri metalice amplasate în zone seismice. Preocupari actuale”, Timisoara, Romania, 25 mai 2007, Ed. Orizonturi Universitare, Timisoara 2008, p. 141-156. (CNCSIS categoria D).

**Bordea, S.**, 2007, „*Retrofitting of Reinforced Concrete Frames in Seismic Areas with a Buckling Restrained Bracing System and Fibre Reinforced Polymers*” in „Scientific Bulletin” of The „Politehnica” University of Timisoara, Romania, Transactions on Civil Engineering and Architecture, Tomul 52 (66), Fascicola 1, 2007 Ed. Politehnica, p. 55-64. (CNCSIS categoria D).

**Bordea, S.**, 2006, „*Evaluarea Performantei Seismice a unui Cadru de Beton Armat Existent printr-o Analiza de tip Pushover*”, Special Prize at “Sesiunea Națională de Comunicări Științifice Studentești – cu participare internațională”, Cluj Napoca, Romania.

**Bordea, S.**, Stratan, A., Dogariu, A., Dubina, D., 2006, “*Performance of nonseismic reinforced concrete frame retrofitted with bracing systems*”, – Summer School “Advanced studies in structural engineering and CAE”, Weimar, Germany.

**Bordea, S.**, Dubina, D., 2006 “*Evaluarea performantei seismice a unui cadru de beton armat existent printr-o analiza de tip pushover*”, Sesiunea Nationala de Comunicari Stiintifice Studentesti – cu participare internationala, Cluj Napoca, Romania.



## Bibliography

- [1] PROHITECH WP6 (Leader Darko Beg) "SET-UP OF ADVANCED REVERSIBLE MIXED TECHNOLOGIES FOR SEISMIC PROTECTION BUCKLING RESTRAINED BRACES AS SOLUTION FOR SEISMIC UPGRADING OF EXISTING RC STRUCTURES" M. D'Aniello, G. Della Corte, F.M. Mazzolani University of Naples Federico II, Italy Datasheet n. 01.06.01.01
- [2] Ko, E., Field, C., „The Unbonded Brace™: From research to Californian practice”
- [3] Clark, P., Aiken, I., Kasai, K., Ko, E. and Kimura, I., 1999, "Design procedures for buildings incorporating hysteretic damping devices", Proc. 69th Annual Convention of SEAOC, Sacramento, CA
- [4] "NIPON STEEL NEWS", no.333, september 2005, (Published monthly by Public Relations Center General Administration Div. Nippon Steel Corporation, (<http://www.nsc.co.jp>))
- [5] Clark, P., Aiken, I., Ko, E., , Kasai, K., Kimura, I., „Design Procedures for Building Incorporating Hysteretic Damping Devices”
- [6] Wada, A., Iwata, M., and Huang, Y.H., 1997, "Seismic Design Trend of Tall Buildings After the Kobe Earthquake," Proceedings of International Post-SMiRT Conference Seminar on Seismic Isolation, Passive Energy Dissipation, and Control of Vibrations of Structures, Taormina, Italy, August 25-27.
- [7] Escudero, E. O. supervisor: Dr. Masayoshi Nakashima, 2003, "Comparative parametric study on normal and buckling restrained steel braces", M.Sc. thesis, Rose School, Pavia, Italy.
- [8] Sabelli, R., Lopez, W., "Design of Buckling-Restrained Braced frames”
- [9] Tremblay, R., Poncet, L., Bolduc, P., Neville, R., and DeVall, R., 2004, "Testing and design of buckling restrained braces for Canadian application", Proceedings of the 13th World Conference on Earthquake Engineering, Vancouver, BC, Paper No. 2893
- [10] Mazzolani, F.M., 2006, "Seismic upgrading of RC buildings by advanced techniques" The ILVA-IDEM Research Project, Polimerica International Scientifical Publisher ([www.polimerica.com](http://www.polimerica.com)), ISBN 99-7699-038-0 Printed edition, ISBN 88-7699-039-9 electronic edition
- [11] Bozorgnia, Y., Bertero, V.V., (2004) "Earthquake engineering: from engineering seismology to performance-based engineering" (chapter XVI "Steel Buckling-Restrained Braced Frames" Chia-Ming Uang, Masayoshi Nakashima), Ed. Taylor & Francis e-Library, ISBN 0-203-48624-2 Master e-book ISBN, 2006
- [12] Clark P., Aiken, I., Kasai, K., Ko, E., and Kimura, I., 1999, "Design procedures for buildings incorporating hysteretic damping devices", Proc. 69th Annual Convention of SEAOC, Sacramento, CA.
- [13] Wada, A., Saeki, E., Takeuchi, T., and Watanabe, A., 1998, "Development of Unbonded Brace," Nippon Steel's Unbonded Braces (promotional document), pp. 1-16, Nippon Steel Corporation Building Construction and Urban Development Division, Tokyo, Japan
- [14] Black, C., Makris, N., and Aiken, I., 2002, "Component testing, stability analysis and characterization of buckling restrained braces". Report No. PEER-2002/08, Pacific Earthquake Engineering Research Center, University of California, Berkeley, CA.



- [15] TSAI, K.C., LAI, J.W., HWANG, Y.C., LIN, S.L. and WENG, C.H., 2004, „Research and Application of Buckling Restrained Braces in Taiwan”, 13th World Conference on Earthquake Engineering Vancouver, B.C., Canada August 1-6, Paper No. 2179
- [16] Tsai, K.C. and Lai, J.W., 2002, "A study of buckling restrained seismic braced frame", *Structural Engineering*, a7 (2), (in Chinese)
- [17] AISC, 2005, "Seismic Provisions for Structural Steel Buildings". American Institute of Steel Construction, Inc. Chicago, Illinois, USA.
- [18] Plumier, A.; Doneux, C.; Castiglioni, C.; Brescianini, J.; Crespi, A.; Dell'Anna, S.; Lazzarotto, L.; Calado, L.; Ferreira, J.; Feligioni, S.; Bursi O.; Ferrario, F.; Sommavilla, M.; Vayas, I.; Thanopoulos, P.; Demarco, T.: "Two Innovations for Earthquake Resistant Design, The INERD Project" – Final Report. CEC Agreement No7210-PR-316 1 July 2001 to 30 June 2004, Research Programme of the Research Fund for Coal and Steel Steel RTD TGS8
- [19] Dubina, D., Stratan, A., Dinu, F., 2008, "Dual high-strength steel eccentrically braced frames with removable links", *Earthquake Engineering & Structural Dynamics*, Vol. 37, No. 15, p. 1703-1720
- [20] Dubina, D., Dinu, F., Stratan, A., 2009, "Post-earthquake intervention procedure on dual eccentrically braced frames with removable links", a 4-a conf. nationala de inginerie seismica, Bucuresti
- [21] Cruz, S.T., Lopez-Almansa, F., Oller, S., 2007, "Numerical simulation of the seismic behavior of building structures equipped with friction energy dissipators", *computers and structures* 85, 30-42 available online at [www.sciencedirect.com](http://www.sciencedirect.com), [www.elsevier.com/locate/compstruc](http://www.elsevier.com/locate/compstruc)
- [22] Chen, S.J., Jhang, C., 2006, "Cyclic behavior of low yield point steel shear walls", *Thin-Walled Structures* 44, 730-738, available online at [www.sciencedirect.com](http://www.sciencedirect.com), [www.elsevier.com/locate/tws](http://www.elsevier.com/locate/tws)
- [23] Chou, C.C., Lai, Y.J., 2009, "Post-tensioned self-centering moment connections with beam bottom flange energy dissipators", *journal of constructional steel research* 65, 1931-1941, contents list available at ScienceDirect, [www.elsevier.com/locate/jcsr](http://www.elsevier.com/locate/jcsr)
- [24] Song, G., Ma, N., Li, H.-N., 2006, „Applications of shape memory alloys in civil structures"
- [25] Shuhaibar, C., López, W.A. and Sabelli, R., 2002, „Buckling-restrained braced frames", *Proceedings, Seminar on Response Modification Technologies for Performance-Based Seismic Design, ATC-17-2, ATC and MCEER*, pp. 321-328
- [26] Isao Kimura, 2002, "The Unbonded Brace A New Alternative for Seismic Lateral Systems Steel Structure" Div., Nippon Steel Corporation Tokyo, JAPAN, (ppt. presentation)
- [27] López, W.A., Rutherford & Chekene Oakland, 2001, "Design Of Unbonded Braced Frames", *Proceedings 70th Annual Convention, Structural Engineers Association of California, Sacramento, California*
- [28] PROHITECH WP5 - Calado, L., Proença, J.M., Panão, A., Nsieri, E., Rutenbrg, A., Levy, R. "INNOVATIVE MATERIALS AND TECHNIQUES Buckling-Restrained Braces", (Instituto Superior Técnico, Lisbon and Technion - Israel Institute of Technology, Haifa)
- [29] Wakabayashi M., Nakamura, T., Kashibara, A., Morizono, T. and Yokohama, H., 1973, "Experimental study of elasto plastic properties of precast concrete wall panels with built in insulation braces", *Summaries of*

- technical paper of annual meeting, Architectural Institute of Japan, p.p. 1041 – 1044 (in Japanese)
- [30] Fujimoto, M., Wada, A., Saeki, E., Watanabe, A and Hitomi, Y. ,1988, "A study on the unbonded brace encased in buckling restraining and steel tube", *Journal of structural engineering* 034B, 249-258 (in Japanese)
- [31] Tremblay, R., Degrange, G., & Blouin, J., 1999, „Seismic rehabilitation of a four-storey building with a stiffened bracing system” Proc. 8th Can. Conf. on Earthquake Engineering, Canadian Association for Earthquake Engineering, Vancouver, B.C., 549-554
- [32] Nagao, N and Takahashi, S., 1990, "A study on the elasto plastic behavior of unbonded composite bracing", (Part 1: experiments on isolated members under cyclic loading), *Journal of structural engineering*, 415, 105-115 (in Japanese)
- [33] Iwata, M., Kato, T. and Wada, A., 2000, "BRB as hysteretic dampers", Proc. STESSA, Quebec, PQ, pp 33-38
- [34] Clark, P., Frank, K., Krawinkler, H. and Shaw, R., 1997, „Protocol for fabrication, inspection, testing, and documentation of beam-column connection tests and other experimental specimens”, Report No. SAC/BD-97/02, SAC Joint Venture, Sacramento, CA.
- [35] Black, C., Makris, N. and Aiken, I., 2002, „Component testing, stability analysis and characterization of buckling-restrained braces”, Report No. PEER-2002/08, Pacific Earthquake Engineering Research Center, University of California, Berkeley, CA.
- [36] Higgins . C. and Newell. J., 2002, "Development of two hysteretic dampers", Proc. 7<sup>th</sup> U.S. National Conference on Earthquake Engineering, Engineering Research Institute, Oakland, CA
- [37] Staker, R. and Reaveley, L.D. ,2002, „Selected study on unbonded braces”, Proceedings, Seminar on Response Modification Technologies for Performance-Based Seismic Design, ATC-17-2, ATC and MCEER, pp.339-349
- [38] Merritt, S., Uang, C.M. and Benzoni, G., 2003, „Subassemblage testing of corebrace buckling-restrained braces”, Report No. TR-2003/01, University of California, San Diego, La Jolla, CA
- [39] Merritt, S., Uang, C.M. and Benzoni, G., 2003, „Uniaxial testing of associated bracing bucklingrestrained braces”, Report No. TR-2003/05, University of California, San Diego, La Jolla, CA
- [40] Chen, C.C., Chen, S.Y. and Liaw, J.J., 2001, "Application of low yield strength steel on controlled plastification ductile concentrically braced frames", *Canadian Jpurnal of Civil Engineering*, 28, 823-836.
- [41] Chen, C.C., Wang, C.H. and Hwang, T.C., 2001, "Buckling strength of buckling inhibited braces", Proc. 3rd Japan-Korea-Taiwan Joint seminar on Earthquake Engineering for building structures, Taipei, Taiwan.
- [42] Brown, A.P., Ian D. Aiken., F. Jeff Jafarzadeh, 2001, "Buckling Restrained Braces Provide the Key to the Seismic Retrofit of the Wallace F. Bennett Federal Building", to appear in *Modern Steel Construction*
- [43] Lai, J.W., Tsai, K.C., "Research and Application of Buckling Restrained Braces in Taiwan"
- [44] AISC/SEAOC Recommended Provisions for BRBF, Structural Engineers Association of Northern California - Seismology and Structural Standards Committee, Recommended Provisions for Buckling-Restrained Braced Frames (2001)

- [45] Uang, C M, Nakashima, M, 2003, "Steel buckling-restrained braced frames," Chapter 16 in *Earthquake Engineering: Recent Advances and*
- [46] Kalyanaraman, V., Sridhara, B.N. and Mahadevan, K., 1994, "Sleeved column system", *Proc. SSRC Task Group Meetings and Task Force Session, Lehigh University, Bethlehem, PA.*
- [47] P100-1/2006, 2006, "Cod de proiectare seismica - Partea I - Prevederi de proiectare pentru cladiri" (Romanian modern design code regarding the seismic load)
- [48] EN 1998-1, 2004, "Eurocode 8: Design of structures for earthquake resistance. Part 1: General rules, seismic actions and rules for buildings" CEN - European Committee for Standardization
- [49] FEMA 356, 2000, "Prestandard and commentary for the seismic rehabilitation of buildings", Federal Emergency Management Agency, Washington (DC).
- [50] ASCE/SEI 41-06, 2007, "Seismic Rehabilitation of Existing Buildings, American Society of civil Engineering" (formerly FEMA 356), Published by American Society of Civil Engineers, 1801 Alexander Bell Drive, Reston Virginia, 20191, [www.pubs.asce.org](http://www.pubs.asce.org), ISBN 13: 978-0-7844-0884-1; ISBN 10: 0-7844-0884-X, USA
- [51] PROHITECH FP6, Mazzolani, F.M., WP9, Report "Set-up of analytical models for special materials and special devices for the seismic structural control"
- [52] *Seismic Provisions for Structural Steel Buildings, March 9, 2005, incl. Supplement No. 1, AMERICAN INSTITUTE OF STEEL CONSTRUCTION, INC PART I - BUCKLING-RESTRAINED BRACED FRAMES*
- [53] FEMA 273, 1997, "NEHRP guidelines for the seismic Prestandard and commentary for the seismic rehabilitation of buildings", prepared for the Building Seismic Safety Council (BSSC), Washington (DC), by the Applied Technology Council (ATC-33 Project) with funding by Federal Emergency Management Agency (FEMA), Washington, D.C.
- [54] ATC-40, 1996, "Seismic Evaluation and Retrofit of Concrete Buildings, Vol I., by Applied Technology Council 555 Twin Dolphin Drive, Suite 550, Redwood City, California 94065, funded by Seismic Safety Commission State of California, Report No. SSC 96-01.
- [55] SEAOC Vision 2000, Performance based seismic engineering of buildings, vols. I and II: Conceptual framework, Sacramento (CA), Structural Engineers Association of California, 1995.
- [56] Fajfar, P., 2000, "A Nonlinear Analysis Method for Performance Based Seismic Design" in Eurocode 8 Annex B (Informative) "Determination of the target displacement for nonlinear static (pushover) analysis"
- [57] Deierlein, G.G., Krawinkler, H. and Cornell, C.A., 2003, "A framework for performance-based earthquake engineering", *Proc. 2003 Pacific Conference on Earthquake Engineering, Christchurch, New Zealand.*
- [58] Park, R. & Paulay, T, 1975, "Reinforced Concrete Structures", New Zealand, John Wiley & Sons, Inc., New York.
- [59] EN 1992-1-1, 2004, "Eurocode 2: Design of concrete structures - Part 1-1: General rules and rules for buildings" CEN - European Committee for Standardization
- [60] Mazzoni S., McKenna F., Fenves G. L. et al., 2005, "Open System for Earthquake Engineering Simulation User Manual, OpenSees version 1.7.0"

- [61] Enrico Spacone, El-Tawil, 2004, "Nonlinear Analysis of Steel-Concrete Composite Structures: State of the Art" *JOURNAL OF STRUCTURAL ENGINEERING* © ASCE / FEBRUARY 2004
- [62] Nassar, A. and H. Krawinkler (1991). *Seismic demands for SDOF and MDOF systems*, John A. Blume Earthquake Engineering Center, Report 95, Dept. of Civil Engineering, Stanford University.
- [63] Lungu, D., Cornea, T., Craifaleanu, I., Aldea, A. *Seismic Zonation of Romania Based on Uniform Hazard Response Ordinates*, Proceedings of the Fifth International Conference on Seismic Zonation, Nice, France, October 16-19, 1995, Vol. 1, p. 445-452, Quest Editions, Presses Academiques, Nantes
- [64] EN 1993-1-1, 2005, "Eurocode 3: Design of steel structures. Part 1-1: General Rules and Rules for Buildings" CEN - European Committee for Standardization
- [65] Paulay, T. and Priestley, M.J.N., 1992, "Seismic Design of Reinforced Concrete and Masonry Buildings", John Wiley & Sons, Inc., New York.
- [66] Newell, J. & Higgins, C. (n.d.), 2003, "Steel Confined Yielding Damper For Earthquake Resistant Design", NHMJ Young Researchers Symposium June 21, <http://cee.uiuc.edu/sstl/nhmj/ppt/Newell.ppt>
- [67] FIB Bulletin 14, 2001, "Externally bonded FRP reinforcement for RC structures", technical report on the Design and use of externally bonded fibre reinforced polymer reinforcement (FRP EBR) for reinforced concrete structures
- [68] ECCS, 1985, "Recommended Testing Procedures for Assessing the Behaviour of Structural Elements under Cyclic Loads", European Convention for Constructional Steelwork, Technical Committee 1, TWG 1.3 - Seismic Design, No.45
- [69] SAP2000, "Structural Analysis Program", a product of Computers and Structures, Inc. 1995 University Ave., Berkeley, CA 94704 ([www.csiberkeley.com](http://www.csiberkeley.com))
- [70] Steel Retro report, may-july 2008, "Definition of the reinforced concrete benchmark building for the execution of comparative performance analyses between steel intervention techniques (amended version 1.1)", WP 3, 4, 5 and 6: Cost, performance and constructive analyses of steel solution for retrofitting vertical elements, floors, roofs and foundations RIVA Acciaio S.p.A. - Aurelio Braconi, Alessandro Osta, University of Pisa - Luca Nardini, Walter Salvatore
- [71] EN 1990, 2002, "Eurocode 0: Basis of structural design CEN - European Committee for Standardization"
- [72] EN 1991-1-1, 2002, "Eurocode: 1 Actions on structures - Part 1-1: General actions - Densities, self-weight, imposed loads for buildings", CEN - European Committee for Standardization.
- [73] NEHRP, 2003, "NEHRP Recommended provisions for new buildings and other structures (FEMA 450)" Part 1: Provisions and Part 2: Commentary. Building Seismic Safety Council, National Institute of Building Sciences, Washington, D.C.
- [74] P100-3/2005, 2005, Romanian evaluation standard "COD DE EVALUARE SI PROIECTARE A LUCRĂRILOR DE CONSOLIDARE LA CLĂDIRI EXISTENTE, VULNERABILE SEISMIC" VOL. 1 - EVALUARE
- [75] Clipii, T., Cadar, I., Tudor, A., 1999, "Beton Armat", Editura Orizonturi Universitare, ISBN 973-9400-38-8, Timisoara 1999, Romania

- [76] ALLEGATO B ALLE NORME TECNICHE PER LE COSTRUZIONI:  
TABELLE DEI PARAMETRI CHE DEFINISCONO L'AZIONE SISMICA  
([http://www.lt.archiworld.it/norme/leggi08/DMIinfrastrut1\\_08-allB.pdf](http://www.lt.archiworld.it/norme/leggi08/DMIinfrastrut1_08-allB.pdf))
- [77] Stratan, A., 2003, "Studiul comportării clădirilor multietajate cu cadre metalice duale amplasate în zone seismice", Universitatea "Politehnica" din Timișoara, 324 pag

## ANNEX I

Table 1. Beam and column cross sections

Beam elements / cross section		width	height	Φ	rebars	no. of
		[mm]	[mm]	[mm]	position	rebars
Frame nr. 1 & 2 / First and second floor/ Main beam	Edge cross section 1-1	400	600	18	upper part	6
					lower part	3
	Intermediate cross section 2-2	400	600	18	upper part	5
					lower part	4
	Mid-span cross section 3-3	400	600	18	upper part	3
					lower part	6
Frame nr. 1 & 2 / Third floor / Main beam	Edge cross section 1-1	300	550	14	upper part	6
					lower part	3
	Intermediate cross section 2-2	300	550	14	upper part	5
					lower part	4
	Mid-span cross section 3-3	300	550	14	upper part	3
					lower part	6
Frame nr. 1 & 2 / Roof / Main beam	Edge cross section 1-1	300	500	14	upper part	4
					lower part	2
	Intermediate cross section 2-2	300	500	14	upper part	3
					lower part	3
	Mid-span cross section 3-3	300	500	14	upper part	2
					lower part	4
Frame nr. 2 / First and second floor / middle beam	---	300	500	18	upper part	4
					lower part	4
Frame nr. 2 / Third floor / middle beam	---	300	500	14	upper part	4
					lower part	4
Frame nr. 3 / First, second and third floor / Secondary beam	Edge cross section	300	400	14	upper part	4
					lower part	2
	Mid-span cross section	300	400	14	upper part	2
					lower part	4
	Edge cross section	300	400	14	upper part	4
					lower part	2
Frame nr. 4 / First, second and third floor / Secondary	---	300	300	14	upper part	3
					lower part	3
Frame nr. 5 / First, second and third floor / Secondary	---	300	200	14	upper part	2
					lower part	2

Column Elements / CS name		width	height	Φ	rebars	no. of
		[mm]	[mm]	[mm]	position	rebars/cs face
Ground floor / all columns	400	400	18	X direction	4	
				Y direction	2	
First floor / columns ABCDE1, ABCDE3, ABCDE4, ABCDE6	400	400	18	X direction	2	
				Y direction	2	
First floor / columns ABCDE2, ABCDE5	300	400	18	X direction	2	
				Y direction	2	
Second floor / columns ABCDE1, ABCDE3, ABCDE4, ABCDE6	300	300	18	X direction	3	
				Y direction	2	
Second floor / columns ABCDE2, ABCDE5	300	300	18	X direction	2	
				Y direction	2	
Third floor / columns ABCDE1, ABCDE3, ABCDE4, ABCDE6	300	300	18	X direction	5	
				Y direction	2	
Third floor / columns ABCDE2, ABCDE5	300	300	18	X direction	2	
				Y direction	2	



Table 2. Conforming (C) and nonconforming (NC) transverse reinforcement for beams and columns

Element / CS name		Stirrup	RC cs		Rebars	Results		
		spacing [mm]	height [mm]	cover width [mm]	diameter [mm]	d [mm]	d/3	C/NC
Beams	Frame nr. 1 / First and second floor/ Main beam	250	600	25	18	566	189	NC
	Frame nr. 1 / Third floor / Main beam	250	550	25	14	518	173	NC
	Frame nr. 1 / Roof / Main beam	250	500	25	14	468	156	NC
	Frame nr. 2 / First and second floor / Main beam	250	600	25	18	566	189	NC
	Frame nr. 2 / Third floor / Main beam	250	550	25	14	518	173	NC
	Frame nr. 2 / Roof / Main beam	250	500	25	14	468	156	NC
	Frame nr. 2 / First and second floor / middle beam	250	500	25	18	466	155	NC
	Frame nr. 2 / Third floor / middle beam	250	500	25	14	468	156	NC
	Frame nr. 3 / First, second and third floor / Secondary beam	250	400	25	14	368	123	NC
	Frame nr. 4 / First, second and third floor / Secondary beam	250	300	25	14	268	89	NC
	Frame nr. 5 / First, second and third floor / Secondary beam	250	200	25	14	168	56	NC
	Columns	Ground floor / all columns - 1 direction	150	400	25	18	366	122
Ground floor / all columns - 2 direction		150	400	25	18	366	122	NC
First floor / columns ABCDE1, ABCDE3, ABCDE4, ABCDE6 - 1 direction		150	400	25	18	366	122	NC
First floor / columns ABCDE1, ABCDE3, ABCDE4, ABCDE6 - 2 direction		150	400	25	18	366	122	NC
First floor / columns ABCDE2, ABCDE5 - 1 direction		150	400	25	18	366	122	NC
First floor / columns ABCDE2, ABCDE5 - 2 direction		150	300	25	18	266	89	NC
Second floor / columns ABCDE1, ABCDE3, ABCDE4, ABCDE6 - 1 direction		150	300	25	18	266	89	NC
Second floor / columns ABCDE1, ABCDE3, ABCDE4, ABCDE6 - 2 direction		150	300	25	18	266	89	NC
Second floor / columns ABCDE2, ABCDE5 - 1 direction		150	300	25	18	266	89	NC
Second floor / columns ABCDE2, ABCDE5 - 2 direction		150	300	25	18	266	89	NC
Third floor / columns ABCDE1, ABCDE3, ABCDE4, ABCDE6 - 1 direction		150	300	25	18	266	89	NC
Third floor / columns ABCDE1, ABCDE3, ABCDE4, ABCDE6 - 2 direction		150	300	25	18	266	89	NC
Third floor / columns ABCDE2, ABCDE5 - 1 direction		150	300	25	18	266	89	NC
Third floor / columns ABCDE2, ABCDE5 - 2 direction		150	300	25	18	266	89	NC

Table 3 Beams state (C/NC) based on the condition that the strength provided by the hoops (Vs) is at least three quarters of the design shear

Beam Elements / CS name		Vd	3/4Vd	Vs	type of material
pushover in X direction	Frame nr. 1&2 / First and second floor / Main beam	175	131	10	NC (unconfined concrete)
	Frame nr. 1&2 / Third floor / Main beam	116	87		NC (unconfined concrete)
	Frame nr. 1&2 / Roof / Main beam	103	77		NC (unconfined concrete)
	Frame nr. 2 / First and second floor / middle beam	120	90		NC (unconfined concrete)
pushover in Y direction	Frame nr. 2 / Third floor / middle beam	103	77		NC (unconfined concrete)
	Frame nr. 3 / First, second and third floor / Secondary beam	86	64		NC (unconfined concrete)
	Frame nr. 4 / First, second and third floor / Secondary beam	63	47		NC (unconfined concrete)
	Frame nr. 5 / First, second and third floor / Secondary beam	33	25		NC (unconfined concrete)

Table 4 Columns state (C/NC) based on the condition that the strength provided by the hoops (Vs) is at least three quarters of the design shear

Columns	Vd	3/4Vd	Vs	type of material
Ground floor / all columns - MIN1/2 direction	77	58	10	NC (unconfined concrete)
First floor / columns ABCDE1, ABCDE3, ABCDE4, ABCDE6 - MIN1/2 direction	102	77		NC (unconfined concrete)
First floor / columns ABCDE2, ABCDE5 - MIN1/2 direction	75	57		NC (unconfined concrete)
Second floor / columns ABCDE1, ABCDE3, ABCDE4, ABCDE6 - MIN1/2 direction	38	29		NC (unconfined concrete)
Second floor / columns ABCDE2, ABCDE5 - MIN1/2 direction	36	27		NC (unconfined concrete)
Third floor / columns ABCDE1, ABCDE3, ABCDE4, ABCDE6 - MIN1/2 direction	69	52		NC (unconfined concrete)
Third floor / columns ABCDE2, ABCDE5 - MIN1/2 direction	69	52		NC (unconfined concrete)

\*Vs – shear strength provided by the hoops (stirrups).



Table 5 Evaluation of  $\rho_{bal}$  according to Park and Paulay

Beam Elements / CS name		rc cs										
		fc' [N/mm2]	fy [N/mm2]	Es [N/mm2]	$\beta_1$	$\rho_{bal}$	b [mm]	h [mm]	a [mm]	$\Phi$ [mm]	d [mm]	
Frame nr. 1&2 / First and second floor/ Main beam	Edge cross section 1-1	20	230	210000	0.85	0.046	400	600	25	18	566	
	Intermediate cross section 2-2	20	230	210000	0.85	0.046	400	600	25	18	566	
	Mid-span cross section 3-3	20	230	210000	0.85	0.046	400	600	25	18	566	
Frame nr. 1&2 / Third floor / Main beam	Edge cross section 1-1	20	230	210000	0.85	0.046	300	550	25	14	518	
	Intermediate cross section 2-2	20	230	210000	0.85	0.046	300	550	25	14	518	
	Mid-span cross section 3-3	20	230	210000	0.85	0.046	300	550	25	14	518	
Frame nr. 1&2 / Roof / Main beam	Edge cross section 1-1	20	230	210000	0.85	0.046	300	500	25	14	468	
	Intermediate cross section 2-2	20	230	210000	0.85	0.046	300	500	25	14	468	
	Mid-span cross section 3-3	20	230	210000	0.85	0.046	300	500	25	14	468	
Frame nr. 2 / First and second floor / middle beam	---	20	230	210000	0.85	0.046	300	500	25	18	466	
Frame nr. 2 / Third floor / middle beam	---	20	230	210000	0.85	0.046	300	500	25	14	468	
Frame nr. 3 / First, second and third floor / Secondary beam	Edge cross section	20	230	210000	0.85	0.046	300	400	25	14	368	
	Mid-span cross section	20	230	210000	0.85	0.046	300	400	25	14	368	
	Edge cross section	20	230	210000	0.85	0.046	300	400	25	14	368	
Frame nr. 4 / First, second and third floor / Secondary beam	---	20	230	210000	0.85	0.046	300	300	25	14	268	
Frame nr. 5 / First, second and third floor / Secondary beam	---	20	230	210000	0.85	0.046	300	200	25	14	168	

Ratio  $(\rho - \rho') / \rho_{bal}$  is the ratio between the difference of reinforcement in tension  $\rho$  and reinforcement in compression  $\rho'$  and the reinforcement ratio producing balanced strain conditions ( $\rho_{bal}$ ).

Table 6 Evaluation of ratio  $(\rho - \rho') / \rho_{bal}$

Beam Elements / CS name		As				As'				$\rho$	$\rho'$	$\rho - \rho'$	$\rho - \rho'$	Ratio	
		upper	no As	1 x As	As	lower	no As'	1 x As'	As'					$(\rho - \rho') / \rho_{bal}$	$(\rho - \rho') / \rho_{bal}$
Frame nr. 1&2 / First and second floor/ Main beam	Edge cross section 1-1	$\Phi 18$	6	254	1524	$\Phi 18$	3	254	762	0.0067	0.0034	0.0034	-0.0034	0.073	-0.073
	Intermediate cross section 2-2	$\Phi 18$	5	254	1270	$\Phi 18$	4	254	1016	0.0056	0.0045	0.0011	-0.0011	0.024	-0.024
	Mid-span cross section 3-3	$\Phi 18$	3	254	762	$\Phi 18$	6	254	1524	0.0034	0.0067	-0.0034	0.0034	-0.073	0.073
Frame nr. 1&2 / Third floor / Main beam	Edge cross section 1-1	$\Phi 14$	6	154	924	$\Phi 14$	3	154	462	0.0059	0.0030	0.0030	-0.0030	0.065	-0.065
	Intermediate cross section 2-2	$\Phi 14$	5	154	770	$\Phi 14$	4	154	616	0.0050	0.0040	0.0010	-0.0010	0.022	-0.022
	Mid-span cross section 3-3	$\Phi 14$	3	154	462	$\Phi 14$	6	154	924	0.0030	0.0059	-0.0030	0.0030	-0.065	0.065
Frame nr. 1&2 / Roof / Main beam	Edge cross section 1-1	$\Phi 14$	4	154	616	$\Phi 14$	2	154	308	0.0044	0.0022	0.0022	-0.0022	0.048	-0.048
	Intermediate cross section 2-2	$\Phi 14$	3	154	462	$\Phi 14$	3	154	462	0.0033	0.0033	0.0000	0.0000	0.000	0.000
	Mid-span cross section 3-3	$\Phi 14$	2	154	308	$\Phi 14$	4	154	616	0.0022	0.0044	-0.0022	0.0022	-0.048	0.048
Frame nr. 2 / First and second floor / middle beam	---	$\Phi 18$	4	254	1016	$\Phi 18$	4	254	1016	0.0073	0.0073	0.0000	0.0000	0.000	0.000
Frame nr. 2 / Third floor / middle beam	---	$\Phi 14$	4	154	616	$\Phi 14$	4	154	616	0.0044	0.0044	0.0000	0.0000	0.000	0.000
Frame nr. 3 / First, second and third floor / Secondary beam	Edge cross section	$\Phi 14$	4	154	616	$\Phi 14$	2	154	308	0.0056	0.0028	0.0028	-0.0028	0.061	-0.061
	Mid-span cross section	$\Phi 14$	2	154	308	$\Phi 14$	4	154	616	0.0028	0.0056	-0.0028	0.0028	-0.061	0.061
	Edge cross section	$\Phi 14$	4	154	616	$\Phi 14$	2	154	308	0.0056	0.0028	0.0028	-0.0028	0.061	-0.061
Frame nr. 4 / First, second and third floor / Secondary beam	---	$\Phi 14$	3	154	462	$\Phi 14$	3	154	462	0.0057	0.0057	0.0000	0.0000	0.000	0.000
Frame nr. 5 / First, second and third floor / Secondary beam	---	$\Phi 14$	2	154	308	$\Phi 14$	2	154	308	0.0061	0.0061	0.0000	0.0000	0.000	0.000

All formulas and parameters used for the evaluation of parameters from Table 6 are presented below:

$A_s$  – area of the rebars in tension

“upper” – represents the rebars from the upper part of cross section

$n_o A_s$  – represents the number of rebars in tension

$1 \times A_s$  – represents the area of a single rebar in tension

$A_{s'}$  – area of the rebars in compression

“lower” – represents the rebars from the lower part of cross section

$n_o A_{s'}$  – represents the number of rebars in compression

$1 \times A_{s'}$  – represents the area of a single rebar in compression

$\rho$  – Ratio of nonprestressed reinforcement in tension  $\rho = \frac{A_s}{b \cdot d}$  (FEMA 356)

$\rho'$  – Ratio of nonprestressed reinforcement in compression  $\rho' = \frac{A_{s'}}{b \cdot d}$  (FEMA 356)

Observation: In order to consider that during the seismic motion, the upper/lower rebars are subjected alternatively to compression and tension, two ratios were considered  $(\rho - \rho') / \rho_{bal}$ , one for each situation.

**Ratio between axial force (P) and axial strength of the cross section  $A_g \cdot f_c'$**

Table 7 *Determination of ratio  $\frac{P}{A_g \cdot f_c'}$* , using a maximum axial force obtained from applying pushover in X direction

Column Elements / CS name		rc cs					Ratio
		fc' [N/mm2]	b [mm]	h [mm]	Ag [mm2]	P [N]	P/(Agxfc')
pushover in X direction	Ground floor / all columns	20	400	400	160000	870000	0.27
	First floor / columns ABCDE1, ABCDE3, ABCDE4, ABCDE6	20	400	400	160000	459700	0.14
	First floor / columns ABCDE2, ABCDE5	20	300	400	120000	427900	0.18
	Second floor / columns ABCDE1, ABCDE3, ABCDE4, ABCDE6	20	300	300	90000	386400	0.21
	Second floor / columns ABCDE2, ABCDE5	20	300	300	90000	227300	0.13
	Third floor / columns ABCDE1, ABCDE3, ABCDE4, ABCDE6	20	300	300	90000	173800	0.10
	Third floor / columns ABCDE2, ABCDE5	20	300	300	90000	100100	0.06

Table 8 *Determination of ratio  $\frac{P}{A_g \cdot f_c'}$* , using a maximum axial force obtained from applying pushover in Y direction

Column Elements / CS name		rc cs					Ratio
		fc' [N/mm2]	b [mm]	h [mm]	Ag [mm2]	P [N]	P/(Agxfc')
pushover in Y direction	Ground floor / all columns	20	400	400	160000	602100	0.19
	First floor / columns ABCDE1, ABCDE3, ABCDE4, ABCDE6	20	400	400	160000	383230	0.12
	First floor / columns ABCDE2, ABCDE5	20	300	400	120000	400000	0.17
	Second floor / columns ABCDE1, ABCDE3, ABCDE4, ABCDE6	20	300	300	90000	220000	0.12
	Second floor / columns ABCDE2, ABCDE5	20	300	300	90000	200844	0.11
	Third floor / columns ABCDE1, ABCDE3, ABCDE4, ABCDE6	20	300	300	90000	128752	0.07
	Third floor / columns ABCDE2, ABCDE5	20	300	300	90000	91000	0.05

**Ratio between shear force (V) and shear strength of the cross section  $b_w \cdot d \cdot \sqrt{f'_c}$  – both for beams and columns**

Table 9 Determination of ratio  $\frac{V}{b_w \cdot d \cdot \sqrt{f'_c}}$  using a maximum shear force obtained from applying pushover in X and Y direction, in the

case of beams

Beam Elements / CS name		rc cs						rebars Φ [mm]	Ratio V/(bxdxsqrt(fc'))	
		fc' [N/mm <sup>2</sup> ]	V [N]	b [mm]	h [mm]	a [mm]	d [mm]			
pushover in X direction	Frame nr. 1&2 / First and second floor / Main beam	Edge cross section 1-1	20	143600	400	600	25	566	18	0.14
		Intermediate cross section 2-2	20	121100	400	600	25	566	18	0.12
		Mid-span cross section 3-3	20	90700	400	600	25	566	18	0.09
	Frame nr. 1&2 / Third floor / Main beam	Edge cross section 1-1	20	71800	300	550	25	518	14	0.10
		Intermediate cross section 2-2	20	62200	300	550	25	518	14	0.09
		Mid-span cross section 3-3	20	45700	300	550	25	518	14	0.07
	Frame nr. 1&2 / Roof / Main beam	Edge cross section 1-1	20	88200	300	500	25	468	14	0.14
		Intermediate cross section 2-2	20	40200	300	500	25	468	14	0.06
		Mid-span cross section 3-3	20	81200	300	500	25	468	14	0.13
Frame nr. 2 / First and second floor / middle beam	---	20	100800	300	500	25	466	18	0.16	
Frame nr. 2 / Third floor / middle beam	---	20	32300	300	500	25	468	14	0.05	
pushover in Y direction	Frame nr. 3 / First, second and third floor / Secondary beam	Edge c ross section	20	45154	300	400	25	368	14	0.09
		Mid-span cross section	20	45154	300	400	25	368	14	0.09
		Edge c ross section	20	45154	300	400	25	368	14	0.09
	Frame nr. 4 / First, second and third floor / Secondary beam	---	20	18400	300	300	25	268	14	0.05
	Frame nr. 5 / First, second and third floor / Secondary beam	---	20	8908	300	200	25	168	14	0.04

Table 10 Determination of ratio  $\frac{V}{b_w \cdot d \cdot \sqrt{f'_c}}$  using a maximum shear force obtained from applying pushover in X and Y direction, in the

case of columns

Column Elements / CS name		rc cs							Ratio
		fc' [N/mm2]	V [N]	b [mm]	h [mm]	a [mm]	Φ [mm]	d [mm]	V/(bxdxsqrt(fc'))
pushover in X direction	Ground floor / all columns	20	77100	400	400	25	18	366	0.12
	First floor / columns ABCDE1, ABCDE3, ABCDE4, ABCDE6	20	230300	400	400	25	18	366	0.35
	First floor / columns ABCDE2, ABCDE5	20	93200	300	400	25	18	366	0.19
	Second floor / columns ABCDE1, ABCDE3, ABCDE4, ABCDE6	20	29400	300	300	25	18	266	0.08
	Second floor / columns ABCDE2, ABCDE5	20	29200	300	300	25	18	266	0.08
	Third floor / columns ABCDE1, ABCDE3, ABCDE4, ABCDE6	20	68400	300	300	25	18	266	0.19
	Third floor / columns ABCDE2, ABCDE5	20	26635	300	300	25	18	266	0.07
Column Elements / CS name		rc cs							Ratio
		fc' [N/mm2]	V [N]	b [mm]	h [mm]	a [mm]	Φ [mm]	d [mm]	V/(bxdxsqrt(fc'))
pushover in Y direction	Ground floor / all columns	20	50098	400	400	25	18	366	0.08
	First floor / columns ABCDE1, ABCDE3, ABCDE4, ABCDE6	20	52898	400	400	25	18	366	0.08
	First floor / columns ABCDE2, ABCDE5	20	30140	300	400	25	18	366	0.06
	Second floor / columns ABCDE1, ABCDE3, ABCDE4, ABCDE6	20	37976	300	300	25	18	266	0.11
	Second floor / columns ABCDE2, ABCDE5	20	36080	300	300	25	18	266	0.10
	Third floor / columns ABCDE1, ABCDE3, ABCDE4, ABCDE6	20	127574	300	300	25	18	266	0.36
	Third floor / columns ABCDE2, ABCDE5	20	140679	300	300	25	18	266	0.39

**Elements controlled by shear****Beams:**

Table 11 Shear strength determination according to the detailed procedure- for 1'st and 2'nd floor main beam from Frame no. 1 and 2 – in case of cracking opening from the lower part of cs

cracking opening from lower part of cs - Frame nr. 1&2 / First and second floor/ Main beam						
cracks	s1	s2	s3	s4	s5	s6
si [mm]	283	533	783	1033	1283	1415
Qb [kN]	433.7	230.3	156.8	118.8	95.7	86.7
nf etr.	1	2	3	4	5	6
Qe [kN]	0.0	10.4	20.8	31.2	41.6	52.0
Qai [kN]	0.0	0.0	37.4	37.4	37.4	112.1
Qcap [kN]	433.7	240.7	214.9	187.4	174.6	250.9

Table 12 Shear strength determination according to the detailed procedure - for 1'st and 2'nd floor main beam from Frame no. 1 and 2 – in case of cracking opening from the upper part of cs

cracking opening from upper part of cs - Frame nr. 1&2 / First and second floor/ Main beam						
cracks	s1	s2	s3	s4	s5	s6
si [mm]	283	533	783	1033	1283	1415
Qb [kN]	613.4	325.7	221.7	168.0	135.3	122.7
nf etr.	1	2	3	4	5	6
Qe [kN]	0.0	10.4	20.8	31.2	41.6	52.0
Qai [kN]	0.0	0.0	0.0	0.0	0.0	0.0
Qcap [kN]	613.4	336.1	242.5	199.2	176.9	174.7

Bellow are presented all formulas and parameters used for the obtaining of the tables 11 and 12.

*Beams flexural shear computation according to detailed procedure Clippi T. et all (1999 - Beton Armat)[75]*

$Q_{cap}$  - shear strength of a cs  $Q_{cap} = Q_b + Q_e + Q_i$

$Q_b$  - shear strength of concrete  $Q_b = \frac{b \cdot d \cdot \sqrt{p}}{s_i} \cdot m_t \cdot R_t$

b - cross section width

d - distance from extreme compression fiber to centroid of tension reinforcement (h-d')

p - tension reinforcement percentage intersected by inclined crack

$$p = \frac{A_s}{b \cdot d} \cdot 100$$

$s_i$  - the horizontal projection of a considered inclined crack, it was experimentally observed that the critical crack is found in the domain of  $0.5d < s_i < 2.5d$ .

$m_t$  - work condition coefficient (=1 in our case).

$R_t$  – Clippi 1999 - Annexe 2 – characteristic tensile strength of BC25 is 1.65 N/mm<sup>2</sup>

$Q_e$  - shear strength of stirrups  $Q_e = (n_f - 1)n_e \cdot A_e \cdot m_{at} \cdot R_a$

$(n_f - 1)$  - number of stirrups intersected by inclined crack minus 1, which is the stirrup from the end of the inclined crack

$n_e$  - number of the stirrups arms (2 if it is simple stirrup and 4 if it is double stirrup) = 2 in our case

$A_e$  - stirrups area

$m_{at}$  - work conditions coefficient is 0.8 for laminated steel rebars (PC60, PC52, OB37)

$R_a$  - characteristic strength of tensile rebars intersected by crack

$Q_i$  - shear strength of inclined rebars  $Q_i = A_{ai(m)} \cdot m_{at} \cdot R_a \cdot \sin \alpha$

$A_{ai(m)}$  - area of inclined rebars, intersected by inclined crack  $m$ , in the central zone equal with  $\frac{3}{4}$  from the length of inclined part

$\alpha$  - angle of the incline rebar

$nf_{etr}$  - represents the number of stirrups intersected by the inclined crack.

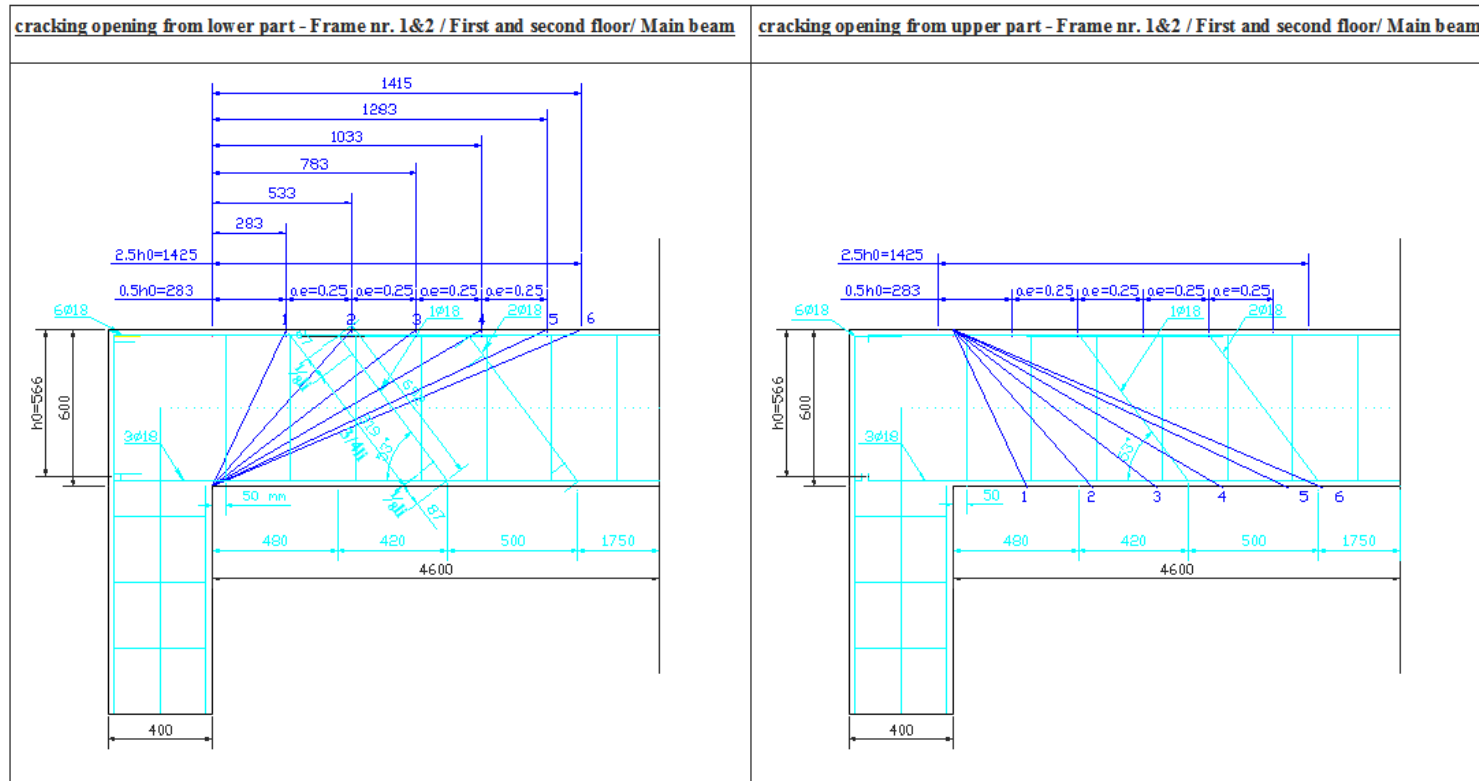


Figure 1 Cracks distribution detail with distances between them in a beam with opening from lower/upper part of the element [75]



Determination of less favorable position of an inclined crack is presented in table 13.

Table 13 Beams element state (controlled/not controlled by shear) due to shear strength vs. shear force, obtained from pushover analysis applied both in X and Y direction

MRF			
Beams - element/cs name	Qcap [KN]	Vx [KN]	Vy [KN]
		Pushover X dir	Pushover Y dir
Frame nr 1&2 / First and second floor / Main beam	175 - s5 lower crack	140	96
Frame nr 1&2 / Third floor / Main beam	116 - s3 lower crack	59	55
Frame nr 1&2 / Roof / Main beam	103 - s5 upper crack	81	80
Frame nr. 2 / First and second floor / Midle beam	120 - s5 lower/upper crack	97	29
Frame nr 1&2 / Third floor / Midle beam	103 - s5 lower/upper crack	28	17
Frame nr. 3 / First, second and third floor / Secondary beam	86 - s4 upper crack	33	45
Frame nr. 4 / First, second and third floor / Secondary beam	63 - s3 lower crack	16	52
Frame nr. 5 / First, second and third floor / Secondary beam	33 - s3 lower crack	7	9

Qcap - shear strength

Vx/y - shear effort in x/y direction (envelopes of pushover analysis in X/Y direction on MRF)

Table 14 Columns element state (controlled/not controlled by shear) due to shear strength vs. shear force on X direction of the cross section obtained from pushover analysis applied both in X and Y direction

MRF				
Columns - element/cs name	Qcap [KN]		Pushover X dir	
	dir X	dir Y	V3 [KN]	V2 [KN]
Ground floor / all columns	125	102	96	104
First floor / columns ABCDE1, ABCDE3, ABCDE4, ABCDE6	102	102	75	87
First floor / columns ABCDE2, ABCDE5	75	94	38	54
Second floor / columns ABCDE1, ABCDE3, ABCDE4, ABCDE6	78	69	20	23
Second floor / columns ABCDE2, ABCDE5	69	69	21	19
Third floor / columns ABCDE1, ABCDE3, ABCDE4, ABCDE6	92	69	65	8
Third floor / columns ABCDE2, ABCDE5	69	69	17	4

Qcap - shear strength

V3 - shear effort in X direction (envelopes of pushover analysis in X direction on MRF)

V2 - shear force in Y direction (envelopes of pushover analysis in X direction on MRF)

MRF				
Columns - element/cs name	Qcap [KN]		Pushover Y dir	
	dir X	dir Y	V3 [KN]	V2 [KN]
Ground floor / all columns	125	102	26	29
First floor / columns ABCDE1, ABCDE3, ABCDE4, ABCDE6	102	102	41	42
First floor / columns ABCDE2, ABCDE5	75	94	12	17
Second floor / columns ABCDE1, ABCDE3, ABCDE4, ABCDE6	78	69	31	30
Second floor / columns ABCDE2, ABCDE5	69	69	28	25
Third floor / columns ABCDE1, ABCDE3, ABCDE4, ABCDE6	92	69	69	69
Third floor / columns ABCDE2, ABCDE5	69	69	22	52

Qcap - shear strength

V3 - shear effort in X direction (envelopes of pushover analysis in Y direction on MRF)

V2 - shear force in Y direction (envelopes of pushover analysis in Y direction on MRF)

Table 15 Beams and columns Lap Length

Elements / CS name		$(l_{b,min})$	$\Phi$ [mm]	$l_{b,rqd}$ [mm]	$\sigma_{sd}$ [N/mm <sup>2</sup> ]	$f_{bd}$ [N/mm <sup>2</sup> ]	LAP length
Beams & Columns Lap Length	Frame nr. 1 / First and second floor/ Main beam	720	18	439	230	2.36	is sufficient
	Frame nr. 1 / Third floor / Main beam	560	14	341	230	2.36	is sufficient
	Frame nr. 1 / Roof / Main beam	560	14	341	230	2.36	is sufficient
	Frame nr. 2 / First and second floor / Main beam	720	18	439	230	2.36	is sufficient
	Frame nr. 2 / Third floor / Main beam	560	14	341	230	2.36	is sufficient
	Frame nr. 2 / Roof / Main beam	560	14	341	230	2.36	is sufficient
	Frame nr. 2 / First and second floor / middle beam	720	18	439	230	2.36	is sufficient
	Frame nr. 2 / Third floor / middle beam	560	14	341	230	2.36	is sufficient
	Frame nr. 3 / First, second and third floor / Secondary beam	560	14	341	230	2.36	is sufficient
	Frame nr. 4 / First, second and third floor / Secondary beam	560	14	341	230	2.36	is sufficient
	Frame nr. 5 / First, second and third floor / Secondary beam	560	14	341	230	2.36	is sufficient
	All columns cross sections	720	18	439	230	2.36	is sufficient

Table 16 Beams element state (sufficient/not sufficient anchorage length) and equivalent yield limit  $f_{y,eq}$ 

Elements / CS name		$(l_{b,min})$	$\Phi$ [mm]	$l_{b,rqd}$ [mm]	$\sigma_{sd}$ [N/mm <sup>2</sup> ]	$f_{bd}$ [N/mm <sup>2</sup> ]	Anchorage length	$f_{y,eq}$
Beams Anchorage Length	Frame nr. 1 / First and second floor/ Main beam	375	18	439	230	2.36	is NOT sufficient	197
	Frame nr. 1 / Third floor / Main beam	375	14	341	230	2.36	is sufficient	230
	Frame nr. 1 / Roof / Main beam	275	14	341	230	2.36	is NOT sufficient	185
	Frame nr. 2 / First and second floor / Main beam	375	18	439	230	2.36	is NOT sufficient	197
	Frame nr. 2 / Third floor / Main beam	375	14	341	230	2.36	is sufficient	230
	Frame nr. 2 / Roof / Main beam	275	14	341	230	2.36	is NOT sufficient	185
	Frame nr. 2 / First and second floor / middle beam	375	18	439	230	2.36	is NOT sufficient	197
	Frame nr. 2 / Third floor / middle beam	275	14	341	230	2.36	is NOT sufficient	185
	Frame nr. 3 / First, second and third floor / Secondary beam	375	14	341	230	2.36	is sufficient	230
	Frame nr. 4 / First, second and third floor / Secondary beam	275	14	341	230	2.36	is NOT sufficient	185
	Frame nr. 5 / First, second and third floor / Secondary beam	275	14	341	230	2.36	is NOT sufficient	185

Bellow are presented all formulas and parameters used for the obtaining of the

$l_{bmin}$  - the existing overlapping,  $40\Phi$  in our case

$\Phi$  - rebars diameter

$\sigma_{sd}$  - design stress of the bar calculus strength for steel =  $f_y$  (characteristic strength of rebars)/ $\gamma_s$  (partial safety factor for steel) - in our case we will work with characteristic strength

$f_{bd}$  - the design value of the ultimate bond stress

$$f_{bd} = 2.25 \cdot \eta_1 \cdot \eta_2 \cdot f_{ctd} = 2.25 \cdot 0.7 \cdot 1 \cdot 1.5 = 2.36$$

$\eta_1$  is a coefficient related to the quality of the bond condition and the position of the bar during concreting = 0.7 (for all other cases and for bars in structural elements built with slip-forms, unless it can be shown that 'good' bond conditions exist)

$\eta_2=1$  is related to the bar diameter = 1,0 for  $\Phi \leq 32$  mm

$f_{ctd}$  - is the design value of concrete tensile strength =  $\alpha_{ct} \times f_{ctk0,05} / \gamma_c$

$\alpha_{ct} = 1$  is a coefficient taking account of long term effects on the tensile strength and of unfavorable effects, resulting from the way the load is applied. Note: The value of  $\alpha_{ct}$  for use in a Country may be found in its National Annex. The recommended value is 1.

$$f_{ctk0,05} = 1.5$$

$\gamma_c = 1.5$  (for concrete, but also it is suggested to use value 1) and because we are dealing only with characteristic strengths =>  $\gamma_c = 1$  (for situations not covered by European standards)

$l_{b,rqd}$  - basic required anchorage length

The basic required anchorage length,  $l_{b,rqd}$ , for anchoring the force  $A_{s,osd}$  in a straight bar assuming constant bond stress equal to  $f_{bd}$  follows from:

$$l_{b,rqd} = (\Phi / 4) (\sigma_{sd} / f_{bd})$$

As conclusion all elements proved to have sufficient lap length as it is presented in previous table  $l_{bmin} > l_{b,rqd}$ .

$$l_{b,min} = h_{column} - a$$

-  $h_{column}$  - cross section height

-  $a$  - minimum concrete cover depth (2.5 cm)

Except  $l_{b,min}$ , all the other parameters are computed the same as in case of lap length presented above.

Table 17 Columns with axial loads exceeding 0.70P<sub>0</sub>

0.7P <sub>0</sub> KN	P <sub>0</sub> KN	P <sub>max</sub> KN		0.7P <sub>0</sub> KN	P <sub>0</sub> KN	P <sub>max</sub> KN	
-2520	-3600	-1070	Ground floor / all columns				
0.7P <sub>0</sub> KN	P <sub>0</sub> KN	P <sub>max</sub> KN	First floor / columns ABCDE1, ABCDE3, ABCDE4, ABCDE6	0.7P <sub>0</sub> KN	P <sub>0</sub> KN	P <sub>max</sub> KN	Second floor / columns ABCDE2, ABCDE5
-2357.6	-3368	-460		-1397.9	-1997	-227	
0.7P <sub>0</sub> KN	P <sub>0</sub> KN	P <sub>max</sub> KN	First floor / columns ABCDE2, ABCDE5	0.7P <sub>0</sub> KN	P <sub>0</sub> KN	P <sub>max</sub> KN	Third floor / columns ABCDE1, ABCDE3, ABCDE4, ABCDE6
-1809.5	-2585	-428		-1643.6	-2348	-174	
0.7P <sub>0</sub> KN	P <sub>0</sub> KN	P <sub>max</sub> KN	Second floor / columns ABCDE1, ABCDE3, ABCDE4, ABCDE6	0.7P <sub>0</sub> KN	P <sub>0</sub> KN	P <sub>max</sub> KN	Third floor / columns ABCDE2, ABCDE5
-1479.8	-2114	-386		-1397.9	-1997	-100	

**Pushover analysis**

Table 18 Shear strength vs. shear force on beam elements obtained from pushover analysis applied both in X and Y directions

MRF+FRP+BRB		
Beams - element/cs name	Q <sub>cap</sub> [KN]	V [KN]
		Pushover X dir
Frame nr 1&2 / First and second floor / Main beam	175	139
Frame nr 1&2 / Third floor / Main beam	116	61
Frame nr 1&2 / Roof / Main beam	103	81
Frame nr. 2 / First and second floor / Midle beam	120	96
Frame nr 1&2 / Third floor / Midle beam	103	35
Frame nr. 3 / First, second and third floor / Secondary beam	86	31
Frame nr. 4 / First, second and third floor / Secondary beam	63	11
Frame nr. 5 / First, second and third floor / Secondary beam	33	6

Q<sub>cap</sub> - shear strength

V - shear effort in X direction (envelopes of pushover analysis in X direction on MRF+FRP+BRB)

MRF+FRP+BRB		
Beams - element/cs name	Q <sub>cap</sub> [KN]	V [KN]
		Pushover Y dir
Frame nr 1&2 / First and second floor / Main beam	175	95
Frame nr 1&2 / Third floor / Main beam	116	56
Frame nr 1&2 / Roof / Main beam	103	79
Frame nr. 2 / First and second floor / Midle beam	120	29
Frame nr 1&2 / Third floor / Midle beam	103	15
Frame nr. 3 / First, second and third floor / Secondary beam	86	45
Frame nr. 4 / First, second and third floor / Secondary beam	63	25
Frame nr. 5 / First, second and third floor / Secondary beam	33	9

Q<sub>cap</sub> - shear strength

V - shear effort in X direction (envelopes of pushover analysis in X direction on MRF+FRP+BRB)

Table 19 Shear strength vs. shear force on column elements for X/Y direction of the cross section obtained from pushover analysis applied both in X and Y direction

MRF+FRP+BRB				
Columns - element/cs name	Qcap [KN]		Pushover X dir	
	dir X	dir Y	V3 [KN]	V2 [KN]
Ground floor / all columns	125	102	78	50
First floor / columns ABCDE1, ABCDE3, ABCDE4, ABCDE6	102	102	61	79
First floor / columns ABCDE2, ABCDE5	75	94	45	46
Second floor / columns ABCDE1, ABCDE3, ABCDE4, ABCDE6	78	69	26	24
Second floor / columns ABCDE2, ABCDE5	69	69	24	21
Third floor / columns ABCDE1, ABCDE3, ABCDE4, ABCDE6	92	69	67	10
Third floor / columns ABCDE2, ABCDE5	69	69	19	4

Qcap - shear strength

V3 - shear effort in X direction (envelopes of pushover analysis in X direction on MRF+FRP+BRB)

V2 - shear force in Y direction (envelopes of pushover analysis in X direction on MRF+FRP+BRB)

MRF+FRP+BRB				
Columns - element/cs name	Qcap [KN]		Pushover Y dir	
	dir X	dir Y	V3 [KN]	V2 [KN]
Ground floor / all columns	125	102	30	30
First floor / columns ABCDE1, ABCDE3, ABCDE4, ABCDE6	102	102	50	50
First floor / columns ABCDE2, ABCDE5	75	94	19	29
Second floor / columns ABCDE1, ABCDE3, ABCDE4, ABCDE6	78	69	23	28
Second floor / columns ABCDE2, ABCDE5	69	69	22	24
Third floor / columns ABCDE1, ABCDE3, ABCDE4, ABCDE6	92	69	71	49
Third floor / columns ABCDE2, ABCDE5	69	69	25	43

Qcap - shear strength

V3 - shear effort in X direction (envelopes of pushover analysis in Y direction on MRF+FRP+BRB)

V2 - shear force in Y direction (envelopes of pushover analysis in Y direction on MRF+FRP+BRB)

**Nonlinear dynamic analysis**

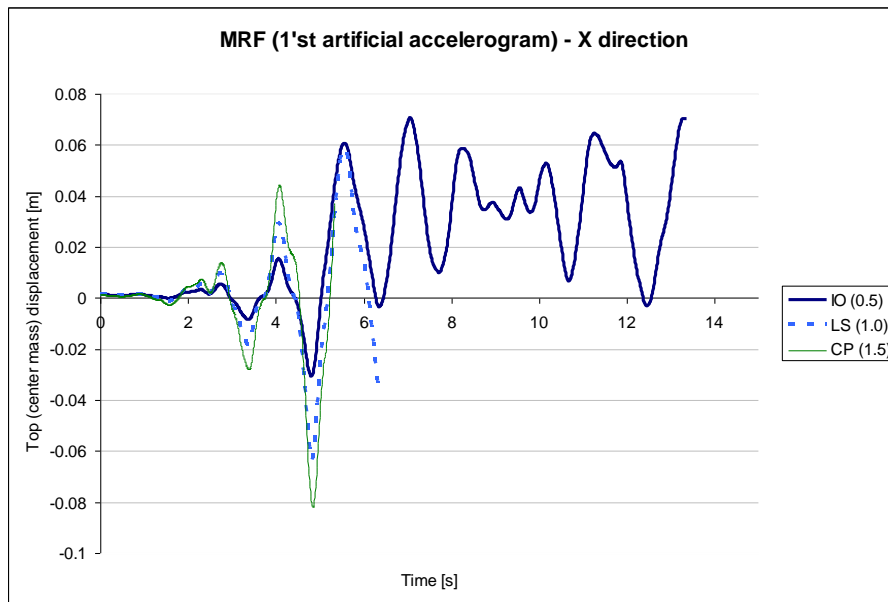


Figure 2 MRF – X direction Top Displacement at the three stages of IO, LS and CP for the 1st artificial accelerogram

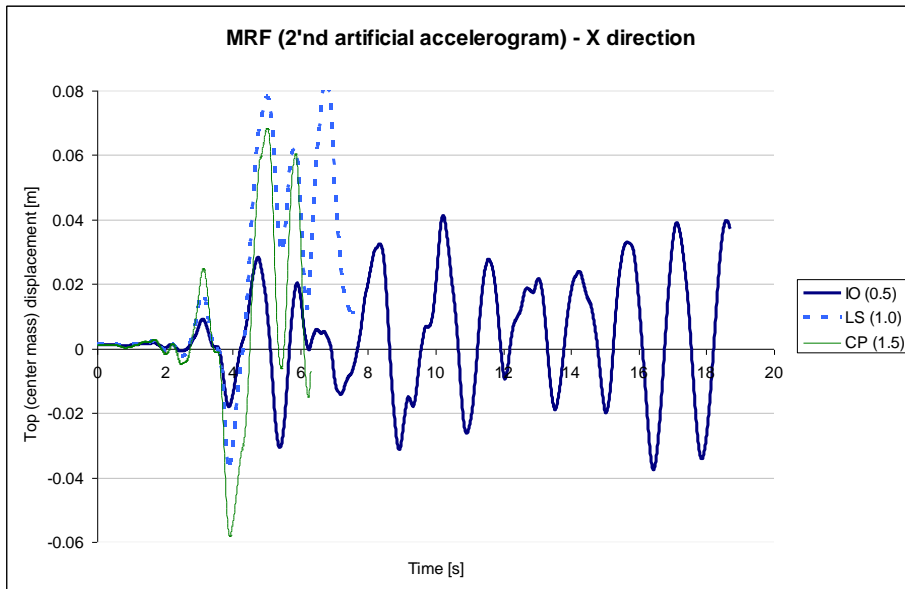


Figure 3 MRF – X direction Top Displacement at the three stages of IO, LS and CP for the 2'nd artificial accelerogram

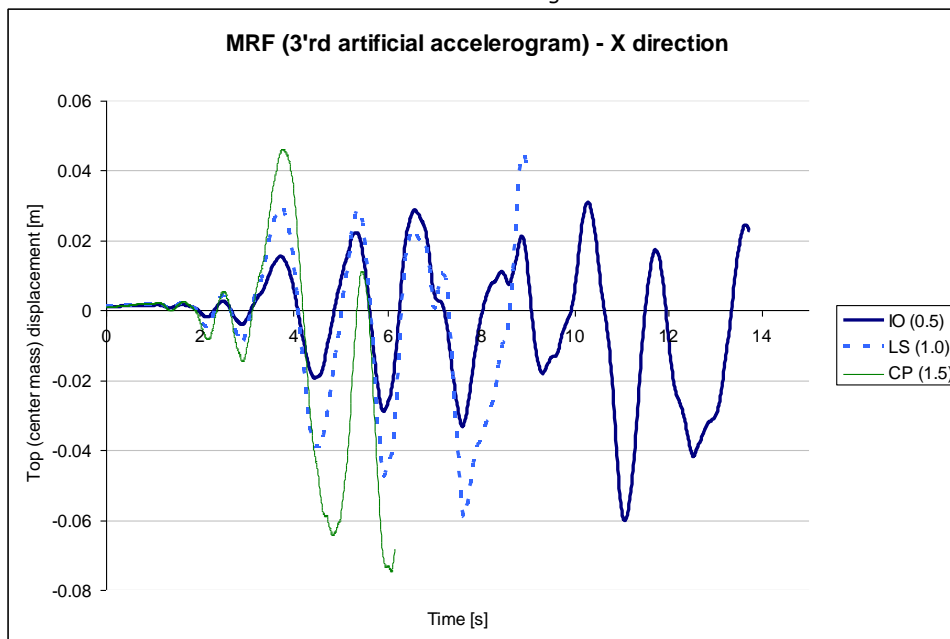


Figure 4 MRF – X direction Top Displacement at the three stages of IO, LS and CP for the 3'rd artificial accelerogram

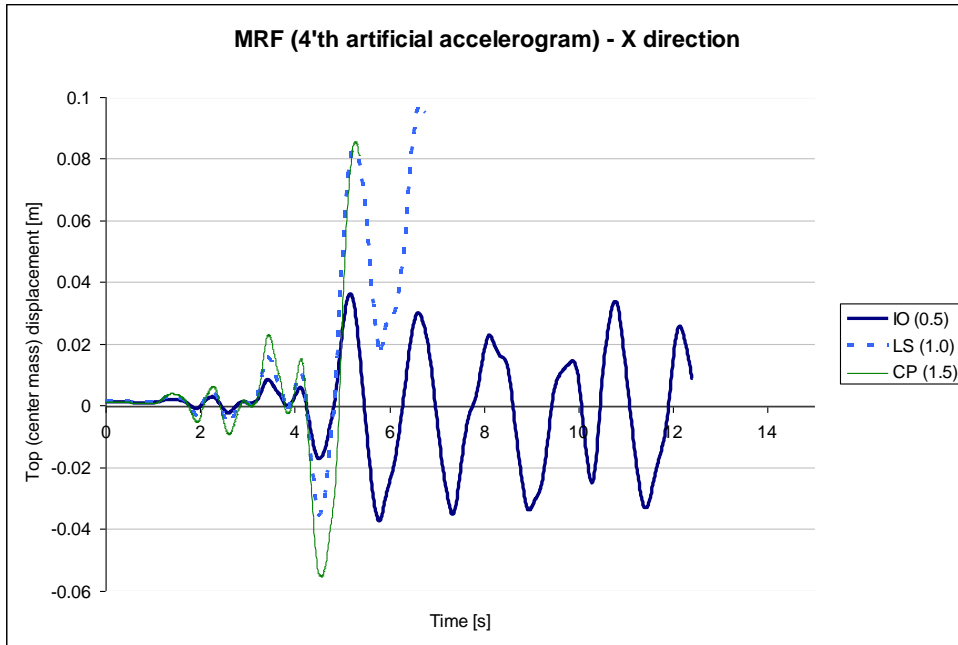


Figure 5 MRF – X direction Top Displacement at the three stages of IO, LS and CP for the 4'th artificial accelerogram

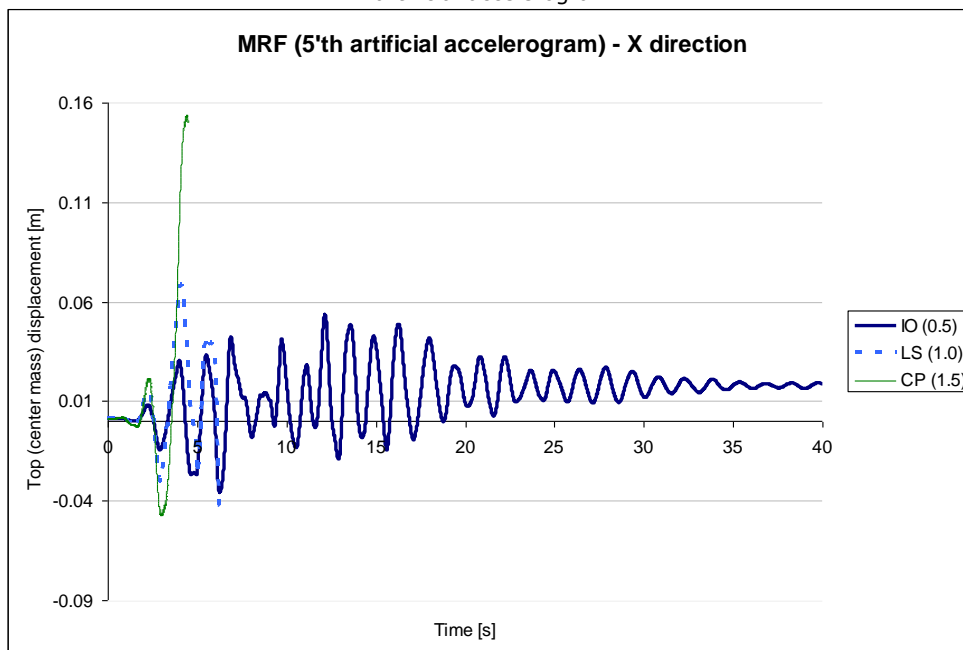


Figure 6 MRF – X direction Top Displacement at the three stages of IO, LS and CP for the 5'th artificial accelerogram

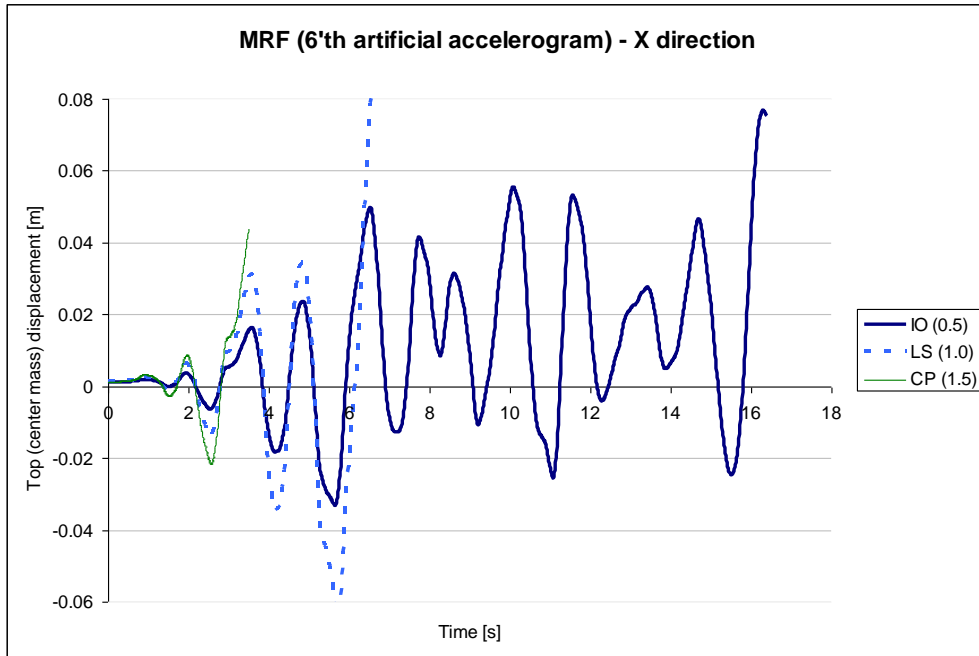


Figure 7 MRF – X direction Top Displacement at the three stages of IO, LS and CP for the 6'th artificial accelerogram

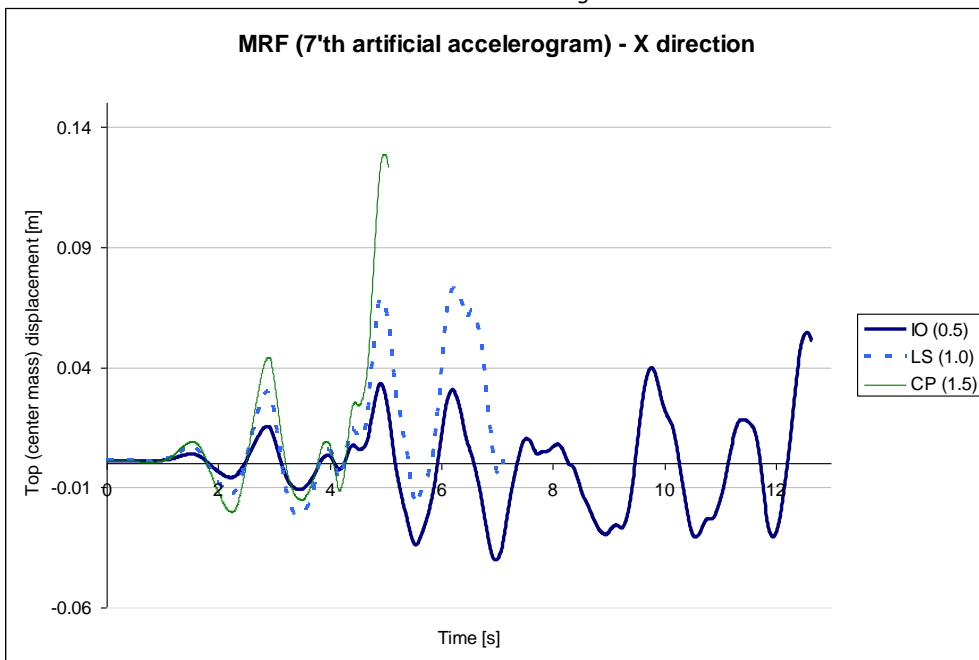


Figure 8 MRF – X direction Top Displacement at the three stages of IO, LS and CP for the 7'th artificial accelerogram



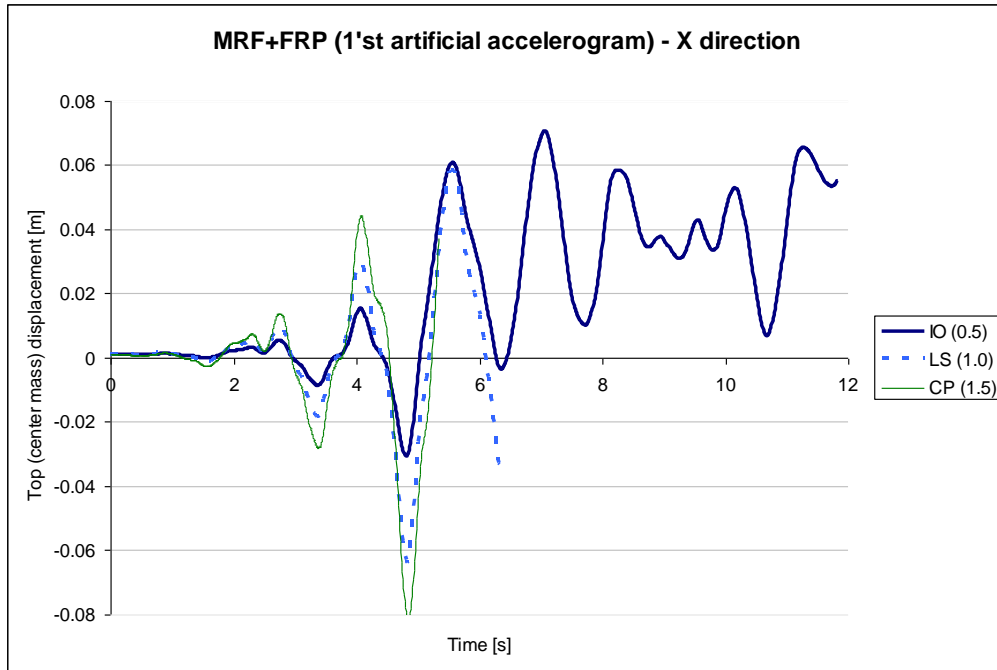


Figure 9 MRF+FRP – X direction Top Displacement at the three stages of IO, LS and CP for the 1'st artificial accelerogram

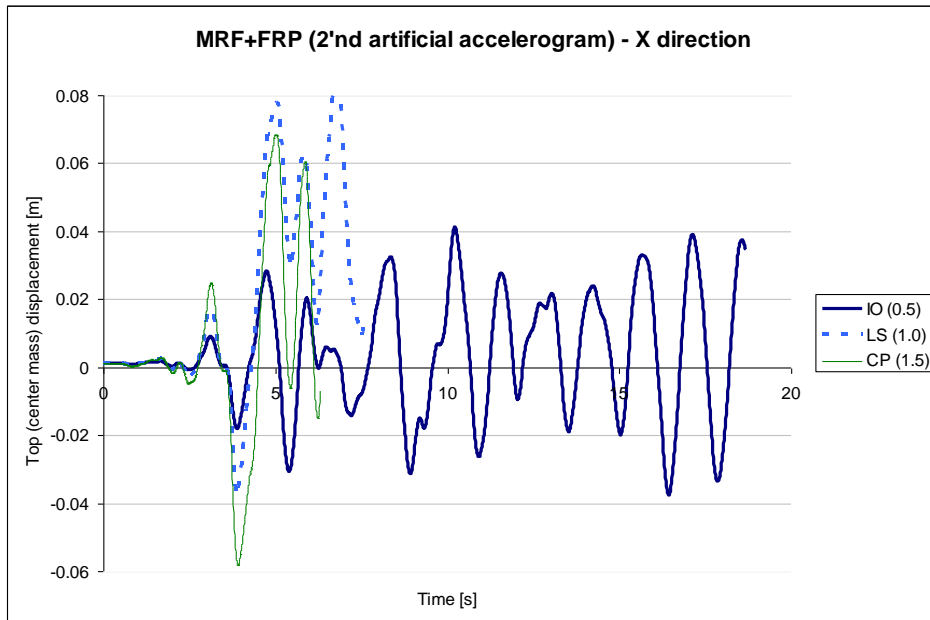


Figure 10 MRF+FRP – X direction Top Displacement at the three stages of IO, LS and CP for the 2'nd artificial accelerogram

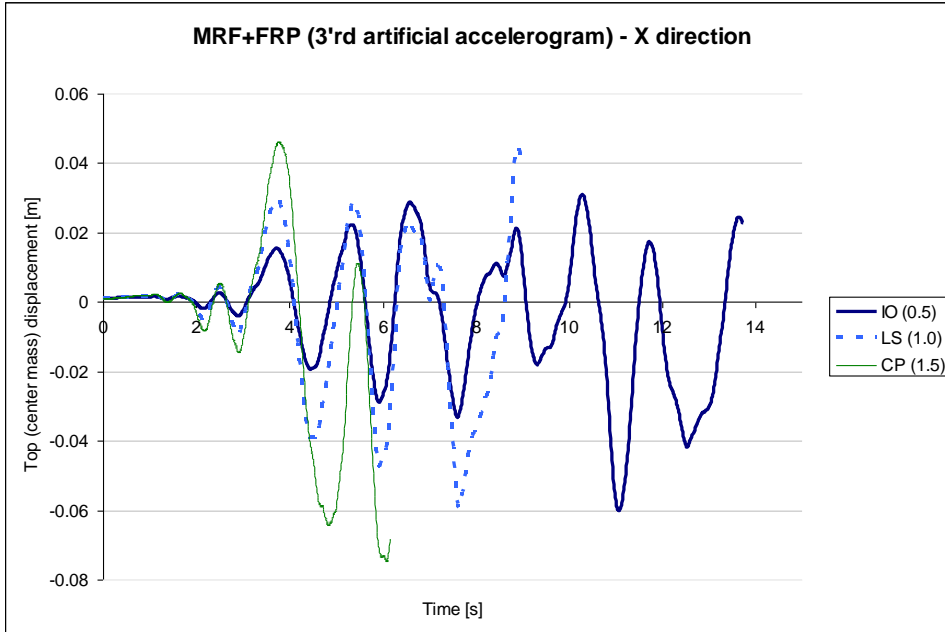


Figure 11 MRF+FRP – X direction Top Displacement at the three stages of IO, LS and CP for the 3'rd artificial accelerogram

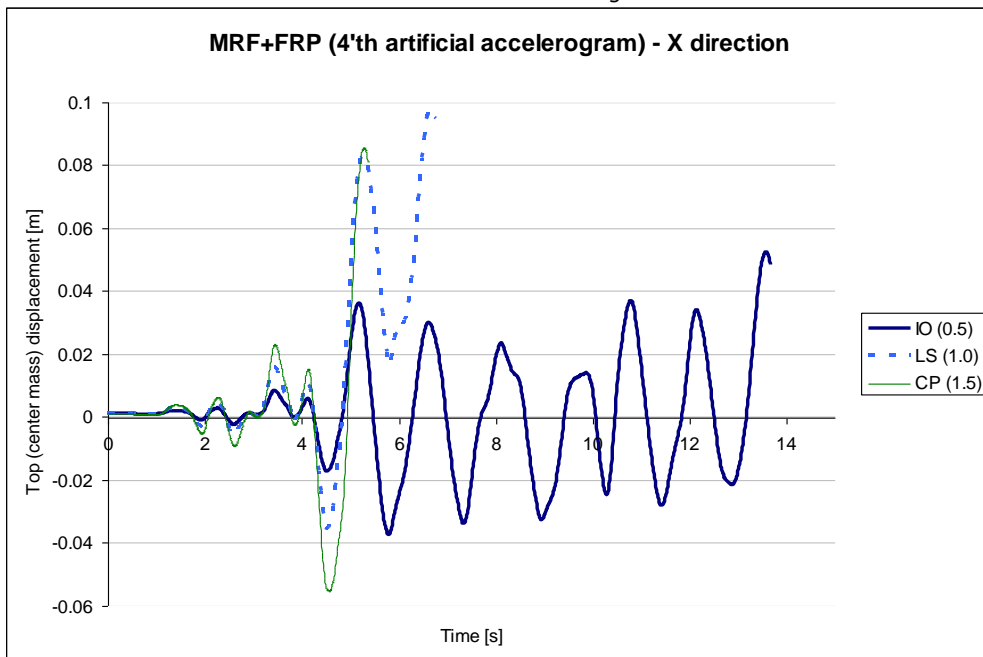


Figure 12 MRF+FRP – X direction Top Displacement at the three stages of IO, LS and CP for the 4'th artificial accelerogram

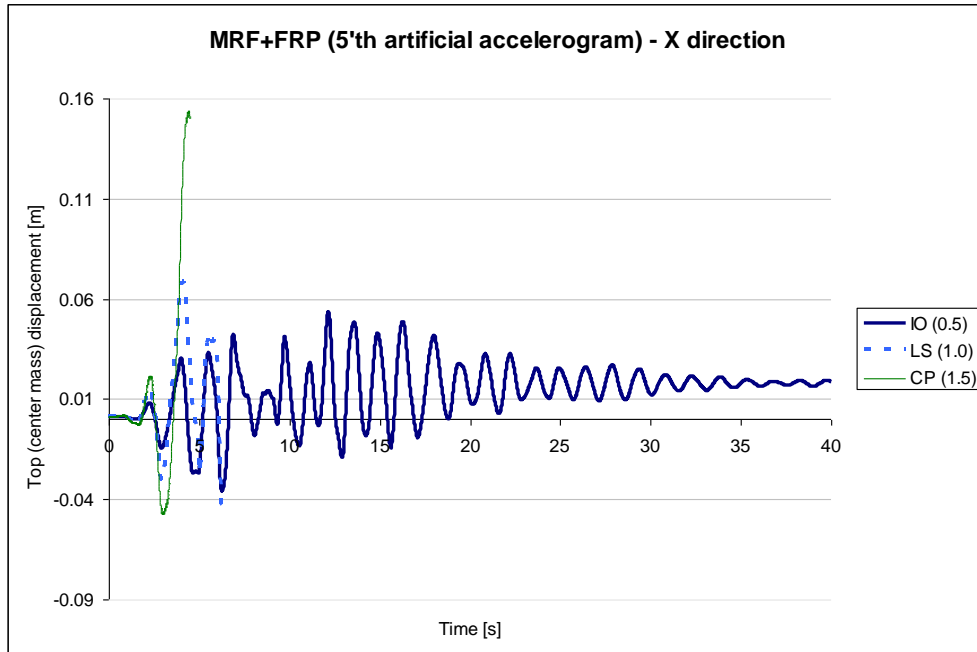


Figure 13 MRF+FRP – X direction Top Displacement at the three stages of IO, LS and CP for the 5'th artificial accelerogram

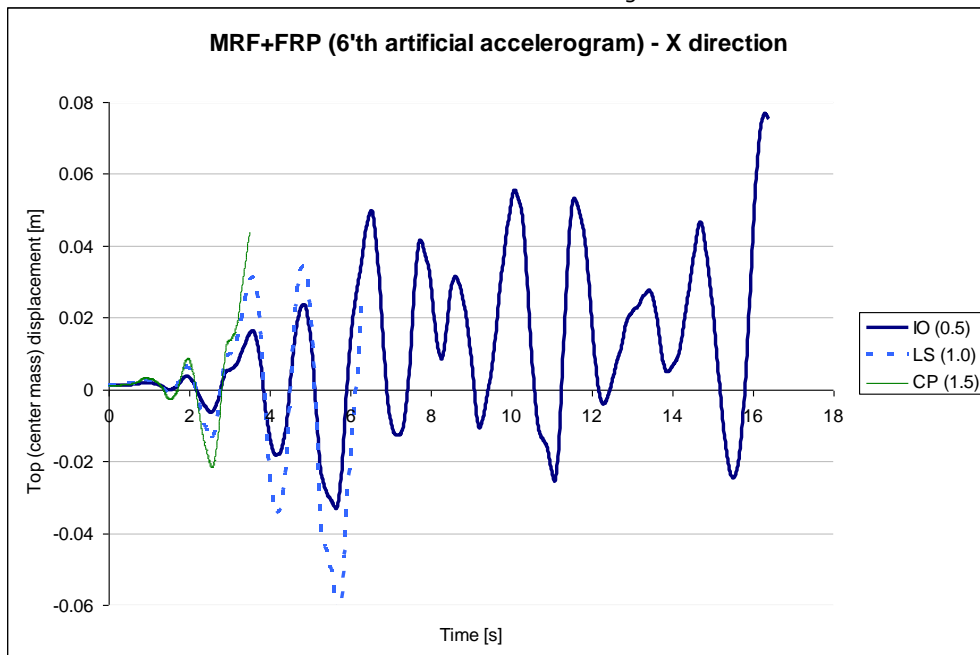


Figure 14 MRF+FRP – X direction Top Displacement at the three stages of IO, LS and CP for the 6'th artificial accelerogram

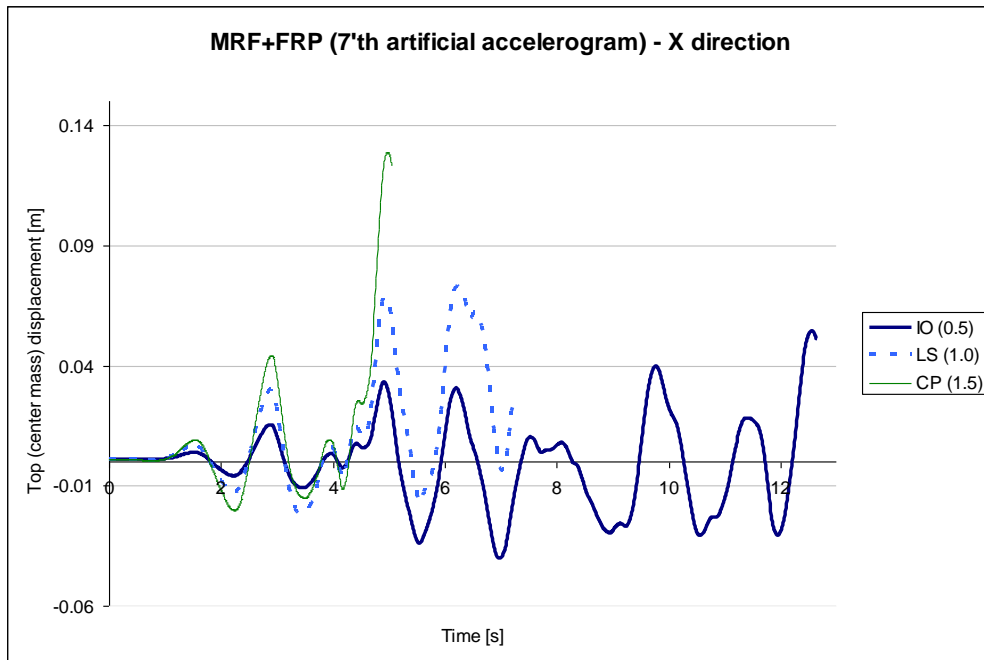


Figure 15 MRF+FRP – X direction Top Displacement at the three stages of IO, LS and CP for the 7'th artificial accelerogram

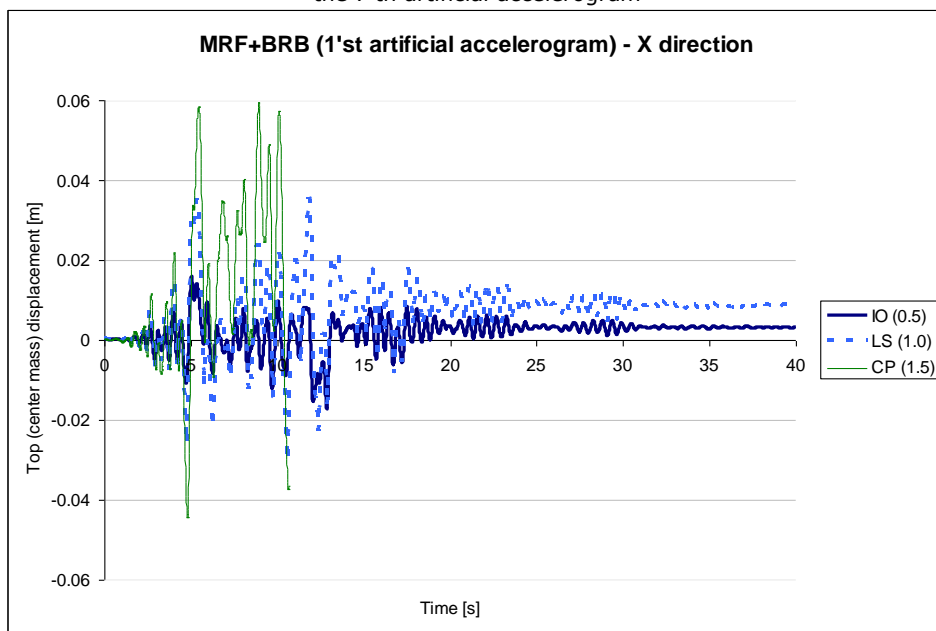


Figure 16 MRF+BRB – X direction Top Displacement at the three stages of IO, LS and CP for the 1'st artificial accelerogram

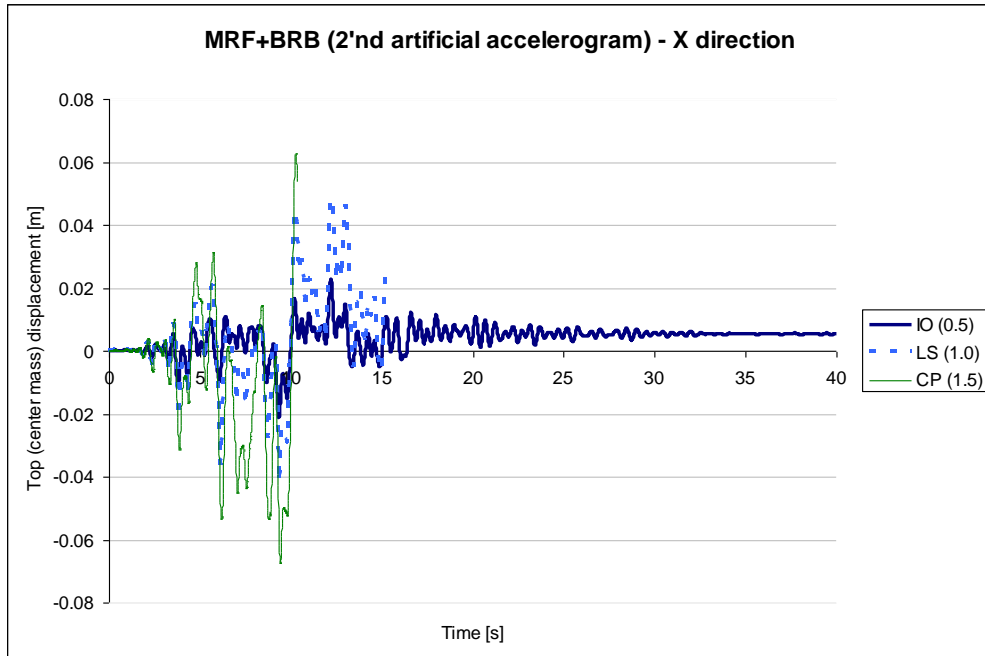


Figure 17 MRF+BRB – X direction Top Displacement at the three stages of IO, LS and CP for the 2'nd artificial accelerogram

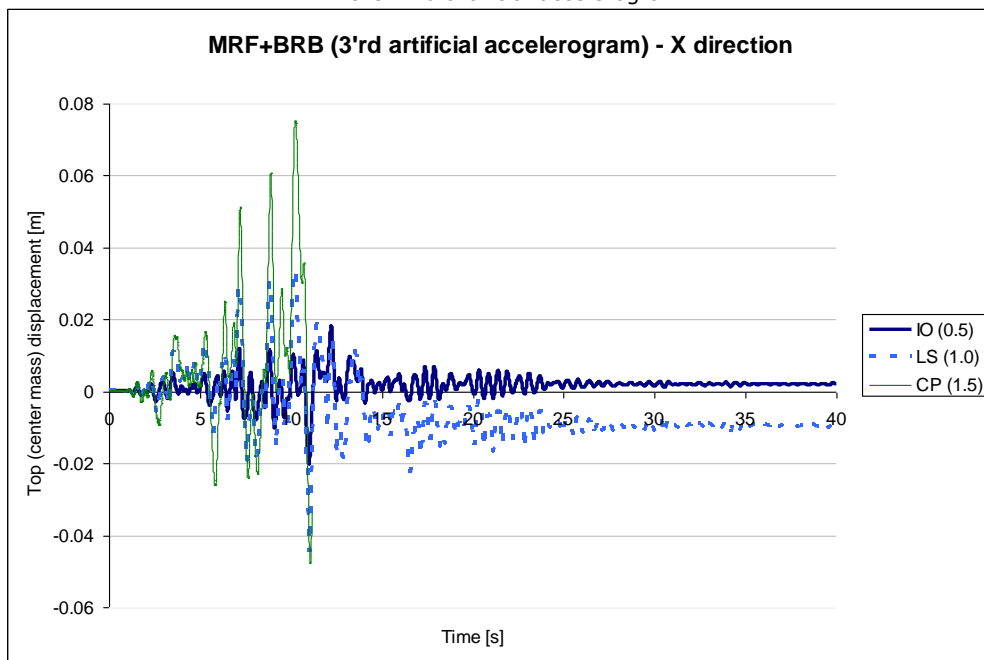


Figure 18 MRF+BRB – X direction Top Displacement at the three stages of IO, LS and CP for the 3'rd artificial accelerogram

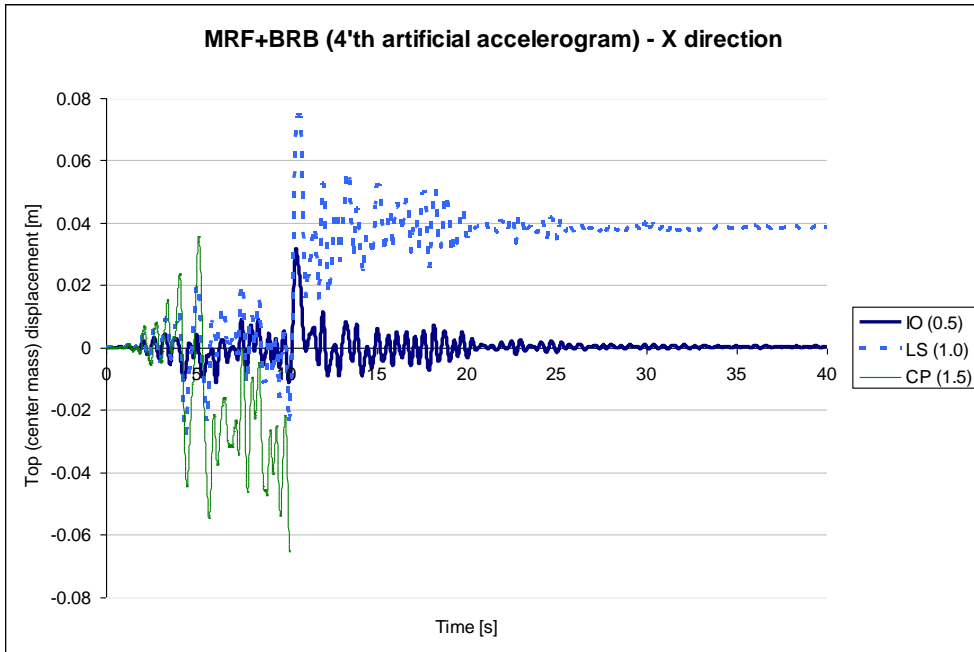


Figure 19 MRF+BRB – X direction Top Displacement at the three stages of IO, LS and CP for the 4'th artificial accelerogram

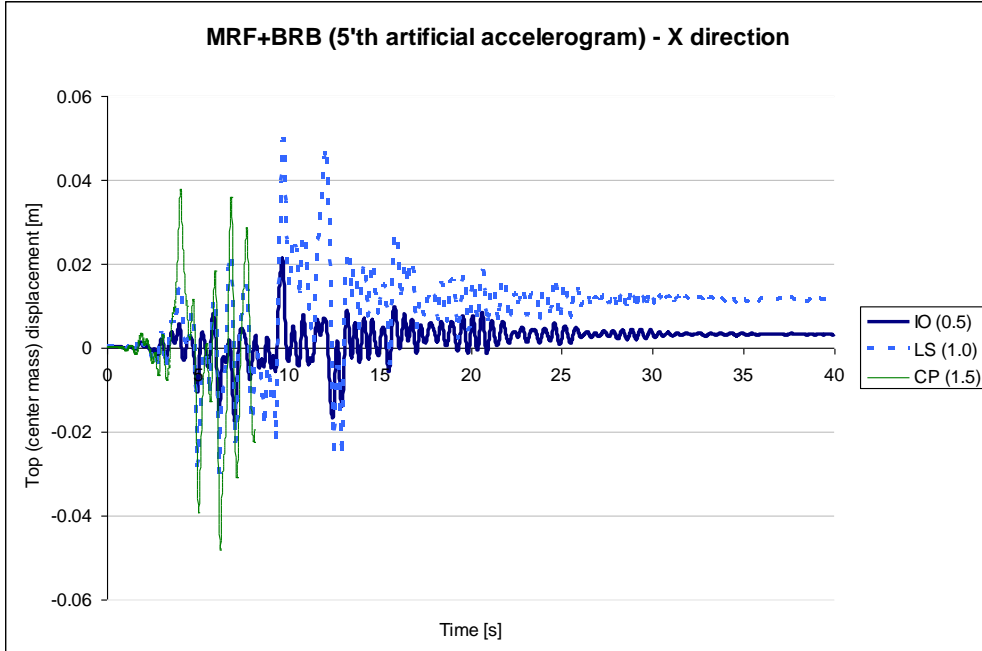


Figure 20 MRF+BRB – X direction Top Displacement at the three stages of IO, LS and CP for the 5'th artificial accelerogram

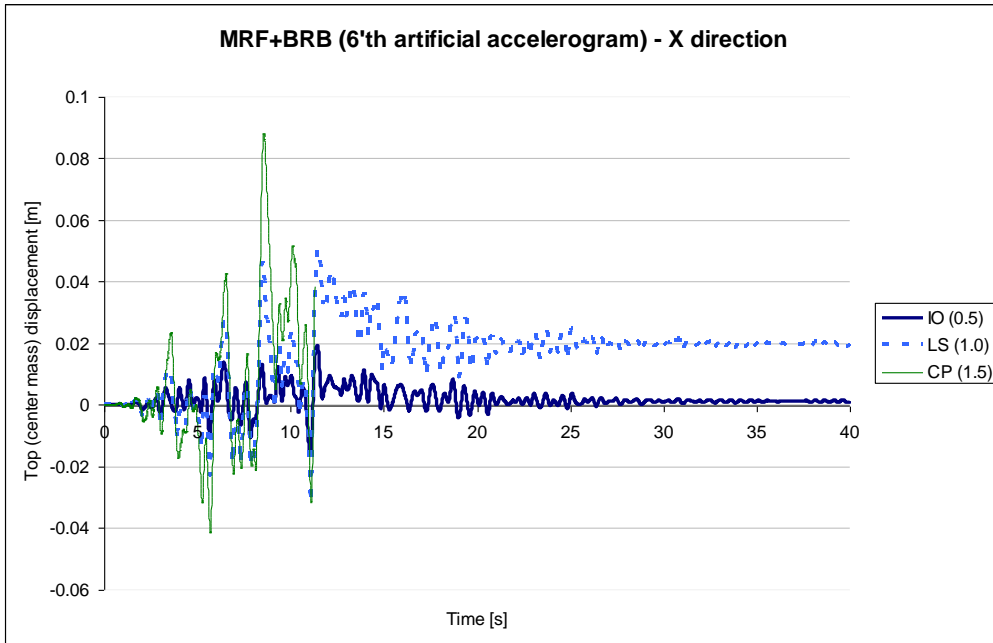


Figure 21 MRF+BRB – X direction Top Displacement at the three stages of IO, LS and CP for the 6'th artificial accelerogram

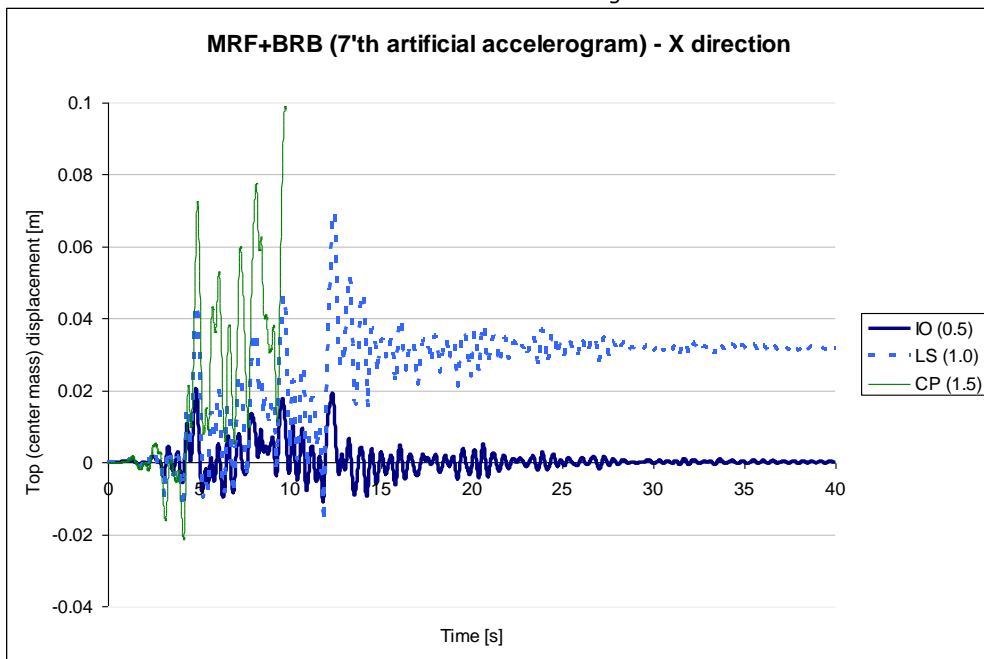


Figure 22 MRF+BRB – X direction Top Displacement at the three stages of IO, LS and CP for the 7'th artificial accelerogram

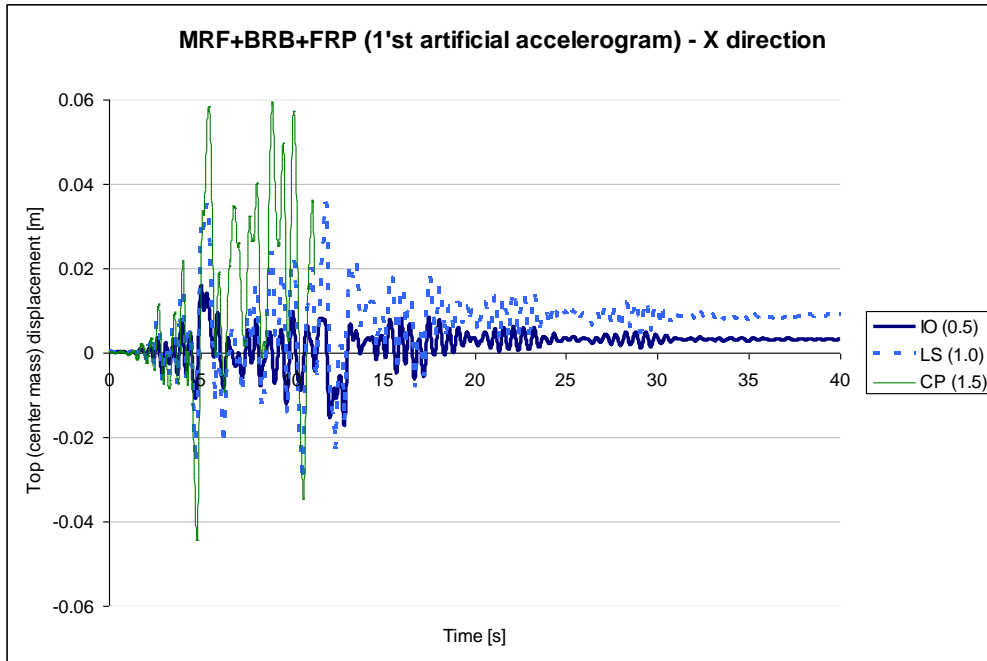


Figure 23 MRF+FRP+BRB – X direction Top Displacement at the three stages of IO, LS and CP for the 1'st artificial accelerogram

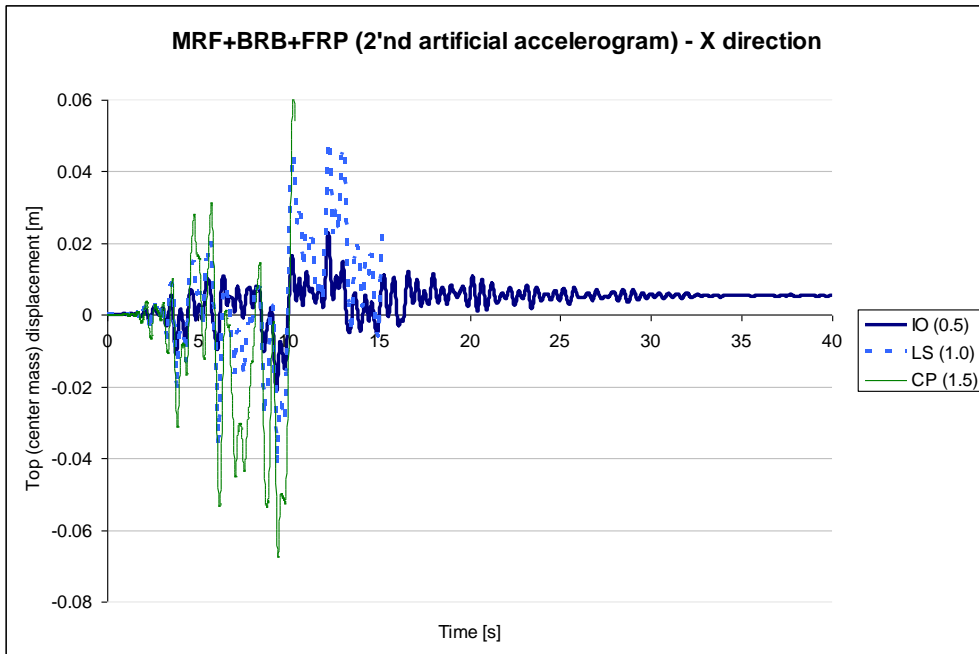


Figure 24 MRF+FRP+BRB – X direction Top Displacement at the three stages of IO, LS and CP for the 2'nd artificial accelerogram



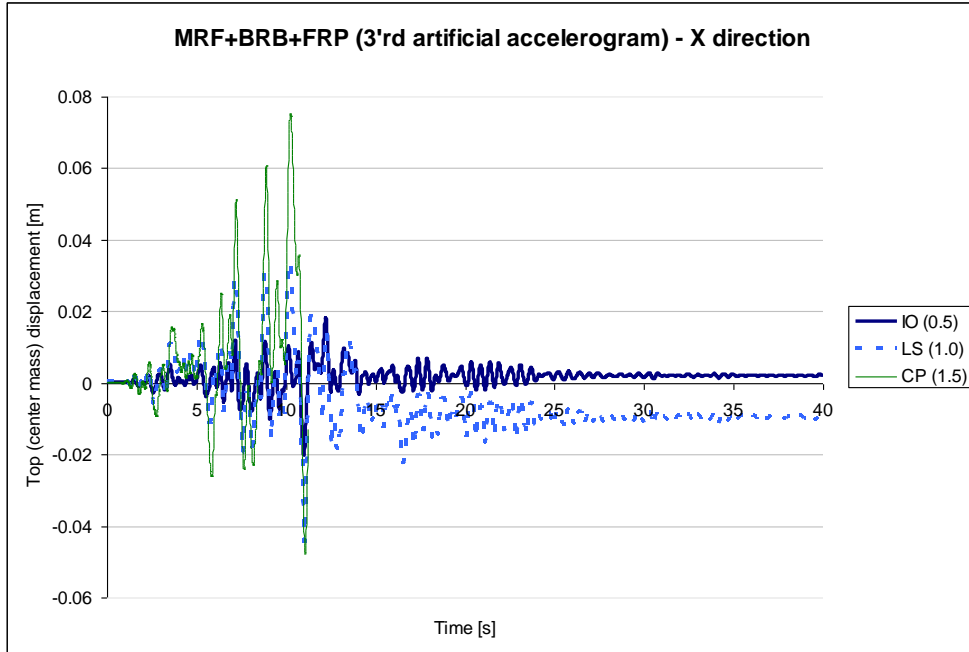


Figure 25 MRF+FRP+BRB – X direction Top Displacement at the three stages of IO, LS and CP for the 3’rd artificial accelerogram

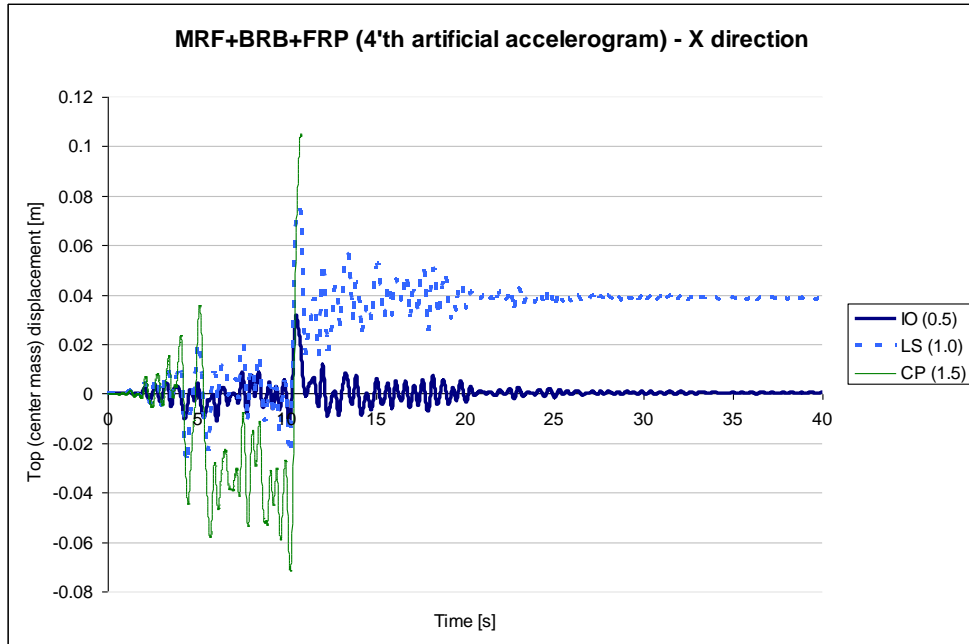


Figure 26 MRF+FRP+BRB – X direction Top Displacement at the three stages of IO, LS and CP for the 4’th artificial accelerogram

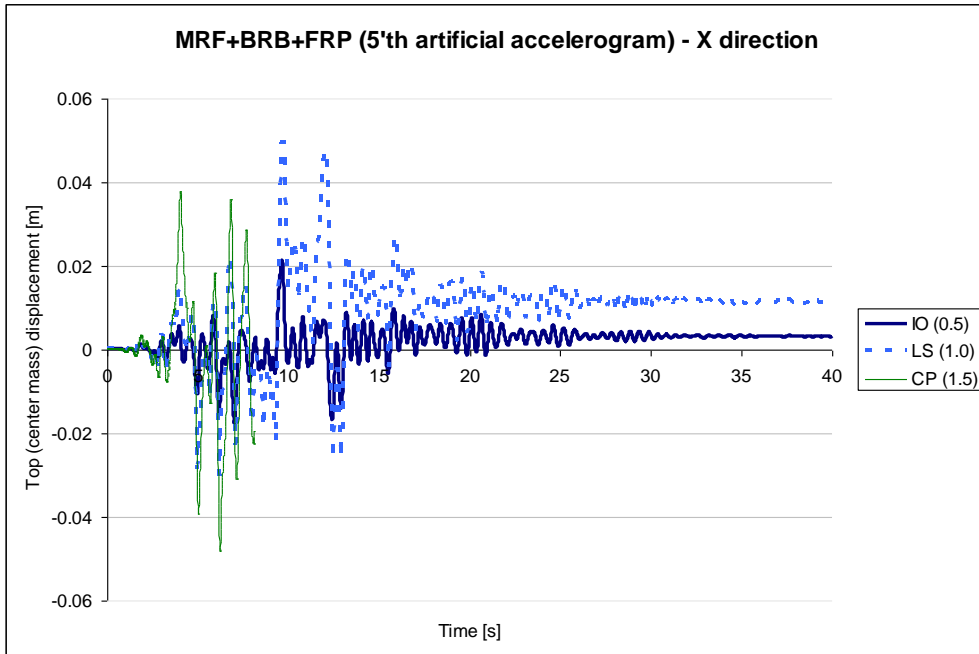


Figure 27 MRF+FRP+BRB – X direction Top Displacement at the three stages of IO, LS and CP for the 5'th artificial accelerogram

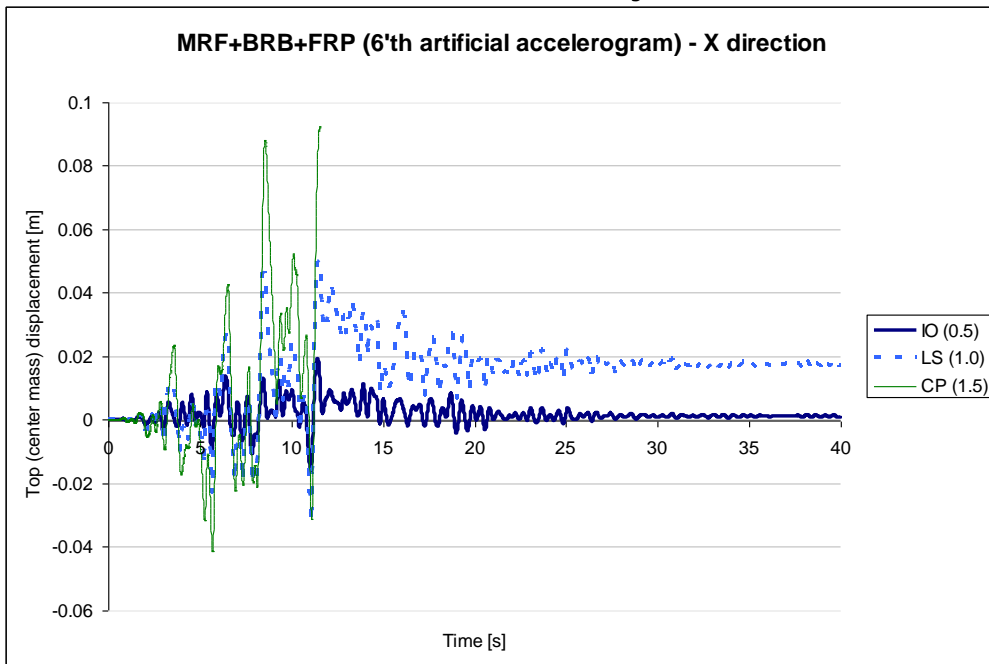


Figure 28 MRF+FRP+BRB – X direction Top Displacement at the three stages of IO, LS and CP for the 6'th artificial accelerogram

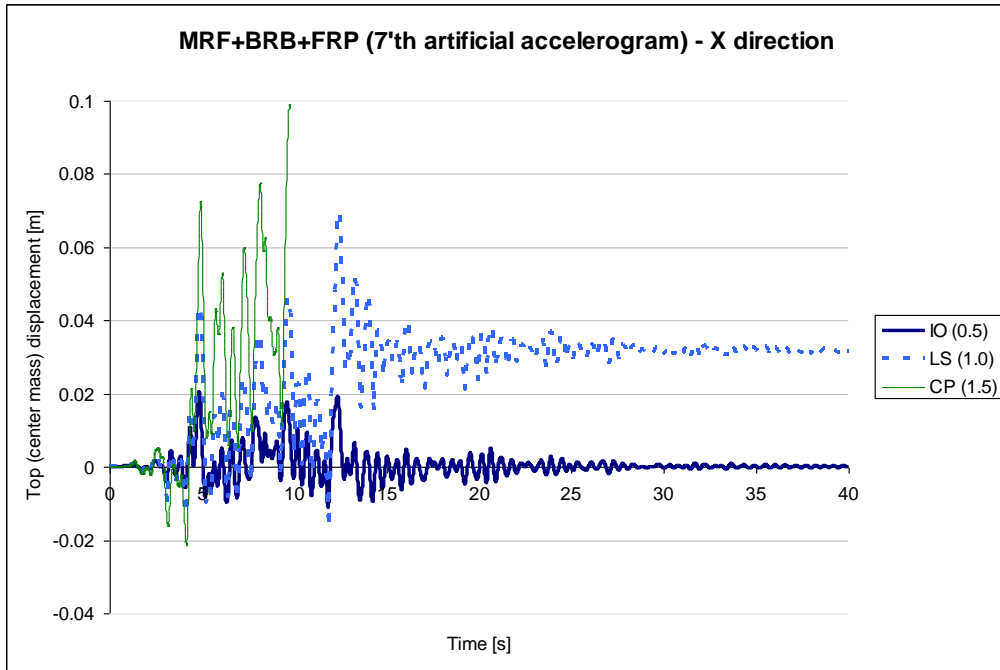


Figure 29 MRF+FRP+BRB – X direction Top Displacement at the three stages of IO, LS and CP for the 7'th artificial accelerogram

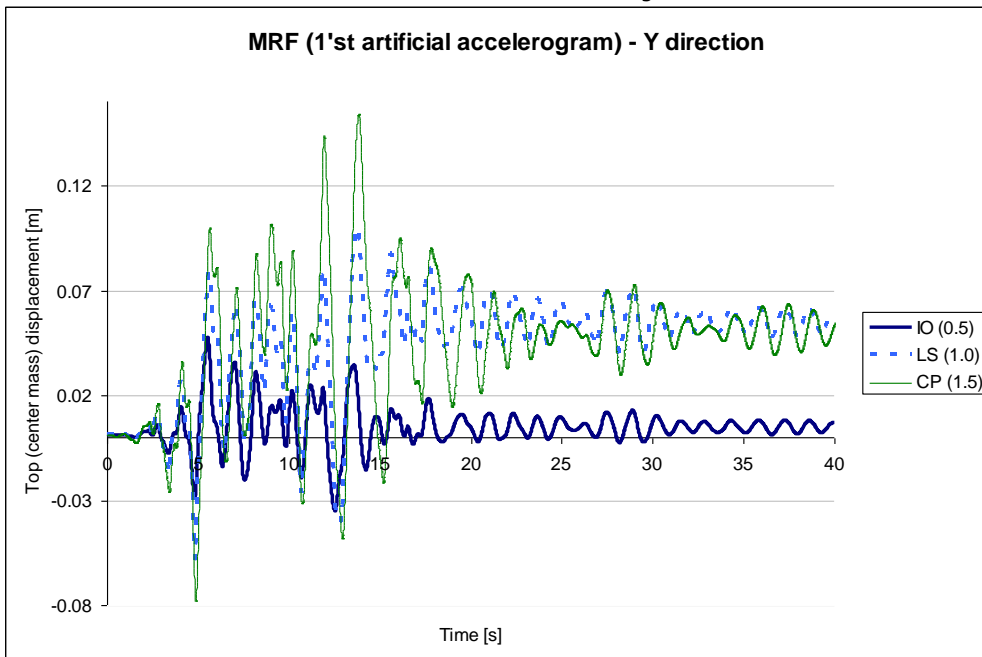


Figure 30 MRF – Y direction Top Displacement at the three stages of IO, LS and CP for the 1'st artificial accelerogram

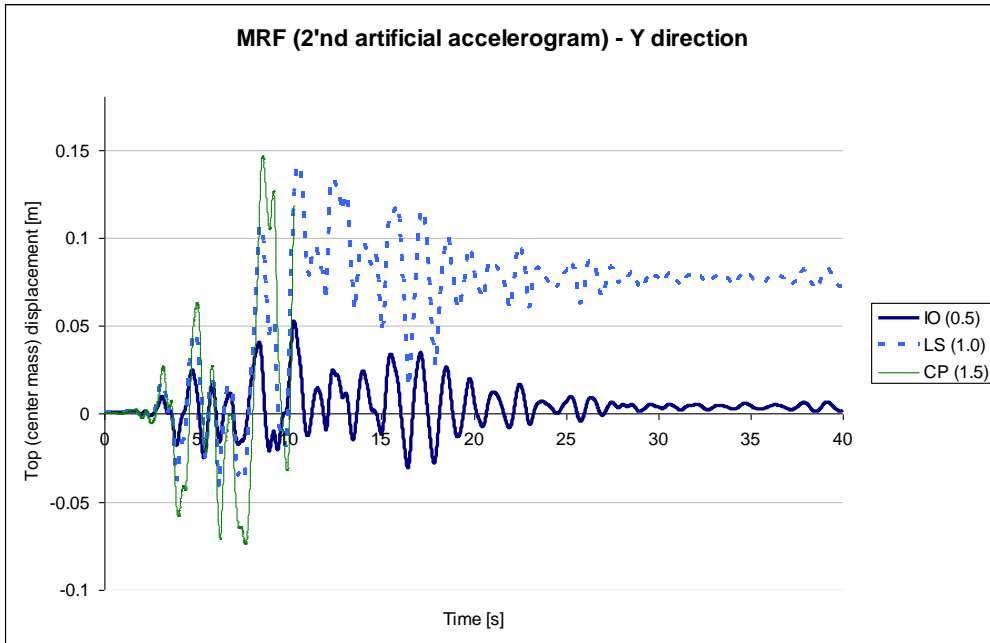


Figure 31 MRF – Y direction Top Displacement at the three stages of IO, LS and CP for the 2'nd artificial accelerogram

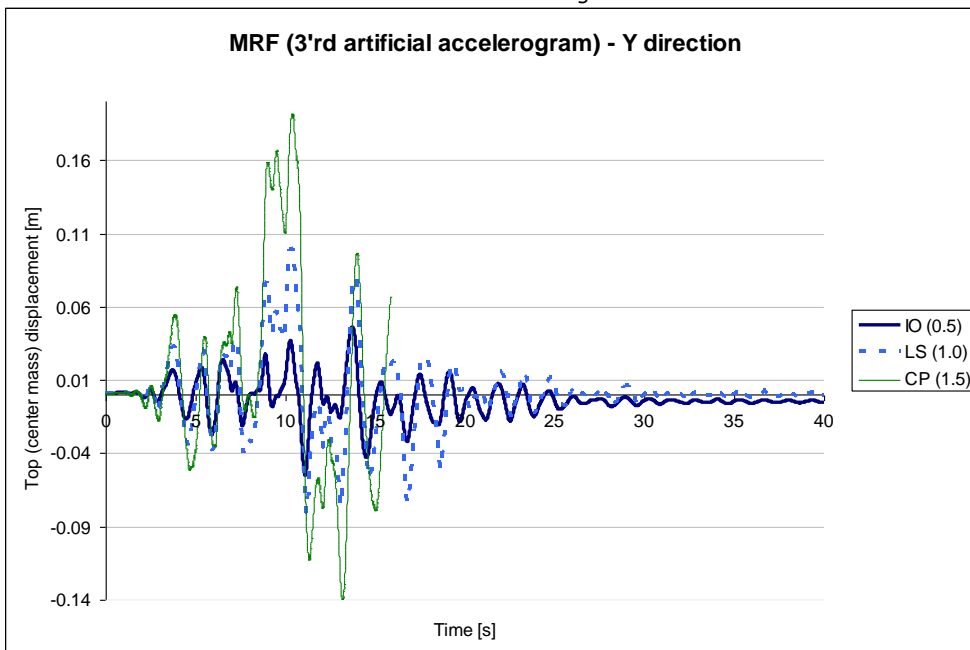


Figure 32 MRF – Y direction Top Displacement at the three stages of IO, LS and CP for the 3'rd artificial accelerogram

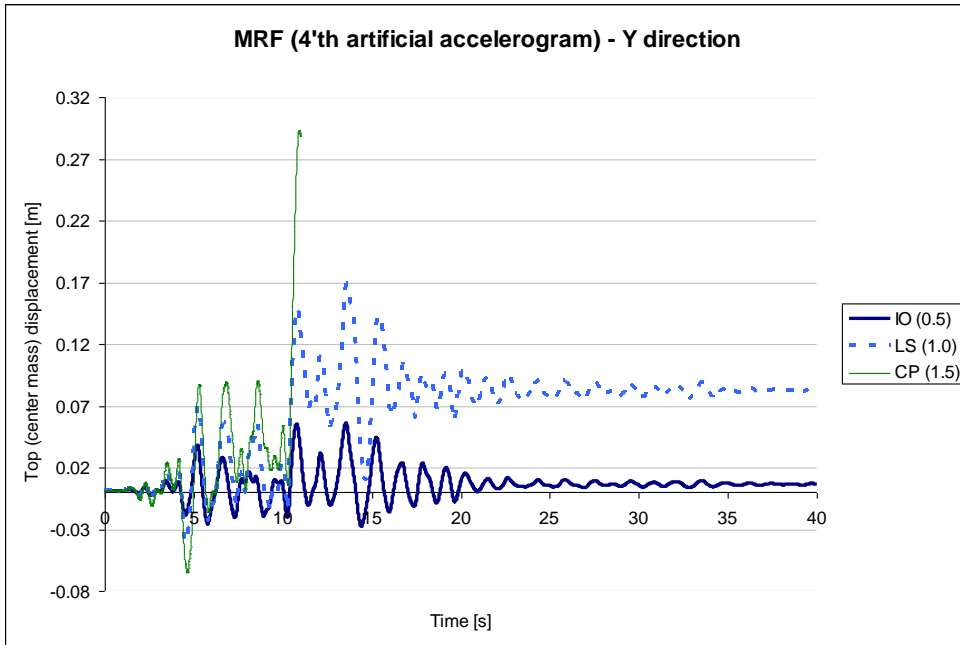


Figure 33 MRF – Y direction Top Displacement at the three stages of IO, LS and CP for the 4'th artificial accelerogram

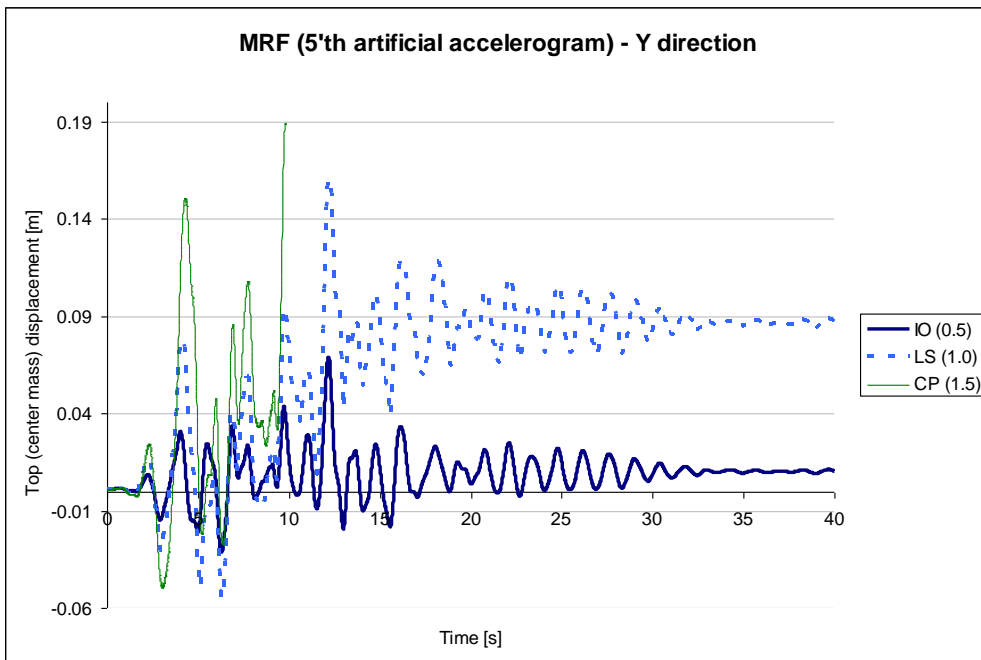


Figure 34 MRF – Y direction Top Displacement at the three stages of IO, LS and CP for the 5'th artificial accelerogram

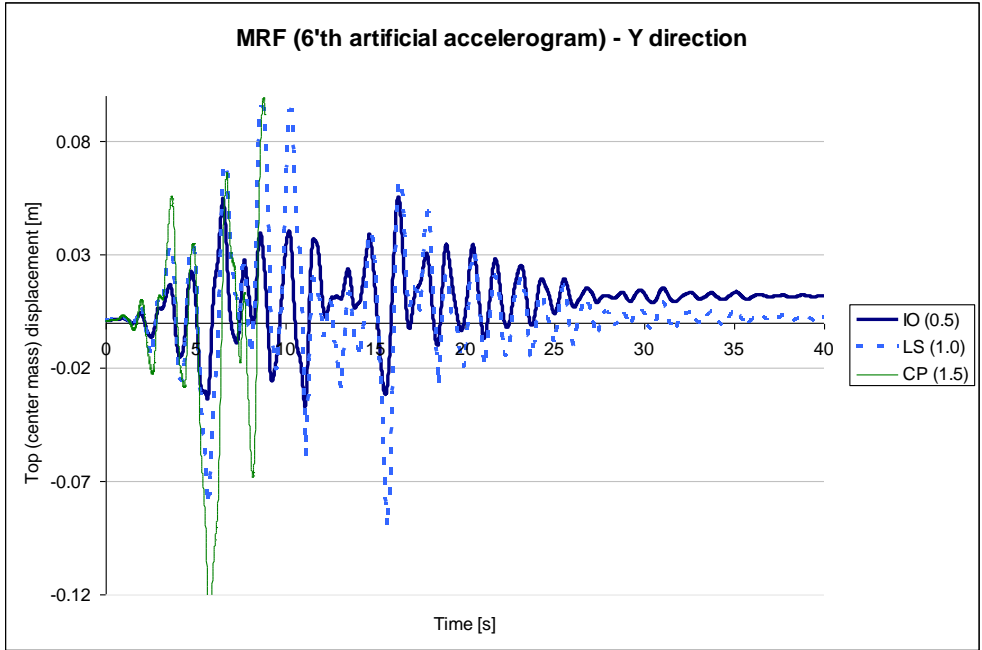


Figure 35 MRF – Y direction Top Displacement at the three stages of IO, LS and CP for the 6'th artificial accelerogram

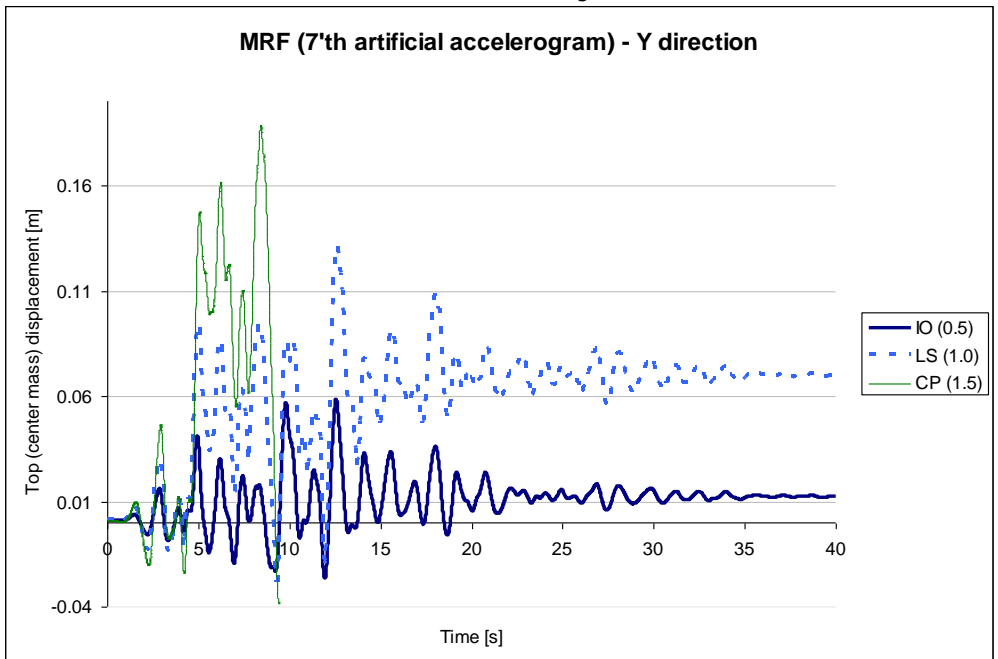


Figure 36 MRF – Y direction Top Displacement at the three stages of IO, LS and CP for the 7'th artificial accelerogram

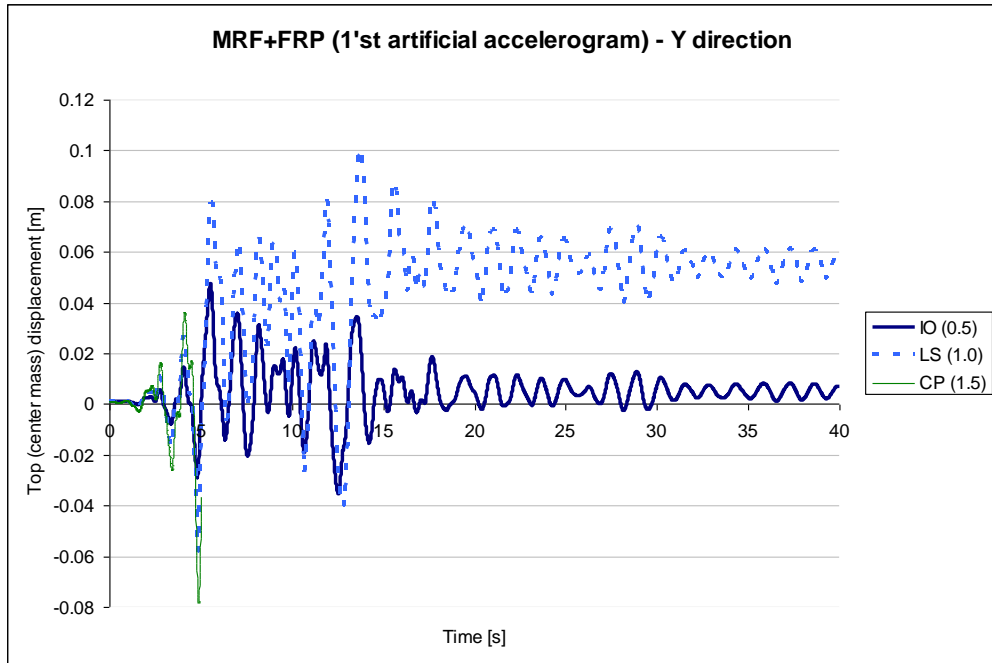


Figure 37 MRF+FRP – Y direction Top Displacement at the three stages of IO, LS and CP for the 1'st artificial accelerogram

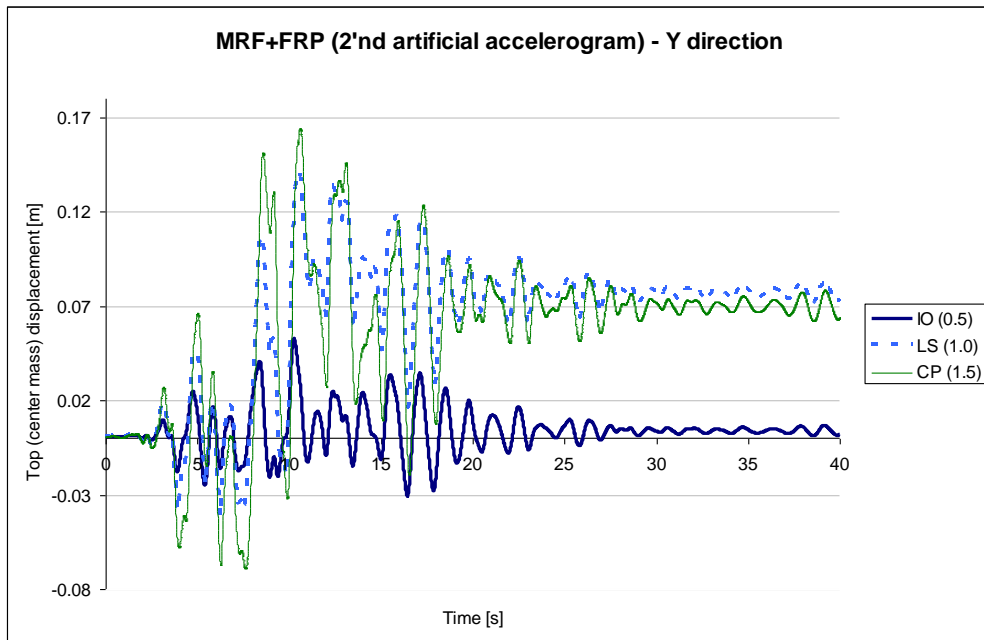


Figure 38 MRF+FRP – Y direction Top Displacement at the three stages of IO, LS and CP for the 2'nd artificial accelerogram

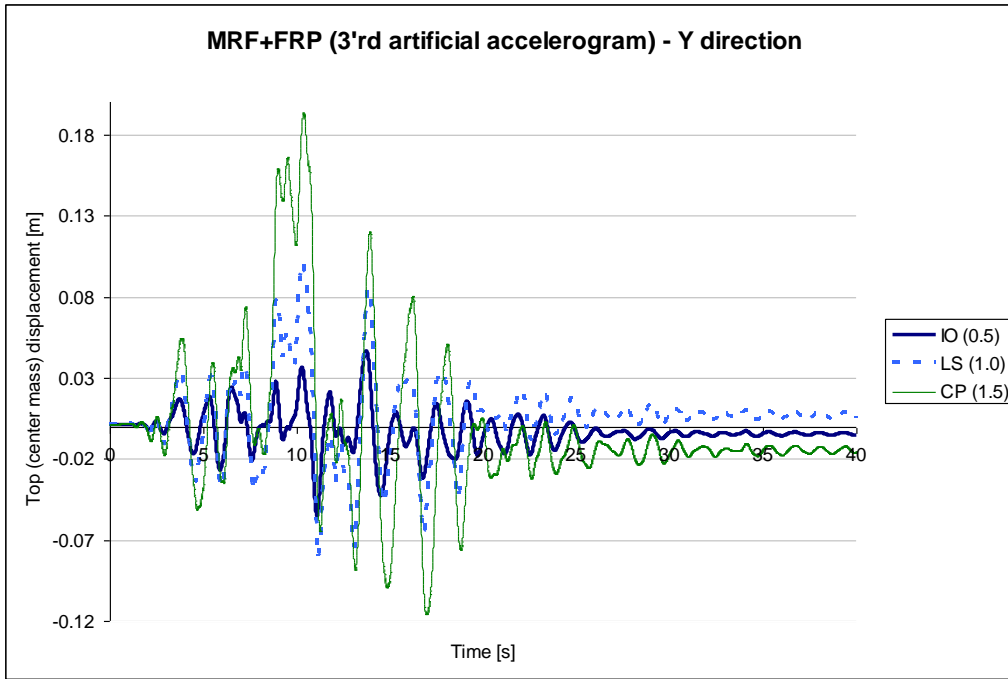


Figure 39 MRF+FRP – Y direction Top Displacement at the three stages of IO, LS and CP for the 3'rd artificial accelerogram

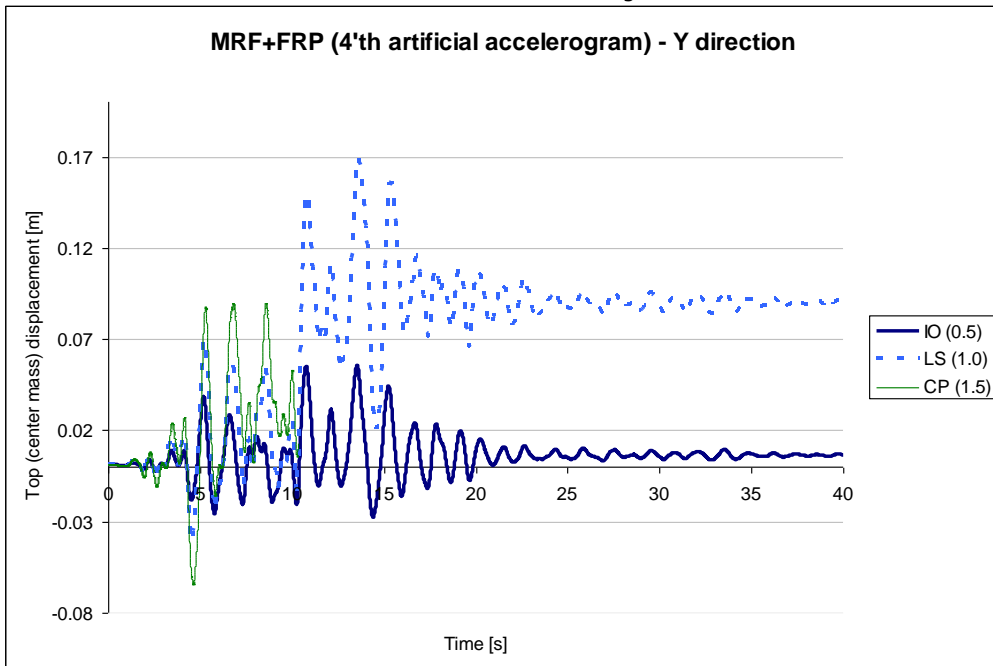


Figure 40 MRF+FRP – Y direction Top Displacement at the three stages of IO, LS and CP for the 4'th artificial accelerogram



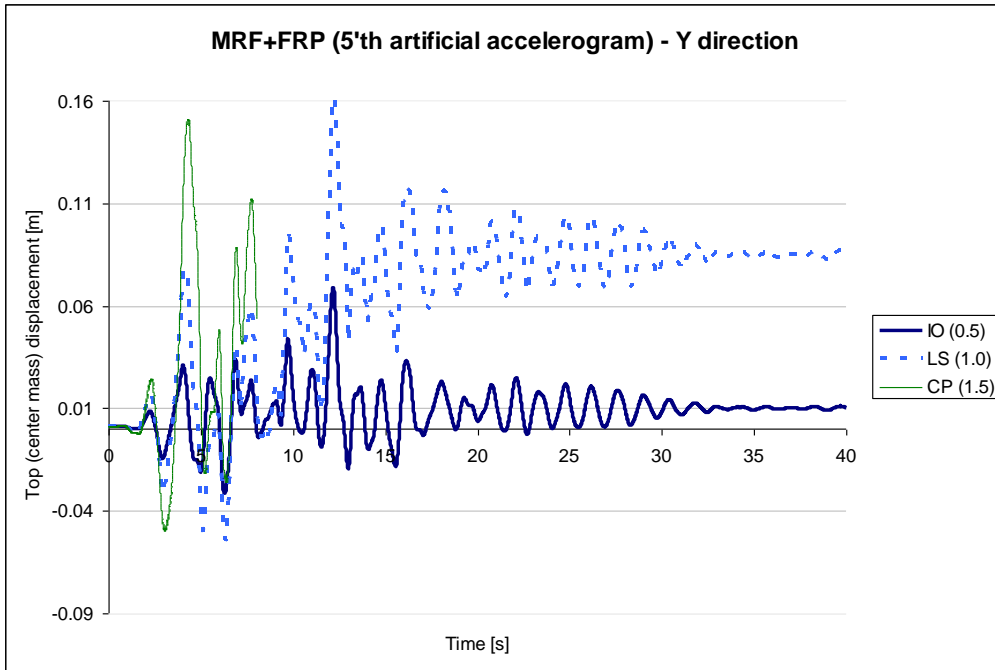


Figure 41 MRF+FRP – Y direction Top Displacement at the three stages of IO, LS and CP for the 5'th artificial accelerogram

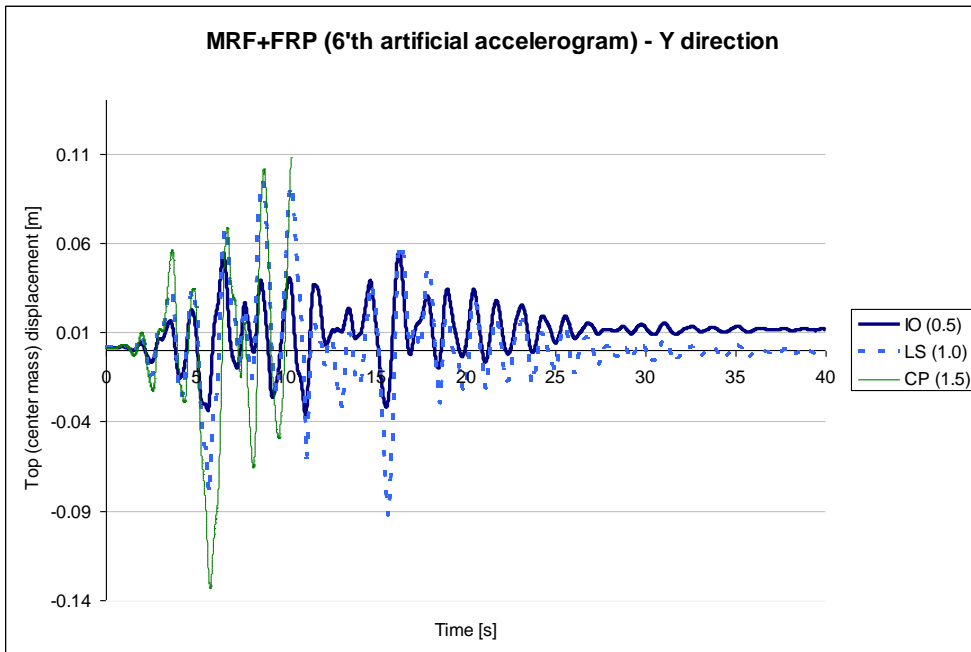


Figure 42 MRF+FRP – Y direction Top Displacement at the three stages of IO, LS and CP for the 6'th artificial accelerogram

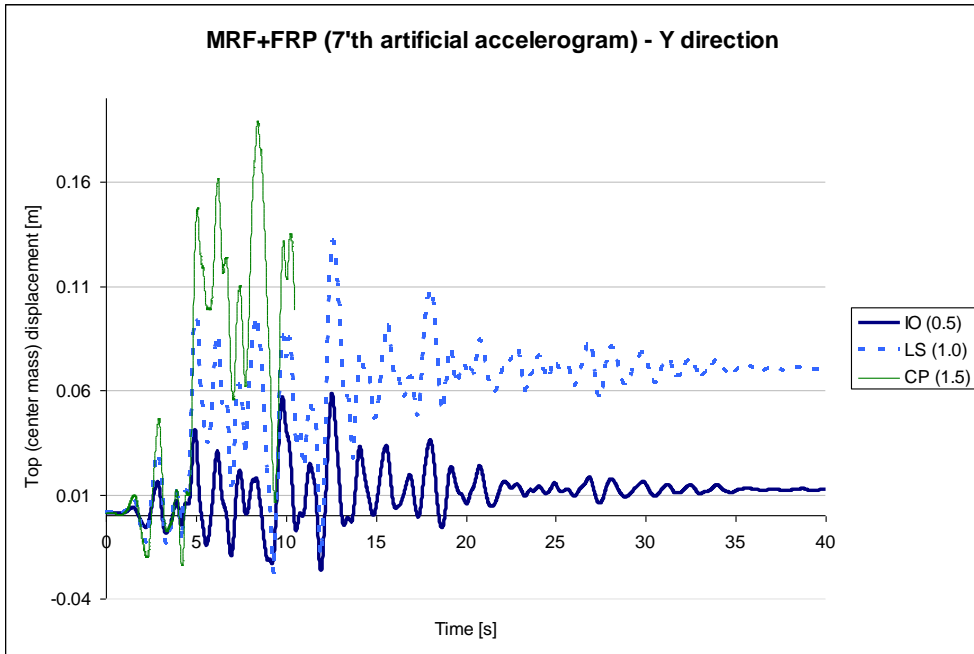


Figure 43 MRF+FRP – Y direction Top Displacement at the three stages of IO, LS and CP for the 7'th artificial accelerogram

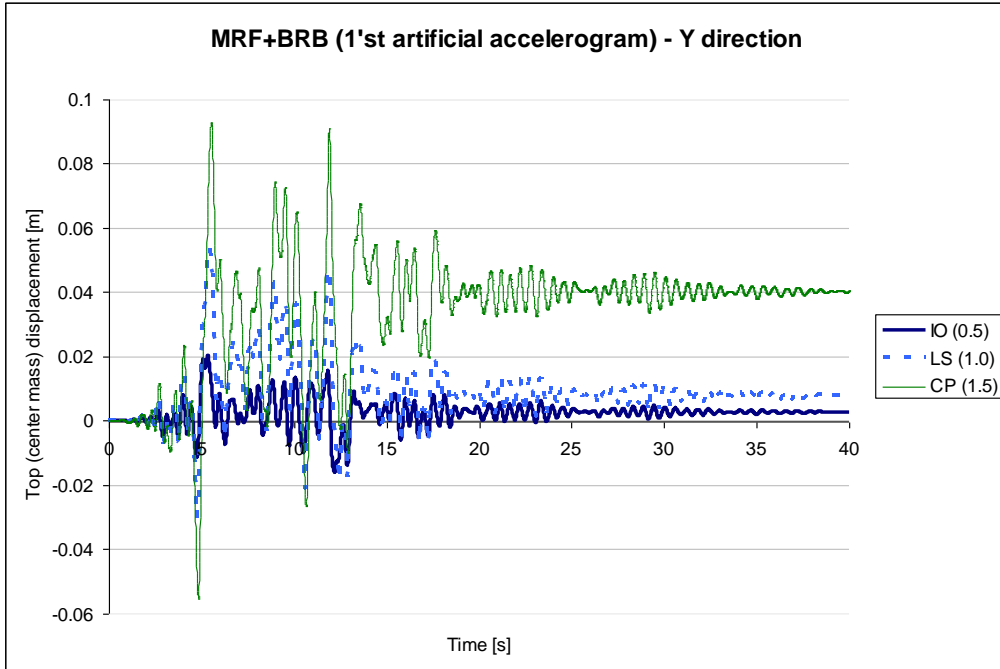


Figure 44 MRF+BRB – Y direction Top Displacement at the three stages of IO, LS and CP for the 1'st artificial accelerogram

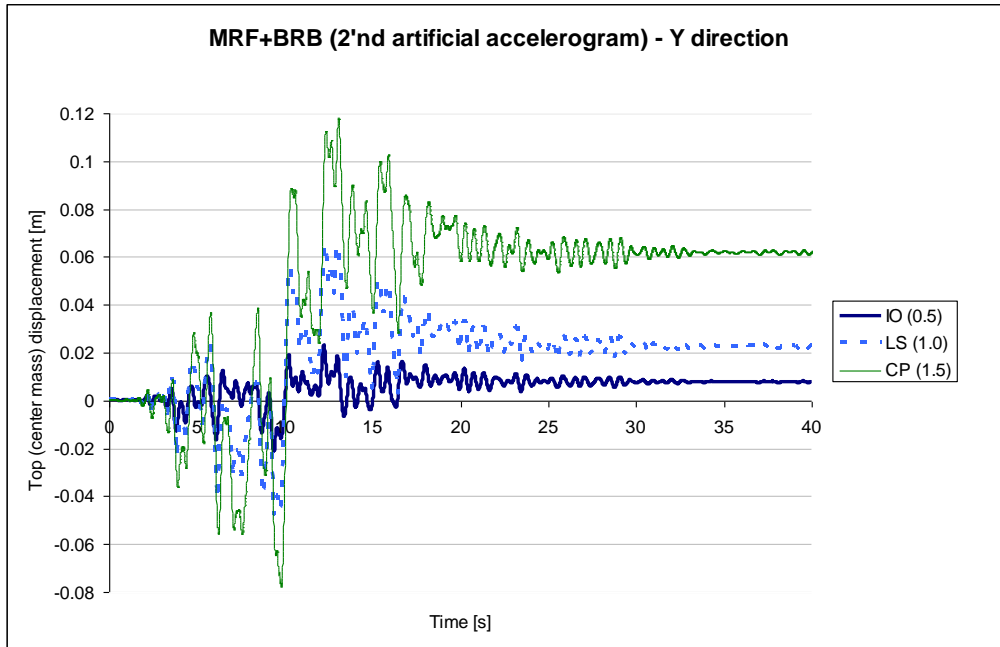


Figure 45 MRF+BRB – Y direction Top Displacement at the three stages of IO, LS and CP for the 2'nd artificial accelerogram

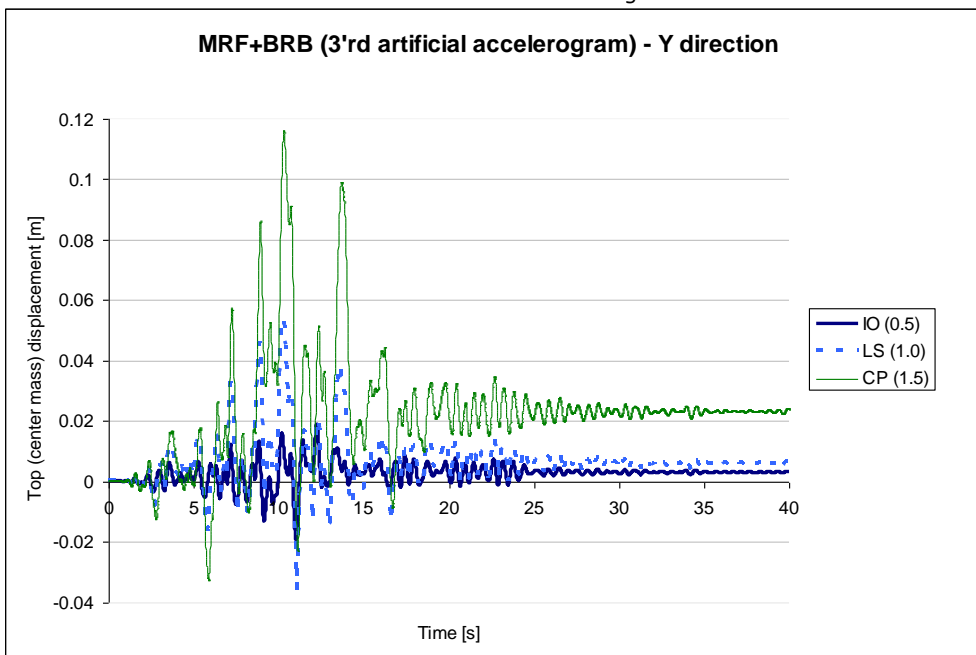


Figure 46 MRF+BRB – Y direction Top Displacement at the three stages of IO, LS and CP for the 3'rd artificial accelerogram

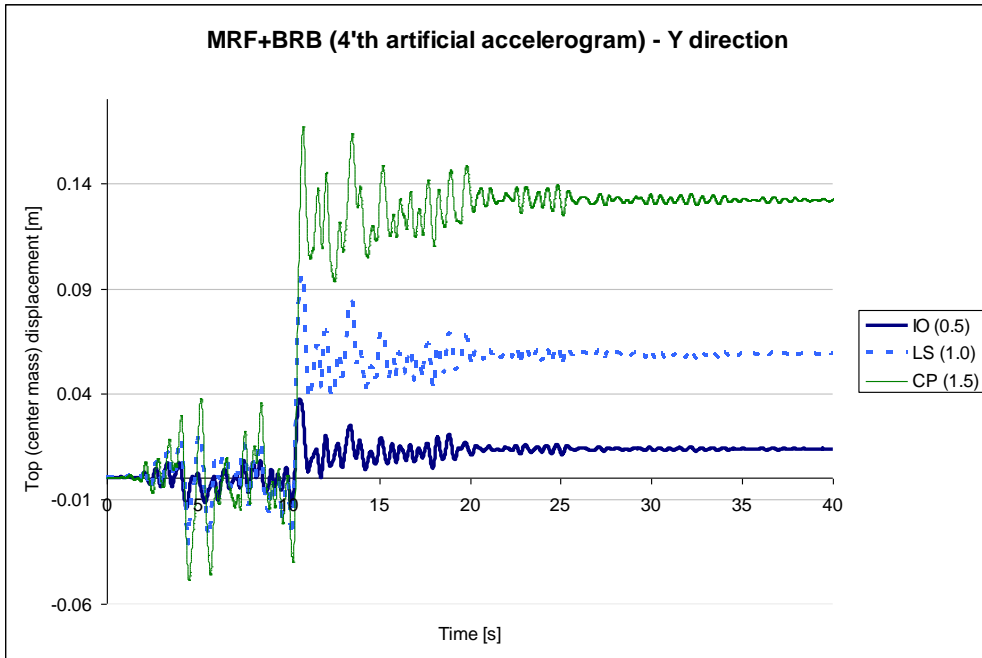


Figure 47 MRF+BRB – Y direction Top Displacement at the three stages of IO, LS and CP for the 4'th artificial accelerogram

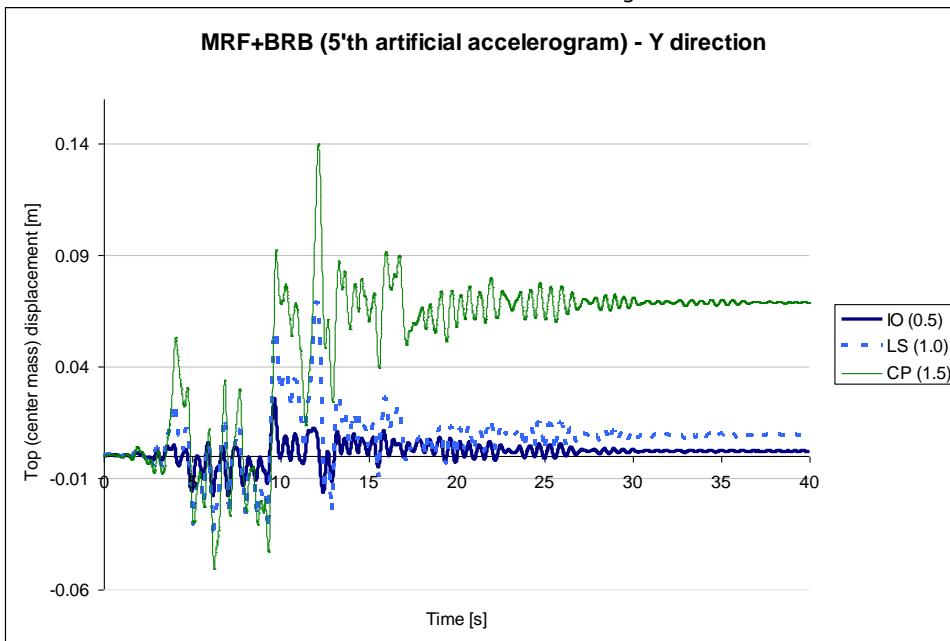


Figure 48 MRF+BRB – Y direction Top Displacement at the three stages of IO, LS and CP for the 5'th artificial accelerogram

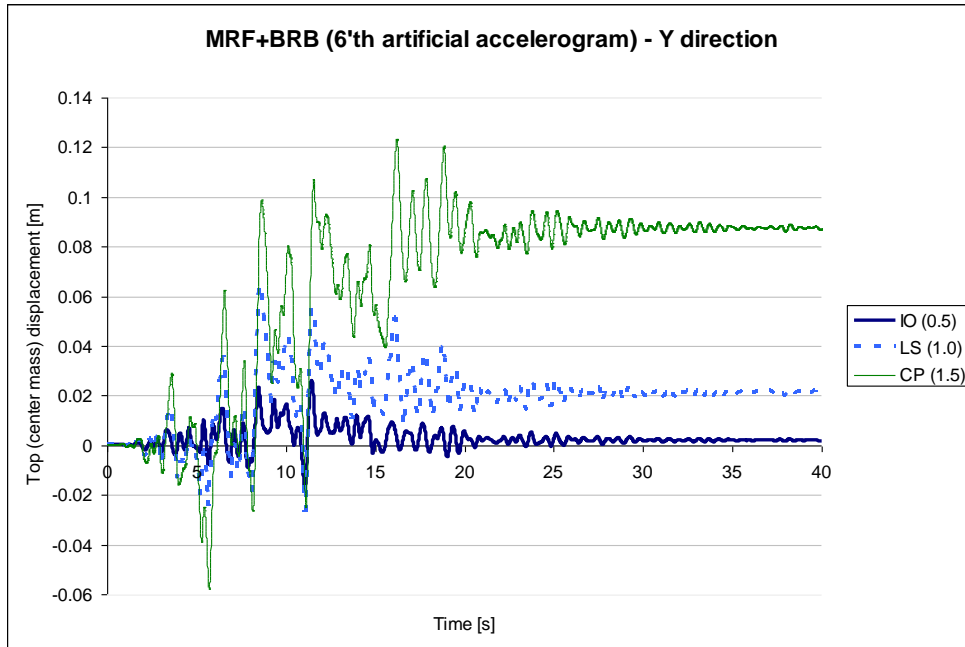


Figure 49 MRF+BRB – Y direction Top Displacement at the three stages of IO, LS and CP for the 6'th artificial accelerogram

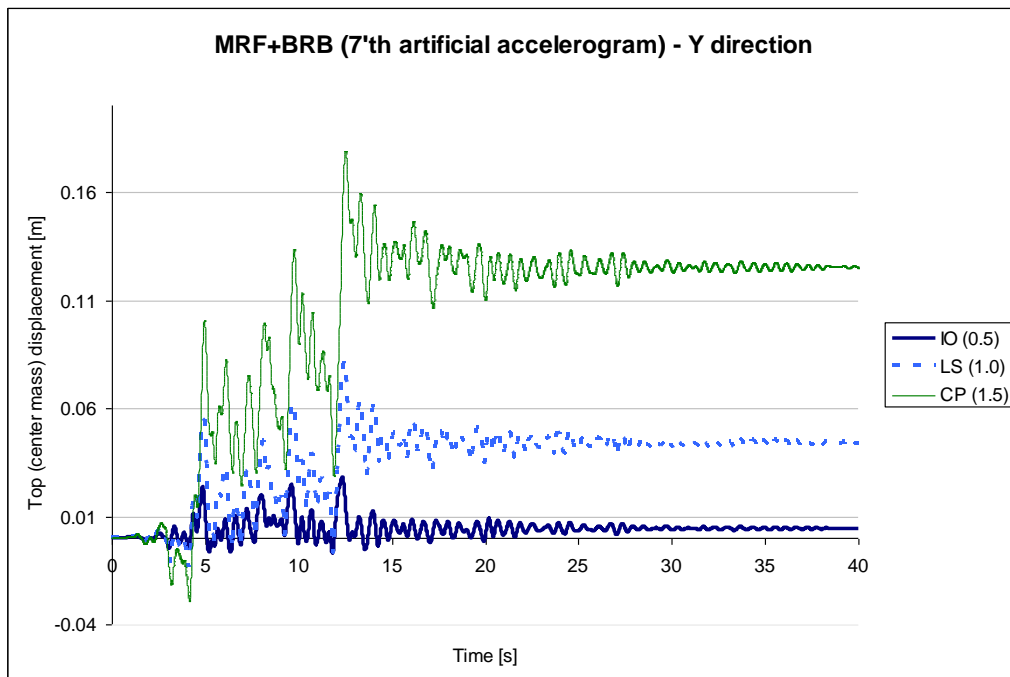


Figure 50 MRF+BRB – Y direction Top Displacement at the three stages of IO, LS and CP for the 7'th artificial accelerogram

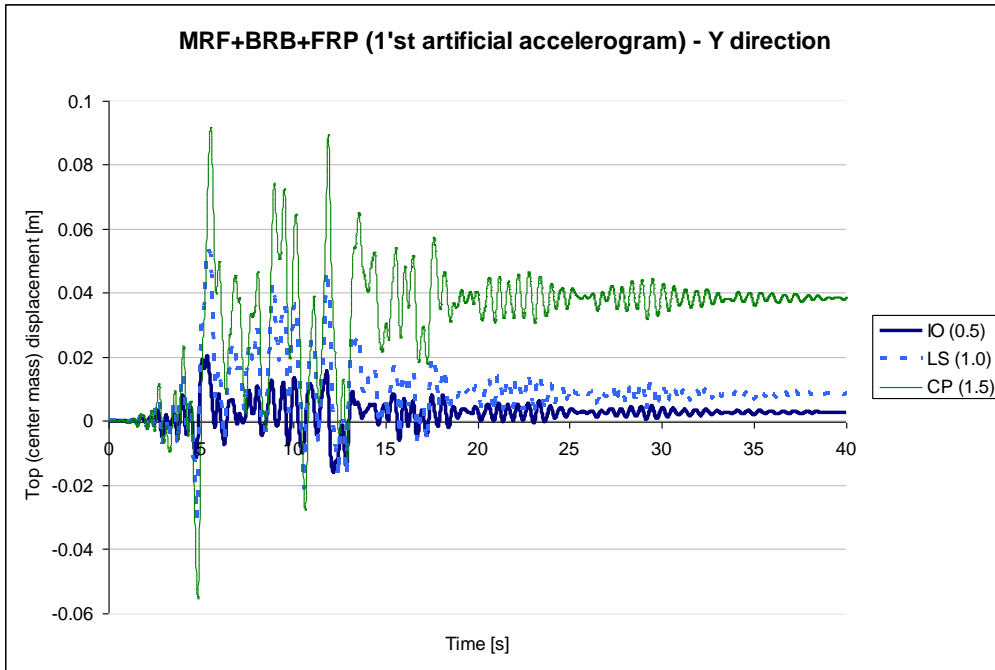


Figure 51 MRF+FRP+BRB – Y direction Top Displacement at the three stages of IO, LS and CP for the 1'st artificial accelerogram

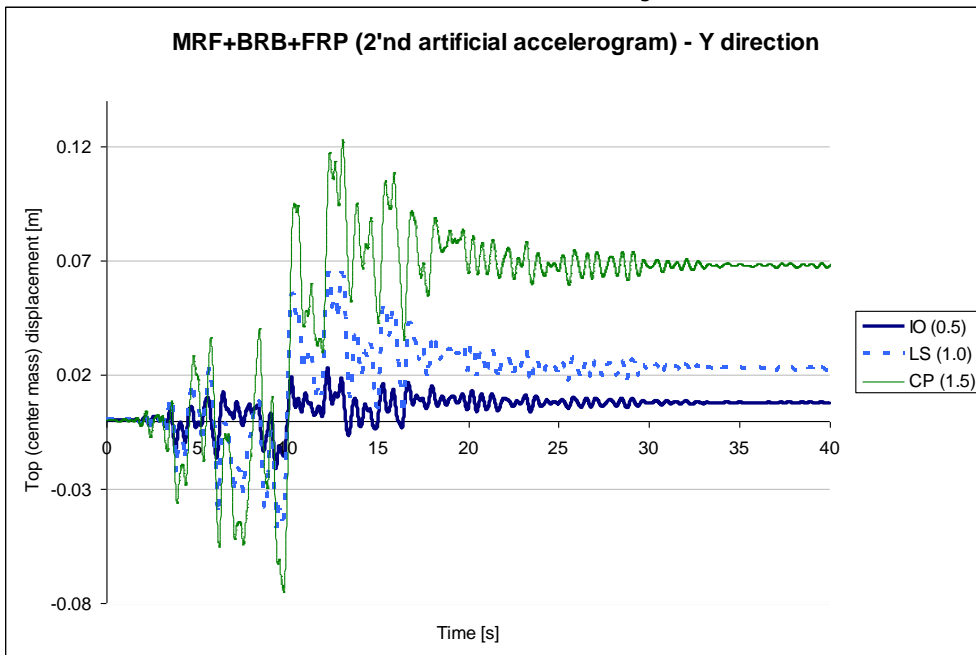


Figure 52 MRF+FRP+BRB – Y direction Top Displacement at the three stages of IO, LS and CP for the 2'nd artificial accelerogram

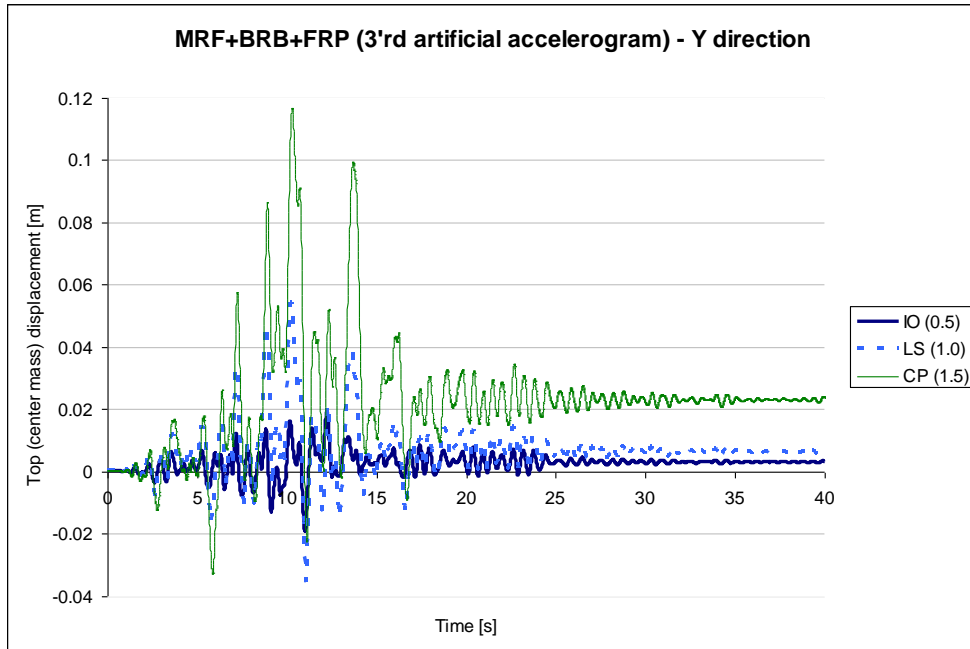


Figure 53 MRF+FRP+BRB – Y direction Top Displacement at the three stages of IO, LS and CP for the 3’rd artificial accelerogram

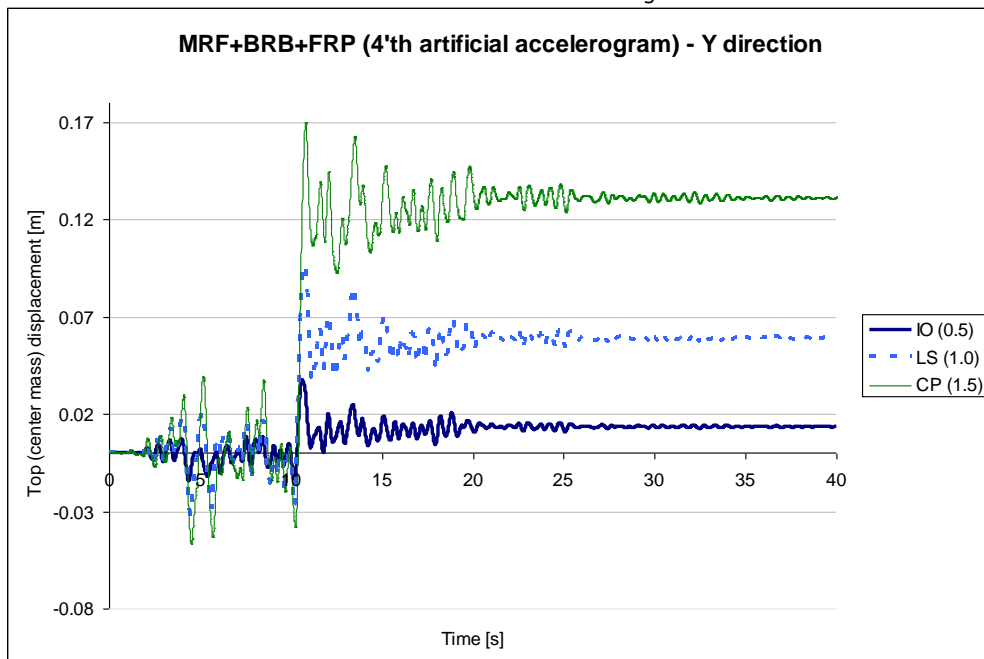


Figure 54 MRF+FRP+BRB – Y direction Top Displacement at the three stages of IO, LS and CP for the 4’th artificial accelerogram

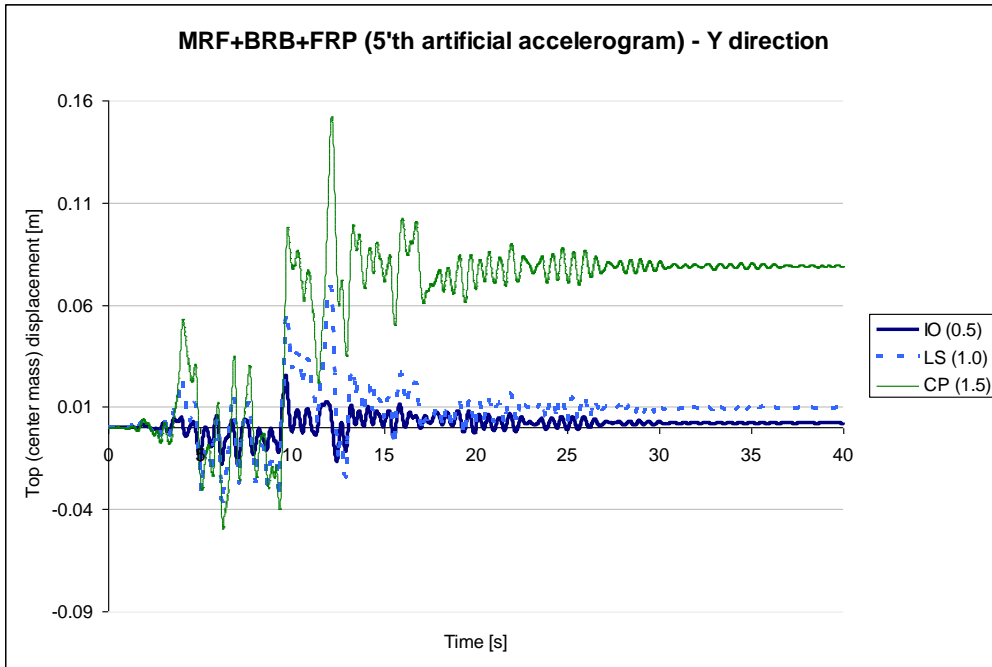


Figure 55 MRF+FRP+BRB – Y direction Top Displacement at the three stages of IO, LS and CP for the 5'th artificial accelerogram

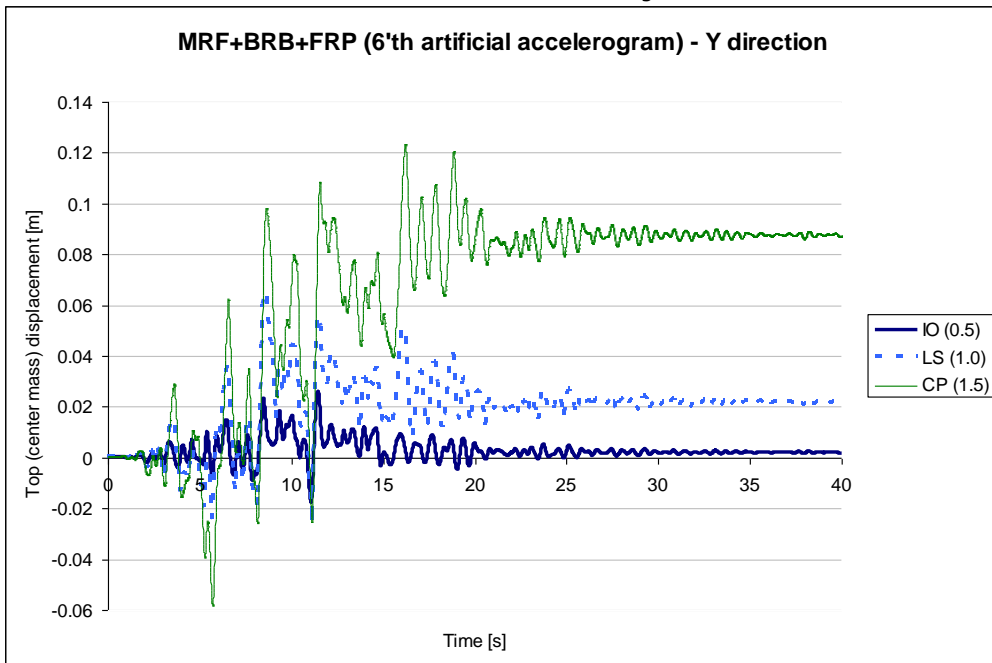


Figure 56 MRF+FRP+BRB – Y direction Top Displacement at the three stages of IO, LS and CP for the 6'st artificial accelerogram



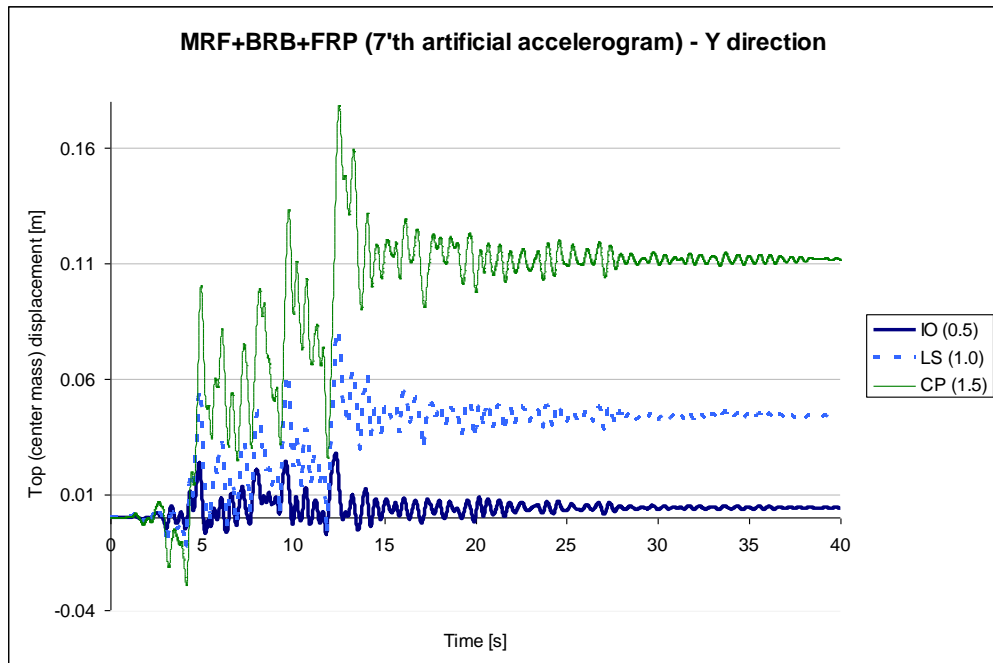


Figure 57 MRF+FRP+BRB – Y direction Top Displacement at the three stages of IO, LS and CP for the 7'th artificial accelerogram



Steps were followed in order to built BRB elements a) and b) mechanical cut; c) welding of the web stiffeners; d) and e) positioning of polystyrene (to permit longitudinal deformations); f) and g) wrapping of the unbonding material (PVC transparent film of 1mm thickness); h), i), j) and k) insertion and calibration of the wrapped steel core into restraining steel tube; l) vertical positioning of the BRB element; m) infill of the restraint material (concrete).